

**CHARACTERISATION OF A NOVEL FLEXING
DIFFUSION CELL (CUTAFLEX™) FOR ASSESSING
DERMAL EXPOSURE TO NANOPARTICLES**

Vanessa Ann Viegas

Submitted to the University of Hertfordshire in fulfilment of the
requirements of the degree of Doctor of Philosophy

July 2014

Abstract

Nanoparticles are thought to present a unique hazard to human health. Furthermore, the increasing use of nanomaterials in consumer products has not been accompanied by relevant risk assessments. It is conceivable that skin flexion may assist the translocation of nanoparticles across the stratum corneum. However, current *in vitro* methodology to study dermal absorption involves the exclusive use of immobile skin within diffusion cells. Therefore, a novel skin-flexing diffusion cell system (“CutaFlex™”) was developed to incorporate reproducible skin flexing (2 flexes min⁻¹; 6 mm maximum amplitude). The initial aims of this Thesis were to characterise the CutaFlex™ system to eliminate the possibility of flexion-induced (experimental) skin damage, demonstrate equivalence with historical permeability data to model compounds and assess the effect of skin flexing on barrier disruption. Subsequent work aimed to investigate the hypothesis that nanoparticles require dermal flexion to penetrate intact skin. In supporting these aims, this Thesis also performed work to assess the correlation between direct measurements of skin barrier function (using tritiated water) and transepidermal water loss (TEWL), the effect of flexing on the performance of topical skin protectants (barrier creams) and to further validate *in vitro* diffusion cell measurements against *in vivo* data acquired under identical conditions.

The results demonstrated that skin flexing did not alter skin barrier function and that the CutaFlex™ system was in general agreement with historical measurements of skin permeability. Furthermore, controlled chemical or physical damage to the stratum corneum was not exacerbated by skin flexing. Skin flexion did not facilitate the dermal absorption of a range of nanoparticles (quantum dots). However, differences in the partitioning of nanoparticles into the stratum corneum were observed (independent of the degree of flexing), with greater amounts of negatively charged nanoparticles found in the superficial layers of the stratum corneum in comparison with positive or neutral nanoparticles. Flexing had a modest effect on the performance of a skin barrier cream which was limited to low dose applications; an effect tentatively ascribed to flexion-induced movement of cream to previously untreated areas. A poor correlation was found between ³H₂O water permeability and TEWL flux. Most importantly, there was excellent agreement between *in vitro* skin permeability studies and *in vivo* studies (which used a surrogate measure of skin permeability).

To summarise, the data in this Thesis has led to the development and characterisation of a novel diffusion cell (CutaFlex™), capable of simultaneously flexing skin whilst performing dermal absorption measurements comparable with the OECD-compliant models.

Acknowledgements

Firstly, I would like to thank Public Health England (formerly Health Protection Agency) for sponsoring this PhD. In particular I would like to thank Dr. Simon Bouffler, Miss Kerry Foxall, Mr. Paul Finnon, Mr. James Warren, Mr. Alan Hodgson, Dr. Stacey Wyke, Dr. Peter Pellow, Dr. Alison Buckley and Dr. Rachel Smith for their help, expertise and lab space. A special thanks to Miss Kerry Foxall for being my honorary student support officer whilst at HPA! I would also like to thank the staff within the Toxicology and Biological Effects Departments whom I have not named specifically. I would also like to acknowledge and thank Bracco Diagnostics Inc. (Princeton, New Jersey, U.S.A.) who primarily funded the work in Chapter 5.

I would like to thank the staff at the University of Hertfordshire's School of Life and Medical Sciences especially Mr. James Stanley, Dr. Liam McAuley, Dr. Anong Smith, Mrs. Sue Rawlins, Dr. Janet Evans and Mrs. Diana Francis; my colleagues in the UH TDDT group at BioPark, namely Mrs. Karen Atkinson, Miss Sneha Kansagra, Dr. Jo Lerner, Mr. Neil Redding, Dr. Nick Kassouf, Miss Sara Syed and Mr. Scott Townend; and an especially huge thank you to my fellow PhD students at UH (for help and moral support in times of need!)- Mr. Satyajit Shetage, Mr. Francesco Caserta, Miss Irene Parisini, Miss Mubinah Beebeejaun, Dr. Andy Edwards, Miss Liz Osoba, Miss Rama Camara and Miss Michelle Botha.

I would like to thank my supervisory team of Prof. Robert Chilcott, Prof. Marc Brown, Dr. James Wakefield and Dr. Matthew Traynor. I would like to give an extra thank you to Prof. Brown for his support over the last few years. Majorly, and most importantly, I would like to thank Prof. Chilcott for without his support, expertise and imagination this project would never have succeeded.

Lastly, I am very grateful to all my family (especially Mom) and friends both in Canada and the UK for all their support, kindness and encouragement throughout the many long years of this PhD- especially, Dr. Haz Matar.

I would like to end this acknowledgement with a special thank you to my parents without whom I would not have made it this far in life or science.

Table Of Contents

Abstract	i
Acknowledgements	ii
Table Of Contents	iii
Abbreviations	viii
Chapter 1: Introduction	1
1.1 Anatomy Of The Skin	2
1.1.1 The Epidermis	4
1.1.2 The Dermis And Hypodermis	10
1.1.3 Appendages	11
1.2 Dermal Absorption Theory	12
1.2.1 Routes of Absorption	13
1.2.2 Absorption Kinetics	16
1.2.3 Laws Of Diffusion.....	18
1.2.4 Partitioning And Diffusivity	19
1.3 Factors Affecting Dermal Absorption	20
1.3.1 Biological Factors	20
1.3.1.1 Anatomical Site.....	20
1.3.1.2 Age	22
1.3.1.3 Species Variation	23
1.3.1.4 Skin Metabolism	25
1.3.1.5 Skin Preparation And Storage Conditions	25
1.3.2 Mechanical Properties Of The Skin	27
1.3.2.1 Skin Damage Models	28
1.3.3 Physicochemical Properties Of The Penetrant.....	30
1.3.3.1 Molecular Weight	30
1.3.3.2 Volatility	31
1.3.3.3 Lipophilicity.....	31
1.3.3.4 Charge	32
1.3.3.5 Hydrogen Bonding.....	32
1.4 Dermal Absorption: Measurement And Techniques	33
1.4.1 <i>In Vitro</i> Diffusion Cell Studies	33
1.4.1.1 Skin	33
1.4.1.2 Receptor Fluid.....	34
1.4.1.3 <i>In Vitro</i> Diffusion Cell Systems.....	34
1.4.1.4 Skin Integrity Measurements	38
1.4.1.5 Model Compounds	41

1.4.1.6 Limitations Of In Vitro Experimentation.....	51
1.4.2 <i>In Vivo</i> Dermal Absorption	51
1.4.2.1 Model Compounds (Methyl Nicotinate)	52
1.4.2.2 Skin Response	53
1.5 Dermal Toxicity	55
1.5.1 Incontinence Associated Dermatitis.....	55
1.5.1.1 Disease	55
1.5.1.2 Prevention (Barrier Creams)	57
1.5.2 Nanoparticles.....	58
1.5.2.1 Definition And Routes Of Exposure	58
1.5.2.2 Nanoparticle Characterisation	62
1.5.2.3 Dermal Absorption Of Nanoparticles	64
1.5.2.4 Systemic Distribution Of Nanoparticles	72
1.6 Summary	74
Chapter 2: General Methods	76
2.1. <i>In Vitro</i> Dermal Absorption Studies.....	77
2.1.1. Chemicals	77
2.1.2. Skin Preparation	80
2.1.3. Diffusion Cells	81
2.1.4. Barrier Integrity Testing.....	86
2.1.4.1. Transepidermal Water Loss	86
2.1.4.2. Tritiated Water Permeability Testing.....	86
2.1.5. Standard Penetrant Studies.....	87
2.1.5.1. Bladder Adherence Studies	87
2.1.5.2. Tritiated Water Dermal Absorption Studies	88
2.1.5.3. Carbon-14 Benzoic Acid, Caffeine and Testosterone Studies	89
2.1.6. Skin Damage Studies	91
2.1.6.1. Phase I: Baseline Studies	91
2.1.6.2. Phase II: Chemical Damage (Sodium Lauryl Sulphate)	92
2.1.6.3. Phase III: Physical Damage	92
2.1.7. Quantum Dot Nanoparticle Characterisation	94
2.1.7.1. Transmission Electron Microscopy (TEM)	94
2.1.7.2. Dynamic Light Scattering	94
2.1.8. Dermal Absorption Of Nanoparticles	94
2.1.9. Fluorimeter Analysis Of Skin Surface Swabs And Receptor Fluid.....	95
2.1.10. UV-Light Box Images Of Skin Surface	95
2.1.11. Histology	96
2.1.11.1. Paraffin Embedding	96
2.1.11.2. H&E Staining	98
2.1.12. Laser Scanning Confocal Microscopy	100
2.1.13. <i>In Vitro</i> Barrier Cream Efficacy Studies.....	100
2.1.13.1. Evaporation Rate Of ¹⁴ C-Methyl Nicotinate And ³ H-Water.....	100
2.1.13.2. Optimal Thickness Studies.....	101
2.1.13.3. Duration Of Efficacy Studies	103
2.2. Clinical Trial.....	104

2.2.1. <i>In Vivo</i> Measurements.....	104
2.2.1.1. Visual Erythema Scoring	104
2.2.1.2. Laser Doppler Imaging	106
2.2.1.3. Tissue Viability Imaging.....	106
2.2.1.4. Transepidermal Water Loss	106
2.2.2. Optimal Thickness Study	106
2.2.3. Duration Of Efficacy Study	107
2.3. Sample And Statistical Analysis	109
2.3.1. Scintillation Counting	109
2.3.2. Statistical Testing	110

Chapter 3: The Effect Of Flexing On Skin Penetration Of Model Compounds 111

3.1 Introduction.....	112
3.2 Materials And Methods	113
3.3 Results	114
3.3.1 Skin Flexion	114
3.3.2 Skin Damage Studies	116
3.3.2.1 Chemical Damage (Sodium Lauryl Sulphate)	116
3.3.2.2 Physical Damage (Punctures)	118
3.3.3 Tritiated Water Permeability And Transepidermal Water Loss Correlation	120
3.3.4 Standard Penetrant Studies.....	123
3.3.4.3 ³ H-Water Dermal Absorption Studies	123
3.3.4.4 ¹⁴ C-Benzonic Acid Dermal Absorption Study	126
3.3.4.5 ¹⁴ C-Caffeine Dermal Absorption Study	131
3.3.4.6 ¹⁴ C-Testosterone Dermal Absorption Study.....	136
3.3.4.7 Dermal Absorption Parameters For All Carbon-14 Chemicals	141
3.4 Discussion.....	143

Chapter 4: The Effect Of Flexing On Quantum Dot Nanoparticle Skin Absorption 154

4.1. Introduction.....	155
4.2. Materials and Methods.....	157
4.3. Results	158
4.3.1. Quantum Dot Nanoparticle Characterisation	158
4.3.2. Transepidermal Water Loss Rates	161
4.3.3. Skin Surface Recovery of QDots	163
4.3.4. Skin Surface Distribution of QDots	165
4.3.4.1. Quantum Dot 565 vs 655 nm	165
4.3.4.2. Flexed vs Static Skin Sections	165
4.3.4.3. PEG-Amine, PEG-Carboxyl And PEG Attachments.....	165

4.3.5. Haematoxylin And Eosin Stained Quantum Dot Skin Sections	168
4.3.6. Laser Scanning Confocal Micrographs Of Quantum Dot And PBS Treated Skin Samples.....	172
4.3.7. Receptor Fluid Fluorescence Recovery Of Quantum Dots.....	179
4.4. Discussion.....	181
Chapter 5: An <i>In Vitro-In Vivo</i> Evaluation Of CutaFlex™ For Assessing Topical Skin Protection Against Methyl Nicotinate..	193
5.1 Introduction.....	194
5.2 Materials and Methods	195
5.3 Results	196
5.3.1 <i>In Vitro</i> Optimal Thickness Study	196
5.3.1.1 ¹⁴ C-Methyl Nicotinate And ³ H-Water Surface Evaporation	196
5.3.1.2 Measured Thickness Applied- RD-1433 and Vaseline®	198
5.3.1.3 Barrier Viability Measurements	200
5.3.1.4 RD-1433 Treated Groups- Optimal Thickness Study.....	203
5.3.1.5 Vaseline® Treated Groups- Optimal Thickness Study.....	206
5.3.1.6 Dose Distribution Of ¹⁴ C-Methyl Nicotinate: RD-1433 And Vaseline®	210
5.3.2 <i>In Vivo</i> Optimal Thickness Study	212
5.3.2.1 Thickness Applied.....	212
5.3.2.2 <i>In Vivo</i> Barrier Integrity Measurement- TEWL.....	214
5.3.2.3 Visual Erythema Scoring	216
5.3.2.4 Tissue Imaging Viability.....	218
5.3.2.5 Laser Doppler Imaging- Blood Flow	220
5.3.2.6 Laser Doppler Imaging- Maximum Blood Flow	222
5.3.3 <i>In Vitro</i> Duration Of Efficacy Study.....	224
5.3.3.1 Barrier Integrity Measurements	224
5.3.3.2 RD-1433 Treated Groups- Duration Of Efficacy Study	227
5.3.3.3 Vaseline® Treated Groups- Duration Of Efficacy Study	230
5.3.3.4 Dose Recovery Of ¹⁴ C-Methyl Nicotinate- Duration Of Efficacy Study	234
5.3.4 <i>In Vivo</i> Duration Of Efficacy Study.....	237
5.3.4.1 Barrier Integrity Measurement- TEWL	237
5.3.4.2 Visual Erythema.....	239
5.3.4.3 Tissue Viability Imaging.....	241
5.3.4.4 Laser Doppler Imaging- Blood Flow	243
5.3.4.5 Laser Doppler Imaging- Maximum Blood Flux	245
5.3.5 Summation Of <i>In Vitro And In Vivo</i> Results.....	247
5.4 Discussion.....	249
Chapter 6: General Discussion	263
6.1. General Discussion	264

6.2. Summary	268
6.3. Future Studies	268
References	270

Abbreviations

¹⁴C- Carbon-14 isotope
³H₂O- Tritiated water
3Rs- reduction, refinement, replacement of animals
C_v- Concentration of penetrant in vehicle
C_{Sc}- Concentration of penetrant in stratum corneum
CdSe- Cadmium-selenium
Ci- Curies (unit of radioactivity)
CNS- Central nervous system
D- Diffusion coefficient
DPM- Disintegrations per minute
DLS- Dynamic light scattering
ECVAM- European centre for the validation of alternative methods
EDX/S- Energy dispersive x-ray spectroscopy
GC-MS- Gas chromatography- mass spectrometry
H&E- Haematoxylin and eosin
HPLC- High performance liquid chromatography
IAD- Incontinence-associated dermatitis
J_{ss}- Steady state flux
J_{Max}- Maximum flux
K_p- Permeability coefficient
K_{Sc}- Membrane partition coefficient
LC-MS- Liquid chromatography- mass spectrometry
LDI- Laser Doppler imaging
LSCM- Laser scanning confocal microscopy
Log P- octanol-water partition coefficient
MASD – moisture-associated skin damage
MN- Methyl nicotinate
MW- Molecular weight
µm- Micrometers
nm- Nanometers
NTA- Nanoparticle tracking analysis
OECD- The organisation for economic co-operation and development
PBS- Phosphate buffered saline
PCS- Photon correlation spectroscopy (also known as DLS)
QD- Quantum dot
Q_T- Cumulative amount penetrated (amount per cm⁻²) at study end
SEM- Scanning electron microscopy
SLS- Sodium lauryl sulphate
Tau (τ)- Lag time
TER- Transepidermal electrical resistance
TEM- Transmission electron microscopy
TEWL- Transepidermal water loss
TiVi- Tissue viability imaging
ZnS- Zinc sulphide

Chapter 1: Introduction

1.1 Anatomy Of The Skin

The skin is the largest organ of the human body and a very important line of defence against harmful factors present in the external environment. As a veneered structure, the three primary layers of the skin are represented by the outer epidermis, dermis and inner hypodermis (Figure 1.1). The epidermis is further subdivided into the stratum corneum, stratum granulosum, stratum spinosum and stratum basale layers and is responsible for protection against xenobiotics, micro-organisms and certain types of radiation (Monteiro-Riviere, 1991). The dermis provides elasticity as well as structural and immunological support for the epidermis (Monteiro-Riviere, 1996). As the innermost layer, the hypodermis functions as insulation and in energy metabolism. On the whole, the stratum corneum is a good but imperfect barrier against the absorption of xenobiotics as well as reducing ‘insensible’ water loss to the environment (Chilcott, 2008). In addition to physical barrier importance, other crucial roles of the skin include temperature regulation, endocrine and apocrine modulation, metabolism and neurosensory roles (Monteiro-Riviere, 1996). The viable epidermis measures approximately 50-100 μm , the dermis 1-2 mm and the hypodermis 1-2 mm (Schaefer and Redelmeier, 1996). An average human adult weighing approximately 65 kg will have a skin surface area of approximately 18,000 cm^2 (Schaefer and Redelmeier, 1996). This is a large area in terms of potential exposure, but much smaller than the lung and gastrointestinal tract, organs that are associated with the exchange or absorption of xenobiotics.

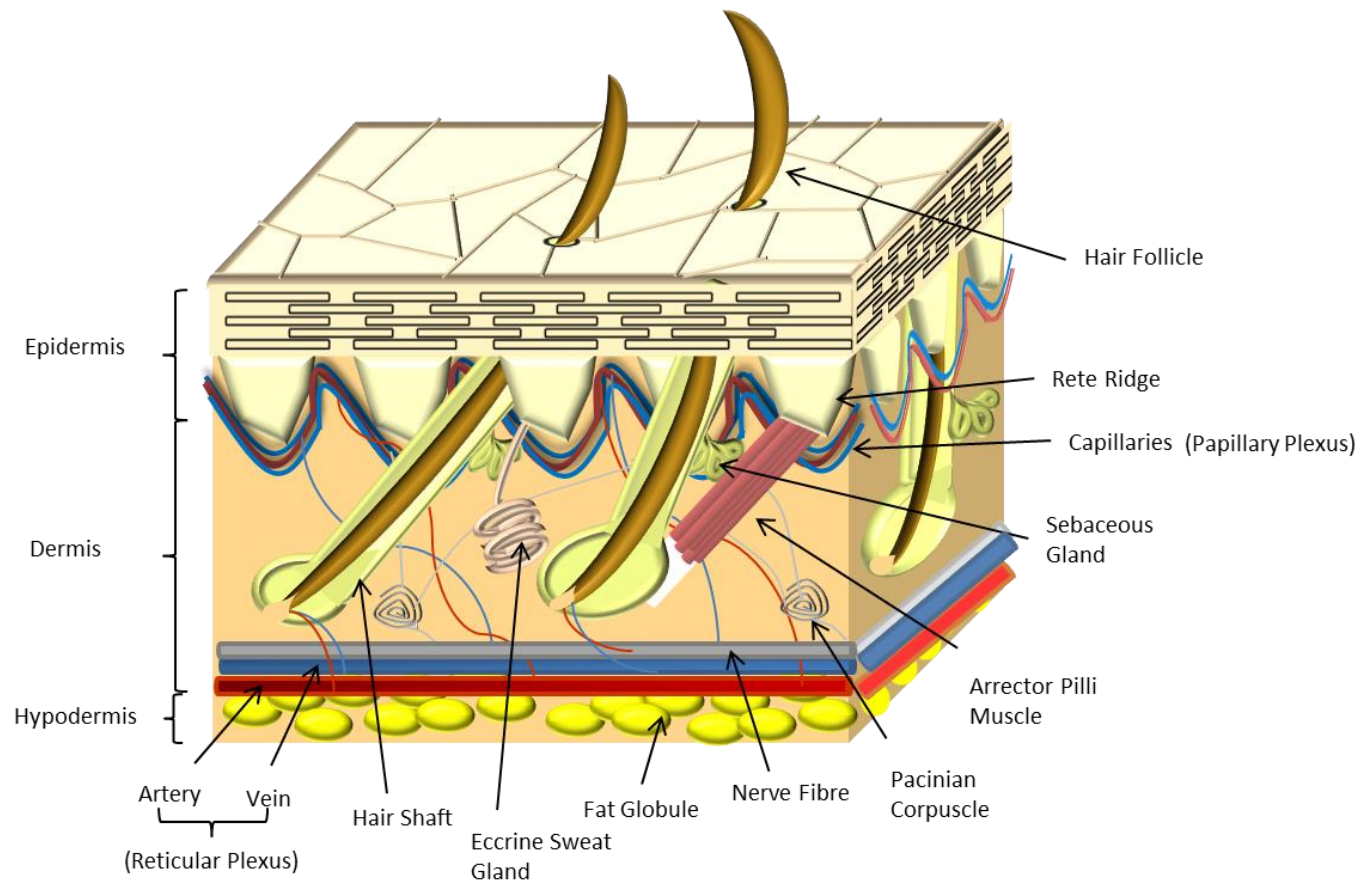


Figure 1.1: Skin Structure And Appendages. The outermost layer of the skin is the epidermis, this is followed by the dermis and lastly, the hypodermis. Appendages such as hair follicles, sebaceous glands and sweat glands exist in the integument. Beneath the downgrowths of epidermis (rete ridges) exists a network of capillaries in the dermis which are connected to arteries and veins that exist in the deeper part of the dermis. A network of nerve fibres also exist in the dermis (Viegas, 2014).

1.1.1 The Epidermis

The epidermis is responsible for limiting transcutaneous water loss, immune-surveillance, protection against solar radiation and temperature regulation. The protective element of the skin begins with the stratum corneum (horny layer), as well as the thin film that lies on top of this layer known as the acid mantle. The acid mantle is made up of sebum, corneocyte debris and remnant material from sweat (Chilcott, 2008). Sebum is the principal part of the acid mantle and is mainly composed of triglycerides, wax esters, and squalene in which the composition and secretion of these components differ by anatomical region (Kligman, 1963). Although hard to measure, the stratum corneum has been acknowledged as having an acidic pH, as low as 5.0 (Katz and Poulson, 1971), whereas the pH of the viable epidermis has been measured as around 7.4 (Sage *et al.*, 1993, Aly *et al.*, 1978).

The stratum corneum is on average 5-20 μm thick (Lademann, 1988). This layer is composed of approximately 15 cell layers, which can increase by five to ten-fold at pressure-bearing sites (Schaefer and Redelmeier, 1996). The stratum corneum is populated with terminally differentiated keratinocytes (corneocytes) in a lipid matrix. Corneocytes are tight bundles of intracellular keratin surrounded by a cornified cell envelope; covalently cross-linked proteins and covalently bound lipid (Eckert, 1989, Steinert, 1993, Reichert *et al.*, 1993). Corneocytes are flat, polyhedral-shaped anuclear cells which are approximately 40 μm in diameter and 0.5 μm in thickness (Marks and Barton, 1983). The intercellular region in the stratum corneum is composed of lipids that originate primarily from the exocytosis of lamellar bodies during the terminal differentiation of keratinocytes (Elias and Menon, 1991, Downing *et al.*, 1993, Grayson *et al.*, 1985, Lademann, 1986, Menon *et al.*, 1992a).

The upper layer of the stratum corneum is known as the stratum disjunctum and normally consists of approximately 3-5 cell layers and is actively undergoing desquamation (sloughing). The lower layer of the stratum corneum is known as the stratum compactum and consists of approximately 3 cell layers: it is thicker and more densely packed than the stratum disjunctum and more closely reflects the underlying viable epidermis (Hou *et al.*, 1991, Fartasch, 1995). The stratum compactum also has a higher density of corneodesmosomes than the stratum disjunctum (Mils *et al.*, 1992). The stratum disjunctum contains 15% by weight of associated water compared to the water associated with the stratum compactum at 30% by weight, both of which are less hydrated than the viable dermis (70% by weight) (Warner *et al.*, 1988, von Zglinicki *et al.*, 1993). Thus, a gradient of water exists through the skin, with deeper viable layers presenting with higher hydration levels. Desquamation of the stratum corneum must be continuous in order to maintain thickness and must be tightly regulated to prevent hyperkeratinosis or alternatively, ablation (Egelrud *et al.*, 1996, Wilkinson, 2008).

The stratum corneum is also responsible for the barrier properties of the skin (Scheuplein and Blank, 1971). The corneocytes and lipids are present in the stratum corneum as a distinct structure represented in a brick and mortar model (further described in Section 1.2.1). The corneocyte bricks are attached to adjacent cells through corneodesmosomes. The lipid mortar is a lamellar arrangement predominantly composed of ceramides, free fatty acids, triglycerides and cholesterol (Table 1.1). It has been acknowledged that there is a complex relationship between stratum corneum lipid composition and biophysical properties, which ultimately influences the behaviour of the overall lipid system (Netzlaff *et al.*, 2006).

Table 1.1. Stratum Corneum Lipids (Adapted from Wilkinson (2008))

Lipid Type	Abundance
Ceramides	40%
Free Cholesterol	27%
Cholesterol Esters	2-5%
Cholesterol Sulphate	3%
Free Fatty Acids (mainly 22-24°C saturates)	9%
Other Lipids (e.g. triglycerides)	11%

Lipid systems have the ability to exist in three different main phases; namely, the solid crystalline, crystalline (gel) and liquid crystalline phases (Schaefer and Redelmeier, 1996). Lipids are rigid in the crystalline phase, relatively rigid in the gel phase and present with rapid lateral mobility in the liquid crystalline phase. The liquid crystalline phase is found in all biological cell membranes (Schaefer and Redelmeier, 1996). Lipid phase transitions in model membranes can be initiated through a change in pressure, hydration, solvent, salt concentration, pH, cations, temperature and proteins (Schaefer and Redelmeier, 1996). In terms of dermal absorption, Potts and Franceour (1991) studied the biophysics of water loss through the skin and concluded that skin permeability was dependent upon conformational disorder in the lipid hydrocarbon chains, with enhanced penetration associated with a change to the liquid crystal phase.

The stratum corneum is subject to continuous renewal of cells as a result of apical migration of cells from the stratum basale every 2 weeks in the mature adult (Monash and Blank, 1958, Montagna, 1961, Egelrud *et al.*, 1996). Present underneath the stratum corneum are 10-20 layers of stratified epidermis, consisting of the keratinising epithelial cells responsible for the synthesis of the stratum corneum. The keratinisation process begins at the stratum basale layer, which is made up of cuboidal to columnar shaped cells attached by desmosomes to each other and to the basement membrane through hemidesmosomes. At this cell layer, two populations of basal cells exist, in which one group function as stem cells and the second as an anchor to the basement membrane (Monteiro-Riviere, 1996). During the keratinisation process, nuclei and organelles are broken down, lipids are expelled into the inter-corneocyte spaces, water content is decreased from 70% to 15% and cells are filled with keratin (Marks, 2004). Keratinocyte cells begin to flatten and

increase in diameter from 10-12 μm to 20-30 μm , with a concomitant (10-20 fold) increase in volume from the stratum basale layer to the stratum corneum (Teumer *et al.*, 1994).

During terminal differentiation, keratinocytes produce keratohyalin granules, cornified envelopes, lamellar bodies and desmosome plaques (Manabe and O'Guin, 1992, Wertz *et al.*, 1989, Schwarz *et al.*, 1990, Odland and Holbrook, 1987). Keratohyalin granules are dense, irregular amorphous deposits that contain profilaggrin, loricrin, cysteine-rich progein and keratins (Harding and Scott, 1983, Adams and Watts, 1993, Tezuka and Takahashi, 1987, Takahashi *et al.*, 1992). Profilaggrin facilitates the bundling of keratin which represents the majority of proteins in the corneocytes (Schaefer and Redelmeier, 1996). Loricrin and cystatin A are major compounds of the cornified envelope (Steven *et al.*, 1990). Desmosome plaques connect keratinocytes in the viable epidermis and are predominately present in the stratum spinosum. Lamellar bodies are present in keratinocytes of the upper stratum spinosum and stratum granulosum. These bodies contain lipid precursors of the intercellular lipid domains of the stratum corneum (Menon *et al.*, 1992b). In order for degradation of the corneodesmosomes to occur (as part of the sloughing process) serine, cysteine and aspartic proteases are excreted into the extracellular spaces in the stratum corneum (Milstone, 2004).

In addition to keratinocytes, the viable epidermis also contains (to a lesser extent) melanocytes (which produce the melanin pigment), Langerhans cells (responsible for antigen presentation and immune response) and Merkel cells which have a role in sensory perception (Jimbow *et al.*, 1993, Stingl *et al.*, 1993, Kim and Holbrook,

1995). Also present in the viable epidermis are terminal nerve fibres which provide a sensory function (pain, touch, heat, etc.) (Hillings *et al.*, 1995).

Keratinocytes in the stratum basale are anchored into a structure known as the basement membrane which is present in the dermal-epidermal junction (Paulsson, 1992, Yancey, 1995). The basement membrane is synthesised by the cells of the stratum basale and is made up of large macromolecules organised into a complex thin extracellular matrix (Monteiro-Riviere, 1996). The adhesion between the basal keratinocytes in this region provides continuous cellular signals which regulate cell proliferation and differentiation (Adams and Watts, 1993, Fuchs, 1993). The basement membrane consists of four components: the cell membrane of the basal epithelial cell, the lamina lucida (possibly an artefact of electron microscopy; Chan and Inoue (1994)), the lamina densa (an electron-dense area beneath the lamina lucida) and the subbasal lamina (containing anchoring fibrils, microfibril-type elements, and single collagen fibres) (Briggaman and Wheeler, 1975). The basement membrane has a variety of functions such as a role in maintaining epidermal-dermal adhesion and in restricting diffusion of large molecules between the epidermis and dermis (Monteiro-Riviere, 1996). The dermal-epidermal junction is a region which contains papillae that increases the surface area between the epidermis and dermis (Schaefer and Redelmeier, 1996). This area consists of downgrowths of epidermis which form 'rete' ridges in the skin, under which the superficial capillary plexus is located (Chilcott, 2008). This increase in surface area is responsible for facilitating diffusion of nutrients, growth factors and xenobiotics between the epidermis and dermis (Schaefer and Redelmeier, 1996).

1.1.2 The Dermis And Hypodermis

The dermis consists of a network of fibrous, filamentous and amorphous connective tissue that provides both tensile strength and elasticity of the skin as well as structural support for both the nerve and vascular networks (Schaefer and Redelmeier, 1996). The connective tissue in the dermis is primarily composed of collagenous fibres and elastic connective tissue. The collagenous fibres form a scaffold that is present throughout the dermis and the elastic tissue provides elasticity for shape retention of the skin (Schaefer and Redelmeier, 1996). The cell populations present in the dermal tissue include fibroblasts, endothelial cells and mast cells. In addition, if conditions such as inflammation or wound healing occur, macrophages, lymphocytes and leukocytes may infiltrate this layer (Schaefer and Redelmeier, 1996). The dermal layer also contains appendages such as hair follicles, sebaceous glands and sweat glands.

There also exists a vast vascular network in the dermis, which is involved in processes such as nutrition, heat exchange, repair, immune responses and thermal regulation (Schaefer and Redelmeier, 1996). The vascular network in the dermis can be divided into an upper, papillary plexus and a lower, reticular plexus (Figure 1.1). The system of capillaries reach the upper epidermis, in which the capillary loops line the papillae which is in contact with the epidermis (Schaefer and Redelmeier, 1996). Also present in the dermis is the lymphatic system, which functions to regulate pressure from interstitial fluid (Schaefer and Redelmeier, 1996).

The hypodermis functions to anchor the dermis to the underlying muscle and bone. This layer is comprised of connective and adipose tissue and has functions which include systemic metabolism and thermoregulation (Svesson, 2009).

1.1.3 Appendages

Several appendages exist in the integument, such as sweat glands, hair follicles and sebaceous glands.

The sweat glands consist of either eccrine glands (two-thirds of all glands) or apocrine glands (one-third of all glands), which secrete an isotonic solution in response to elevated skin temperatures and are the most numerous of all the appendages (Schaefer and Redelmeier, 1996). The glands consist of a coiled duct connected to the skin surface through a secretory tube and spiral channel (acrosyringium) which permeates the epidermis (Schaefer and Redelmeier, 1996).

Hair follicles are classified into either fine vellus hair, which extend less than 1 millimeter into the dermis or coarse terminal hair which extends more than 3 millimeters into the hypodermis (Schaefer and Redelmeier, 1996). Both arrector pilli muscles and sebaceous glands are associated with hair follicles. The hair bulb is present within a region of connective tissue, termed the follicular papilla, which brings the hair in close proximity to blood vessels (Schaefer and Redelmeier, 1996). The appendageal route has also been under investigation as a potential transdermal route for nanoparticle dermal penetration. It has been demonstrated that particles ranging in size from 1.5 to 750 μm can deposit in the follicular duct as well as penetrating into terminal scalp follicles and superficial penetration into vellus hair follicles (Rolland *et al.*, 1993, Toll *et al.*, 2004, Sumian *et al.*, 1999, Mordon *et al.*, 2003).

Sebaceous glands are found in all regions of the body, however, the density of the glands per follicle and activity of the glands vary according to site and age (Wester and Maibach, 1993, Blume *et al.*, 1991, Saint-Léger, 1994). This type of gland is

associated with hair follicles approximately 0.5 mm below the skin surface where the afferent ducts join (Schaefer and Redelmeier, 1996). The sebaceous glands consist of one or several lobes connected with a duct to the hair follicle. Sebaceous glandular activity is not present in infants and is reduced in the elderly (Schaefer and Redelmeier, 1996). The highest sebaceous gland activity occurs in the facial region and is absent in the palms of the hands and soles of the feet (Schaefer and Redelmeier, 1996). The sebaceous gland duct is not lined with stratum corneum and instead is surrounded by a single epidermal cell layer under which the dermis is present (Wilkinson, 2008). The sebaceous gland is a highly lipophilic environment due to the presence of sebum, whilst the dermis is a largely hydrophilic area due to the collagen and elastin gel matrix. Therefore, if a compound was able to partition from one to another, diffusion would immediately occur into the dermal tissue (Wilkinson, 2008).

1.2 Dermal Absorption Theory

The stratum corneum provides a good (but imperfect) barrier to the absorption of xenobiotics. The barrier has been acknowledged as the rate limiting step in the permeation and penetration of chemicals, initially identified through studies on the penetration of water and subsequent tape stripping of the stratum corneum (Blank, 1953, Monash and Blank, 1958). Interestingly, this role of the stratum corneum was first alluded to by Smith *et al.* (1919). The outermost layer of the epidermis has also been exploited as a route of entry for topically applied therapeutic drugs. Percutaneous penetration is a process based on passive diffusion as no known active transport mechanisms exist in the stratum corneum (Ng *et al.*, 1992, Hadgraft, 2001). Water is acknowledged as having a role as a skin penetration enhancer, as hydrated skin is generally more permeable than its non-hydrated counterpart (Roberts and

Walker, 1993). Water is capable of forming substantial interactions with amide linkages and protein side groups through acceptor and donor hydrogen bonds, and has almost no affinity for stratum corneum lipids besides transient hydrogen bonds with polar head groups in ceramides and phospholipids (Schaefer and Redelmeier, 1996). Due to protein-water binding, the stratum corneum has the capacity to absorb five to six times its original weight in strongly bound water (Scheuplein, 1966, Scheuplein and Morgan, 1967). When skin is occluded, the water lost naturally to the environment becomes trapped within the intercellular spaces of the stratum corneum causing an increase in stratum corneum hydration (Warner *et al.*, 2003). When occlusion of the skin occurred with human volunteers, it was seen that a higher water content was equivalent to an increase in permeability and penetration (Zhai and Maibach, 2002). The penetration enhancing effect of occlusion is complex and dependent on a number of other variables which also influence penetration (Bucks and Maibach, 1999).

1.2.1 Routes of Absorption

The stratum corneum has been described as a ‘brick and mortar’ model (Figure 1.2) due to the arrangement of corneocytes and lipids in this layer (Michaels *et al.*, 1975). Due to steric hindrance, molecules greater than 500 Da are thought to be potentially excluded from crossing the stratum corneum (Bos and Meinardi, 2000). If penetration was to occur, it would happen via three possible routes, namely the intercellular, transcellular and transfollicular routes (Figure 1.2).

The intercellular route is a tortuous pathway through the lipid lamellae around corneocytes, in comparison to the relatively lateral transcellular route through the corneocyte cells and the lipid lamellae. However, it should be noted that permeation

through multiple layers of corneocytes and lipids is both thermodynamically and kinetically un-favourable (Flynn, 1990).

The third potential route (transfollicular) involves the passage of chemicals through hair follicles and sweat glands, a route thought to circumvent the stratum corneum. The entrance to the hair follicle could serve to trap particles and possibly prevent the uniform distribution of formulations over the skin surface (Schaefer and Redelmeier, 1996). However, this route is still lined with corneocytes as well as sebum and metabolising enzymes, thereby creating another barrier to absorption (Chilcott, 2008).

If a molecule were to take the intercellular route through the stratum corneum, then the stacking of the corneocytes would be important, as this directly influences the path length for diffusion (Christophers *et al.*, 1974). Both vertical and lateral distances between the corneocytes have been reported as 75 nm (Elias and Friend, 1975). The tortuous path around corneocytes is thought to be a structural aspect of the human stratum corneum which could partly account for the barrier properties of the skin (Potts and Francoeur, 1991).

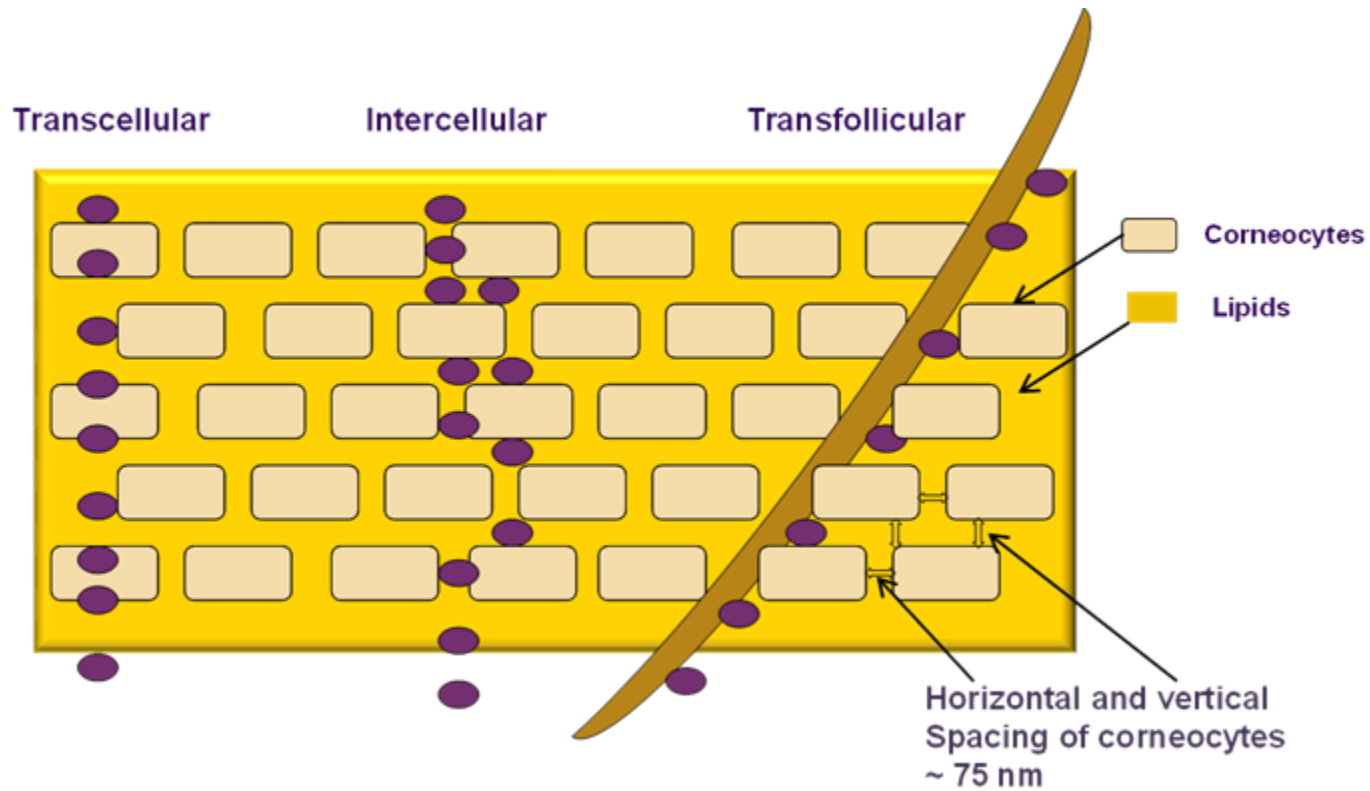


Figure 1.2: Brick And Mortar Model Of Human Stratum Corneum. The transcellular route is a route through the corneocyte cells and lipid bilayer. The intercellular route is through the lipid bilayer alone. The transfollicular route is a pathway down through the hair follicles. The distances between corneocytes in the stratum corneum (horizontal and vertical) have been acknowledged as approximately 75 nm in diameter (Viegas, 2014).

1.2.2 Absorption Kinetics

Percutaneous penetration is governed by the basic laws of thermodynamics (Higuchi, 1960). For example, a thermodynamic gradient may exist between a substance within a vehicle and the stratum corneum, in which case a lipophilic molecule present in an aqueous vehicle would preferentially partition into a lipid rich environment of the stratum corneum. The thermodynamic activity of a molecule in a vehicle is more important than its absolute concentration (Lippold and Schneemann, 1984, Hori *et al.*, 1990, Moser *et al.*, 2001).

In order to experimentally determine the parameters of dermal absorption, two main skin exposure scenarios are used (Figure 1.3). ‘Infinite dose’ is a condition in which a substance is applied to the skin surface at a concentration which does not appreciably deplete over time. The infinite dose regime results in a steady-state penetration where the amount of substance penetrating the skin becomes constant over time. The time taken to reach steady-state is known as the ‘lag time’ (Pugh and Chilcott, 2008). Penetration rate (flux) is determined from the graph at steady-state (J_{ss}). Kinetic parameters such as steady-state flux (J_{ss}), permeability coefficient (K_p), diffusion coefficient (D) and lag time (τ) can be determined using the infinite dose situation (Equation 1.1-1.5). However, the infinite dose is unrealistic as it does not generally reflect a ‘normal’ dermal exposure. Thus, finite dose is a more appropriate situation, in which a substance and its vehicle applied to the skin surface deplete steadily over time due to absorption into deeper layers of the skin (Pugh and Chilcott, 2008). Using finite dosing conditions, the pseudo steady-state can be used to determine the maximum rate of penetration (J_{Max}) using the linear portion of the penetration curve (Figure 1.3).

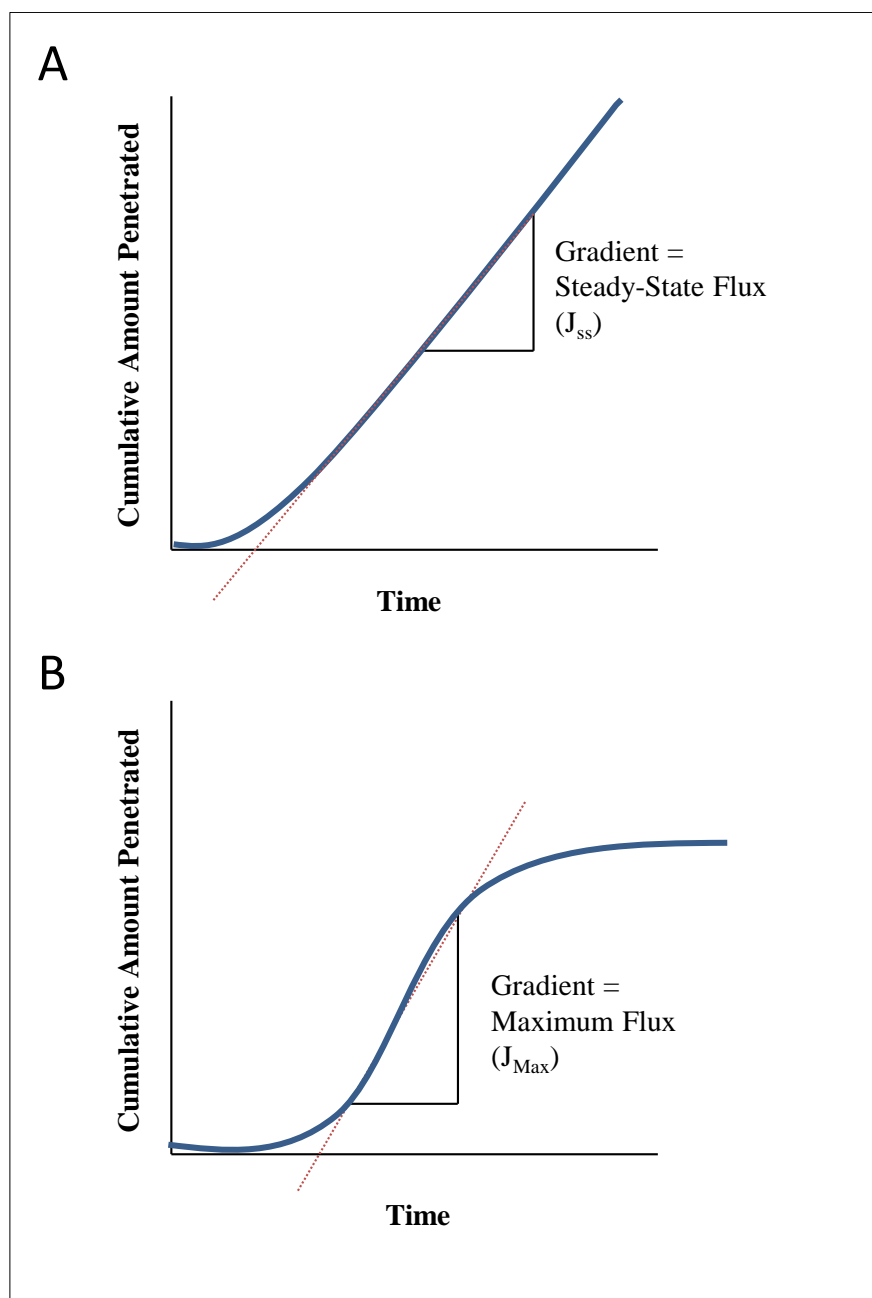


Figure 1.3: Infinite (A) And Finite (B) Dose Regimes. The infinite dose (A) results in ‘steady-state’ penetration (J_{ss}) in which the time taken to reach steady state is ‘lag time’. The finite dose (B) results in a pseudo steady state which can be used to determine maximum flux (J_{Max}) using the linear part of the curve.

1.2.3 Laws Of Diffusion

A common definition for diffusion is, “the process by which matter is transported from part of a system to another as a result of random molecular motions” (Crank, 1975).

One of the earliest modellers of diffusion was Fourier, who proposed that the heat energy current density or flux (J) was proportional to the change in temperature with distance travelled, and in which the relationship is linear with respect to the constant (k) (Fourier, 1878). Adolf Fick then extrapolated the relationship between conduction of heat (as found by Fourier) to diffusion of molecules in order to describe chemical diffusion.

Fick’s first law can be applied to the diffusion of molecules across a membrane at steady state and can be represented by Equation 1.1:

Equation 1.1

$$J_{SS} = K_p \Delta C$$

In which case, the steady state flux (J_{ss}) for a specific molecule potentially penetrating the skin (amount per unit area, per hour e.g. $\mu\text{g cm}^{-2} \text{hr}^{-1}$) is directly related to the permeability coefficient (K_p) and the difference in concentration (ΔC) across the skin (Grandjean 1990). Using infinite dose conditions, it is assumed that ΔC remains constant and that infinite sink conditions maintain the concentration at zero leading to ΔC representing the concentration of a substance in the vehicle/solvent applied to the skin surface.

1.2.4 Partitioning And Diffusivity

Skin absorption can essentially be divided into three distinct stages (Pugh and Chilcott, 2008). The first stage is partitioning of the penetrant from the vehicle into the stratum corneum, a process that depends upon the thermodynamic activity of the penetrant in the vehicle versus the stratum corneum. The second stage is the diffusion of the penetrant through the stratum corneum, a process driven by a thermodynamic gradient. The third stage involves the partitioning of the penetrant from the stratum corneum into the deeper tissue (Pugh and Chilcott, 2008).

After topical application of a compound, an equilibrium will gradually form between the concentration of penetrant in the vehicle (C_v) and concentration in the stratum corneum (C_{sc}). These two concentrations are related by the partition coefficient/membrane partition coefficient (K_{sc}) according to Equation 1.2 (Pugh and Chilcott, 2008):

Equation 1.2

$$K_{sc} = \frac{C_{sc}}{C_v}$$

The amount of penetrant in the stratum corneum affects the thermodynamic gradient through the stratum corneum and is related to the permeability coefficient (K_p) as follows in Equation 1.3:

Equation 1.3

$$K_p = \frac{K_{sc}D}{x}$$

Where D -diffusion coefficient; x - thickness of the stratum corneum.

When substituting the previous equation into Fick's first law of diffusion, the following equation is created to show the relationship between the main factors affecting skin absorption in Equation 1.4:

Equation 1.4

$$J_{ss} = \frac{K_{sc}C_vD}{x}$$

Where D (the diffusion coefficient) is a measure of the diffusivity (or mobility) of a compound in the stratum corneum and is dependent on the size, shape and bonding capacity of the compound with components of the stratum corneum. The relationship of the diffusion coefficient to lag time (τ) and stratum corneum thickness (x) is represented as follows in Equation 1.5 (Pugh and Chilcott, 2008):

Equation 1.5

$$\tau = \frac{x^2}{6D}$$

1.3 Factors Affecting Dermal Absorption

There are many factors thought to affect the percutaneous absorption of chemicals through the skin, both biological factors and physicochemical properties of the penetrant will be discussed.

1.3.1 Biological Factors

1.3.1.1 Anatomical Site

Skin surface morphology is well documented as differing between anatomical sites (Maibach *et al.*, 1971). These regional differences in the skin include epidermal

thickness, density of hair follicles and sweat and sebaceous ducts (Chilcott, 2008). It is not known as to why differences in skin permeability are seen for different anatomical sites. Specifically, the palm and forearm displayed similar permeability (Marzulli, 1962). When compared to forearm skin, the abdomen and dorsum of the hand had twice the permeability (Maibach *et al.*, 1971). Human back skin showed a higher penetration rate of ^{14}C -hydrocortisone compared to that of the forearm (Feldmann and Maibach, 1967). In the domestic pig, anatomical variability was seen as a greater increase in the absorption of parathion in the dorsum compared to the abdomen (Qiao *et al.*, 1994). When comparing methyl nicotinate application sites on the forehead, forearm and palm of human skin, it was found that penetration was greatest through the forehead, intermediate through the forearm and the least through the palm (Tur *et al.*, 1983).

Studies have demonstrated that the thickness and number of cell layers of the human stratum corneum are variable for each anatomical region (Holbrook and Odland, 1974). It should be noted that at present, no conclusive evidence exists to link skin barrier thickness to dermal absorption, moreso a lack of correlation has been found between skin barrier thickness between anatomical sites and percutaneous penetration (Chilcott, 2008, Schaefer and Redelmeier, 1996). In addition to thickness, an increase in corneocyte cell layers and corneocyte surface area has been documented as increasing the diffusional pathlength of dermal absorption of a penetrant (Rougier *et al.*, 1988). However, no concrete evidence exists to prove that corneocyte size and/or thickness of the stratum corneum contributes to regional differences in permeation.

A correlation was thought to be found between methyl nicotinate absorption and appendageal density (Tur *et al.*, 1983). However, appendageal density is known to increase the skin surface area available for absorption, with denser follicular areas presenting with increases in skin absorption.

Intracellular lipid content has been documented as differing between anatomical locations (Lampe *et al.*, 1983). However, it has not been conclusively established that alterations in lipid content of the stratum corneum are responsible for differences in anatomical variations in dermal absorption.

Therefore, anatomical variation is likely to affect dermal absorption through a variety of mechanisms that include density of appendages, corneocyte surface area, intercellular lipid content and even blood flow (Schaefer and Redelmeier, 1996).

1.3.1.2 Age

Age is also thought to be another factor in affecting dermal absorption of compounds. In general, morphological organisation and thickness of the human stratum corneum does not change with age (Lavker, 1979, Christophers and Kligman, 1965). However, age and gender-related differences in fatty acid composition of the stratum corneum lipids were found to be factors in influencing skin permeability (Nazzaro-Porro *et al.*, 1979). Lipid content and cohesion of corneocytes in the stratum corneum has been shown to decrease with age and microscopic changes such as flattening of the epidermal-dermal junction, retraction of epidermal downgrowths, thinness, reduction in the output of sweat glands and a more heterogenous basal cell population were seen (Lavker, 1979, Lavker *et al.*, 1986, Lavker *et al.*, 1987, Hull and Warfel, 1983, Gilchrest, 1984, Kligman *et al.*, 1985a, Kligman and Balin, 1989, Rapaport, 1973, Leveque *et al.*, 1984). However,

Bronaugh *et al.* (1986) determined that there was no correlation between water permeability and time of harvest, adult age of skin, sex or race of skin samples, indicating that age-related differences in skin morphology do not necessarily affect skin permeability.

Ageing of skin involves a multitude of factors, including many biological factors (e.g. lipid composition and blood flow) that can produce compound-dependent effects and affect percutaneous penetration (Monteiro-Riviere, 1996). However, there does not appear to be any conclusive evidence that ageing affects skin permeability in adults.

1.3.1.3 Species Variation

Excised human skin is widely considered the ‘gold standard’ for *in vitro* percutaneous absorption measurements (OECD, 2004). Different animal species have been put forward as alternatives to human skin, however, it has widely been acknowledged that animal skin is more permeable than human skin (Vecchia and Bunge, 2006, Walker *et al.*, 1986). The thickness of the stratum corneum has been considered as a factor that contributes to species variation (Bronaugh *et al.*, 1982, Scheuplein and Bronaugh, 1983). An additional factor attributing to the difference in permeation between species is thought to be the variation in skin surface lipids (Sato *et al.*, 1991).

The skin of the monkey and pig have been found to be better models in terms of predictive permeability than that of rodent skin (Wester and Maibach, 1984, Meyer *et al.*, 1978, Monteiro-Riviere and Riviere, 1996, Reifenrath and Spencer, 1985). (Elias and Friend, 1975). Corneocytes are stacked and not-offset in murine stratum corneum, potentially allowing for a more direct route of penetration through the

barrier layer of skin which may explain the unusually permeable skins of mice compared to other species (Bergstresser and Chapman, 1980). Domestic pig skin is both morphologically and functionally closest to human skin than other animal models (Meyer *et al.*, 1978, Monteiro-Riviere and Riviere, 1996, Calabrese, 1984) and can be readily obtained. Porcine skin has been acknowledged as a good animal model for percutaneous penetration based on the similarities to human skin, viz., a sparse hair coat, well-differentiated epidermal tissue, a dermis containing a well-differentiated papillary body, high elastic-tissue content as well as similarities in vasculature (Monteiro-Riviere and Riviere, 1996, Simon and Maibach, 2000, Forbes, 1969, Montagna and Yun, 1964). Moreover, the epidermis of porcine skin is known to be similar to human epidermal tissue in terms of epidermal turnover kinetics and characterisation of keratinous proteins (Weinstein, 1966). Squalene, a wax ester, is the major lipid in human skin, whilst most animal species have substantial amounts of diester waxes: this difference has been suggested as a major factor in species variation in skin permeability (Nicolaidis *et al.*, 1968).

Follicular density also differs between species, with porcine dorsum and human abdominal skin presenting with approximately 11 ± 1 hair follicles per cm^2 in comparison to the back of rat skin (289 ± 21), murine skin (658 ± 38) and hairless murine (75 ± 6 follicles per cm^2) (Bronaugh *et al.*, 1982). It has been debated if anatomical areas with a higher density of hair follicles allow for a greater penetration of chemicals than less hirsute areas. However, it should be noted that the hair follicles are mainly lined with stratum corneum and the increase in surface area could have attributed to the higher rates of penetration in dense follicular areas (Monteiro-Riviere, 1996) rather than trans-follicular penetration. Scalp skin for example, has a 20 fold increase in surface area of the stratum corneum and consequently increases

the area available for skin absorption (Chilcott, 2008). Moreover, it has been previously demonstrated that hair follicles are not a major route for xenobiotics with the exception of metal ions (Scheuplein, 1976).

1.3.1.4 Skin Metabolism

The extent to which a compound is metabolised after percutaneous penetration can influence the extent of the total dose absorbed, as well as the toxic effect from any accompanying metabolites. Kao *et al.* (1985) found that the *in vitro* penetration of topically applied testosterone and benzo[a]pyrene was greatly affected by metabolic viability in a number of species. The parent compounds and full spectrum of metabolites from testosterone and benzo[a]pyrene were found in the viable skin preparations whereas only the parent compounds were found in previously frozen skin samples (Kao *et al.*, 1985). The metabolism of the compounds was seen to differ with species, most likely due to the different expression of enzymes present in the epidermis of each animal skin (Kao *et al.*, 1985). Overall, these results suggest that diffusion of chemical compounds into the epidermis may be influenced by metabolic activity and provide an additional mechanism for species differences.

1.3.1.5 Skin Preparation And Storage Conditions

If additional dermal tissue is present in the skin sample this could affect the percutaneous penetration of a compound, based upon associated physicochemical properties. Hydrophilic compounds were found to exhibit only small differences in absorption through a membrane containing extra hydrophilic dermis (Bronaugh, 1996). Hydrophobic compounds on the other hand, exhibited with a slower penetration than the *in vivo* scenario (Bronaugh, 1996). Skin thickness was not found to influence the *in vitro* penetration of caffeine and benzoic acid, however

testosterone showed a higher maximum absorption rate when using dermatomed skin membrane and a higher amount in the skin after 24 hours (van de Sandt *et al.*, 2004). When the epidermis of the skin was removed, compounds with lower log P values were absorbed more rapidly than compounds with a higher log P (Hawkins and Reifenrath, 1986).

Full thickness skin should be chosen when animal skin is very thin, such as in the mouse and rabbit or when studying dermal or hypodermal delivery routes (Pendlington, 2008). A dermatome has been acknowledged as the most efficient way to prepare membranes for *in vitro* percutaneous absorption testing due to the ability to use this instrument with both hairy and hairless skin whilst retaining barrier integrity (Bronaugh, 1996). Human epidermal membranes can also be prepared from full-thickness skin by submerging the skin into 60°C water, after which the epidermis will separate from the underlying tissue (Bronaugh *et al.*, 1981, Scheuplein, 1965). Epidermal membranes are thought to more relevant than full-thickness or split thickness skin for *in vitro* transdermal testing, as there is no dermal tissue in this preparation to provide an additional barrier to penetration. Epidermal membranes can be prepared from human skin and weanling porcine ear skin. However, haired skin sections cannot be used in epidermal membrane preparation as hair shafts will remain in the dermis which will result in holes as the epidermis is separated. Skin barrier measurements should be performed on epidermal membranes in order to determine if the process of separation led to damage of the epidermis.

Storage conditions of the skin may potentially affect skin permeability (Reifenrath and Kemppainen, 1991). Several researchers have experimentally determined that skin could be stored frozen up to one year without a significant change in water

permeability (Bronaugh *et al.*, 1986, Franz, 1975, Harrison *et al.*, 1984). However, Hawkins and Reifenrath (1984) found that pig skin stored frozen for more than 1 week become more permeable to *N, N*-diethyl-*m*-toluamide. Hawkins and Reifenrath (1986) further measured radiolabelled benzoic acid, caffeine, *N, N*-diethyl-*m*-toluamide, fluocinolone acetonide and lindate in both fresh and previously frozen porcine skin and found no significant differences in permeability after freezing skin for eight hours. It has been recommended that skin integrity should be evaluated following frozen storage (OECD, 2004).

1.3.2 Mechanical Properties Of The Skin

The effect of physical or mechanical properties of the skin on dermal absorption has been largely overlooked, with very few studies directly comparing the impact of both. The keratin in the skin forms a filamentous network allowing for cohesion, flexibility and elastic recovery in the stratum corneum (Young and Heath, 2000, Monteiro-Riviere, 2006). The stratum corneum maintains a high level of mechanical resistance due to the corneocyte cell structure (Egelrud *et al.*, 1996).

The slope of Young's modulus (stress-strain curve) has been used to determine a true elasticity value of individual corneocytes (Lévêque *et al.*, 1988). Under physiological conditions, the stretching/deformation of the stratum corneum is not due to elongation of corneocytes but to a conformational change provided by multiple intersecting furrows (Lévêque *et al.*, 1988). Transepidermal water loss is influenced by skin stretching, due to the decrease in surface area facilitated by stretching, leading to lower rates of TEWL than un-stretched skin (Pinnagoda *et al.*, 1990).

It is thought that energy provided by flexing could provide the additional force required for particle translocation from the skin surface. An *in vitro* skin flexing

device was first reported by Tinkle *et al.* (2003) and further used experimentally in studies reported by Rouse *et al.* (2007) and Zhang and Monteiro-Riviere (2008). The flexing apparatus consisted of two rectangular platforms attached to a 3-inch hinge, in which one platform was attached to a rotational motor and the other to a drawer slider. As the motor performed a rotation, the skin along the centre of the hinge underwent both vertical and horizontal movement in which both tensile and compressive forces were applied (Rouse *et al.*, 2007). Normal physiological movement (i.e. flexing or stretching of skin) is thought to influence the percutaneous penetration of a range of ultra-fine particles (see Section 1.5.2.3). When using the Rouse *et al.* flexing device, particles were seen to penetrate into the viable epidermis and dermis. However these studies did not measure skin barrier integrity, and applied the particles after flexing, so it cannot be determined if the particles penetrated through an intact or damaged skin barrier layer and/or whether this was a direct result of skin flexing.

1.3.2.1 Skin Damage Models

Chemical Damage (Sodium Lauryl Sulphate)

Sodium lauryl sulphate (SLS) is a small (288 Da) amphiphilic and anionic surfactant present in many consumer products due to its emulsifying and detergent properties (Effendy and Maibach, 1996). Sodium lauryl sulphate has been found to penetrate skin and interact with both lipid and protein, causing a disruption in barrier function as well as an increase in TEWL (Scheuplein and Ross, 1970, Elias, 1983). Detergents are known to deplete certain lipids from the intercellular spaces of the skin barrier layer (Imokawa *et al.*, 1989). However, *in vitro* studies have discovered that after low concentrations of SLS exposure, the stratum corneum maintained a regular lamellar lipid arrangement (Fartasch, 1995, Fartasch, 1997). This is in accordance

with biochemical studies which found experimentally induced scaly skin had the same amount of ceramides as healthy control skin (Froebe *et al.*, 1990). A leading theory behind the basis of SLS-induced damage lies in the hyperhydration of the stratum corneum layer leading to eventual disorganisation of the lipid bilayers (Lévêque *et al.*, 1993). Previous studies have shown when SLS is used at high volume, but identical concentration, a more intense skin reaction was seen (Frosch and Kligman, 1979). Surface area dose is also important for SLS-induced reactions, with smaller test areas found to elicit a limited irritant response in comparison to larger areas (Frosch and Kligman, 1979).

Physical Damage

Mechanical damage of the skin can provoke irritant dermatitis through physical processes such as friction, causing hyperkeratosis, erythema, scaling and vesicle formation (Morris-Jones *et al.*, 2002, McMullen and Gawkroeder, 2006). *In vitro* abrasion of the epidermis alone is known to cause a two-fold increase in penetration in both human and rat skin (Bronaugh and Stewart, 1985).

Tape stripping has been used in the past for enhancement of percutaneous penetration and as a model for studying diseased and irritated skin (Moon *et al.*, 1990, Benfledt and Serup, 1999). Tape stripping is the sequential removal of superficial stratum corneum by repeat topical application of adhesive tape and involves the determination of the amount of compound penetrated in the different layers of the stratum corneum (Dupuis *et al.*, 1984, Rougier *et al.*, 1986). However, this particular model of skin damage produces a large variability due to the practical difficulty associated with removing single, uniform layers of keratinocytes (Martin *et al.*, 1996, van der Molen and Riviere, 2005). The number of cells removed may

not be proportional to the number of tape strips due to factors such as force of strip removal, skin hydration, anatomical site and inter-individual variations in technique (Marttin *et al.*, 1996).

The change in percutaneous absorption through damaged skin must be characterised, as topical preparations are occasionally applied to a compromised barrier layer. Bronaugh and Stewart (1985) investigated the effect of damage (abrasion) on percutaneous penetration through human and rat skin. It was found that of all chemicals investigated, the increase in absorption through damaged skin was related to the initial extent to which the compounds were absorbed by the skin, with poorly absorbed chemicals showing the greatest increase in penetration.

1.3.3 Physicochemical Properties Of The Penetrant

There are a wide range of physicochemical properties that may affect dermal absorption of chemicals, with the primary factors generally considered to be molecular weight, volatility, lipophilicity, charge and hydrogen bonding (Brain and Chilcott, 2008).

1.3.3.1 Molecular Weight

Transdermal penetration of molecules with a molecular weight greater than 500 Daltons is highly unlikely due to physical constraints in the stratum corneum (Bos and Meinardi, 2000). This is based upon the fact that the molecular weight of contact allergens, pharmaceutical agents used in topical dermatotherapy and topical drugs in drug delivery systems, are consistently less than 500 Daltons. However, passive and active methods have been developed to enhance percutaneous penetration, such as hydration of the stratum corneum, ultrasound, iontophoresis and skin abrasion (Barry

and Williams, 1995, Mitragotri *et al.*, 1995, Bhatia and Singh, 1998, Brown *et al.*, 2008).

1.3.3.2 Volatility

Volatile chemical compounds will affect dermal absorption and cumulative amount penetrated. This is due to the fact that the amount of chemical present on the skin surface will deplete in proportion to the volatility of the compound (Chilcott, 2012). This is an effect which may be exacerbated when using non-occluded exposure. Extremely volatile chemicals may not have sufficient contact time with the skin surface in order to partition into the skin (Gilpin *et al.*, 2009). An example of a highly volatile chemical would be the nerve agent sarin (GB), in which higher temperatures reduced the amount of liquid chemical in contact with the skin and therefore reduced the dermal penetration hazard (Chilcott, 2012). This is in direct contrast to VX (a non-volatile chemical warfare agent) which may remain present at relatively high temperatures and will therefore continue to be a dermal penetration hazard (Chilcott, 2012).

1.3.3.3 Lipophilicity

The inter-corneocyte lipid matrix is primarily composed of ceramides, free fatty acids and cholesterol (Table 1.1), rendering it a predominantly lipophilic environment and thus a factor influencing the percutaneous absorption of molecules. To determine solubility, the partitioning of a substance is measured between two immiscible liquids (e.g. octanol and water) at equilibrium. Generally, an octanol-water partition coefficient ($\log P$) between 1 and 3 is thought to be optimal for skin absorption (Brain and Chilcott, 2008). Although the stratum corneum is highly lipophilic, the underlying dermis is a largely hydrophilic area. Therefore, in order for a substance to successfully traverse the epidermis to the viable dermis and/or site of

action, it must not be highly lipophilic or hydrophilic, or there is a risk it will get trapped or excluded from either layer (Brain and Chilcott, 2008). Pro-drugs have been used as a strategy for targeting of compounds to the viable skin tissue (Anderson, 1993, Higuchi and Yu, 1987). Briefly, compounds are modified in order to enhance percutaneous absorption into the stratum corneum. The modification involves the synthesis of a lipophilic precursor drug which, on entry to the viable epidermis, is metabolised to the active drug by esterases. Esterification of drugs is employed as a modification due to the relatively high activity of esterases present in the viable epidermis, after which, the compounds are expected to clear the target site as based upon pharmacokinetics (Schaefer and Redelmeier, 1996, Kao and Carver, 1990).

1.3.3.4 Charge

In addition to the hydrophobic lipid domains, the stratum corneum also provides protection against the absorption of ions due to proteins present at the epidermal surface conferring both types of charge. However, more negative groups are present in the stratum corneum therefore aiding the absorption of cations over anions (Brain and Chilcott, 2008). For ions and non-electrolyte penetrants with many polar groups that are capable of hydrogen bonding with hydrated keratin, shunt diffusion (i.e. hair follicles) may be the predominant pathway (Scheuplein, 1976). This is due to relatively slow penetration of these compounds through keratin, attributing almost all penetration to the transfollicular route (Scheuplein, 1976).

1.3.3.5 Hydrogen Bonding

Hydrogen-bonding groups exist in the stratum corneum, allowing for transient hydrogen bonds to form with incoming penetrants. The influence of hydrogen

bonding on the rate of absorption depends upon the strength and number of bonds involved. Contemporary models of dermal absorption include a consideration of both acceptor and donor hydrogen bonding groups, in order to improve the predictive accuracy of percutaneous penetration (Moss *et al.*, 2014).

1.4 Dermal Absorption: Measurement And Techniques

Measuring the dermal absorption of a particular penetrant is important, as the amount of compound penetrated could be sufficient to produce a toxic effect and thus may present a greater risk to human health. Chemicals that are too hazardous to test on human volunteers can be assessed for dermal absorption using an *in vitro* diffusion cell system.

1.4.1 *In Vitro* Diffusion Cell Studies

1.4.1.1 *Skin*

The membrane chosen for *in vitro* testing should simulate the skin barrier layer as closely as possible, as well as model the condition being simulated (Bronaugh, 1996). The 'skin barrier layer' refers to the thickness of the skin which a compound must diffuse through *in vivo* before absorption by capillaries in the upper dermis (papillary plexus) and removed by the systemic circulation (Bronaugh, 1996). The distance to the papillary plexus varies with skin type, being approximately 100 μm for human skin (Bronaugh, 1995a). Considerations for skin type as well as skin preparation and storage methods have been previously discussed in detail in Section 1.3.1.5.

1.4.1.2 Receptor Fluid

The choice of receptor fluid is dependent on the compound under study. For a hydrophilic compound, a physiological buffer (e.g. normal saline or isotonic buffer) may suffice (Bronaugh, 1996). The selection of receptor fluids for more lipophilic compounds is more complicated as these molecules will diffuse into the stratum corneum readily but may not partition from the skin into the receptor fluid. Thus, it is important to ensure that the penetrant has sufficient solubility in the receptor fluid and that the receptor fluid of choice does not alter skin barrier function (as chemicals that solubilise hydrophobic compounds could potentially remove lipids from the skin) (Bronaugh, 1996). This consideration further emphasises the need to perform skin integrity analysis prior to performing dermal absorption studies. Partitioning of a penetrant from the skin into the receptor fluid and mixing of the receptor chamber fluid are known to influence percutaneous absorption, especially for highly lipophilic penetrants (Crutcher and Maibach, 1969). The use of 50% aqueous ethanol as a receptor fluid has been shown to provide a good correlation between *in vitro* and *in vivo* absorption data when using lipophilic penetrants (Scott and Ramsey, 1987). Alternatively, aqueous based fluid can be mixed with excipients such as polyethylene glycol 20 oleyl ether (Volpo 20) and serum albumin to improve penetrant solubility (Schaefer and Redelmeier, 1996).

1.4.1.3 In Vitro Diffusion Cell Systems

Two types of diffusion cell exist to measure *in vitro* percutaneous penetration, static and flow-through cells (Figure 1.4). Recent designs of static diffusion cells have been based upon publications by T.J. Franz in the mid-1970s (Franz, 1975, Franz, 1978) and flow-through cells from R.L. Bronaugh (Bronaugh, 1995a, Bronaugh, 1995b). However, it should be noted that versions of both static and flow-through

diffusion cells have been used in percutaneous absorption studies since at least the 1940s (Pendlington, 2008).

Static cells consist of several parts; the (upper) donor chamber, (lower) receptor chamber, clamp, sampling arm, heated jacket (optional) and skin tissue (Figure 1.4- A). The skin (or relevant tissue under study) is securely clamped between the donor and receptor chambers. The donor area of the skin is then dosed with the substance under study and the amount that has permeated through the skin can then be measured in the receptor chamber via the sampling arm.

The receptor chamber fluid is mixed thoroughly with magnetic stir bars and either placed in a water bath or incorporates a heated jacket to maintain the temperature of the skin at $32^{\circ}\text{C} \pm 1^{\circ}\text{C}$.

In contrast, flow-through diffusion cells (Figure 1.4- B) require a peristaltic pump to continuously deliver fresh receptor chamber fluid to each cell. The accuracy of the flow rate through the receptor chamber is important, as it is known to significantly influence skin penetration (Crutcher and Maibach, 1969). Flow-through diffusion cells are more practical for longer collection periods than the static cell, due to the use of automated samplers. The static cell allows for accumulation and quantification of slow penetrating compounds in the receptor fluid, whereas the samples may be too dilute for analysis using the flow-through diffusion cells (Pendlington, 2008). The van de Sandt *et al.* study (2004) determined that there were no differences found in the penetration of all three model compounds (benzoic acid, caffeine and testosterone) between different diffusion cell types. Whilst both types of cell provide equivalent results, the constant replacement of receptor fluid makes the flow-through diffusion cell more suitable for metabolic analysis, as the nutrients in the fluid do not

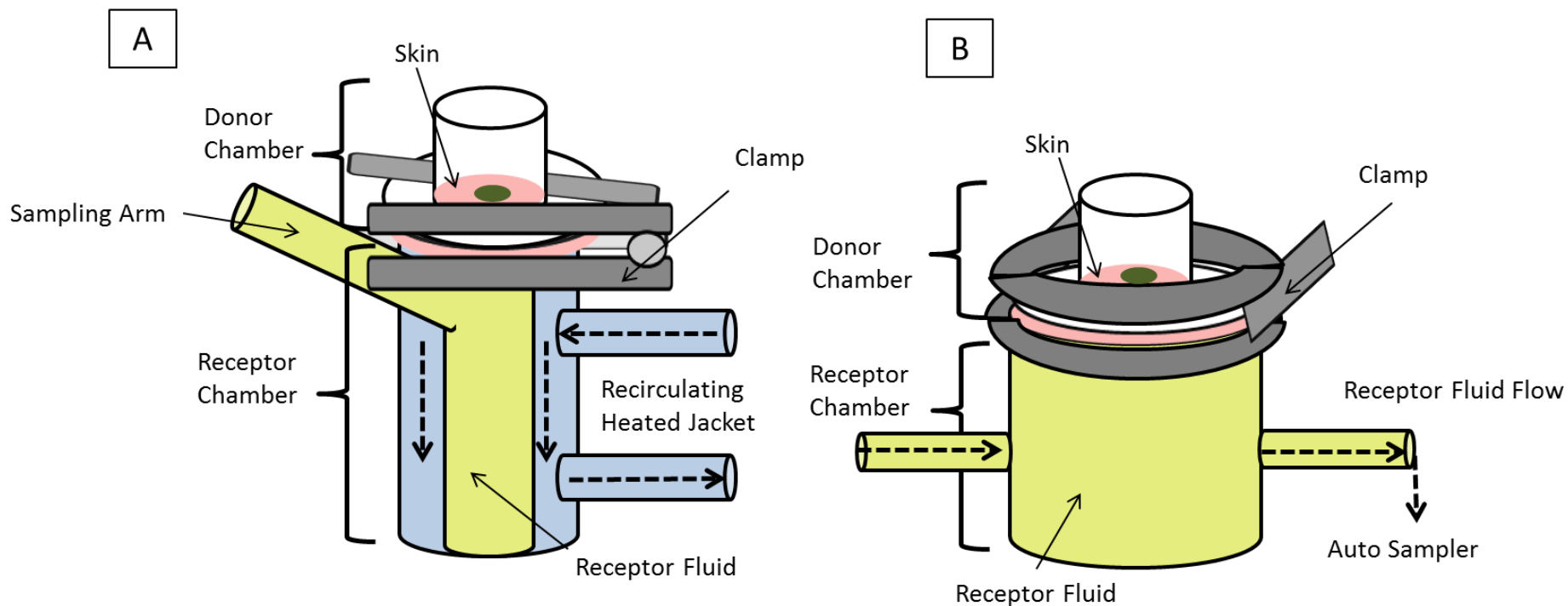


Figure 1.4: Static (A) And Flow-Through (B) Diffusion Cell Systems. Used for *in vitro* dermal absorption studies and consist of a donor chamber (where penetrant is applied) and a receptor chamber (where absorbed penetrant is collected). The tissue (e.g. skin) is clamped between the donor and receptor chamber. The sampling arm is used to collect aliquots of the receptor fluid which contains thoroughly mixed (inserted stir bars) substance that has penetrated through the skin. In the static cell, a heated jacket ensures that the skin is maintained at a temperature of $32^{\circ}\text{C} \pm 1^{\circ}\text{C}$ through connection to a heated re-circulating pump. In the flow-through cell, receptor fluid is pumped through each cell by a peristaltic pump which controls flow rate and the sampling arm allows for automated fraction collection (Viegas, 2014).

deplete over time and the biochemical viability of the skin can be maintained for longer periods (Bronaugh, 1996, Clowes *et al.*, 1994).

The OECD 428 method provides guidelines to measure the diffusion of chemicals onto and through the skin using either static or flow-through diffusion cells fabricated from inert materials. In a finite dose scenario, the guidelines recommend a skin surface 'dose' of 1-5 mg cm⁻² for all solids and semi-solids and up to 10 µl cm⁻² for liquids (OECD, 2004). During a dermal absorption study, the compound under study is left in contact with the skin surface for a predetermined duration (reflecting practical exposure) and under stringent environmental conditions. Removal of the compound from the skin surface takes place after the exposure duration with a relevant cleansing method. The OECD recommends an exposure duration of 24 hours as a maximum, but concedes that longer periods may be justified. It recommends that the skin be maintained at constant 32 ± 1°C and receptor fluid should be well-mixed and sampled at pre-determined time points throughout the experiment. Aliquots of receptor fluid samples and skin sections can then be analysed for the test chemical and/or metabolites. In order to validate the performance and reliability of the test system, a result for an appropriate reference chemical should be undertaken and compared to published literature for the method used. The reference chemical should be close in lipophilicity to the test subject or a number of reference substances of different lipophilicities that are known should be provided (OECD, 2004).

1.4.1.4 Skin Integrity Measurements

There are several established methods to measure integument integrity and these include transepidermal electrical resistance (TER), permeability of tritiated water ($^3\text{H}_2\text{O}$) and transepidermal water loss (TEWL).

Transepidermal Electrical Resistance

Skin electrical resistivity is known to be a quantitative indicator of the structural integrity of the skin barrier layer (Allenby *et al.*, 1969). Two electrodes are used to apply a voltage across a skin sample, in which the skin's electrical current is then measured using an ammeter. The electrical resistance of the skin is obtained from using the skin electrical current and Ohm's Law. The electrical resistance of the skin is multiplied by the available surface area to obtain electrical resistivity. If the electrical resistivity of excised skin is less than $50 \text{ k}\Omega \text{ cm}^{-2}$, the barrier layer is then considered damaged (Kasting and Bowman, 1990, Rosell *et al.*, 1998). A cut-off value is determined for the type of skin preparation and species of skin in use, with a higher value associated with skin damage due to the electrolytes leaking from the top solution through the skin into the lower solution. This technique has been adopted by the OECD as a recommended test for skin barrier integrity (OECD, 2004).

Tritiated Water Permeability

Water permeability has been extensively assessed through the skin both *in vitro* and *in vivo* (Bettley and Grice, 1967, Blank, 1952, Blank, 1953, DeLong *et al.*, 1954, Idson, 1973, Scheuplein and Morgan, 1967). The water permeability coefficient (K_p) for skin has long been used to determine skin viability (Harrison *et al.*, 1984, Bronaugh *et al.*, 1981, Galey *et al.*, 1976, Bronaugh and Stewart, 1985). As water is hydrophilic, the stratum corneum would be the rate limiting step in absorption and a

defect in the barrier layer would reflect in a higher absorption of tritiated water (Bronaugh *et al.*, 1986).

A relatively rapid (20 minute) tritiated water test was designed in order to determine skin integrity (Bronaugh *et al.*, 1986). This test involved applying tritiated water at volume of $312.5 \mu\text{l cm}^{-2}$ and an activity of $0.33 \mu\text{Ci}$ per diffusion cell. The tritiated water was left on the skin for 20 minutes, after which the excess water was removed by blotting and the skin surface was rinsed once with distilled water. The receptor fluid was sampled for 60 minutes after removal of tritiated water. This procedure was advantageous in measuring skin integrity prior to assessment of chemical penetration due to the relatively small amount of radioactivity needed and the diffusion of all tritiated water within an 80 minute period. The evaluation of water in the assessment of skin integrity was also compared against model compounds of varying polarity (Bronaugh *et al.*, 1986). It was found that regardless of polarity, increases in water absorption in the 20 minute test were always accompanied by increases in the permeability of the chemical under study. The average permeability coefficient (K_p ; Equation 1.1) of water through *ex-vivo* human abdominal skin ranged from $1.0\text{-}1.5 \times 10^{-3} \text{ cm h}^{-1}$, as reported by several researchers (Bronaugh *et al.*, 1986, Harrison *et al.*, 1984, Scheuplein, 1965). The K_p cut-off value for water permeation through human skin was determined to be $2.5 \times 10^{-3} \text{ cm h}^{-1}$ as this equivalent to the upper limit for steady state water permeation (Bronaugh *et al.*, 1986).

Transepidermal Water Loss

Transepidermal water loss has been defined as the “constitutive outward loss of water from deeper epidermal layers of the skin in the absence of sweat gland activity” (Pinson 1941). Transepidermal water loss functions as a surrogate

measurement of skin barrier integrity by relating skin integrity to water loss from deeper layers of the skin to the skin surface. Rates of TEWL are measured using different types of evaporimeters (instrument to measure water evaporation) such as open and closed chamber probes (Schaefer and Redelmeier, 1996, Taylor, 2008).

Evaporimetry is a surrogate measure of TEWL, since it relies on measuring a water vapour gradient above the skin surface: It is assumed that changes in the water vapour gradient above the skin equates to a change in permeability of the skin. Importantly, the appearance of water vapour above the skin is primarily based upon the phase transition from liquid to vapour. Therefore, any variable that can affect that phase transition will affect the apparent permeability of the skin. Many additional factors can therefore influence the water vapour gradient, such as environmental conditions and experimental conditions, which has necessitated the development of guidelines to minimise such artefacts (Pinnagoda *et al.*, 1990).

Transepidermal water loss has been previously used as a measure of barrier integrity for identifying undamaged and damaged skin (Lamaud *et al.*, 1984, Lotte *et al.*, 1987, Aalto-Korte and Turpeinen, 1993, Tsai *et al.*, 2003). Historically, TEWL has also been used *in vivo* as a test for both baseline skin barrier function and to quantify any subsequent damage. An increase in transepidermal water loss may be measured before visible inflammation occurs after exposure to ionic, polar and water-soluble irritants (e.g. sodium hydroxide, soaps and detergents) (Malten and Thiele, 1973). In contrast, exposure to un-ionised polar irritants (e.g. dimethyl sulfoxide) and un-ionised non-polar, water-soluble irritants (e.g. hexanediol diacrylate and butanediol), did not increase TEWL until visible inflammation had occurred (Malten and den Arend, 1978, Malten *et al.*, 1979). Several potential sources of interference for *in*

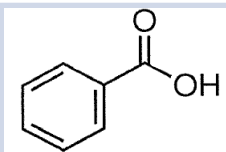
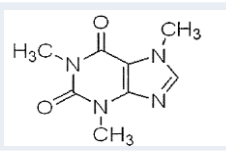
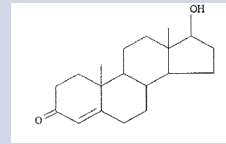
in vivo TEWL measurements may include blood perfusion, metabolism, temperature variation and sweat gland activity (Benowitz *et al.*, 1992, Kao *et al.*, 1984, Blank and Scheuplein, 1969, Pinnagoda *et al.*, 1990). Using an evaporimeter to measure transepidermal water loss flux has been contested as a measurement of *in vitro* barrier integrity as studies have shown that measurements of TEWL rates do not always relate to skin permeability (Chilcott *et al.*, 2002).

Both TEWL and tritiated water permeability have been recommended by the OECD and the European Centre for the Validation of Alternative Methods (ECVAM) in assessing skin barrier integrity due to the relatively quick assessment of the quality of skin (OECD 2004; Howes *et al.* 1996).

1.4.1.5 Model Compounds

The OECD guideline 428 advises that novel diffusion cells be fully characterised before use by measuring and comparing the absorption of model (or reference) chemicals to OECD-compliant models. The reference compound(s) can be applied at the same time as a penetrant under study or can be compared to historic percutaneous penetration data relating to the model compound. Three commonly used reference compounds are benzoic acid, caffeine and testosterone (Table 1.2) and have been used to characterise such parameters as a comparison of animal skin to human skin, skin damage and skin storage conditions.

Table 1.2: Physicochemical Properties Of Benzoic Acid, Caffeine And Testosterone. Synonyms of each compound as well as chemical abstracts service (CAS) number, molecular weight (MW), solubility (Log P) and chemical structure.

Compound	Synonyms	CAS	MW	Log P	Structure
Benzoic Acid	Benzenecarboxylic acid	65-85-0	122.10	1.83	
Caffeine	3, 7-dihydro-1, 3, 7-trimethyl-1H-purine-2, 6-dione	58-22-0	194.19	-0.01	
Testosterone	4-androsten-17 β -ol-3-one	58-08-2	288.42	3.32	

In order to validate the use of animal skin in place of human skin *in vitro*, studies should be carried out with standard compounds to provide an estimation of dermal absorption parameters with the animal skin system. Reifenrath *et al.* (1984) found a significant correlation between human skin grafted onto athymic nude mice and human skin ($r = 0.74$) as well as between weanling Yorkshire pig skin and human skin ($r = 0.83$). There were no significant correlations found between human skin compared to hairless dog, or pig skin grafted onto athymic mice. Porcine skin was validated *in vitro* by Hawkins and Reifenrath (1986), in which permeability to 11 compounds correlated well with that of human skin ($r = 0.79$). The correlation between porcine and human skin was further improved when split-thickness (dermatomed) skin was used rather than full thickness. Bartek *et al.* (1972) found that skin permeability was of the order: rabbit > rat > pig \geq man and that the skin of the miniature swine had the closest percutaneous penetration properties to man.

An important aspect for interpreting skin absorption data of model compounds (or indeed any penetrant) is the statistical distribution of data and hence appropriate statistical test. The distribution of K_p values for a range of model compounds (e.g. 5-fluorouracil, oestradiol, water) was found to be best described as log-normal rather than normal (Williams *et al.*, 1992, Cornell and Barry, 1995, Fasano *et al.*, 2002). Khan *et al.* (2005) found that when using silicone membranes, the permeability coefficients of two model compounds (caffeine and testosterone) fitted a normal distribution. This statistical disparity is most likely indicative of the fact that artificial membranes comprise a homogenous barrier to diffusion whereas stratum corneum is a hybrid of different anatomical and biochemical barriers.

It is difficult to compare studies of model compounds performed by different laboratories, due to differences in skin membranes, dose regimes, penetrant solution preparation and study design. A multi-centre study sought to characterise the skin absorption of three model compounds (benzoic acid, caffeine and testosterone) in human and rat skin across ten different laboratories (van de Sandt *et al.*, 2004). The maximum absorption of benzoic acid was greatest compared to both caffeine and testosterone (see Tables 1.3 - 1.5). In the majority of laboratories, benzoic acid and caffeine showed a higher penetration rate than testosterone (van de Sandt *et al.*, 2004).

When comparing previous studies involving the use of benzoic acid, caffeine and testosterone, several points are apparent (see Table 1.3, Table 1.4 and Table 1.5). Generally, benzoic acid and caffeine have similar cumulative penetration kinetics, whereas testosterone is a much slower penetrant. This is to be expected, as testosterone has a relatively high log P value and high molecular weight compared to both benzoic acid and caffeine, both factors which will affect dermal absorption. As expected, skin damage (caused by abrasion) resulted in a 2-fold increase in skin absorption of benzoic acid and caffeine (Bronaugh and Stewart, 1985). Comparison of *in vivo* and *in vitro* porcine skin studies demonstrated that permeability to benzoic acid and caffeine remained relatively similar (Hawkins and Reifenrath, 1986). These data indicate good *in vivo/in vitro* correlation (Hawkins and Reifenrath, 1986). Moreover, the *in vitro* studies were performed both with split thickness and full thickness skin and so confirm that the presence of (hydrophilic) dermal tissue does not substantially alter the percutaneous penetration of hydrophilic penetrants (Hawkins and Reifenrath, 1986). The van de Sandt *et al.* (2004) multi-centre study consistently produced the highest skin absorption rates compared to other

researchers. This could be due to the higher dose that was used, due to the majority of other studies investigating the use of these compounds at a dose of $4 \mu\text{g cm}^{-2}$, as well as in some cases, a shorter exposure time of 24 hours. It should be noted that the calculations in Tables 1.3 to 1.5 do not take into account the lag times of the penetrants when converting from the applied dose penetrated to a mass amount per cm^{-2} per hour and therefore will underestimate the actual flux.

Table 1.3: Studies Investigating Dermal Absorption Of Benzoic Acid. Cumulative amount penetrated is represented as the applied dose of testosterone (%) penetrated. The amounts in brackets are converted values from applied dose penetrated (%) to mass amount ($\mu\text{g cm}^{-2} \text{h}^{-1}$) for the reported exposure duration.

Chemical	Paper	Study	Skin	Dermal Absorption Parameter
Benzoic Acid	Reifenrath <i>et al.</i> (1984)	<i>In vivo</i>	Weanling Pig	Applied Dose Penetrated: 12% ($0.001 \mu\text{g cm}^{-2} \text{h}^{-1}$)
		<i>In vivo</i>	Human- Graft onto nude mice	Applied Dose Penetrated: 40% ($0.07 \mu\text{g cm}^{-2} \text{h}^{-1}$)
		<i>In vivo</i>	Pig- Graft onto nude mice	Applied Dose Penetrated: 42% ($0.07 \mu\text{g cm}^{-2} \text{h}^{-1}$)
	Bronaugh and Stewart (1985)	<i>In vitro</i>	Human Human- Abraded	Applied Dose Penetrated: 28% ($0.05 \mu\text{g cm}^{-2} \text{h}^{-1}$) Applied Dose Penetrated: 58% ($0.10 \mu\text{g cm}^{-2} \text{h}^{-1}$)
			Rat Rat- Abraded	Applied Dose Penetrated: 20% ($0.03 \mu\text{g cm}^{-2} \text{h}^{-1}$) Applied Dose Penetrated: 40% ($0.07 \mu\text{g cm}^{-2} \text{h}^{-1}$)
	Hawkins and Reifenrath (1986)	<i>In vivo</i> <i>In vitro</i> <i>In vitro</i>	Porcine Porcine- Full Thickness Porcine- Split Thickness	Applied Dose Penetrated: 28% ($0.02 \mu\text{g cm}^{-2} \text{h}^{-1}$) Applied Dose Penetrated: 21% ($0.02 \mu\text{g cm}^{-2} \text{h}^{-1}$) Applied Dose Penetrated: 20% ($0.02 \mu\text{g cm}^{-2} \text{h}^{-1}$)
	van de Sandt <i>et al.</i> (2004)	<i>In vitro</i>	Human- Split Thickness	Applied Dose Penetrated: $69 \pm 15\%$ ($2.9 \pm 0.6 \mu\text{g cm}^{-2} \text{h}^{-1}$)

Table 1.4: Studies Investigating Dermal Absorption Of Caffeine. Cumulative amount penetrated is represented as the applied dose of testosterone (%) penetrated. Dermal absorption parameters listed include; permeability coefficient (K_p), the diffusion coefficient (D), membrane partition coefficient (K_m), lag time and steady state flux (J_{ss}) in mass amount per cm^{-2} per hour. The amounts in brackets are converted values from applied dose penetrated (%) to mass amount ($\mu\text{g cm}^{-2} \text{h}^{-1}$) for the reported exposure duration.

Chemical	Paper	Study	Skin	Dermal Absorption Parameter
Caffeine	Bartek <i>et al.</i> (1972)	<i>In vivo</i>	Porcine	Applied Dose Penetrated: 32% ($0.01 \mu\text{g cm}^{-2} \text{h}^{-1} \mu\text{g}$)
	Reifenrath <i>et al.</i> (1984)	<i>In vivo</i>	Weaning Pig	Applied Dose Penetrated: 20% ($0.002 \mu\text{g cm}^{-2} \text{h}^{-1}$)
		<i>In vivo</i>	Human Graft	Applied Dose Penetrated: 42% ($0.07 \mu\text{g cm}^{-2} \text{h}^{-1}$)
		<i>In vivo</i>	Porcine Graft	Applied Dose Penetrated: 30% ($0.05 \mu\text{g cm}^{-2} \text{h}^{-1}$)
	Bronaugh and Stewart (1985)	<i>In vitro</i>	Human	Applied Dose Penetrated: 41% ($0.07 \mu\text{g cm}^{-2} \text{h}^{-1}$)
			Human- Abraded	Applied Dose Penetrated: 63% ($0.1 \mu\text{g cm}^{-2} \text{h}^{-1}$)
Rat			Applied Dose Penetrated: 56% ($0.09 \mu\text{g cm}^{-2} \text{h}^{-1}$)	
Rat- Abraded			Applied Dose Penetrated: 90% ($0.2 \mu\text{g cm}^{-2} \text{h}^{-1}$)	
Hawkins and Reifenrath (1986)	<i>In vivo</i>	Porcine	Applied Dose Penetrated: 23% ($0.02 \mu\text{g cm}^{-2} \text{h}^{-1}$)	
	<i>In vitro</i>	Porcine - Full Thickness	Applied Dose Penetrated: 20% ($0.02 \mu\text{g cm}^{-2} \text{h}^{-1}$)	
	<i>In vitro</i>	Porcine - Split Thickness	Applied Dose Penetrated: 21% ($0.02 \mu\text{g cm}^{-2} \text{h}^{-1}$)	
Boucad <i>et al.</i> (2001)	<i>In vitro</i>	Human	$J_{\text{Max}} - 1.1 \text{ ng cm}^{-2} \text{ h}^{-1}$ Lag Time- 0.6 h	
		Human- Ultrasound	$J_{\text{Max}} - 4 \text{ ng cm}^{-2} \text{ h}^{-1}$ Lag Time- 0.5 h	
		Rat	$J_{\text{Max}} - 0.2 \text{ ng cm}^{-2} \text{ h}^{-1}$	
		Rat- Ultrasound	$J_{\text{Max}} - 15 \text{ ng cm}^{-2} \text{ h}^{-1}$	

	Van de Sandt <i>et al.</i> (2004)	<i>In vitro</i>	Human	Applied Dose Penetrated: $27 \pm 11\%$ ($1.1 \pm 0.5 \mu\text{g cm}^{-2} \text{h}^{-1}$)
	Khan <i>et al.</i> (2005)	<i>In vitro</i>	Porcine (Ear)	$K_p - 1.4 \times 10^{-3}$

Table 1.5: Studies Investigating Dermal Absorption Of Testosterone. Cumulative amount penetrated is represented as the applied dose of testosterone (%) penetrated. Dermal absorption parameters listed include; permeability coefficient (K_p), the diffusion coefficient (D), membrane partition coefficient (K_m), lag time and steady state flux (J_{ss}) in mass amount per cm^{-2} per hour. The amounts in brackets are converted values from applied dose penetrated (%) to mass amount ($\mu\text{g cm}^{-2} \text{h}^{-1}$) for the reported exposure duration.

Chemical	Paper	Study	Skin	Dermal Absorption Parameter
Testosterone	Scheuplein <i>et al.</i> (1967)	<i>In vitro</i> <i>In vivo</i>	Human- Intact	$K_p - 4 \times 10^{-6} \text{ cm h}^{-1}$ $D - 2 \times 10^{-11} \text{ cm}^2 \text{ h}^{-1}$ $K_m - 23$ Lag Time- 38h $J_{ss} \text{ (in vitro)} - 40 \text{ moles cm}^{-2} \text{ h}^{-1}$ $J_{ss} \text{ (in vivo)} - 150 \text{ moles cm}^{-2} \text{ h}^{-1}$
	Bartek <i>et al.</i> (1972)	<i>In vivo</i>	Porcine (Ear)	Applied Dose Penetrated: 29% ($0.01 \mu\text{g cm}^{-2} \text{h}^{-1}$)
	Kao <i>et al.</i> (1985)	<i>In vitro</i>	Human- Fresh Human- Frozen	Applied Dose Penetrated: 50% ($0.05 \mu\text{g cm}^{-2} \text{h}^{-1}$) Applied Dose Penetrated: 62% ($0.06 \mu\text{g cm}^{-2} \text{h}^{-1}$)
	Hawkins and Reifenrath (1984)	<i>In vitro</i>	Porcine	Applied Dose Penetrated: 3% ($0.002 \mu\text{g cm}^{-2} \text{h}^{-1}$)
	Reifenrath <i>et al.</i> (1984)	<i>In vivo</i> <i>In vivo</i> <i>In vivo</i>	Weaning Pig Human Skin Graft- Nude Mice Porcine Skin Graft- Nude Mice	Applied Dose Penetrated: 5% ($0.0005 \mu\text{g cm}^{-2} \text{h}^{-1}$) Applied Dose Penetrated: 40% ($0.07 \mu\text{g cm}^{-2} \text{h}^{-1}$) Applied Dose Penetrated: 41% ($0.07 \mu\text{g cm}^{-2} \text{h}^{-1}$)
	Hawkins and Reifenrath (1986)	<i>In vivo</i> <i>In vitro</i> <i>In vitro</i>	Porcine Skin Porcine Skin- Split Thickness Porcine Skin- Full thickness	Applied Dose Penetrated: 13% ($0.01 \mu\text{g cm}^{-2} \text{h}^{-1}$) Applied Dose Penetrated: 3% ($0.002 \mu\text{g cm}^{-2} \text{h}^{-1}$) Applied Dose Penetrated: 6% ($0.005 \mu\text{g cm}^{-2} \text{h}^{-1}$)

	Tang et al (2002)	<i>In vitro</i>	Porcine (Dorsum)- Split Thickness	K_p (experimental 22-25h)- $2 \times 10^{-3} \text{ cm h}^{-1}$ K_p (predicted 41-48h) 2×10^{-3}
	van de Sandt <i>et al.</i> (2004)	<i>In vitro</i>	Human- Split Thickness	Applied Dose Penetrated: $23 \pm 14\%$ ($0.9 \pm 0.6 \mu\text{g cm}^{-2} \text{ h}^{-1}$)
	Khan et al (2005)	<i>In vitro</i>	Porcine (Ear)- Full Thickness	K_p - $1 \times 10^{-2} \text{ cm h}^{-1}$

1.4.1.6 Limitations Of In Vitro Experimentation

Many distinct advantages are associated with *in vitro* experimentation such as precise control over experimental parameters, the ability to test potentially toxic materials using human skin, direct measurements of the penetration and distribution of the penetrant within the skin and corresponding contribution to the 3Rs of reduction, refinement and replacement of animals in scientific research (Pendlington, 2008). Most notably however, the limitations that exist in this model are the lack of pharmacokinetic data available after percutaneous penetration (e.g. systemic distribution), an inability to perform a test to investigate metabolism within the skin without going to great lengths to ensure viability and a missing factor of pharmacodynamics (e.g. vasoconstriction and vasodilation) (Pendlington, 2008) and the lack of overt toxic responses such as erythema, blistering or other immune responses.

1.4.2 In Vivo Dermal Absorption

The dermal absorption of penetrants can be measured using human volunteers using a variety of methods. This is arguably the ‘gold standard’ for developing human risk assessment or optimising drug delivery systems or skin protectants, but can only be performed if the chemicals or drugs are of sufficiently low toxicity to justify their use in volunteers. Historically, radioisotope tracers have been used in the past with human volunteers to assess percutaneous absorption (Feldmann and Maibach, 1967, Feldmann and Maibach, 1965). It is now more common to use non-radiolabelled compounds to assess dermal absorption and to quantify amounts of the penetrant or metabolite(s) in blood and urine using analytical methods such as HPLC, GC-MS or LC-MS (Pendlington *et al.*, 2001, Sampol *et al.*, 2000, Jakasa *et al.*, 2004). Local absorption and assessment of the depth of penetration can be assessed using

minimally invasive methods such as tape stripping and microdialysis. Non-invasive measurements of percutaneous penetration based on quantifying a local relevant biological response can also be assessed through visual erythema scoring, tissue viability imaging and laser Doppler imaging (erythema), infrared thermography (skin temperature), pH of the skin surface, transepidermal water loss (viability of the barrier layer), and skin reflectance spectroscopy (Patil *et al.*, 1996).

Further in-depth discussion about the use of vasodilators on human volunteers and two non-invasive monitoring methods (visual erythema scoring and laser Doppler imaging) relevant to this Thesis will be discussed.

1.4.2.1 Model Compounds (Methyl Nicotinate)

Nicotinates were examined in the latter part of the 20th century as markers for skin permeation for studying both physicochemical properties and formulation effects (Albery and Hadgraft, 1979a, Albery and Hadgraft, 1979b, Albery and Hadgraft, 1979c, Baker *et al.*, 1969, Cronin and Stoughton, 1962, Hadgraft *et al.*, 1973, Hadgraft *et al.*, 1972, Stoughton *et al.*, 1960). Following topical application to skin, nicotinic acid derivatives are known to rapidly elicit vasodilation of the peripheral blood vessels in the dermal papillae and produce notable erythema (Fulton *et al.*, 1959, Stoughton *et al.*, 1960). When using an identical exposure time and concentration of methyl nicotinate, the time of onset of erythema is reproducible (Guy and Maibach, 1982). In terms of methyl nicotinate, Laser Doppler velocimetry has been reported as a rapid and sensitive technique for identifying and quantifying skin blood flow (Wester and Maibach, 1984).

1.4.2.2 Skin Response

Visual Erythema Scoring

Acute irritation and corrosion have been evaluated using a modified version of the Draize test, first outlined by John Draize and colleagues (Draize *et al.*, 1944). The grading scale used in Draize-type tests ranges from a score of 0-4 for a description of both erythema and oedema formation, this was previously used to evaluate skin reactions using animals and can also be used for evaluating human skin responses (Table 2.4). Integrated scales, with the addition of papular, vesicular and bullous responses, ranging from 4-16 points have also been proposed (Patil *et al.*, 1996). It should be noted that reliance of animal studies on the Draize test is being phased out in favour of more humane endpoints and alternative models (Balls *et al.*, 1995).

Laser Doppler Imaging

Laser Doppler velocimetry (LDV) was shown to indicate changes in microvascular perfusion as early as 1975 (Stern, 1975). Laser Doppler velocimetry is a non-invasive technique that detects changes in the microvasculature of the skin and was validated and developed for clinical evaluation of superficial blood flow in the skin (Holloway and Watkins, 1977, Watkins and Holloway, 1978, Stern *et al.*, 1977). This technique was subsequently employed to detect blood perfusion changes after injection trauma and mild burns from transcutaneous oxygen monitoring (Holloway, 1980, Enkema *et al.*, 1981). Laser Doppler imaging built upon the principles of LDV as this technique uses the Doppler shift principle to determine the velocity of red blood cells in the papillary plexus using a 632 nm helium-neon (He-Ne) laser source which is directed towards skin tissue, penetrating to a depth of 1-1.5 mm. Laser light back-scattered from stationary particles remains at the same frequency as the light that entered the skin, whereas laser light from moving particles (i.e. red blood cells)

undergoes a shift in frequency according to the Doppler effect (Holloway and Watkins, 1977). Guy *et al.* (1983) found that LDV and photopulse plethysmography correlated well during *in vivo* monitoring of methyl nicotinate exposure in human volunteers, providing a useful non-invasive technique to explore drug disposition in the skin after topical application.

Laser Scanning Confocal Microscopy

When fluorescent samples are imaged using a conventional light microscope, the fluorescence in regions outside the area of interest interferes with the resolution of the areas in focus. This is especially true for specimens greater than 2 μm in thickness (Paddock, 1999). The optical principle of laser scanning confocal microscopy is to eliminate out of focus light in the specimen through spatial filtering (Paddock, 1999). This is physically achieved by incorporating the use of strategically placed pinholes into the apparatus. The point of light is focused by an objective lens into the specimen with any transmitted light that passes through focused using a second objective lens at a second pinhole (with identical focus to the first pinhole). Therefore, the pinholes were ‘confocal’ (Paddock, 1999). Any light passing through the second pinhole struck a low-noise photomultiplier which amplified the signal which was related to the brightness of the light. The second pinhole prevented light from above and below the plane of focus from striking the photomultiplier (Paddock, 1999). Confocal microscopy has been used to visualise nanoparticle-cell interaction, with many studies documenting uptake of nanoparticles into cells (Calvo *et al.*, 1994, Dailey *et al.*, 2003, Gorelik *et al.*, 2002, Kemp *et al.*, 2008). Confocal microscopy has also been commonly used to visualise fluorescent nanoparticles and the skin (Rouse *et al.*, 2007, Ryman-Rasmussen *et al.*, 2006, Tinkle *et al.*, 2003).

An alternative to single-photon confocal microscopy is multi-photon microscopy. Multi-photon microscopy allows for the deeper imaging of biological samples without the accompanying loss in resolution, light scattering or increase in photobleaching in comparison to wide-field and confocal microscopy (Williams *et al.*, 2001, Denk *et al.*, 1990). Multiphoton microscopy is a technique which uses longer wavelength photons, which are scattered less by biological tissue, and therefore is a better technique than confocal microscopy in visualising fluorescence through thick tissues (Halbhuber and Konig, 2003). Multiphoton has been used with quantum dot nanoparticles to visualise detailed cell structures (Ferrara *et al.*, 2006).

1.5 Dermal Toxicity

The use of *in vitro* techniques can be beneficial in the testing of topical products such as barrier creams. However, such ‘static’ models fail to reproduce the normal movement of skin which could potentially alter the thickness and hence protective effect of barrier creams measured *in vitro*. This issue is discussed further when analysing potential nanoparticle penetration through the skin (see Section 1.5.2.3).

One potential application of barrier creams is in the prevention and treatment of skin disorders such as incontinence associated dermatitis (IAD).

1.5.1 Incontinence Associated Dermatitis

1.5.1.1 Disease

Incontinence associated dermatitis presents as inflammation of the skin surface, erythema and, in severe cases, oedema and blister formation (Voegeli, 2012). There are four primary objectives in managing moisture-associated skin damage; (1) adoption of a structured skin-care regimen, (2) use of products that prevent moisture

on 'at-risk' skin, (3) control of the cause behind excessive moisture and (4) treatment of any secondary infection (Gray *et al.*, 2011). As many as 3-25% of the population in care homes within the United Kingdom have suffered from incontinence-associated dermatitis (Newman *et al.*, 2007). However, this number could be vastly underestimated, as prevalence of IAD has been acknowledged as being under-reported due to a lack of validated assessment tools in addition to the stigma of the condition (Borchert *et al.*, 2010).

Incontinence-associated dermatitis has been defined as, "inflammation and erosion of the skin caused by prolonged exposure to various sources of moisture, including faeces, urine, perspiration and wound exudate" (Gray *et al.*, 2007). This type of dermatitis falls under the category of moisture-associated skin damage (MASD). It has been theorised that there are several factors leading to the causation of incontinence-associated dermatitis. Possible changes in the pH of the skin's acid mantle due to ammonia from urine as well as excessive moisture is thought to lead to disruption of the intercellular lipids and corneocytes in the skin barrier layer leading to skin irritation and breakdown (Warner *et al.*, 2003, Langemo *et al.*, 2011). Previous histological results have corroborated the disruption of the intercellular lipids and corneocyte structure, essentially leading to physical damage of the stratum corneum with associated loss of barrier function (Warner *et al.*, 2003). Over-hydration of the skin barrier layer is also known to elicit damage and as a consequence, irritants found in urine and faecal matter may penetrate the skin. Physical irritation such as the skin cleansing can further contribute to the breakdown of the epidermis (Gray, 2010). Therefore, topical skin protectants would provide an additional barrier to decrease exposure to both wash and irritant substances and in theory, result in a decrease in IAD.

1.5.1.2 Prevention (*Barrier Creams*)

Skin barrier creams have been proposed in the past to prevent and/or reduce dermal absorption from hazardous agents known to cause contact dermatitis (Schaefer and Redelmeier, 1996). However, researchers have been divided as if topical skin protectants have provided protection or exacerbated irritation (Wigger-Alberti *et al.*, 1998, Frosch *et al.*, 1993, Schluter-Wigger and Elsner, 1996). Schliemann *et al.* (2013) found that the protective efficacy of the creams was dependant on the amount of product applied per unit skin surface area and recommended the use of protective creams at doses less than 2 mg cm^{-2} . Basic preparations have consisted of a lipid or water emulsion, in addition to anti-microbials such as zinc oxide and titanium oxide (Voegeli, 2012). Water repellent silicone-based preparations such as dimethicone, in addition to mild antiseptic agents such as cetrimide and benzalkonium have also been employed (Voegeli, 2012). In addition to the above, pure white petrolatum (i.e. Vaseline) has also been used as a skin protectant due to inherent water-repellent properties as well as allowing for barrier recovery (Ghadially *et al.*, 1992).

The experimental formulation RD-1433 is a topical skin protectant initially developed to protect members of the armed forces against exposure to toxic chemicals. *In vivo* data has shown that this cream can reduce the size of skin lesions following exposure to skin damaging agent as well as decreasing mortality rate and protecting red blood cell activity when animals were exposed to organophosphorus nerve agents (Liu *et al.*, 1999). Moreover, the perfluorinated composition of RD-1433 may inhibit bacterial growth. The composition of RD-1433 also provides lubrication thereby eliminating possible skin friction and further associated damage from IAD.

1.5.2 Nanoparticles

Nanoparticles are considered a relatively new dermal absorption risk as more consumer products have incorporated these particles without the relevant risk assessments. Nanoparticles are thought to be a unique dermal absorption hazard, as on average these particles are too large in size to penetrate through the stratum corneum. However, it is thought that with additional energy provided through skin flexing, these particles could have enough energy to then translocate into deeper (viable) layers of skin (Rouse *et al.*, 2007).

The potential for dermal absorption of nanoparticles has been investigated using both *in vitro* and *in vivo* methods (Rouse *et al.*, 2007, Ryman-Rasmussen *et al.*, 2006, Gratieri *et al.*, 2010, Zhang and Monteiro-Riviere, 2008). The *in vitro* assessment of nanoparticle dermal penetration using standard diffusion cells (static/flow-through) may not be entirely appropriate as evidence exists to suggest skin movement could alter the absorption of nanoparticles (see Section 1.5.2.3). Hence, the main purpose of work outlined in this Thesis was to develop a more appropriate dermal exposure model for assessing percutaneous absorption of nanoparticles.

1.5.2.1 Definition And Routes Of Exposure

Nanoparticles can be defined as single particles with at least one dimension measuring less than 100 nm and are a subset of nanomaterials (Royal Society and Royal Academy of Engineering, 2004). These particles have unique size-dependent properties due to a larger surface area per unit mass, culminating in a more reactive species compared to the same material at a larger size (Zuin *et al.*, 2007). The increase in surface area is an important factor which determines the bulk properties of each material, with the ratio of surface to total atoms or molecules increasing

exponentially with decreasing particle size. The increase in surface reactivity of nanoparticles could mean that these particles exhibit a greater biological activity per mass than larger particles should they enter a living organism and remain solid rather than dissolved into ions.

Due to high surface energy resulting in inter-particle attraction through London, van der Waals and electrostatic forces, nanoparticles are often found in aggregates (physically connected) or agglomerates (loosely connected) (Werth *et al.*, 2003). The physicochemical properties of nanoparticles such as size, shape, chemical composition, lattice structure, surface chemistry, surface charge and aggregation state make it particularly difficult to predict how these particles will react when studied in biological systems (Zuin *et al.*, 2007).

Nanomaterials have been used in a variety of industries encompassing sporting goods, tyres, electronic components, food packaging, sunscreens, cosmetics and antimicrobial and antifungal preparations (Table 1.6). Humans are also exposed to nanosized particles unintentionally through natural combustion processes such as forest fires and volcanoes (Table 1.6). An indirect source of exposure has been through ultrafine particulate matter present in air pollution from sources such as automobile engines and manufacturing industries (Table 1.6).

Ingestion, inhalation and skin penetration are all potential exposure routes for both engineered and natural nanomaterials (Oberdörster *et al.*, 2005). Inhalation is considered the most likely route of exposure from nanoparticles, however concerns have been raised by the possibility of dermal penetration and further systemic exposure (Borm *et al.*, 2006).

Table 1.6. Nanoparticle Origins And Sources (table from Oberdörster *et al.* (2005))

Natural	Anthropogenic	
	Un-intentional	Intentional
Forest fires	Combustion engines	Metals, semi-conductors, metal oxides, carbon, polymers
Volcanoes	Power plants	Nano-wires, -spheres, needles, -tubes, -shells, -rings
Viruses	Incinerators	Un-treated, coated particles in cosmetics, medical, fabrics, electronics, optics, displays, etc.
Ferritin (12.5 nm)	Jet engines	
Microparticles in active cells (< 100 nm)	Metal, polymer fumes	
Biogenic magnetite	Frying, broiling, grilling	
	Electric motors	

Quantum Dot Nanoparticles

Quantum dots (QDots) are nanocrystals comprising of a metallic core (usually cadmium and selenium) surrounded by an inorganic shell coating (commonly zinc sulphate). Quantum dot nanoparticles are fluorescent semi-conductor materials used for therapeutic, diagnostic and semi-conductor applications (Ryman-Rasmussen *et al.*, 2006). One of the properties exhibited by quantum dots is photoluminescence. Two advantages that quantum dot nanoparticles hold over traditional fluorophores are a greater resistance to light-dependent oxidation (photobleaching) and a greater brightness due to high quantum yield and large molar extinction coefficient values (Ho and Leong, 2010). The high density of electrons present within quantum dots also make these nanoparticles ideal for visualisation by transmission electron microscopy (TEM) (Nisman *et al.*, 2004).

Quantum dots are atom clusters consisting of a distinct core, shell and coating. The core of the quantum dot consists of a few hundreds to thousands of atoms of semi-conductor material, in some cases, cadmium mixed with selenium. This core is then stabilised by a surrounding semi-conductor shell (i.e. zinc sulphide), to enhance both optical and physical properties of the material. The shell has been shown to minimise leaching of cadmium from the core (Cho *et al.*, 2007). Lastly, an amphiphilic polymer coating (i.e. polyethylene glycol) can be applied to provide a water-soluble surface that can be modified. A majority of quantum dots have the amphiphilic inner coating covalently bonded to a functionalised polyethylene glycol outer coating to decrease the possibilities of non-specific bonding. It has been demonstrated that quantum dot toxicity is dependent upon surface charge and surface coating (Hoshino *et al.*, 2004). In order to introduce quantum dots into a biological system, water-soluble dots are preferable. Therefore, dots have been synthesised with water-soluble

ligands, silanisation and encapsulation within block-copolymer micelles to improve hydrophilicity (Chan and Nile, 1998, Mattoussi *et al.*, 2000, Gerion *et al.*, 2001).

1.5.2.2 Nanoparticle Characterisation

The synthesis of nanomaterials can occur through either a bottom-up or top-down approach. The bottom-up approach, as described by Whitesides *et al.* (1991) involves one of the following processes: building structures using covalent bonds through chemical synthesis; covalent polymerization; ionic, hydrogen-bond or van der Waals interactions used to instigate self-assembly of crystal and colloid structures and lastly, molecular self-assembly using a combination of synthetic processes.

When suspended in a liquid medium, nanoparticles may carry a surface electrical charge, dependent upon the physicochemical properties of the particle and the surrounding media (Eastman, 2005). The size and charge of a nanoparticle are two major factors that affect dispersion through adsorption of ions, contaminants and biomolecules (Powers *et al.*, 2006). Additional energy may need to be provided in order to further disperse nanoparticle aggregates. Sonication involves the use of ultrasonic energy to physically break apart loose bonds between aggregates in solution (Zuin *et al.*, 2007). Step-wise centrifugation has also been employed to further narrow the distribution range of nanoparticles.

It has been recognised that no individual technique can provide the entire characterisation of a nanoparticulate sample (UK NanoSafety Partnership Group, 2012). Multiple techniques are required for different sample forms (e.g. aerosol, suspension, dry powder, etc.) and the optimum set of required techniques is dependent upon the nanoparticle type, formulation under study and purpose of study (UK NanoSafety Partnership Group, 2012).

Dynamic Light Scattering

Dynamic light scattering (DLS) or photon correlation spectroscopy (PCS) is a conventional characterisation technique used for measuring nanoparticle size in suspension. DLS measures the speed at which particles are diffusing within a suspension (due to Brownian motion) then detects the rate in which the intensity of the scattered light fluctuates. The hydrodynamic diameter of a nanoparticle is calculated from the translational diffusion coefficient using the Stokes-Einstein equation (Equation 1.6):

Equation 1.6

$$d(H) = \frac{kT}{3\pi\eta D}$$

Where **d(H)**- hydrodynamic diameter; **k** – Boltzmann's constant; **T**- absolute temperature ;**η** – viscosity; **D**- translational diffusion coefficient

This type of particle sizing is affected by ions in suspension as well as total ionic charge, as ions that are covalently attached to nanoparticles will be included in the hydrodynamic diameter. An alternative to DLS is nanoparticle tracking and analysis (NTA) which allows for each nanoparticle in suspension to be tracked in real-time and sized on a particle-by particle basis by a dedicated particle tracking image analysis program. Dynamic light scattering estimates particle size by using intensity weighted (z-average) distributions whereas NTA provides a particle size distribution due to a direct number/frequency distribution measurement. Both NTA and DLS allow for the measuring of the zeta potential (ζ) of a particle in suspension. Zeta potential is a physical property that is exhibited by any particle in suspension: greater than +30 mV and less than -30 mV indicates a stable suspension (Everett, 1994, Lyklema, 2000).

Transmission Electron Microscopy

The characterisation technique favoured for both shape and aggregation state/size is transmission electron microscopy because this is a direct rather than inferred measurement. Transmission electron microscopy also provides a visual image of the nanoparticulate matter at a higher resolution. Transmission electron microscopy can also be coupled with energy dispersive x-ray spectroscopy (EDX) for identifying the sample composition. However, due to preparation methods for samples undergoing transmission electron microscopy (carbon grid room temperature desiccation) nanoparticle shape and size can differ from what is seen in a suspension.

1.5.2.3 Dermal Absorption Of Nanoparticles

The concerns for human health include a potential for cytotoxicity, accumulation in skin and other organs resulting in toxicity, metabolism of nanoparticles to smaller particles with increased toxicity, and toxicity of photo-activated nanoparticles (Tsuji *et al.*, 2006). The dimensions of nanoparticles are important for potential percutaneous penetration as the pilosebaceous pores are reportedly 10-70 μm in diameter (Lauer *et al.*, 1996), sweat gland pores are 60-80 μm in diameter (Roberts, 2004) and lastly, the lipid matrix surrounding the dead corneocytes fills a gap of only 75 nm (Elias and Friend, 1975). It has been suggested that receptor-mediated pathways into the cell would not work for a nanoparticle greater than 100 nm (Royal Society and Royal Academy of Engineering, 2004). The size constraints for entry into the nucleus and epithelial barriers are 40 nm and less than 35 nm, respectively (Oberdörster *et al.*, 2005). However, these size guidelines vary with surface modifications and nanoparticulate material.

As with all xenobiotics, the main barrier to dermal absorption of nanoparticles is the stratum corneum. In addition to the lipid lamellae, the varying polarities of the skin layers contribute to reducing penetration into the deeper viable skin layers (Labouta *et al.*, 2011). Surface hydrophobicity was found to favour the passage of nanoparticles into the stratum corneum (Labouta *et al.*, 2011). A skin exposure time of 6 hours (or greater) was determined as the minimum exposure time needed to see significant penetration for studying factors such as physicochemical properties, formulation effects and environmental conditions (Labouta *et al.*, 2011).

Studies investigating the dermal absorption of nanoparticles have used a variety of skin types, nanoparticles and exposure conditions, with some studies rejecting skin penetration (Pflücker *et al.*, 2001, Schulz *et al.*, 2002, Alvarez-Román *et al.*, 2004, Gamer *et al.*, 2006, Mavon *et al.*, 2007, van der Merwe *et al.*, 2009, Senzui *et al.*, 2010, Szikszai *et al.*, 2010) and others which found evidence for the percutaneous penetration of nanoparticles (Alvarez-Román *et al.*, 2004, Kertész *et al.*, 2005, Lademann *et al.*, 1999, Menzel *et al.*, 2004, Ryman-Rasmussen *et al.*, 2006, Tan *et al.*, 1996, Larese *et al.*, 2009, Wu *et al.*, 2009a, Baroli *et al.*, 2007).

Dermal Absorption Studies Of Micro- And Nanoparticles

The hypothesis that external force can provide the necessary energy for percutaneous absorption of ultrafine particles has been researched by several scientists. It is thought that mechanical stimulation occurring through repetitive skin movement may alter the structural organisation of the skin barrier layer, leading to increased penetration of nanoparticles. This theory is preceded by evidence from individuals who walked barefoot in the African rift valleys, amongst which there was a high prevalence of podoconiosis. This elephantiasis of the feet and legs was believed to be

caused by mechanical stressors due to the exposure of unprotected feet to soils with high concentrations of zirconium and beryllium particles (Blundell *et al.*, 1989, Corachan *et al.*, 1988). Particles were identified in both the lymph nodes and the dermis of individuals affected. This finding suggested that normal physiological movement can influence percutaneous absorption of particles. Both Tan *et al.* (1996) and Lademann *et al.* (1999) reported *in vivo* titanium dioxide penetration into the upper layers of the stratum corneum and hair follicles using repeated rubbing of sunscreen onto the volar forearm (which would induce skin flexing, as well as an additional effect of pressure).

Tinkle *et al.* (2003) incorporated skin flexion *in vitro* for consideration of particulate penetration through human stratum corneum. Through mechanical flexing of human skin, beryllium particles were reported to penetrate the stratum corneum into the viable epidermis and, occasionally, reached the dermis. It was hypothesised that the flexing motion (20 flexes per minute at a 45 degree angle) provided the energy necessary for the particles to penetrate the stratum corneum. Subsequently, this device was used to assess the dermal absorption of a fullerene-substituted phenylalanine (Baa) and found that flexed samples showed a greater epidermal and dermal penetration compared to static samples (Rouse *et al.*, 2007). Importantly, TEM showed nanoparticles localised in intercellular spaces of the stratum granulosum, suggesting migration through the skin occurred via an intercellular pathway. These results led to the hypothesis that the force applied to the skin during flexing could have caused a change in the morphology and architectural lipid organisation in the stratum corneum leading to a transient increase to the intercellular spaces and causing nanoparticle penetration (Rouse *et al.* 2007). The ability for these nanoparticles to translocate through the lipid matrix of the stratum corneum raises

the potential for absorption into circulation and accumulation at different sites in the body leading to possible systemic toxicity. However, it should be emphasised that the flexing took place before exposure to the nanoparticles and no test of skin integrity was performed in these studies. It is not unreasonable to assume that the relatively energetic flexing (20 flexes per minute) caused an irreversible increase in permeability due to physical damage.

Quantum dot nanoparticles are photostable and inherently fluorescent, with wavelengths of emission directly related to the size of the material. Quantum dots allow for reliable multi-colour imaging of biological samples, even in living tissues where auto-fluorescence is a problem for traditional fluorophores (Chan *et al.*, 2002). A number of studies have been performed with quantum dots, with conflicting outcomes (Table 1.7).

Quantum dot nanoparticles are not able to penetrate intact skin when topically applied at a physiological pH, with accumulation observed in the hair follicles and skin furrows (Prow *et al.*, 2012, Gratieri *et al.*, 2010, Wu *et al.*, 2009b). When skin flexing and massaging was studied, quantum dots were still found localised and retained on the surface of the stratum corneum, although the pattern of surface

Table 1.7: Quantum Dot Dermal Absorption Studies. A review of *in vitro* and *in vivo* dermal absorption studies involving quantum dot nanoparticles using intact and damaged skin of different species. Absorption of quantum dot nanoparticles varied according to treatment.

Quantum Dot	Paper	Study	Skin	Treatment	Absorption
QD 505-525nm	Paliwal <i>et al.</i> (2006)	<i>In vitro</i>	Porcine Full-Thickness	Sonophoresis and SLS	Yes- Dots found within lipids in stratum corneum at barrier of stratum granulosum
QD 565 and 655 nm Neutral, Cationic and Anionic pH 8.3 and 9.0	Ryman-Rasmussen <i>et al.</i> (2006)	<i>In vitro</i>	Porcine Split-Thickness	Intact	Yes- QD 565 all attachments in epidermis and dermis by 8h, QD 655 PEG and PEG-Amine in epidermis by 8h, QD 655 PEG-Carboxyl in epidermis at 24h.
QD 565 and 655 nm Neutral, Cationic and Anionic pH 8.3 and 9.0	Zhang and Monteiro-Riviere (2008)	<i>In vitro</i>	Rat Skin	Intact Flexed Tape-Stripped (10) Abraded	No No- Increase of dots on skin surface No Yes- penetration of QD 655 at 8h and with QD565 at 24h
QD 621nm Neutral	Zhang <i>et al.</i> (2008)	<i>In vitro</i>	Porcine Split-Thickness	Intact	No- In upper stratum corneum and hair follicles
QD 621nm Cationic	Gopee <i>et al.</i> (2009)	<i>In vivo</i>	Mouse Dorsum	Intact Tape-Stripped (5-20) Acetone-Treated Abraded	No No No Yes- viable epidermis, dermis

					and accumulation in liver and lymph nodes
QD 565nm Cationic	Jeong <i>et al.</i> (2010)	<i>In vivo</i> <i>In vitro</i>	Human Volunteers (2) EpiDerm	Intact	No- upper layers of the stratum corneum No- upper layers of stratum corneum
QD 613nm	Gratieri <i>et al.</i> (2010)	<i>In vitro</i>	Human Skin	Intact Massaged Tape Stripped (20)	No No- only affected pattern of distribution on skin surface Yes- small amounts in deeper stratum corneum of fully tape-stripped and 10 minutes flexed skin
Hydrophilic	Seto <i>et al.</i> (2010)	<i>In vitro</i>	Human Full and Split Thickness Porcine Full and Split Thickness	Intact Sonophoresis and SLS	No Yes- Increase in penetration in split-thickness skin
QD Cd/Se Core, Zn/S Shell Neutral, Cationic and Anionic	Lopez <i>et al.</i> (2011)	<i>In vitro</i>	Porcine Skin- Full thickness	Intact Sonophoresis and SLS	Yes- 0.01% of applied dose Yes- 5 to 13 fold increase using follicular route and cavitations
QD 565nm Neutral, Cationic and Anionic	Prow <i>et al.</i> (2012)	<i>In vitro</i>	Human Skin	pH 7.0 pH 8.3 and 9.0 Tape-Stripped (30)	No Yes- QD 565 and QD 655 PEG Yes- All dots found in upper dermis at 24h

QD 800 nm Anionic	Lee <i>et al.</i> (2013)	<i>In vitro</i>	Nude Mice	Intact Laser irradiation (4 mJ)	No- In outermost stratum corneum No- Increased amounts in stratum corneum and hair follicles
QD 620nm Anionic	Mortensen <i>et al.</i> (2013)	<i>In vivo</i>	Nude Mice	Intact Ultraviolet irradiation	No- Penetration into furrows and hair follicles Yes- In-frequently found in stratum corneum of damaged skin

spreading and total amount retained had increased (Zhang and Monteiro-Riviere, 2008, Gratieri *et al.*, 2010). Quantum dots are often supplied in alkaline vehicles (e.g. pH 8-9). When quantum dot nanoparticles were applied to the skin surface at a pH of 8.3 and 9.0, penetration of these particles was seen to the level of the stratum granulosum in human skin and into the dermis of porcine skin (Prow *et al.*, 2012, Ryman-Rasmussen *et al.*, 2006). These data indicate that skin absorption of nanoparticles may occur when the skin barrier is disrupted. When the barrier was disrupted through active means (e.g. sonophoresis, SLS, etc.) quantum dot nanoparticles of different sizes and charges were seen in the dermis (Paliwal *et al.*, 2006, Lopez *et al.*, 2011, Seto *et al.*, 2010, Lee *et al.*, 2013).

Ultraviolet (UV) irradiation can also lead to damage of the skin barrier layer. This environmental stressor is particularly relevant to certain types of sunscreens which contain nanoparticles, as these are intended for use during UV skin exposure. Following UV exposure (360 mJ cm^{-2}), QDots were sometimes found within the damaged areas of the stratum corneum where there was disorganisation of the corneocyte and lipid bilayer, allowing for looser junctions and alterations in the shape and morphology of the cells (Mortensen *et al.*, 2013).

Interestingly, following using UV skin irradiation *in vivo*, barrier disruption lead to significant increases in liver levels of cadmium in treated mice following exposure to quantum dot nanoparticles (Mortensen *et al.*, 2013).

Abraded skin has also been shown to allow the penetration of QDots to the level of the dermis after 8-24 hours (Zhang and Monteiro-Riviere, 2008, Gopee *et al.*, 2009). The penetration of the dots into the viable epidermis and dermis led to accumulation of cadmium in the liver and lymph nodes of mice (Gopee *et al.*, 2009). In contrast,

skin that was tape-stripped presented with a large variation in penetration, with either a lack of penetration or penetration into the upper layer of the dermis (Gratieri *et al.*, 2010, Zhang and Monteiro-Riviere, 2008, Gopee *et al.*, 2009, Prow *et al.*, 2012). Tape-stripping is known to be a highly variable procedure and as such, the actual amount of stratum corneum removed may be inconsistent, thereby leading to variation in percutaneous absorption.

When quantum dots were injected transdermally, the dots were found in the capillaries of the skin and the regional lymph nodes (Larson *et al.*, 2003, Kim *et al.*, 2004). These particles were mapped as travelling from the injection sites through the lymphatic system and finally to regional lymph nodes (Gopee *et al.*, 2007). Transport mechanisms to the lymph nodes were likely macrophages and dendritic (Langerhans) cells (Ohl *et al.*, 2004, Sato *et al.*, 1998). It is thought that the quantum dot nanoparticles could be expelled from the body before the breakdown of the outermost polymer coating occurred, allowing the body protection from the cadmium core (Larson *et al.*, 2003). However, other studies have demonstrated a time-dependent loss of cadmium from injection sites and subsequent deposition in the liver, regional draining lymph nodes, kidney, spleen and hepatic lymph nodes after injection of QDots (Gopee *et al.*, 2007). Kulvietis *et al.* (2013) demonstrated that, after subcutaneous injection in mice, dots were found in the dermis, hypodermis and muscle tissue. The basement membrane prevented upwards movement of these dots into the epidermal layers.

1.5.2.4 Systemic Distribution Of Nanoparticles

The rise in products incorporating nanotechnology has not been concurrently followed by the corresponding risk assessment of these products to human health and

the environment. If it is possible for nanoparticles to enter and distribute through the body, an understanding of accumulation or excretion of these particles needs to be determined.

Proteins are known to adsorb onto the surface of nanoparticles, creating a structure referred to as a 'protein corona'. It is thought that different proteins, when attached to the surface of a nanoparticle, can facilitate uptake into cells by active transport (Lynch *et al.*, 2007). It has been argued that it is the amount and type of proteins making up the corona that evoke a biological response and not the physicochemical properties of the nanoparticle itself (Lynch *et al.*, 2007). Blood protein coronas are especially durable and, when coming into contact with a cellular membrane, it is the protein that signals cellular uptake (Walczyk *et al.*, 2010). The proteins in the outer layer of the corona are slowly exchanged and it is believed that as the nanoparticle-corona complex is transported throughout the body, the proteins change (Walczyk *et al.*, 2010). Different proteins are thought to influence differential uptake by specific target organs (Walczyk *et al.*, 2010). As nanoparticle and associated protein corona move within the body, it is thought these particles will reach areas of the body not possible by just the nanoparticle itself (Walczyk *et al.*, 2010).

The dermal penetration and body distribution of titanium dioxide (TiO₂) nanoparticles has been reported following dermal exposure of mice, as well as induction of delayed pathological lesions in major organs two months after exposure (Wu *et al.*, 2009). The TiO₂ particles (21 nm) were found in the brain with no accompanying pathological lesions. However, the skin and the liver displayed severe pathological changes along with excess superoxide dismutase (SOD) and

malondialdehyde (MDA) levels which are associated with oxidative stress (Wu *et al.*, 2009a)

The size and charge of QDot nanoparticles was found to affect elimination of these particles from the body as zwitterionic and neutral coatings prevented adsorption of serum proteins and allowed for excretion due to a size of < 15 nm (Choi *et al.*, 2007). When injected, inert gold nanoparticles were found localised in macrophages, Kupffer liver cells, spleen, small intestine and mesenteric lymph node macrophages, possibly through endocytosis (Sadauskas *et al.*, 2007). The ideal size of excretion has been debated with the size of < 5.5 nm resulting in the rapid and efficient clearance and elimination from the body by macrophages as well as filtration by the renal glomeruli (Sadauskas *et al.*, 2007).

1.6 Summary

The skin is the first line of defence against the ingress of xenobiotics and a plethora of *in vitro* and *in vivo* techniques have been developed to characterise, assess, measure and elucidate the mechanisms of dermal absorption.

Nanoparticles, in particular, present a contemporary risk to humans. However, an *in vitro* skin exposure model which offers an improvement on the current, static skin system is needed to fully elucidate the dermal hazard of nanoparticles. A flexing skin system is required to provide additional energy for translocation of particles which, under normal circumstances, would be physically excluded by their size. Moreover, a flexing skin system would provide a more practically relevant model for testing topical skin protectants, as the current (static skin) models cannot reproduce the effects of normal skin movement which may affect the patency of topical application.

Therefore, the aims of this Thesis were:

- To produce a novel *in vitro* diffusion cell (CutaFlex™) capable of producing reproducible flexion
- To assess the dermal absorption of reference compounds measured with CutaFlex™ compared to the standard OECD-compliant Franz-type cell.
- To characterise the effects of flexing on skin barrier function after chemical and physical damage of the skin barrier layer.
- To characterise the effect of *in vitro* skin flexing on performance of a skin barrier cream.
- To assess the effect of skin flexing on the dermal absorption of quantum dot nanoparticles of different sizes, shapes and charges.

Chapter 2: General Methods

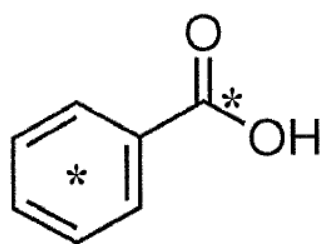
2.1. *In Vitro* Dermal Absorption Studies

2.1.1. Chemicals

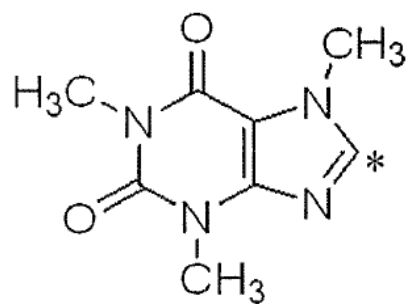
Tritiated water ($^3\text{H}_2\text{O}$) was purchased from American Radiolabelled Chemicals (ARC) U.K. Ltd. (St. Louis, U.S.A.) with a specific activity of 1 mCi ml^{-1} and was mixed with deionised water (dH_2O : obtained from the municipal water supply via a MilliQ Direct Q5 purification system, Watford, U.K.) to achieve a stock solution with a nominal activity of $0.0023 \text{ } \mu\text{Ci } \mu\text{l}^{-1}$.

Carbon-14 radiolabelled “model compounds” benzoic acid, caffeine and testosterone were purchased from ARC U.K. Ltd with specific activities of $165 \text{ mCi mmol}^{-1}$, 55 mCi mmol^{-1} and 55 mCi mmol^{-1} , respectively (Figure 2.1). Unlabelled benzoic acid, caffeine and testosterone were purchased from Sigma Aldrich (Gillingham, U.K.) and were reported to be more than 99% pure. The saturated solubility of each chemical in aqueous ethanol (22 ml) at 32°C was determined¹ to be 90, 84 and 10 mg ml^{-1} for benzoic acid, caffeine and testosterone, respectively. To maintain the specific activity of each chemical solution, the equilibrium between dissolved to undissolved chemical had to be identical for both the radiolabelled and cold chemical. Therefore, equilibrated, unfiltered saturated solutions were prepared by mixing appropriate amounts of ^{14}C -radiolabelled and unlabelled model compounds to achieve stock solutions with a nominal activity of $0.0113 \text{ } \mu\text{Ci } \mu\text{l}^{-1}$. Prior to dosing each chemical onto the skin surface, the radioactive stock solution was cooled to 0°C (using ice) and heated to 40°C (using heat blocks) and cycled 5 times (thermo-cycling) with rigorous stirring between each step. The solutions were then dosed onto the skin surface at 32°C . All suspensions were then stored at 5°C until further usage.

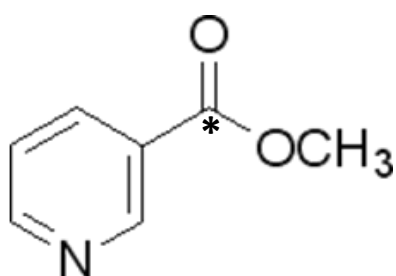
¹Solubility was determined by UV absorption spectroscopy using an appropriate range of calibration standards.



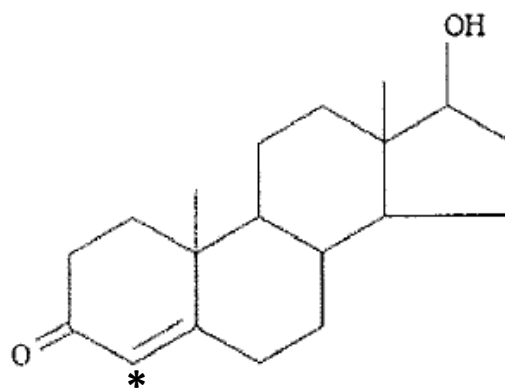
Benzoic Acid



Caffeine



Methyl Nicotinate



Testosterone

Figure 2.1: Radiolabelled Carbon-14 Benzoic Acid, Caffeine, Methyl Nicotinate And Testosterone. The position of the carbon-14 isotope is indicated in each compound by an asterisk (*).

Ring-labelled ^{14}C - methyl nicotinate was purchased from ARC as a dry powder with a specific activity of 55 mCi mmol^{-1} (Figure 2.1). Non-radioactive methyl nicotinate (MN) was reported to be more than 99% pure and was purchased from Sigma-Aldrich (St. Louis, U.S.A.). A working solution of ^{14}C -methyl nicotinate was prepared using 0.624 mg of radiolabelled methyl nicotinate supplemented with 1.09 mg of non-radioactive methyl nicotinate in distilled water to achieve a 5 mM solution with a nominal activity of $0.1 \mu\text{Ci } \mu\text{l}^{-1}$.

Ultima Gold™ liquid scintillation cocktail and Soluene® - 350 tissue solubiliser were purchased from PerkinElmer (Waltham, U.S.A.). Phosphate buffered saline tablets, sodium lauryl sulphate, 10% neutral buffered formalin (NBF), Harris' haematoxylin solution and eosin Y alcoholic solution were ordered from Sigma-Aldrich (St. Louis, U.S.A.). Phosphate buffered saline solution was prepared by adding 1 tablet to 200 ml of distilled water. Absolute ethanol, propan-2-ol (isopropyl alcohol), xylene, 1M hydrochloric acid and paraffin wax pellets were purchased from Fisher Scientific (Loughborough, U.K.). Absolute ethanol was diluted 50:50 with distilled water to produce a 50% aqueous ethanol solution.

QTracker® quantum dot nanoparticles were purchased from Molecular Probes, Invitrogen Corp. (Carlsbad, U.S.A.). QTracker® 565 and 655 nm PEG-Amine and PEG-Carboxyl quantum dots were supplied as $8 \mu\text{M}$ in $250 \mu\text{l}$ borate buffer. QTracker® 565 and 655 nm PEG coated quantum dots were supplied as $2 \mu\text{M}$ in $200 \mu\text{l}$ borate buffer. Both the PEG-Amine and PEG-Carboxyl quantum dots were diluted 1:7 and the PEG quantum dots by 1:2 using phosphate buffered saline to achieve a working solution of $1 \mu\text{M}$ at a pH of 7. All quantum dots were originally supplied in borate buffer, but were diluted using phosphate-buffered saline as it was confirmed

to have little or no effect on size or stability of the nanoparticle suspension (Invitrogen Corp, private communication). Immediately prior to each study, nanoparticle suspensions were subjected to cuphorn sonication at 12.7 kJ using an S-4000 sonicator purchased from Misonix (Farmingdale, U.S.A.).

White pearl bactericidal hand cleaning and caring lotion was purchased from DYSYS Chemical Systems (Baltinglas, Ireland). The topical skin protectant (barrier cream) “RD-1433” was provided by BRACCO Diagnostics Ltd and was reported to be of clinical research grade and so in compliance with the MHRA requirements in Annex I of the Council Directive 93/42/EEC of 1993 concerning medical devices (European Commission, 1993). Vaseline[®] petroleum jelly was obtained from a local pharmaceutical retailer. The density of each product was measured before study² and determined as 2.24 g cm⁻³ for RD-1433 and 0.95 g cm⁻³ for Vaseline[®].

2.1.2. Skin Preparation

Full thickness porcine skin was obtained post-mortem from female pigs (*Sus scrofa*, large white strain, 3 months of age and weight approximately 25 kg) purchased from a reputable supplier. Pigs were euthanised using a captive bolt. Skin was close clipped prior to removal from the dorsal aspect of each animal, after which all sections were wrapped in aluminium foil and stored flat at -20°C for up to 3 months before use. Skin was defrosted for approximately 24 hours at 5°C and dermatomed to a thickness of 500 µm using a Humecca D42 dermatome purchased from EuroSurgical Ltd. (Guildford, U.K.) before each study. Skin thickness was confirmed using a digital micrometer purchased from Tooled-Up (Middlesex, U.K.). Dermatomed skin

² The density of each product was calculated from weighing a known volume (1 ml) of product.

was then cut into squares measuring approximately 3 x 3 cm in preparation for mounting into diffusion cells.

2.1.3. Diffusion Cells

Static (Franz-type) glass diffusion cells were purchased from PermeGear (Hellertown, U.S.A.) and were of the horizontal, glass-jacketed variety (Figure 2.2- A) with an available surface area of 1.77 cm² and receptor chamber volume of approximately 14 ml. The flexing skin system (CutaFlex™) was based upon a modification of the standard Franz cell and was manufactured by BM Injections (Winchester, UK). The modified cells were constructed from inert (PTFE) plastic and incorporated a bifurcated receptor sampling arm (Figure 2.2- B). The upper arm was modified to accommodate a removable air-tight cap. The lower arm accommodated a latex bladder which was connected to an external Watson-Marlow 520Di peristaltic pump (Falmouth, U.K.), controlled by bespoke software provided by Watson-Marlow (v1.0) which allowed for timed control of the pump (to control inflation/deflation of the latex bladder).

After mounting the skin sections and clamping the donor chamber in place, the receptor chamber in each (static and CutaFlex™) diffusion cell was filled with either 50% (v/v) aqueous ethanol or phosphate buffered saline as appropriate. The assembled diffusion cells were then placed in a metal chamber (Figure 2.3) on a magnetic stirrer, which mixed the receptor chamber fluid via two (12 x 6 mm) Teflon™ coated iron stir bars placed in each receptor chamber. The jacket of each diffusion cell was connected to a Grant Instruments GD120 (Cambridge, U.K.) recirculating water heater via the diffusion cell manifold (Figure 2.3) in order to ensure a skin temperature of approximately 32°C ± 1°C (as confirmed using infrared

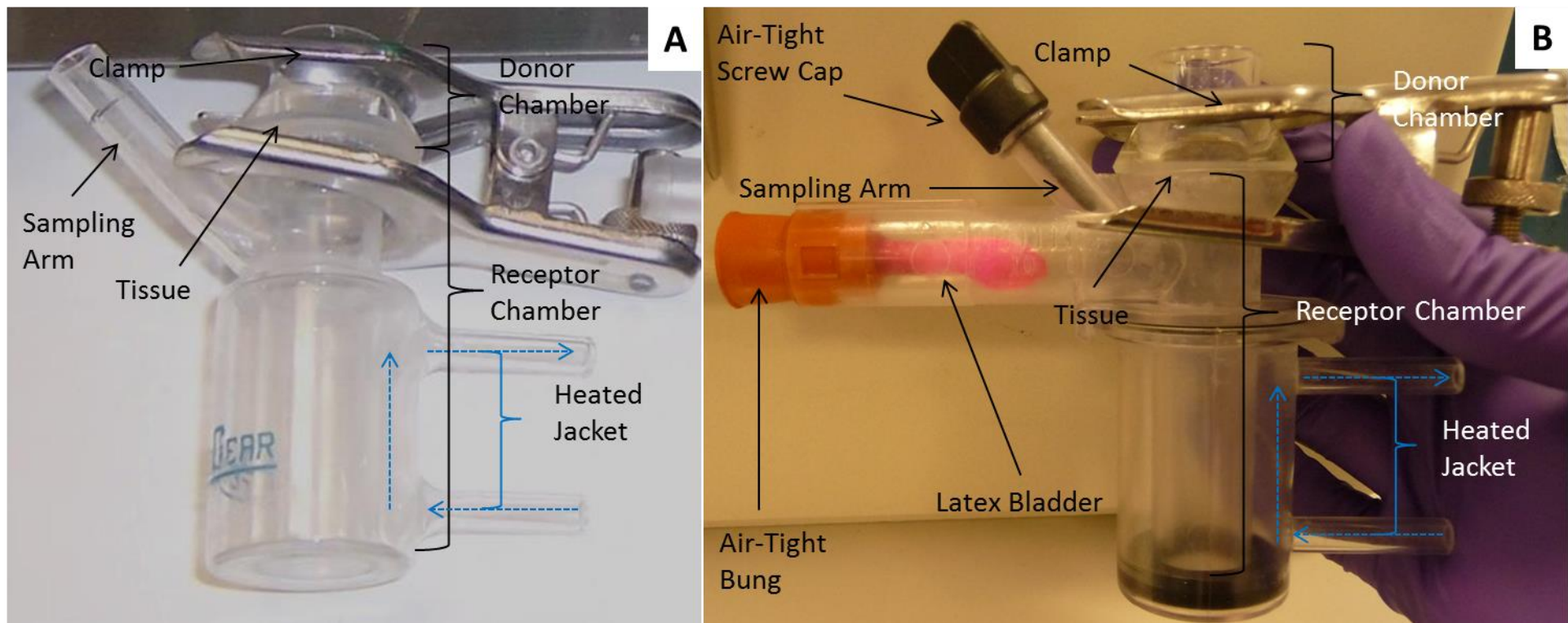


Figure 2.2: Two *In Vitro* Diffusion Cells Used For Percutaneous Penetration Testing: Franz-Type (A) and CutaFlex™ (B). The Franz-type (Left) static diffusion cell is comprised of a donor chamber (application of penetrant under study); receptor chamber (collection of penetrant that passes through membrane); skin section (clamped between the two chambers); sampling arm for removing aliquots of receptor fluid and a heated jacket to keep the skin at a constant temperature. CutaFlex™ is a novel flexing diffusion cell based upon the OECD-compliant Franz-type cell and consists of a latex bladder attached to an air-tight bung which is connected to a peristaltic pump; an air-tight screw cap seals the sampling arm of which receptor fluid samples are taken; a donor chamber; skin section; receptor chamber and a heated jacket (Viegas, 2014).



Figure 2.3: Diffusion Cell Apparatus Comprising Peristaltic Pump, Diffusion Manifolds Containing Franz-Type And CutaFlex™ Diffusion Cells And Re-Circulating Heated Pump. The peristaltic pump operated through the use of computer software, to inflate the latex bladder in CutaFlex™ cells. Both Franz-type and CutaFlex™ cells sat in metal chambers in the diffusion manifolds on top of stir blocks, in order to ensure constant mixing of receptor fluid contents. The re-circulating heated pump was connected to the diffusion cells via the diffusion manifold and ensured constant temperature of the skin within the cells (Viegas, 2014).

imaging; FLIR Model P620 Camera, Cambridge, U.K.). Diffusion cells were subsequently left to equilibrate overnight (minimum period of 12 hours) before use.

Skin deflection in the CutaFlex™ diffusion cell was driven by air displacement generated by the peristaltic pump under controlled parameters (Figure 2.4). Peristaltic pump tubing with a bore size of 2.54 mm (internal diameter) was purchased from Scientific Laboratory Supplies (Wilford, U.K.) to connect the peristaltic pump directly to the latex bladders in each cell. Gauze inserts were not used under the skin in the CutaFlex™ or Franz-type diffusion systems (as this would prevent concave flexing).

Skin deflection height was measured using a custom-made laboratory apparatus that sat on top of the skin surface and contained a piston with a ruler displaying millimetre markings. Characterisation of skin flexion height was performed using six CutaFlex™ cells and repeated approximately three times per cell. For the displacement of air as facilitated by the peristaltic pump, twelve revolutions per minute was the chosen speed for both forward (upwards) movement of 14 seconds and reverse (downwards) movement of 13 seconds. These values led to approximately 2 flexes per minute. Each diffusion cell was filmed for flexion using a digital camera, with both the start and end position of the top of the piston manually recorded. It was found that the maximum average of height displacement was approximately 3 millimetres.

Based on the skin deflection height of 6 mm, volume displacement within the receptor chamber was calculated using the formula below:

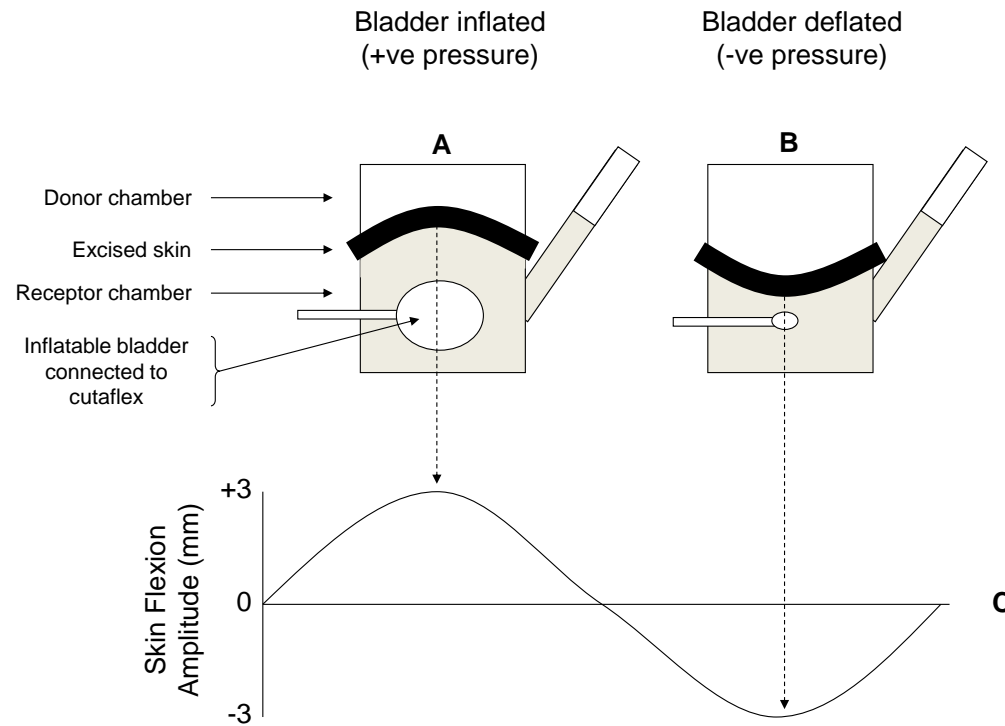


Figure 2.4: Schematic Representation Of CutaFlex™ Skin Flexion. Air is introduced through the latex bladder via a peristaltic pump controlled using bespoke programmable computer software. The increase in air leads to an expansion of the latex bladder which displaces receptor fluid within the air-tight diffusion cell. The displacement of receptor fluid results in stretching of the skin outwards from the diffusion cell (maximum vertical displacement of 3 mm). When air is consequently pulled out of the diffusion cell system, vertical displacement of the skin occurs in the opposite (concave) direction to a maximum displacement of 3 mm (Viegas, 2014).

Equation 2.1

$$V_{dome} = \frac{\pi (3a^2 + h^2)}{6}$$

Where a = 0.75 cm and h = 0.3 cm

Therefore, the volume of receptor fluid being pumped into/out of the receptor chamber to attain a maximum displacement as induced by a vertical displacement height of 6 mm was 279 μl (~ 2% of receptor chamber volume).

2.1.4. Barrier Integrity Testing**2.1.4.1. Transepidermal Water Loss**

Where applicable, an indirect measurement of structural integrity was performed on skin sections in each diffusion cell using an AquaFlux AF 200 closed-chamber evaporimeter with software (AquaFlux version 7.03) purchased from Biox (London, U.K.). The evaporimeter was calibrated prior to each use according to manufacturer's instructions. Briefly, the evaporimeter probe was set to accumulate approximately 0.02 mg of ice and a baseline value was taken after a 30 minute stabilisation period using a closed cap. The cap was then replaced with a measurement cap with an adapter specific for a 1.5 cm diameter donor chamber (used in this study) using a correction factor of 2.1 (applied by the software to account for the increased measurement height from the skin surface). Measurements of TEWL rates were subsequently acquired at equilibrium, defined as a standard deviation of 0.075 $\text{g m}^{-2} \text{h}^{-1}$ over a 5 second time period (as per manufacturer's instructions).

2.1.4.2. Tritiated Water Permeability Testing

Where applicable, the structural integrity of skin samples was measured directly using a modification of the "twenty minute test" (Bronaugh *et al.*, 1986). Briefly, an

aliquot (250 μl) of fluid was removed from each receptor chamber prior to the addition of 442.5 μl of $^3\text{H}_2\text{O}$ working solution (2.3 nCi μl^{-1}) to the skin surface (occluded) of each donor chamber (equating to a dose of 250 mg cm^{-2}). A second aliquot (250 μl) of each receptor fluid was taken 30 minutes after application of the $^3\text{H}_2\text{O}$. In both cases, the receptor fluid was replenished with fresh PBS solution (250 μl) in order to ensure the volume of each chamber was kept constant. Aliquots were placed into vials containing 5 ml of LSC fluid. Any residual $^3\text{H}_2\text{O}$ was carefully removed from the skin surface with a syringe, followed by a wet swab and a dry swab of the skin surface. Standard solutions were prepared on the day of each experiment by addition of 100 μl of $^3\text{H}_2\text{O}$ to (a) cotton wool swabs and (b) unexposed skin tissue dissolved in 10 ml of Soluene-350. Each standard solution was prepared in triplicate and was subjected to an identical sampling regime of 250 μl aliquots into vials containing 5 ml of LSC fluid. A standard receptor chamber solution was prepared in triplicate by the addition of 442.5 μl of $^3\text{H}_2\text{O}$ working solution to 557.5 μl of fresh receptor fluid (phosphate buffered saline solution) from which a range of triplicate samples (25, 50, 75 and 100 μl) were taken and placed into vials containing 5 ml of LSC scintillation to produce a standard (calibration) curve. All vials were then subject to liquid scintillation counting as described in Section 2.3.1.

2.1.5. Standard Penetrant Studies

2.1.5.1. Bladder Adherence Studies

An aliquot (442.5 μl) of either $^3\text{H}_2\text{O}$ or Carbon-14 chemical working solution was added to either 13.6 ml or 16 ml of PBS or 50% aqueous ethanol, in a Franz-type or CutaFlex™ receptor chamber. Receptor chambers were then sealed using Parafilm® and aliquots (250 μl) of receptor fluid were withdrawn from each diffusion cell at

regular intervals for up to 8 hours (tritiated water) or 51 hours (Carbon-14 chemicals). Each aliquot was placed into a vial containing 5 ml of liquid scintillation counting fluid. Each receptor chamber was then replenished with an equivalent volume (250 μ l) of fresh fluid to maintain constant volume after each sample was removed. After each study, the latex bladders were removed from each CutaFlex™ cell and placed into vials containing 20 ml of absolute ethanol and aliquots (250 μ l) were taken after 1 week and placed into vials containing 5 ml of LSC fluid. Standard calibration solutions were prepared as described in Section 2.1.4.2. All aliquots were subject to liquid scintillation counting as described in Section 2.3.1.

2.1.5.2. Tritiated Water Dermal Absorption Studies

Each experiment was initiated by the addition of 442.5 μ l (250 mg cm⁻²) ³H₂O working solution to the skin surface (occluded) in each donor chamber. Franz-type and CutaFlex™ diffusion cells (flexed for 0, 30, 60, 90, 120, 240, 360 and 480 minutes) were tested for tritiated water permeability, with 9 diffusion cells per group. Samples of receptor fluid (250 μ l) were withdrawn from each diffusion cell at regular intervals up to 9 hours post-exposure and were placed into vials containing 5 ml of liquid scintillation counting fluid. Each receptor chamber was topped up with an equivalent volume (250 μ l) of fresh fluid to maintain a constant volume in the receptor chamber. Standard calibration solutions were prepared as previously described in Section 2.1.4.2. Aliquots (250 μ l) of each sample (i.e. swabs, skin and receptor fluid) were placed into vials containing 5 ml of LSC and subject to liquid scintillation counting (Section 2.3.1).

2.1.5.3. Carbon-14 Benzoic Acid, Caffeine and Testosterone Studies

Skin Partition Coefficients

Skin partition coefficients of benzoic acid, caffeine and testosterone were determined in triplicate: Dermatomed skin sections were weighed and then placed into separate vials containing 557.5 μl of 50% aqueous ethanol. An aliquot (442.5 μl) of each Carbon-14 working solution was added to a vial containing the skin section, which was then exposed for 3 days at $32^\circ\text{C} \pm 1^\circ\text{C}$ with occasional stirring. Sections were then removed, blotted and briefly rinsed with 50% aqueous ethanol. Each section was then added to a vial containing 5 ml of Soluene-350. After two weeks, aliquots (250 μl) were removed from each skin sample and analysed through liquid scintillation counting as described in Section 2.3.1.

Dermal Absorption Studies

An aliquot (250 μl) of fluid was removed from each receptor chamber prior to the addition of 442.5 μl ($0.113 \mu\text{Ci } \mu\text{l}^{-1}$) of either ^{14}C -benzoic acid, caffeine or testosterone to the skin surface (occluded) of each donor chamber. Samples of receptor fluid (250 μl) were withdrawn from each diffusion cell at regular intervals up to 51 hours post-exposure and were placed into vials containing 5 ml of liquid scintillation fluid. Each receptor chamber was replenished with an equivalent volume (250 μl) of 50% aqueous ethanol to maintain a constant volume in the receptor chamber. After 51 hours, any remaining ^{14}C -chemical was removed from the skin surface using a wet swab followed by a dry swab (repeated twice) which were each placed into vials containing 20 ml of absolute ethanol. After two weeks (with occasional shaking), aliquots (250 μl) were removed and placed into vials containing 5 ml of liquid scintillation counting fluid. Skin samples were removed from diffusion cells and placed into vials containing 10 ml of Soluene-350 for two weeks, after

which aliquots (250 µl) were taken from each sample and placed into vials containing 5 ml of LSC fluid.

Standard solutions were prepared on the day of each experiment by addition of 221 µl of relevant ¹⁴C-chemical to (a) 6 cotton wool swabs in 20 ml of absolute ethanol and (b) un-exposed skin tissue dissolved in 10 ml of Soluene-350. Each solution was prepared in triplicate and was subjected to an identical sampling regime of 250 µl aliquots into vials containing 5 ml of LSC fluid. A standard receptor chamber solution was prepared in triplicate by the addition of 442.5 µl of ¹⁴C-chemical working solution to 557.5 µl of fresh receptor fluid (50% aqueous ethanol) from which a range of triplicate samples (25, 50, 75 and 100 µl) were taken and placed into vials containing 5 ml of LSC scintillation to produce a standard (calibration) curve. All vials were then subject to liquid scintillation counting as described in Section 2.3.1.

Representative sections (3) from each treatment group were taken for autoradiography by the Typhoon FLA 7000 Typhoon System (GE Healthcare; Amersham, U.K.). After analysis, skin samples were placed into 5 ml of Soluene-350 for two weeks, after which aliquots (250 µl) were placed into vials containing 5ml of LSC fluid. All vials were then subject to scintillation counting.

Surface Spreading Of Carbon-14 Chemicals Visualised Using Autoradiography

Representative carbon-14 treated skin samples as well as skin blanks were stored in a Kodak exposure cassette at -70°C until autoradiography was performed. Samples were defrosted at room temperature on the day of analysis. The re-usable exposure film was first wiped clean for 15 minutes using white light and read on the Typhoon system in order to ensure no residual signal was present from the previous use. The

exposure cassette was then lined with cellophane onto which the skin samples were placed. A layer of cellophane was then placed over the surface of all skin samples, to protect the exposure film from direct contact and the exposure cassette was then exposed to the skin in the dark for 3 hours at room temperature. After 3 hours, the film was removed from the exposure cassette and placed into the Typhoon system. The system was calibrated for the photomultiplier tubes set at 800 units, a resolution of 25 μ M, latitude of L5 and a mode for a large film (20 x 40 cm). After the images were taken, the skin was dissolved in Soluene-350 and analysed using scintillation counting. All autoradiographs were subsequently analysed using public domain software (Image J, National Institute of Health, Version 1.74) to quantify intensity per unit area values, after which all treatment groups were compared to a non-treated control.

2.1.6. Skin Damage Studies

The purpose of these experiments was to compare the effects of skin damage between un-flexed and flexed skin. Skin damage was quantified by measurements of TEWL rates and $^3\text{H}_2\text{O}$ permeability (Section 2.1.4) performed before and after skin damage. Standard solutions were prepared as previously described in Section 2.1.4.2.

2.1.6.1. Phase I: Baseline Studies

The initial studies were performed to determine baseline values of tritiated water and transepidermal water loss (TEWL) before and after flexion of the skin in the absence of damage. Briefly, transepidermal water loss and tritiated water measurements were taken both before and after skin flexion for 0, 30, 60, 90 or 120 minutes (Figure 2.5-I).

2.1.6.2. Phase II: Chemical Damage (Sodium Lauryl Sulphate)

After initial measurements of transepidermal water loss and tritiated water permeation, a solution of 5% (v/v) SLS was applied to the skin at 442.5 μl (250 $\mu\text{l cm}^{-2}$) for a duration of 1 hour³. The SLS solution was then removed and the skin was swabbed with a wet and dry cotton swab (repeated in triplicate) to remove any residual SLS. After SLS removal, the diffusion cells were then flexed (or remained un-flexed) for up to two hours after which final TEWL and tritiated water measurements were taken (Figure 2.5- II).

2.1.6.3. Phase III: Physical Damage

Initial measurements of both transepidermal water loss and tritiated water permeation were taken before each piece of skin was punctured twice *in situ* (centrally) using a 25 gauge hypodermic needle and were then flexed (or remain static) for up to two hours after which a second set of TEWL and tritiated water measurements were taken (Figure 2.5- III) .

³ One hour was deemed the minimum time to produce significant skin damage in a series of pilot studies (data not shown).

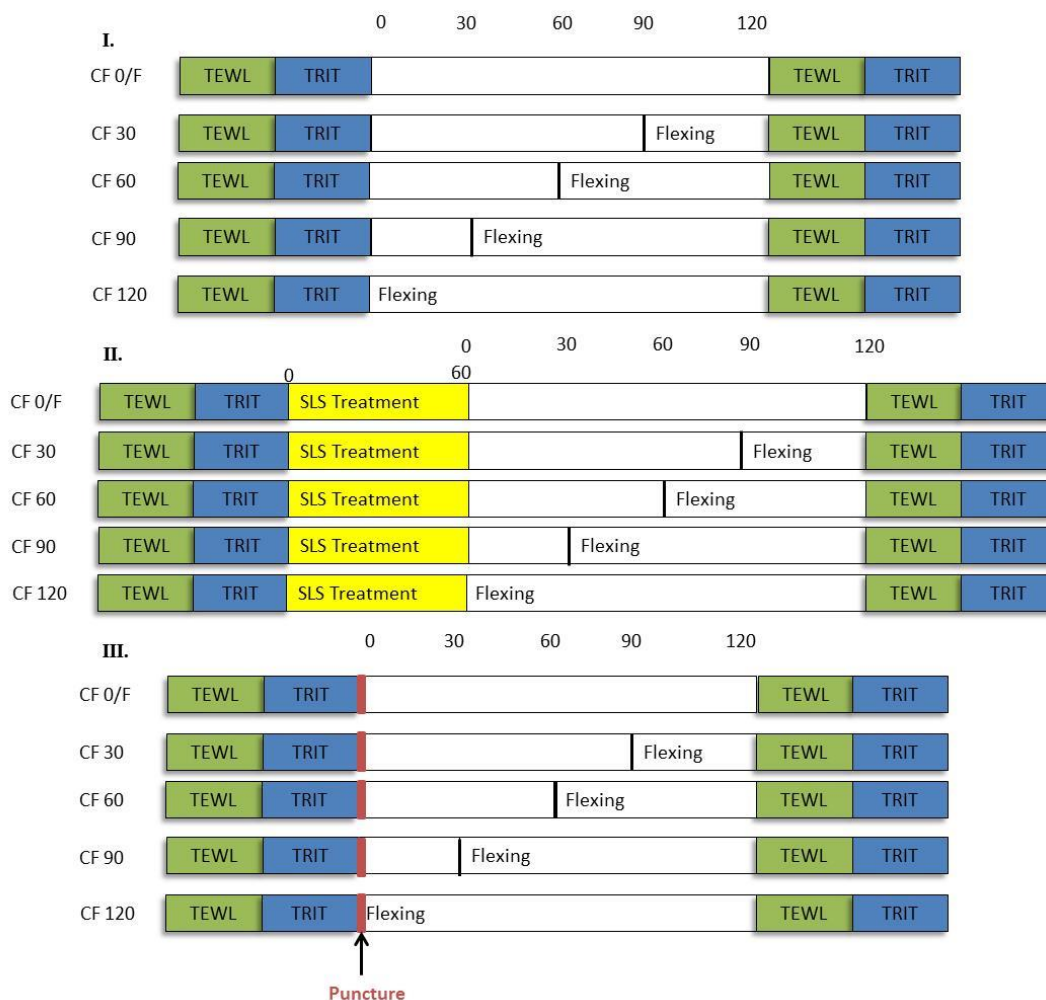


Figure 2.5: Skin Damage Study Design: Baseline And Flexing Study Outline (I), Chemical Damage Study Outline (II) And Physical Damage Study Outline (III). Tritiated water permeability and transepidermal water flux measurements were used to assess barrier integrity. Both Franz-type cells (F) and CutaFlex™ (CF) diffusion cells were tested in either static (0) or flexing (30-120 minutes) conditions. The first phase of study evaluated the effect of flexing on skin integrity. The second set of studies assessed chemical damage (using sodium lauryl sulphate) of the skin when using flexing. The last phase of study assessed the effect of physical damage (punctures) of the skin when using flexing.

2.1.7. Quantum Dot Nanoparticle Characterisation

2.1.7.1. *Transmission Electron Microscopy (TEM)*

Aliquots (20 μ l) of each quantum dot nanoparticle working suspension were applied to a standard carbon-mesh TEM grid purchased from Agar Scientific (Standsted, U.K.) and left to dry at room temperature. Samples were then hand delivered to BegbrokeNano (Yarnton, U.K.) for analysis⁴. Nanoparticle morphology and size were determined using a JOEL analytical TEM with a LaB6 electron gun with an accelerating voltage of 200 kV. Energy-dispersive x-ray analysis (EDX) was simultaneously performed to confirm elemental presence of analysed nanoparticles.

2.1.7.2. *Dynamic Light Scattering*

An aliquot (50 μ l) of each quantum dot working suspension was placed into small volume (40 μ l) cuvettes and characterised for median peak size (number-based) as well as overall distribution size and polydispersity index at 25°C using a Zetasizer NS purchased from Malvern (Malvern, U.K.). Each measurement was determined from up to 17 runs and a final average recorded from five replicates.

2.1.8. Dermal Absorption Of Nanoparticles

An indirect measurement of structural integrity was performed on skin sections in each diffusion cell using an evaporimeter to determine transepidermal water loss flux (Section 2.1.4.1). An aliquot (300 μ l) of quantum dot suspension (1 μ M) was applied to the skin surface of each donor chamber (occluded) for 8 hours. Excess quantum dot nanoparticle solution was removed from the skin surface of each diffusion cell by a dry swab followed by a wet swab, which were both placed into vials containing 20 ml of distilled water. An equilibration time of one hour was observed before the final set of transepidermal water loss measurements in each diffusion cell. After TEWL

⁴ TEM analysis was performed by BegbrokeNano-Oxford Materials Characterisation Service.

measurements were completed, skin sections were taken for visualisation of residual skin surface fluorescence using UV-light as further described in Section 2.1.10. Skin sections were then dehydrated for eventual embedding in paraffin wax and further analysis through H&E staining and laser scanning confocal microscopy as further described in Section 2.1.11.2 and 2.1.12, respectively. Receptor fluid from each diffusion cell, 14 or 16.4 ml for Franz or CutaFlex[™] cells, respectively, was decanted into vials for further analysis through fluorescence spectrophotometry (Section 2.1.9).

2.1.9. Fluorimeter Analysis Of Skin Surface Swabs And Receptor Fluid

Aliquots (3 ml) of skin swab and receptor fluid samples from each diffusion cell were analysed in triplicate for fluorescence intensity using a Cary Eclipse fluorescence spectrophotometer purchased from Agilent (Santa Clara, U.S.A.). An excitation wavelength of 488 nm was chosen with an emission wavelength of either 565 or 655 nm were used for the relevant dots. A standard solution was prepared using aliquots of 2, 4, 8 and 10 μ l of each 1 μ M quantum dot suspension placed into 20 ml of distilled water. Each standard was analysed in triplicate to construct a calibration curve.

2.1.10. UV-Light Box Images Of Skin Surface

Skin sections were placed into a bespoke light box which utilized 4 arrays of 16 LED light bulbs. A Canon EOS 60D digital camera with UV-filter was calibrated with an ISO speed of 1600, shutter speed of 0.2 seconds and an aperture of 5.6. All quantum dot treatment groups were paired with non-treated controls. Each image was analysed using ImageJ (v1.74) to obtain an intensity value per unit area. Each skin section was then compared to an un-treated control.

2.1.11. Histology

2.1.11.1. *Paraffin Embedding*

All skin sections were fixed overnight in 10% neutral-buffered formalin (NBF). Skin was then transferred through the steps outlined in Table 2.1, for dehydration leading to paraffin embedding using a Citadel 2000 tissue processor (ThermoFisher; Waltham, U.S.A).

Molten paraffin wax was poured into 10 ml embedding moulds containing skin sections and allowed to set overnight. The paraffin wax blocks were cut on a Shandon™ Finesse 325 manual microtome (ThermoFisher; Waltham, U.S.A.) into 5 µm sections, through the dermal tissue upwards⁵. Sections were floated on a 45°C water bath to smooth out any wrinkles and mounted onto lysine (positively) coated microscope slides (VWR International; Lutterworth, U.K.). The paraffin wax sections were then baked onto the slides overnight in a 40°C oven. Slides were then loaded into a slide rack and re-hydrated using the steps outlined in Table 2.2.

⁵ This tissue orientation was used to prevent QDot particle translocation from the skin surface through the skin. The microtome blade was cleaned after each section was cut from the paraffin block.

Table 2.1: Skin Processing Schedule For Paraffin Wax Embedding. Skin was progressively dehydrated through graded steps of ethanol (EtOH). Xylene steps were used to displace ethanol in order for wax embedding. Total processing time was 12 hours, after which skin sections were manually embedded into paraffin wax blocks.

Concentration	Duration
70% EtOH	1 h
95% EtOH	1 h
100% EtOH	1 h
100% EtOH	1.5 h
100% EtOH	1.5 h
Xylene	2 h
Xylene	1 h
Xylene	1 h
Wax	1 h
Wax	1 h

Table 2.2: Skin Re-Hydration Schedule For H&E Staining Or Confocal Microscopy Analysis. After sectioning of paraffin blocks, paraffin skin sections on slides were passed through xylene and ethanol (EtOH) steps leading to either H&E staining or confocal analysis.

Concentration	Duration
Xylene	10 min
100% EtOH	6 min
95% EtOH	3 min
70% EtOH	3 min

2.1.11.2. *H&E Staining*

Harris' haematoxylin solution was filtered before each use. A 0.25% v/v hydrochloric acid in 70% ethanol solution was used for differentiation of the haematoxylin stain. Tissue dehydration into H&E stain and subsequent rehydration steps were followed for 5 μ m skin sections for each quantum dot (Table 2.3).

All resulting H&E stained skin sections were imaged using a Leitz LABORLUX 11 purchased from Leica (Solms, Germany) with a 10x (0.25 NA) lens and images were acquired using a Canon PowerShot S5 IS camera with remote shooting software set for an ISO of 800 and tungsten exposure.

Table 2.3: Haematoxylin and Eosin Staining Chart For Quantum Dot Exposed Skin Sections. Skin was re-dehydrated by passing through xylene and a graded series of ethanol steps. Re-hydration was followed by skin staining with Harris' haematoxylin solution after which skin was stained using Eosin Y. Skin was then dehydrated and a coverslip was attached to each slide.

Step	Chemical	Time
1	Xylene	10 min
2	100% Ethanol	6 min
3	95% Ethanol	3 min
4	70% Ethanol	3 min
5	Harris' Haematoxylin Solution	2.5 min
6	Rinse in running tap water	1 min
7	Differentiate in 0.25% HCl in 70% Ethanol	3 dips
8	Rinse in running tap water	1 min
9	95% Ethanol	0.5 min
10	Counterstain in Eosin Y	1 min
11	Rinse in running tap water	0.25 min
12	70% Ethanol	3 min
13	95% Ethanol	3 min
14	100% Ethanol	6 min
15	Xylene	10 min
16	Coverslip	

2.1.12. Laser Scanning Confocal Microscopy

Quantum dots were imaged in exposed skin samples using a C1 confocal laser scanner connected to an Eclipse TE 2000 U inverted fluorescence microscope using a 10x (0.3 NA) Plan Fluor DIC L/N1 dry objective purchased from Nikon (Tokyo, Japan). An Argon-Ion laser was used to excite the quantum dots at a wavelength of 488 nm and a filter-based emission channel of 500-643 nm was used for visualisation. Gain settings for both the red and green channel were set at 100 units. Transmitted light was used to obtain skin structure details. The transmitted light channel gain was set at 37 units. Images were captured using the Nikon EZ-C1 software (Gold version 3.90). Images were chosen at 1024 pixel resolution with each image consisting of an average of 4 laser scans. It should be noted that due to the limited filter settings of the confocal microscope, QDot 565 fluorescence was made to appear red (not green).

2.1.13. *In Vitro* Barrier Cream Efficacy Studies

2.1.13.1. *Evaporation Rate Of ¹⁴C-Methyl Nicotinate And ³H-Water*

Methyl nicotinate working solution was diluted by one third and un-labelled methyl nicotinate was added to achieve a 5 mM working solution (0.033 $\mu\text{Ci } \mu\text{l}^{-1}$). An aliquot (10 μl) of $^3\text{H}_2\text{O}$ stock solution was diluted by one-third to achieve a new working solution (0.033 $\mu\text{Ci } \mu\text{l}^{-1}$). CutaFlex™ diffusion cell groups were used with aluminium foil in the place of skin and heated to 32°C. Following an equilibration time (2h), the aluminium foil in each donor chamber was dosed with either 10 μl of ^{14}C -methyl nicotinate or 10 μl of tritiated water. Aluminium foil was subsequently removed from the manifold at time 0 (control), 5, 10, 15, 20, 30, 45, 60, 90 and 120 minutes after dosing and placed directly into vials containing 5 ml of LSC fluid. Each time-point was replicated in triplicate. A standard calibration solution was

performed in triplicate using aluminium foil dosed with 2, 4, 8 and 10 μl aliquots of working solution and placed into vials containing 5 ml of LSC fluid. All samples were then analysed using scintillation counting as further described in Section 2.3.1.

2.1.13.2. *Optimal Thickness Studies*

Both transepidermal water loss flux and tritiated water measurements relating to skin barrier integrity were performed as previously described in Section 2.1.4. The test products RD-1433 or Vaseline[®] were applied at 3 nominal thicknesses of 0.01, 0.05 and 0.1 mm (1.8, 8.9 and 17.7 μl , respectively) and in addition to an untreated control were assessed (6 diffusion cells per group) for ¹⁴C-methyl nicotinate penetration (Figure 2.6- I). Test products were uniformly spread onto the treated or untreated skin surface using a pre-weighed glove tip after which the glove tip was weighed again, for an estimation of product delivery. Studies were initiated by placing an aliquot (10 μl) of ¹⁴C-labelled methyl nicotinate onto the treated or untreated skin surface in each donor chamber. Samples of receptor fluid (250 μl) were removed from each diffusion cell at regular intervals for up to 180 minutes and placed into vials containing 5 ml of LSC fluid. Each receptor chamber was replenished with an equivalent volume of fresh fluid to maintain a constant volume. Twenty minutes after exposure, excess methyl nicotinate was removed with a cotton bud which was immersed in 20 ml of isopropyl alcohol for 2 weeks with occasional stirring, after which an aliquot (250 μl) was placed into vials containing 5 ml of LSC fluid. After a further 120 minutes had elapsed, the test products were removed from the skin surface using a cotton swab soaked with 0.25% of white pearl handwash solution followed by a dry swab (both repeated twice), all of which were placed into vials containing 20 ml of isopropyl alcohol. An aliquot (250 μl) of each sample was

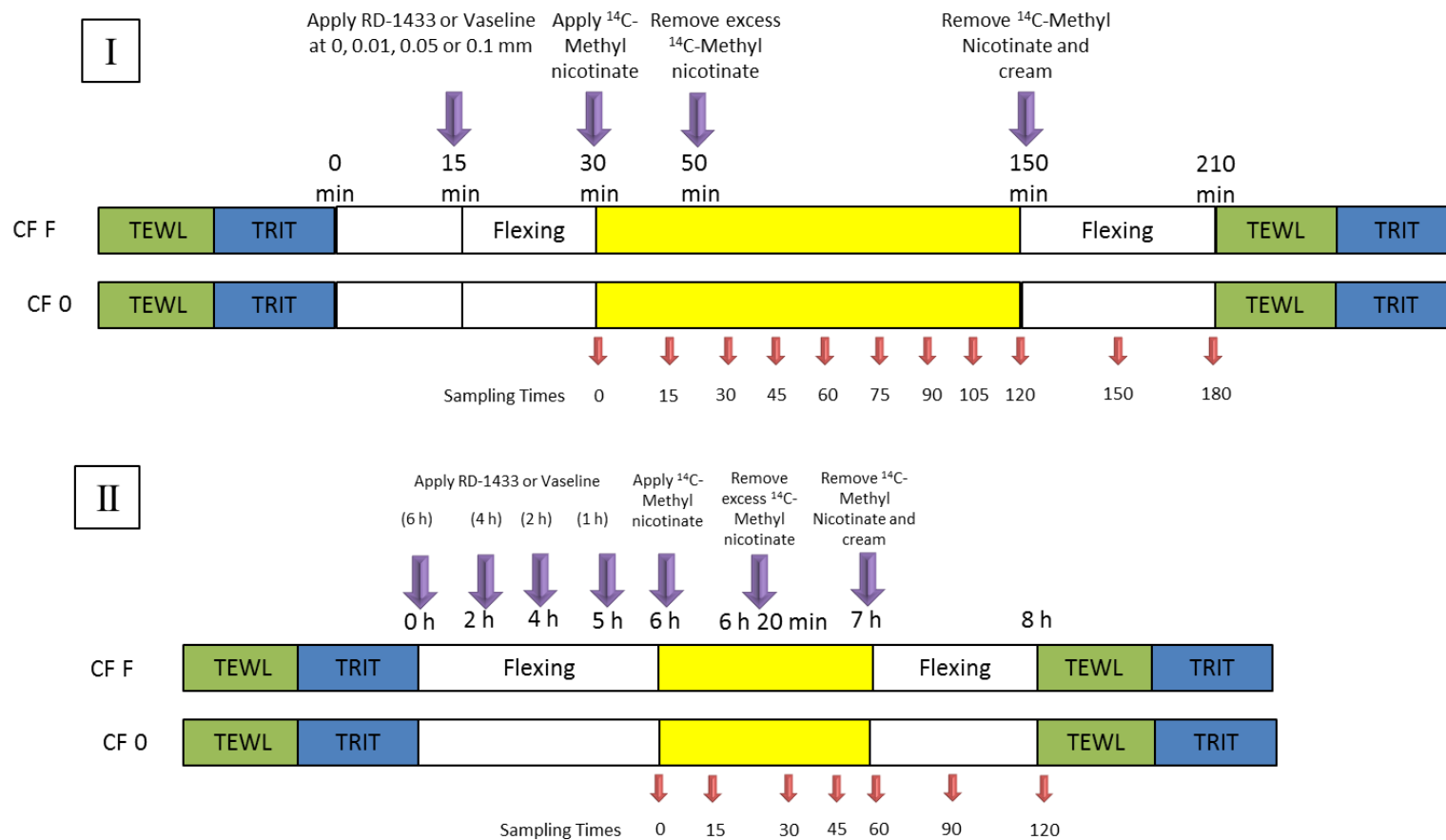


Figure 2.6: *In Vitro* Schedule For Both Optimal Thickness (I) And Duration Of Efficacy Studies (II). CutaFlex™ flexed (CF F) and CutaFlex™ static (CF 0) cells were both tested with RD-1433 and Vaseline at thicknesses of 0, 0.01, 0.05 and 0.1 mm to determine a protective effect against ¹⁴C-methyl nicotinate. Following on from this, a nominal thickness of 0.1 mm was chosen for application at 1, 2, 4 and 6 hours.

then placed into a vial containing 5 ml of LSC fluid. A further flexing (or static) time period of 60 minutes was then observed after which a second set of TEWL and tritiated water permeability measurements were taken.

Standard solutions were prepared on the day of each experiment by an addition of 5 μl ^{14}C -methyl nicotinate to (a) four cotton wool swabs in 20 ml of isopropyl alcohol and (b) un-treated skin tissue dissolved in 10 ml of Soluene-350. Each of the standard solutions was prepared in triplicate and aliquots (250 μl) of each sample were placed into vials containing 5 ml of LSC fluid. A standard receptor chamber solution was also prepared in triplicate by the addition of 10 μl of ^{14}C -methyl nicotinate to 990 μl of fresh receptor fluid (phosphate buffered saline) from which a range of triplicate aliquots (25, 50, 75 and 100 μl) were placed into vials containing 5 ml of LSC fluid. All samples were subject to liquid scintillation counting (Section 2.3.1).

2.1.13.3. Duration Of Efficacy Studies

Measurements of transepidermal water loss flux and tritiated water permeability were performed (Section 2.1.4) to measure barrier integrity. A test product thickness of 0.1 mm (17.7 μl) was chosen for a staggered application of both RD-1433 and Vaseline over a period of 0 (control), 1, 2, 4 or 6 hours (Figure 2.6- II). This dose of test product was determined from the corresponding human volunteer studies (Section 2.2.2). Test products were uniformly spread onto the skin surface using the method previously described in Section 2.1.13.2. An aliquot (10 μl) of working solution of ^{14}C -methyl nicotinate was applied to the skin surface in each donor chamber. Receptor fluid aliquots (250 μl) were removed from each diffusion cell at regular intervals up to 120 minutes. Each receptor chamber was replenished with an

equivalent volume in order to maintain a constant volume of receptor fluid. Twenty minutes after dosing, excess ^{14}C -methyl nicotinate was removed using a cotton bud which was then placed into a vial containing 20 ml of isopropyl alcohol in which aliquots (250 μl) were subsequently placed into vials containing 5 ml of LSC fluid. Sixty minutes after exposure, residual test products were removed from the skin surface using a cotton wool swab moistened with handwash solution followed by a dry swab (repeated twice) which were placed into vials containing 20 ml of isopropyl alcohol. Aliquots (250 μl) were then taken from each swab sample and placed into vials containing 5 ml of LSC fluid. A further skin flexing (or static) time period of 60 minutes was then observed after which a second set of TEWL and tritiated water permeability measurements were taken. Standard solutions were prepared as previously discussed in Section 2.1.13.2

2.2. Clinical Trial

Ethical approval to determine clinical efficacy of RD-1433 was granted by the National Research Ethics Service Committee (North East- Northern & Yorkshire, Reference: 12/NE/0255) and the Medicines and Healthcare Products Regulatory Agency (Reference: CI/2012/0033). All 12 participants provided fully informed consent. This work involved the input of staff from the Research Centre for Transdermal and Topical Drug Delivery and Toxicology. This study was performed ‘double blind’ in accordance with the principles of GCP.

2.2.1. *In Vivo* Measurements

2.2.1.1. *Visual Erythema Scoring*

All treatment sites were evaluated for visual erythema and oedema using a Draize-type scoring system. The grading scale used in Draize-type tests ranges from a score of 0-4 for a description of both erythema and oedema formation (Table 2.4).

Table 2.4. Grading Scale Used In Draize-Type Tests (Draize *et al.* (1944).
Grading of both erythema and oedema on a scale from 0-4.

	Erythema	Oedema
0	No erythema	No oedema
1	Very slight erythema (barely perceptible)	Very slight oedema (barely perceptible)
2	Well-defined erythema	Slight oedema (edges of area well defined by definite raising)
3	Moderate to severe erythema	Moderate oedema (raised approx. 1mm)
4	Severe erythema (beet redness) to slight eschar formations (injuries in depth)	Severe oedema (raised more than 1 mm and extending beyond area of exposure)

2.2.1.2. Laser Doppler Imaging

A laser Doppler imager and software (Moor version 2.2) was purchased from Moor Instruments (Devon, U.K.) to measure cutaneous blood flow at each treatment site. The scanner was placed 15 cm above each treatment site and measurements were taken in triplicate. The scan speed was set at 200 milliseconds per line with a scan area of 15.7 cm x 12.5 cm. The triplicate images were then smoothed and averaged using the Moor software. Using the averaged flux image, circular regions of interest were manually drawn around each exposure site and these values were averaged per treatment.

2.2.1.3. Tissue Viability Imaging

Skin erythema was measured using a Tissue Viability Imager 600 and software (TiVi 600 version 5.0) purchased from WheelsBridge (Linköping, Sweden). The camera was placed on a bespoke stand above the treatment areas. Images were taken in duplicate at a maximum resolution of 2074 x 1556 pixels with a colour span of 400. Percentage of erythema was then averaged per treatment.

2.2.1.4. Transepidermal Water Loss

Transepidermal water loss flux was analysed at each treatment site using a Biox AquaFlux AF200 probe (previously described in Section 2.1.5.1) with an appropriate *in vivo* measuring cap.

2.2.2. Optimal Thickness Study

Human volunteers (both sexes, 31-81 years of age) had six circular areas of 2.3 cm² drawn on the volar forearm of both arms with a non-permanent skin marker. One site on each arm was designated as an untreated control. The volume of Vaseline and RD-1433 dispensed was calculated by dividing the required thickness of the cream

(in mm) by 10 (cm) and then multiplying by the dosing area (2.3 cm^2). Test products RD-1433 and Vaseline were applied at five different nominal thicknesses of 0.01, 0.02, 0.05, 0.1 and 0.2 mm (corresponding to 4.2, 8.3, 20.8, 41.5 and 83.1 μl , respectively) and in addition to an untreated control were assigned a treatment area (Figure 2.7- I). Methyl nicotinate was prepared fresh daily, as a 5 mM solution in distilled water. Initial measurements of TEWL, LDI, tissue viability imaging and visual erythema were taken before application of Vaseline and RD-1433 as outlined in Section 2.2.1. After products were applied to the skin surface, non-contact measurements of LDI, infrared, TiVi and visual erythema were taken. An aliquot (10 μl) of methyl nicotinate was applied to the centre of each skin treatment area, after which non-contact measurements were taken at regular intervals until 120 minutes. Excess methyl nicotinate was removed 20 minutes post-exposure using a cotton bud. This was deemed necessary to avoid participants having to remain perfectly still for the 2 hour exposure period to avoid the droplet moving. A pilot study (data not reported) demonstrated that 20 minutes was sufficient to provide a maximum erythematous response. Both RD-1433 and Vaseline were removed 120 minutes post-exposure using warm water and detergent. Following a 60 minute rest period, the final set of contact and non-contact biophysical measurements were taken. For the purpose of this Thesis, only biophysical measurements of visual erythema scoring, laser Doppler imaging, tissue viability imaging and transepidermal water loss flux will be reported.

2.2.3. Duration Of Efficacy Study

Initial biophysical measurements and preparation of methyl nicotinate solution were performed as previously outlined in Section 2.2.2. Following the results of the

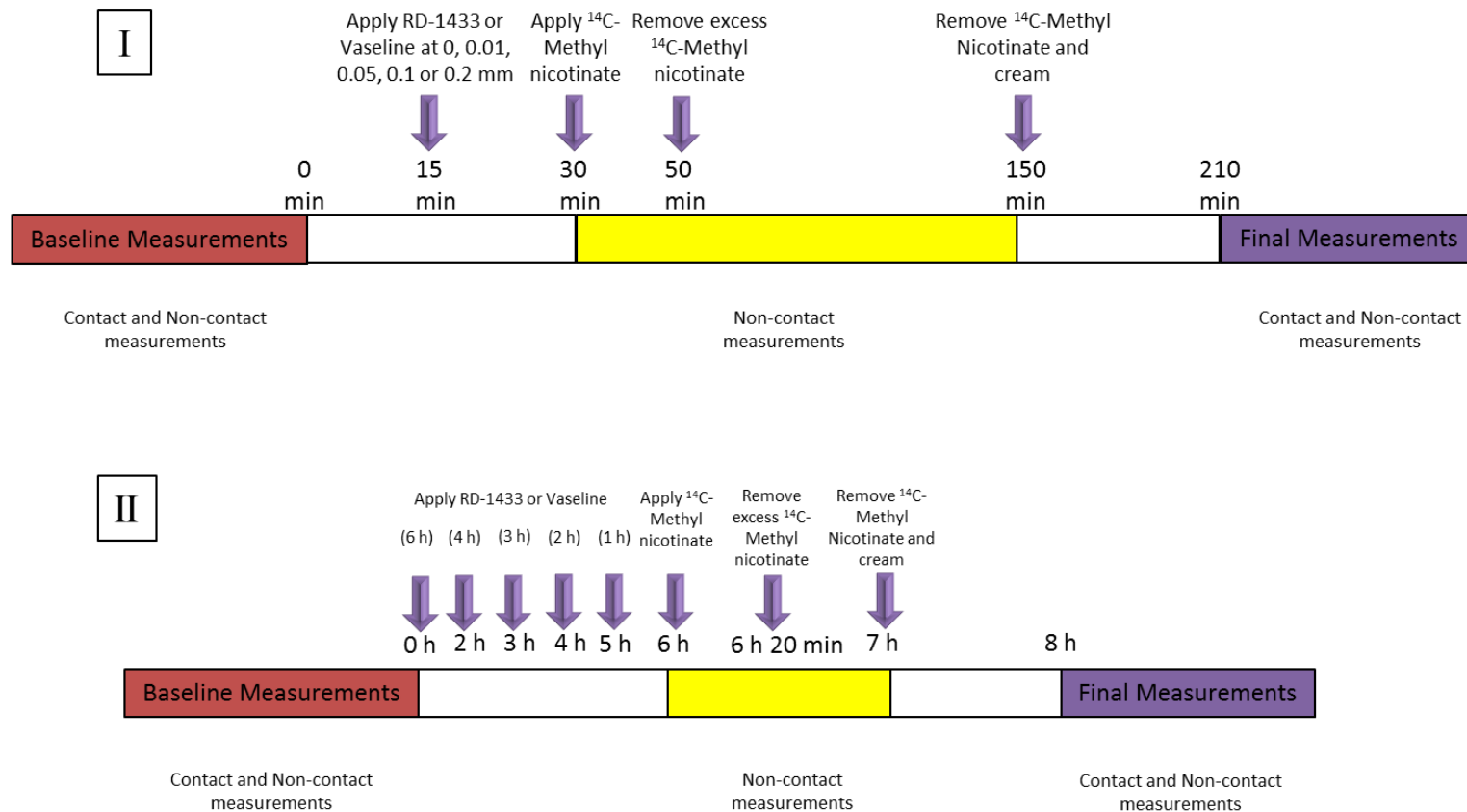


Figure 2.7: Clinical Trial Schedule For Optimal Thickness (I) And Duration Of Efficacy (II) Studies. Volunteers were tested with RD-1433 and Vaseline at thicknesses of 0, 0.01, 0.02, 0.05, 0.1 and 0.2 mm to determine a protective effect against ¹⁴C-methyl nicotinate (Optimal Thickness Study). Following on from this, a nominal thickness of 0.1 mm was chosen for application at 1, 2, 4, 5 and 6 hours (Reapplication Frequency Study).

optimal thickness study⁶, a thickness of 0.1 mm was chosen for staggered application of both RD-1433 and Vaseline application for a period of 1, 2, 3, 4 and 6 hours before exposure to methyl nicotinate (Figure 2.7- II). During the staggered application period, volunteers were allowed to engage in light physical activity. After product application, non-contact biophysical measurements identical to the optimal thickness study measurements were taken. An aliquot (10 µl) of methyl nicotinate was applied to the treatment sites on both arms, after which non-contact biophysical measurements were taken for regular intervals up to 60 minutes. Excess methyl nicotinate was removed 20 minutes post-exposure. After 60 minutes, test products were removed using warm water and a mild detergent (white pearl handwash). Sites were allowed to air dry for a further 60 minutes, after which all biophysical measurements were taken.

2.3. Sample And Statistical Analysis

2.3.1. Scintillation Counting

The radioactivity in all samples (receptor chamber fluid, skin, surface swabs, calibration standards) was quantified using a Tri-Carb 2810TR liquid scintillation analyser purchased from PerkinElmer (Waltham, U.S.A.), using an analysis runtime of 5 minutes per sample and a pre-set quench curve specific to the brand of liquid scintillation fluid (Ultima Gold™). For experiments which used both tritium and carbon-14, the Quanta Smart Tri-Carb software was set with specific limits. In order to count for tritium, the program was set to count in the region between 0 - 18.6 keV. To count for emissions from Carbon-14, the program was set to count in the region between 18.6 - 156 keV.

⁶ The results for the optimal thickness study were used to ascertain the topical dose of RD-1433 and Vaseline® required to determine the duration of efficacy.

The individual disintegrations per minute (DPM) values were normalised by subtraction of baseline samples and then divided by the specific activity of the radioactive substance to achieve a mass per sample. Specific activity was calculated as the amount of radioactivity (in DPM) a radioactive substance possessed per unit mass (in grams). Specific Activity was determined using relevant dose standards (Sections 2.1.4.2, 2.1.5.3 and 2.1.13). Once all time point aliquots were converted to mass quantities, a dilution factor was applied in order to calculate the total amount of radioactivity in the entire receptor chamber which contained either 14 ml (Franz-type) or 16.2 ml (CutaFlex™) of receptor fluid. A cumulative amount was then calculated based on the total amount per receptor chamber as well as the addition of all previous aliquots removed and finally divided by the surface area of application (1.77 cm²).

2.3.2. Statistical Testing

All data were tested for normality using the Kolmogorov-Smirnov test. All treatment groups were then analysed against the relevant control using a Kruskal-Wallis non-parametric ANOVA with Dunn's post test. In regards to inter-group variability, individual Mann Whitney non-parametric tests were performed with a two-tail P value and a Bonferroni correction. Treatments in the same group were tested for significance using a non-parametric Wilcoxon matched-pairs test with a Bonferroni correction. Correlation between values was determined using Spearman's rank correlation coefficient. The level of significance was predetermined at $p < 0.05$. The clinical study was performed 'double blind' in that neither the participants nor scientific staff knew which skin site had been assigned which treatment. The clinical study was only 'unblinded' when the statistical analysis was complete.

**Chapter 3: The Effect Of Flexing On Skin Penetration Of Model
Compounds**

3.1 Introduction

The purpose of the work reported in this chapter was to characterise a novel diffusion cell system in order to determine the effect of *in vitro* flexing on normal skin barrier integrity. To achieve this aim, work was divided into three main stages:

1. To assess the effects of skin flexing on skin barrier function measured directly (using $^3\text{H}_2\text{O}$) and indirectly (TEWL).
2. Characterisation of the novel flexing diffusion cell (CutaFlex[™]) using standard penetrants: ^3H -water, ^{14}C -benzoic acid, caffeine and testosterone.
3. Investigation of the effects of skin flexing on skin barrier function following controlled physical or chemical damage. Barrier function was quantified directly (by measuring $^3\text{H}_2\text{O}$ penetration) and using TEWL.

3.2 Materials And Methods

Tritiated water working solutions and equilibrated, saturated and un-filtered ^{14}C -benzoic acid, caffeine and testosterone solutions were prepared according to Section 2.1.1. Porcine skin and Franz and CutaFlex[™] diffusion cell systems were prepared as outlined in Section 2.1.2 and 2.1.3, respectively. A standard skin absorption protocol was followed for $^3\text{H}_2\text{O}$ (Section 2.1.5.2) and Carbon-14 chemicals (Section 2.1.5.3). Skin damage studies were performed according to protocols outlined in Section 2.1.6. All samples were analysed using radiometric methods (Section 2.3.1). Statistical testing was performed as outlined in Section 2.3.2.

3.3 Results

3.3.1 Skin Flexion

No significant differences ($p > 0.05$) were found in either tritiated water permeation or transepidermal water loss between the Franz static control and CutaFlex[™] static, 30, 60, 90 and 120 minutes flexed groups in either baseline or flexing conditions (Figure 3.1). No significant differences ($p > 0.05$) in tritiated water penetration were seen with static skin or skin flexed from 30-120 minutes in the CutaFlex[™] diffusion cells.

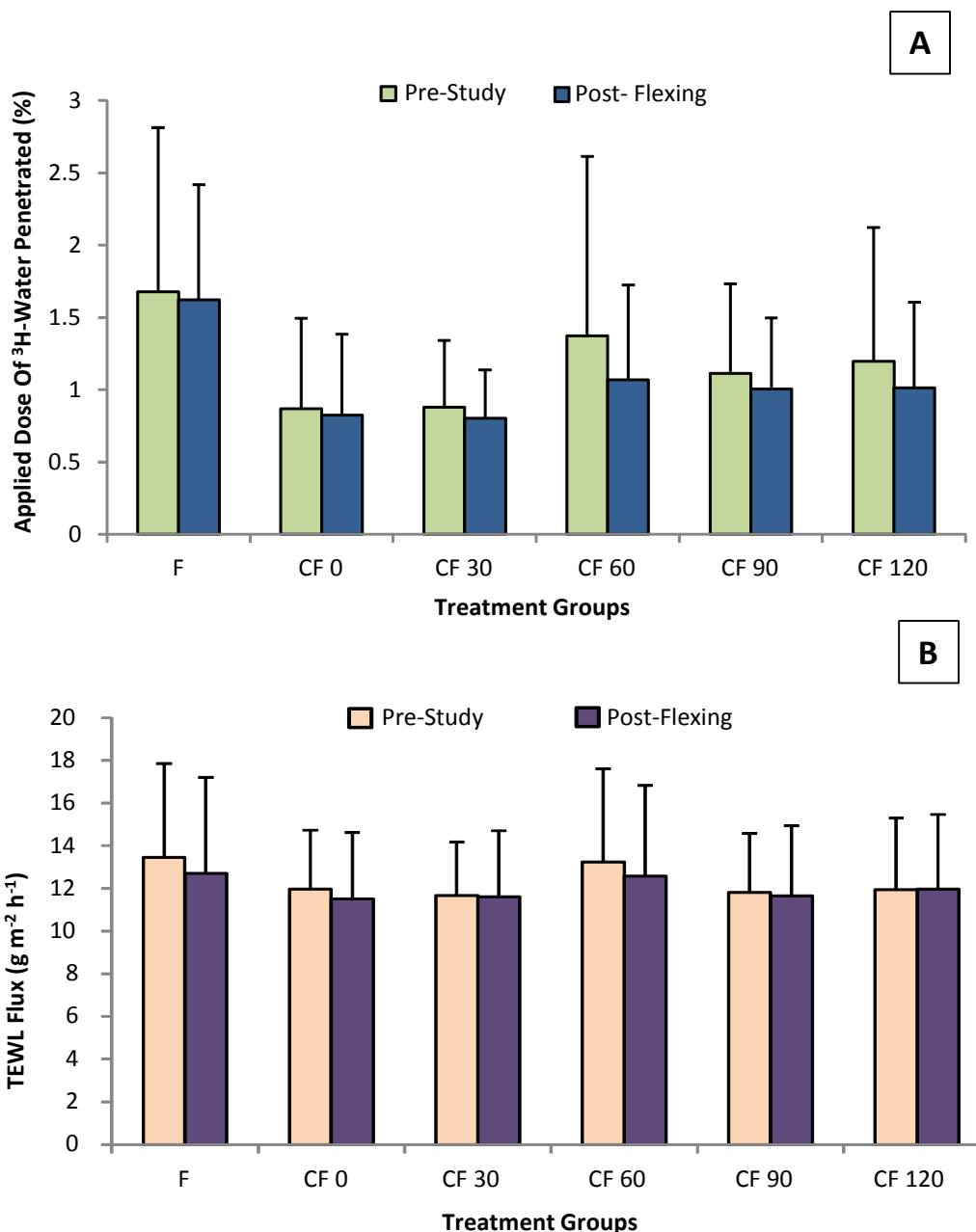


Figure 3.1: Flexing Of Porcine Skin As Measured By Tritiated Water Permeation (A) And Transepidermal Water Loss (B) In Franz (F), CutaFlex™ Static (CF 0) And CutaFlex™ 30-120 Minutes Flexed (CF 30, 60, 90 And 120) Diffusion Cells. Tritiated water was applied (250 mg cm^{-2}) to the skin surface for 30 minutes before and after skin flexion. Transepidermal water loss flux was also measured before and after skin flexion. All data are represented as mean + standard deviation of $n=9$ diffusion cells.

3.3.2 Skin Damage Studies

3.3.2.1 Chemical Damage (*Sodium Lauryl Sulphate*)

Significant differences were found in the amount of tritiated water penetrated between baseline and post-treatment with SLS between the Franz static control ($p < 0.01$), CutaFlex™ static ($p < 0.01$) and CutaFlex™ 30 ($p < 0.01$), 60 ($p < 0.01$), 90 ($p < 0.05$) and 120 ($p < 0.01$) minutes flexed groups (Figure 3.2, A). A decrease in skin integrity was detected in 100% of the treatment groups.

Significant differences ($p < 0.01$) were found in transepidermal water loss flux between baseline and post-SLS treatment within the Franz static control ($p < 0.05$), CutaFlex™ static ($p < 0.05$), and CutaFlex™ 60 minutes flexed ($p < 0.05$) groups (Figure 3.2, B). A decrease in skin integrity was detected in 50% of the treatment groups.

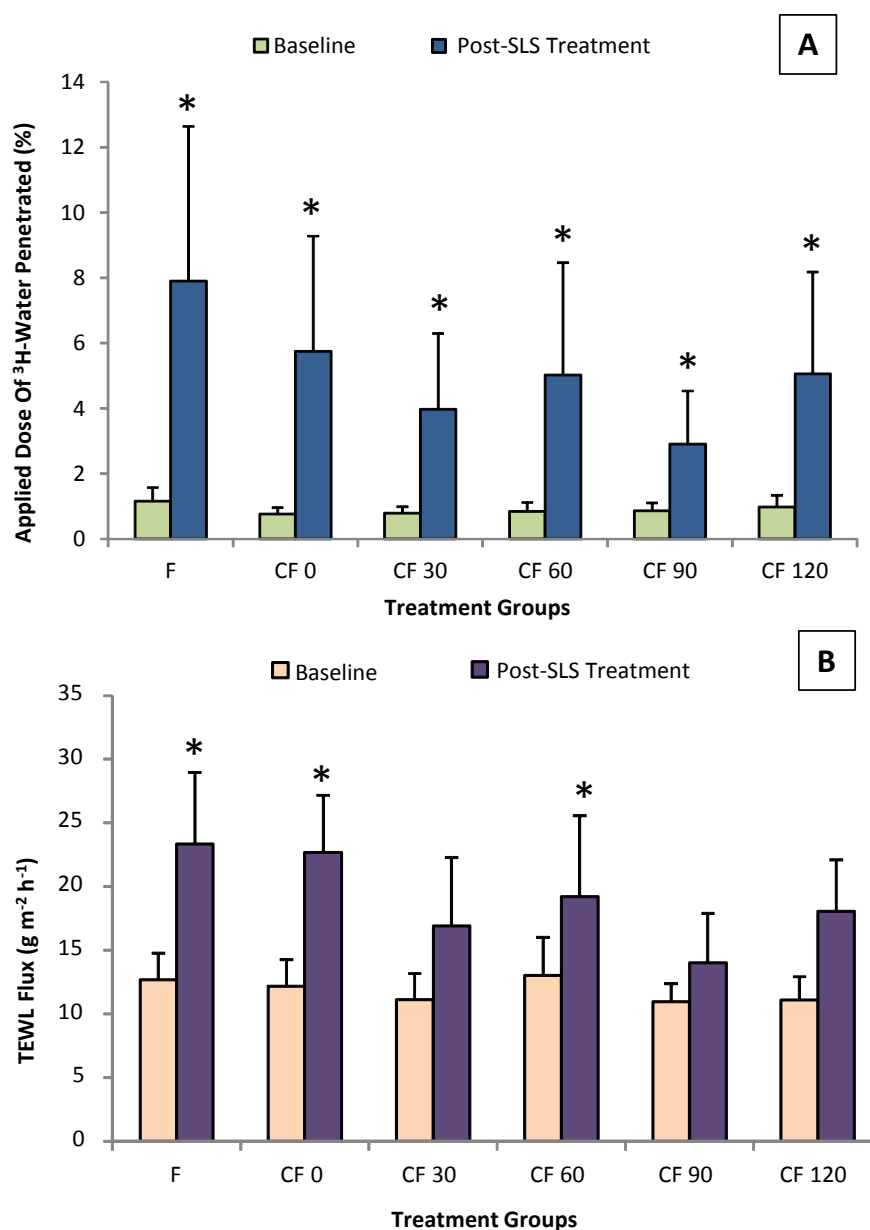


Figure 3.2: Chemical Damage Of Porcine Skin As Measured By Tritiated Water Permeation (Top) And Transepidermal Water Loss (Bottom) In Franz (F), CutaFlex™ Static (CF 0) And CutaFlex™ 30-120 Minutes Flexed (CF 30, 60, 90 And 120 Diffusion Cells. Tritiated water was applied (250 mg cm^{-2}) to the skin surface for 30 minutes before and after SLS treatment. Transepidermal water loss flux was also measured before and after SLS treatment. A 5% (v/v) solution of sodium lauryl sulphate was applied ($250 \text{ } \mu\text{l cm}^{-2}$) to the skin surface for 1 hour. All data are represented as mean + standard deviation of $n=9$ diffusion cells. An asterisk (*) represents a significant ($p < 0.05$) increase in either tritiated water penetration or TEWL flux as compared to baseline values for each treatment group.

3.3.2.2 *Physical Damage (Punctures)*

Significant increases ($p < 0.05$) in tritiated water penetration were found between baseline and post-puncture treatment in all flexed skin treatment groups (Figure 3.3, A). A decrease in skin integrity was seen in 67% of groups treated.

Significant increases ($p < 0.05$) in transepidermal water loss were found between baseline and post-puncture values within the CutaFlex™ static and CutaFlex™ 30, 60, 90 and 120 minutes flexed groups (Figure 3.3, B). A decrease in skin integrity was seen in 83% of the groups tested.

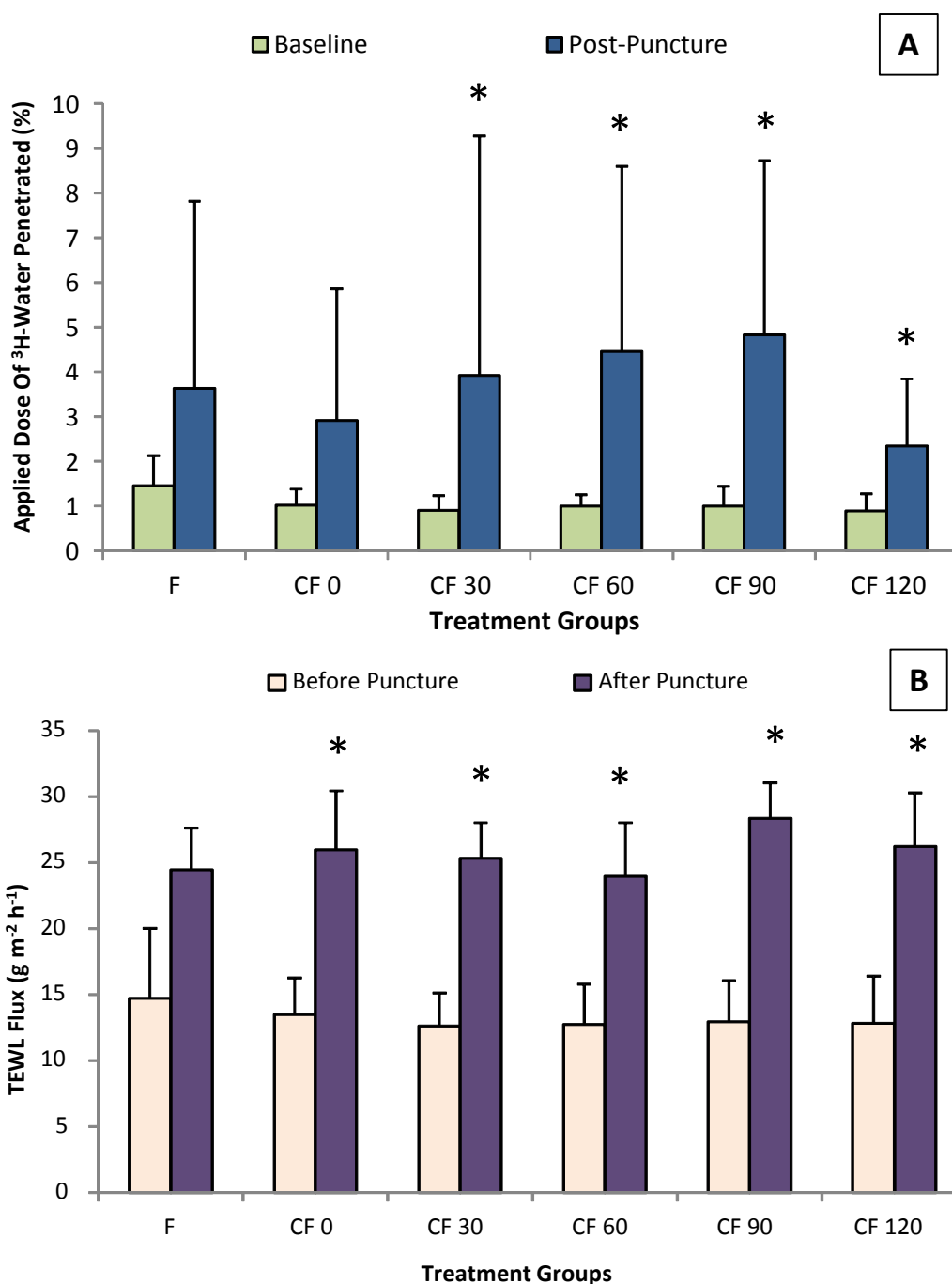


Figure 3.3: Physical Damage Of Porcine Skin As Measured By Tritiated Water Permeation (Top) And Transepidermal Water Loss (Bottom) In Franz (F), CutaFlex™ Static (CF 0) And CutaFlex™ 30-120 Minutes Flexed (CF 30, 60, 90 And 120) Diffusion Cells. Tritiated water was applied (250 mg cm^{-2}) to the skin surface for 30 minutes before and after two punctures were made through the entirety of the skin section in each diffusion cell. Transepidermal water loss flux was also measured before and after puncturing the skin. All data are represented as mean + standard deviation of $n=9$ diffusion cells. An asterisk (*) represents a significant ($p < 0.05$) increase in either tritiated water penetration or TEWL flux as compared to baseline values for each treatment group.

3.3.3 Tritiated Water Permeability And Transepidermal Water Loss

Correlation

Baseline values of the applied amount of tritiated water penetrated and transepidermal water loss from all flexing and chemical and physical damage studies were collated and plotted (Figure 3.4). A poor correlation ($r = 0.52$) was found in baseline values between tritiated water and TEWL flux. The cut-off values between intact and damaged skin were determined as mean plus two standard deviations; Corresponding to 2.3% of the applied dose penetrated ($^3\text{H}_2\text{O}$) and flux of $18.3 \text{ g m}^{-2} \text{ h}^{-1}$ (TEWL rate). When taking these values into consideration, the applied amount of tritiated water penetrated through porcine skin at baseline fell below the threshold value in 96% of all values tested (154 of 160 values). Transepidermal water loss flux measurements fell below the threshold in 94% of all values tested (151 out of 160 values). There was a 46-fold difference found between the minimum and maximum tritiated water values as compared to a 3-fold difference between the minimum and maximum values of TEWL rates.

When measuring the linear regression of baseline values of tritiated water penetration and transepidermal water loss flux, the correlation of the values ranged from 0.1-0.4 (Figure 3.5, A, B and C). When measuring the linear regression of flexed, SLS treated and puncture treated values of tritiated water penetration and transepidermal water loss flux, the correlation of the values ranged from 0.06-0.4 (Figure 3.5, D, E and F). Therefore, there was no correlation found between TEWL rate and tritiated water penetrated.

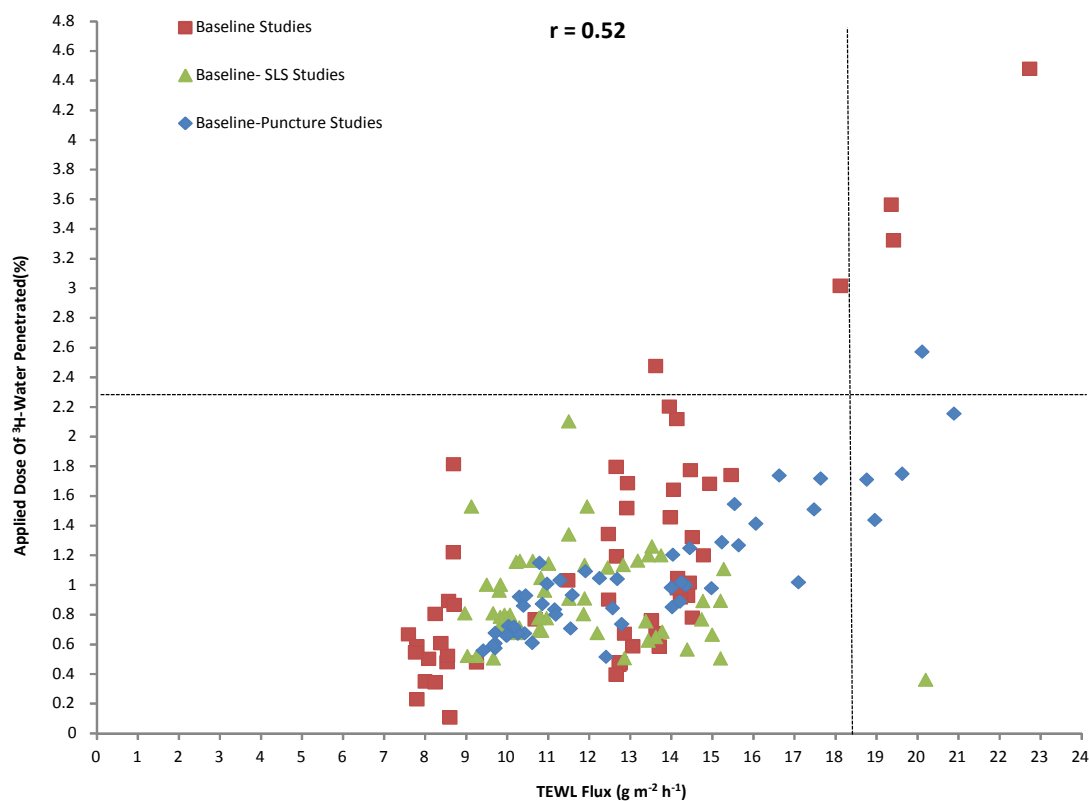


Figure 3.4: Applied Dose Of Tritiated Water Penetrated As Correlated With Transepidermal Water Loss Flux For Baseline Measurements In Skin Damage Studies. Tritiated water was applied to the skin surface for 30 minutes (442.5 mg; 1 μCi) and transepidermal water loss measurements were taken before and after flexion, sodium lauryl sulphate treatment and puncturing of the skin. The cut-off values for tritiated water applied dose penetrated and transepidermal water loss flux were set as mean + two standard deviations. The dotted vertical and horizontal lines represent the cut-off values for TEWL flux and applied dose of tritiated water penetrated, respectively.

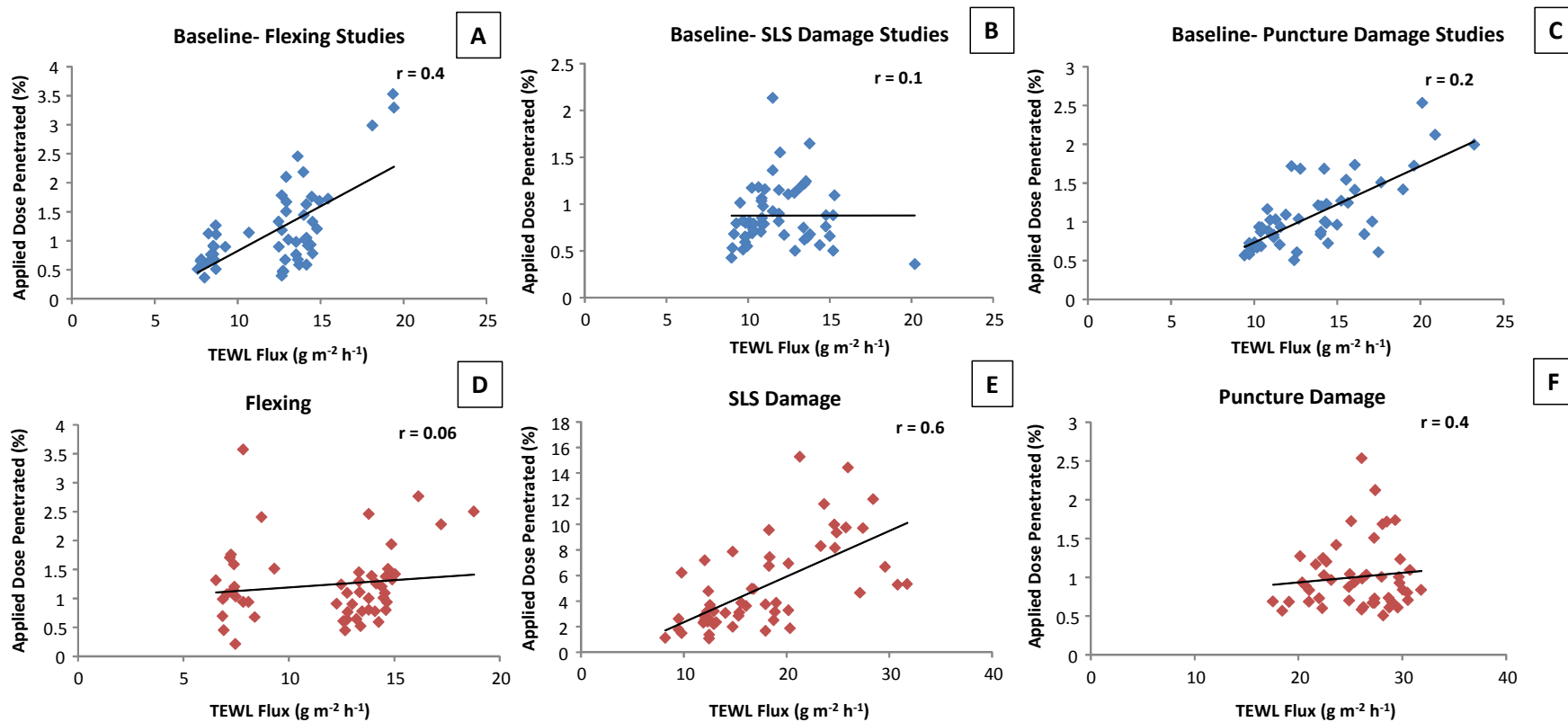


Figure 3.5: Applied Dose Of Tritiated Water Penetrated As Correlated With Transepidermal Water Loss For Baseline (Top) And Flexed, SLS-Damaged And Puncture Damaged Treatments (Bottom) As Measures Of Skin Barrier Integrity. Tritiated water was applied to the skin surface for 30 minutes (442.5 mg; 1 μ Ci) and transepidermal water loss measurements were taken before and after flexion (A and D), sodium lauryl sulphate treatment (B and E) and puncturing of the skin (C and F).

3.3.4 Standard Penetrant Studies

3.3.4.3 ³H-Water Dermal Absorption Studies

Cumulative Amount Penetrated

The cumulative amount of ³H₂O penetrating un-flexed skin mounted in the CutaFlex™ diffusion cells was not significantly different ($p > 0.05$) to that penetrating skin in standard Franz diffusion cells (Figure 3.1). Similarly, flexing of skin (for durations of 30-480 minutes) within the CutaFlex™ cells had no measurable effect on the cumulative absorption of ³H₂O.

Maximum Flux

In terms of the rate of absorption of tritiated water through skin, there was no significant effect of flexing for the majority of the CutaFlex™ treatment groups (Figure 3.7). However, a statistically significant difference ($p < 0.05$) was observed between un-flexed skin in the Franz cell and skin flexed for 120 minutes in the 540 minute study. Overall, the average steady-state flux of ³H₂O ranged from 47 – 86 $\mu\text{g cm}^{-2}\text{h}^{-1}$.

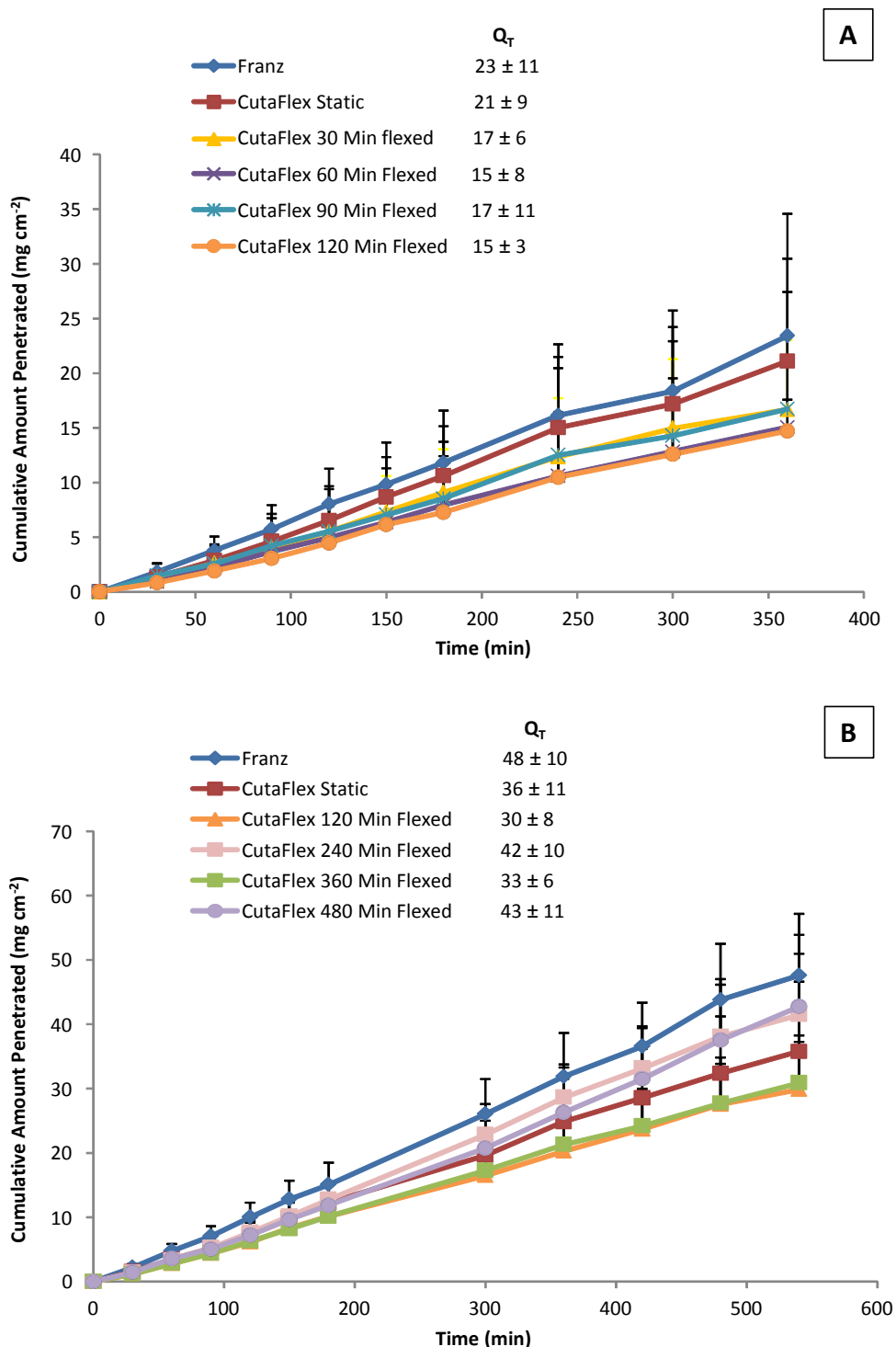


Figure 3.6: Cumulative Amount Of Tritiated Water Penetrated Through Static (Franz, CutaFlex™ Static) And Flexed (CutaFlex™ 30-480 Minutes Flexed) Porcine Skin Over 360 (A) And 540 Minutes (B). Tritiated water was applied (250 $\mu\text{l cm}^{-2}$) to the skin surface at time 0. Skin mounted in CutaFlex™ cells was un-flexed (static) or flexed with a maximum amplitude of 6 mm, twice a minute for durations of 30-480 minutes. All diffusion cells remained static until 30 minutes after tritiated water was applied. All points are mean + standard deviation of n=9 diffusion cells. Values for the cumulative amount penetrated at study end are represented on the graph (Q_T).

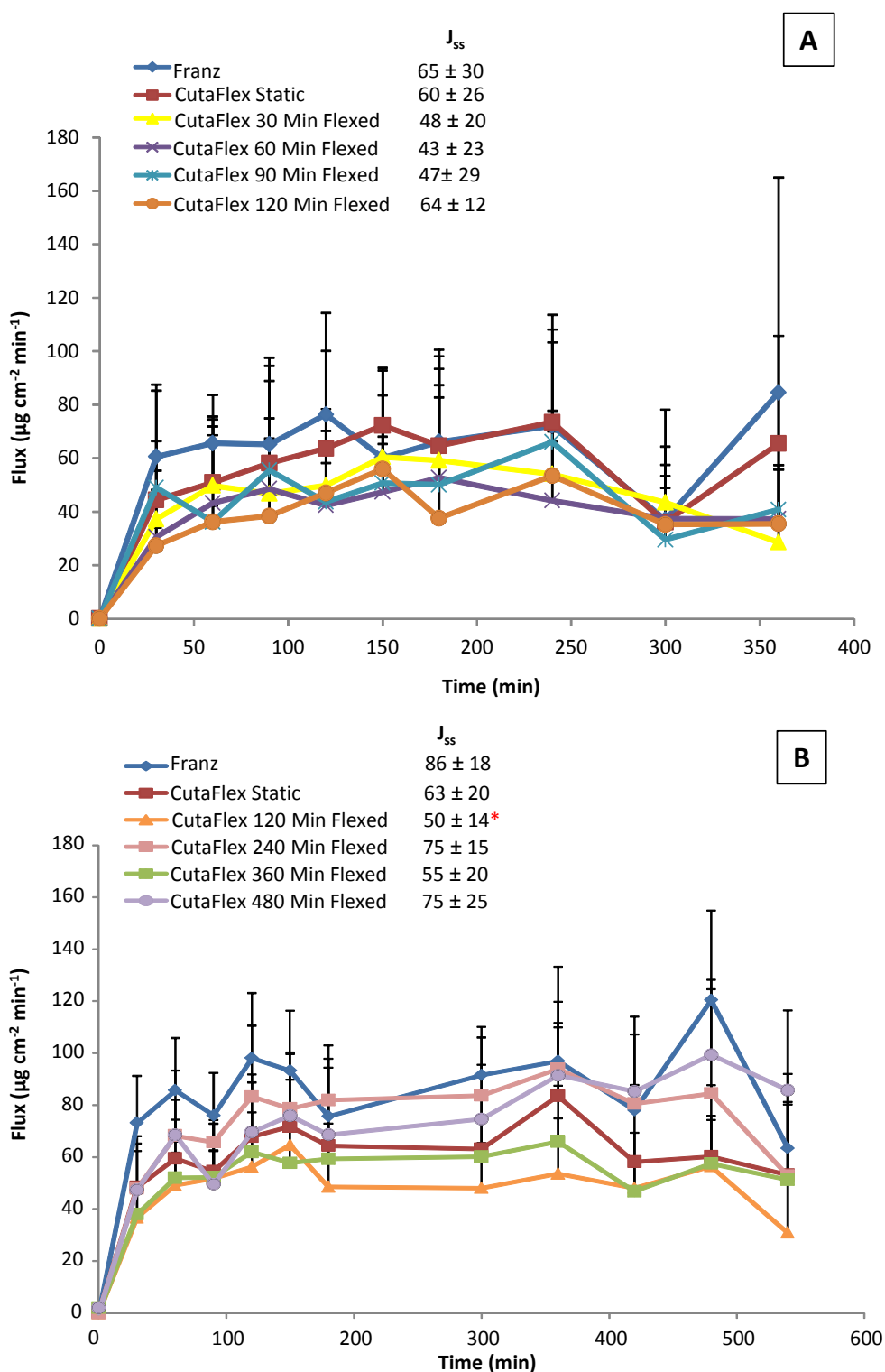


Figure 3.7: Flux Profile Of Tritiated Water Penetrated Through Static (Franz, CutaFlex™ Static) And Flexed (CutaFlex™ 30-480 Minutes Flexed) Porcine Skin Over 360 (A) And 540 Minutes (B). Tritiated water was applied ($250 \mu\text{l cm}^{-2}$) to the skin surface at time 0. All diffusion cells remained static until 30 minutes after tritiated water was applied. Maximum flux (J_{Max} ; $\mu\text{g cm}^{-2} \text{min}^{-1}$) and time (min) of maximum flux are displayed on the graph. All points are mean + standard deviation of $n=9$ diffusion cells. An asterisk (*) represents a significant ($p < 0.05$) decrease in maximum flux compare to Franz (control) group.

3.3.4.4 ¹⁴C-Benzonic Acid Dermal Absorption Study

Transepidermal Water Loss

There were no significant differences ($p > 0.05$) found in transepidermal water loss flux between baseline and post-treatment values within or between treatment groups (Figure 3.8).

Skin Surface Spreading

There were no significant differences ($p > 0.05$) observed in the amount of ¹⁴C-benzoic acid remaining on the skin surface between any of the treatment groups (Figure 3.9).

Cumulative Penetration

There were no significant differences ($p > 0.05$) in the cumulative amount of ¹⁴C-benzoic acid penetrated through the skin of the Franz static control group compared to the CutaFlex™ treatment groups (Figure 3.10). The flux of ¹⁴C-benzoic acid was not significantly different between unflexed skin (in Franz and CutaFlex™ diffusion cells) or flexed skin ($p > 0.05$) and ranged from an average of 200-240 $\mu\text{g cm}^{-2} \text{h}^{-1}$.

Mass-Balance

Skin in the Franz cell system showed significantly ($p < 0.05$) lower amounts of ¹⁴C-benzoic acid recovered from the skin surface as compared to static and flexed skin in the CutaFlex™ system. Quantitatively, the amount of ¹⁴C-benzoic acid recovered from the surface of skin from CutaFlex™ cells was approximately 3-4 fold higher than that from Franz cells. Moreover, there were no significant differences found in the amount of ¹⁴C-benzoic acid recovered in the skin samples and in the receptor fluid of any of the treatment groups (Figure 3.11).

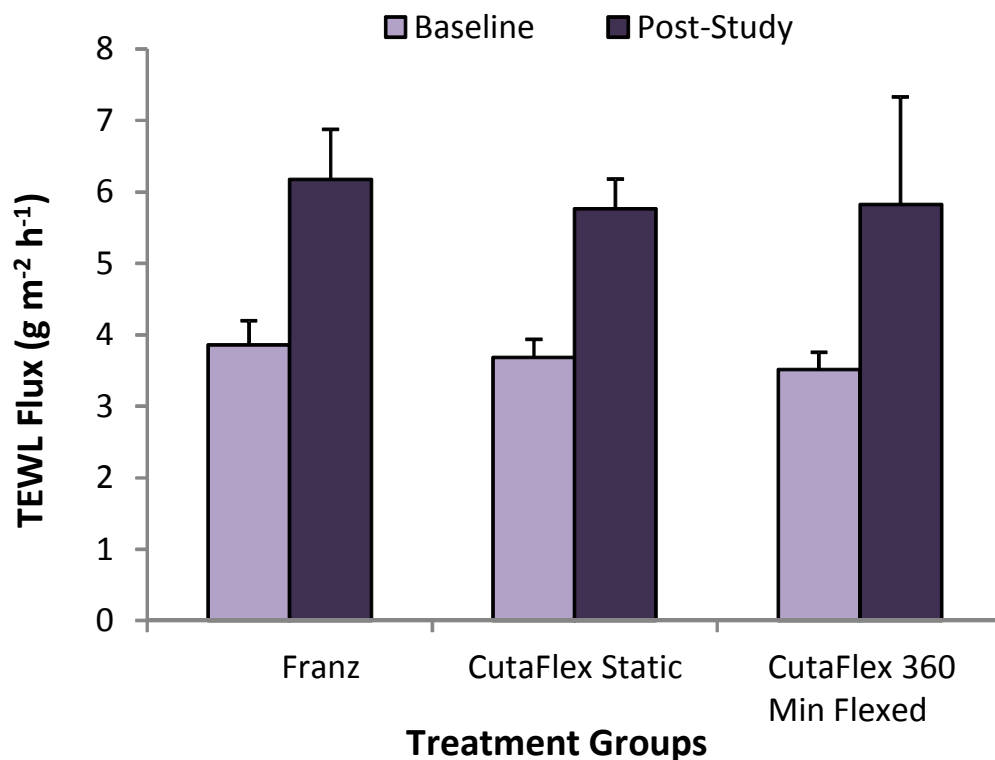


Figure 3.8: Transepidermal Water Loss Flux Before And After ^{14}C -Benzoic Acid Exposure In Static (Franz And CutaFlex™ Static) And Flexed (CutaFlex™ 360 Minutes Flexed) Diffusion Cells. Benzoic acid was applied ($442.5 \mu\text{l}$) to the skin surface in a saturated, equilibrated un-filtered solution for 51 hours. All bars are represented as mean + standard deviation of $n=6$ diffusion cells.

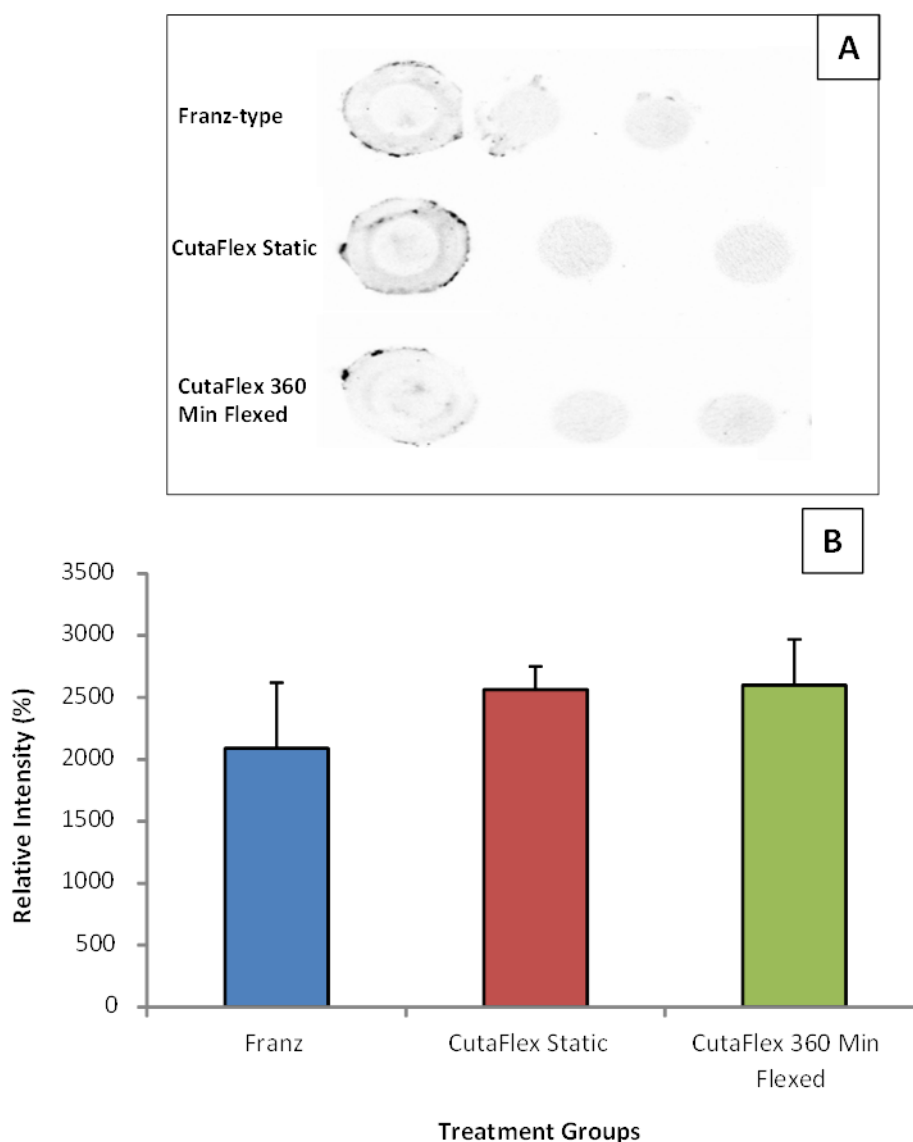


Figure 3.9: Surface Spreading Of ^{14}C -Benzoic Acid Treated Static (Franz And CutaFlexTM Static) And Flexed (CutaFlexTM 360 Min Flexed) Porcine Skin Sections After 51 Hours Of Exposure: Autoradiographs (A) And Intensity Graph (B). Skin was assessed for surface spreading of Carbon-14 using representative autoradiography images (A). The average intensity of staining was quantified by image analysis to produce a relative intensity score by comparison to un-exposed (control) skin. Benzoic acid was applied ($250 \mu\text{l cm}^{-2}$) to the skin surface in a saturated, equilibrated un-filtered solution at a concentration of 90 mg ml^{-1} . All points are mean + standard deviation of $n=3$ skin sections.

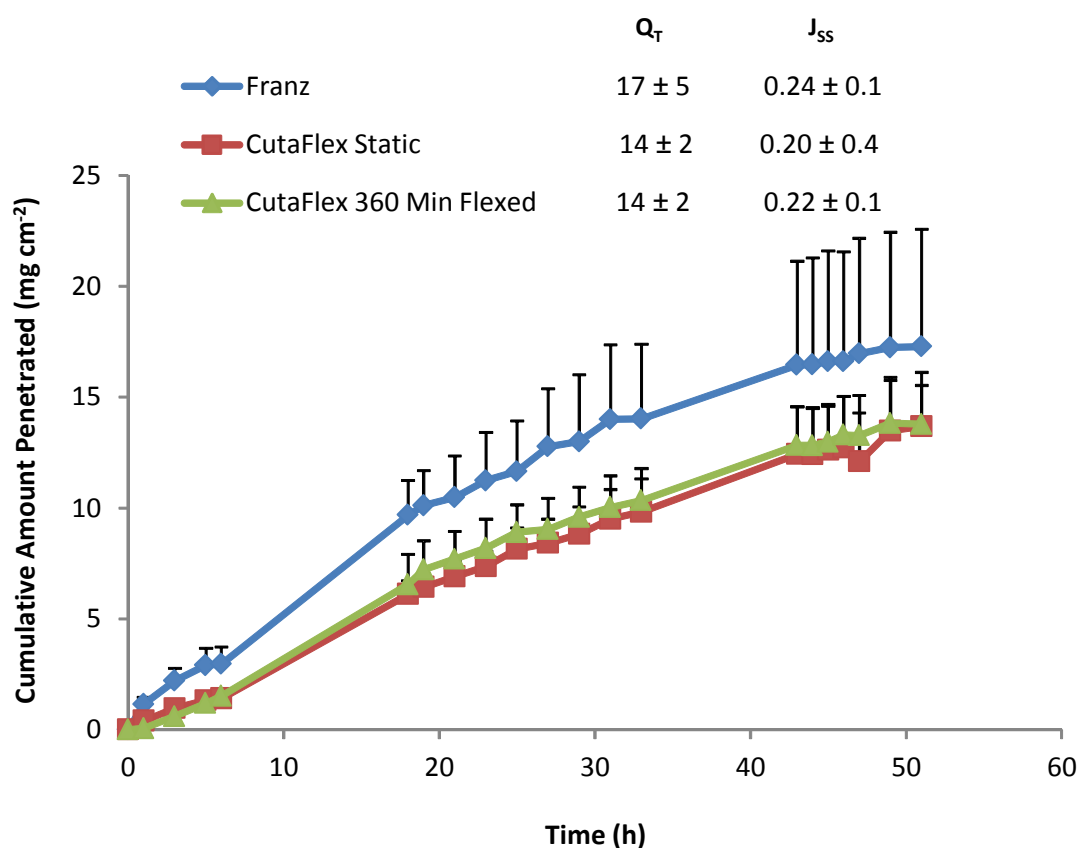


Figure 3.10: Cumulative Amount Of ^{14}C -Benzoic Acid Penetrated Through Static (Franz and CutaFlex™ Static) And Flexed (CutaFlex™ 360 Minutes Flexed) Porcine Skin Over 51 Hours. Benzoic acid was applied ($250 \mu\text{l cm}^{-2}$) to the skin surface in a saturated, equilibrated un-filtered solution at a concentration of 90 mg ml^{-1} and a volume of $442.5 \mu\text{l}$ ($5 \mu\text{Ci}$) for 51 hours. Skin mounted in CutaFlex™ cells was un-flexed (static) or flexed with a maximum amplitude of 6 mm, twice a minute for a duration of 360 minutes. All points are mean + standard deviation of $n=6$ diffusion cells. Values for the cumulative amount penetrated at study end (Q_T) are represented on the graph in units of mg cm^{-2} . Steady-state flux (J_{SS}) values are represented on the graph in units of $\text{mg cm}^{-2} \text{ h}^{-1}$.

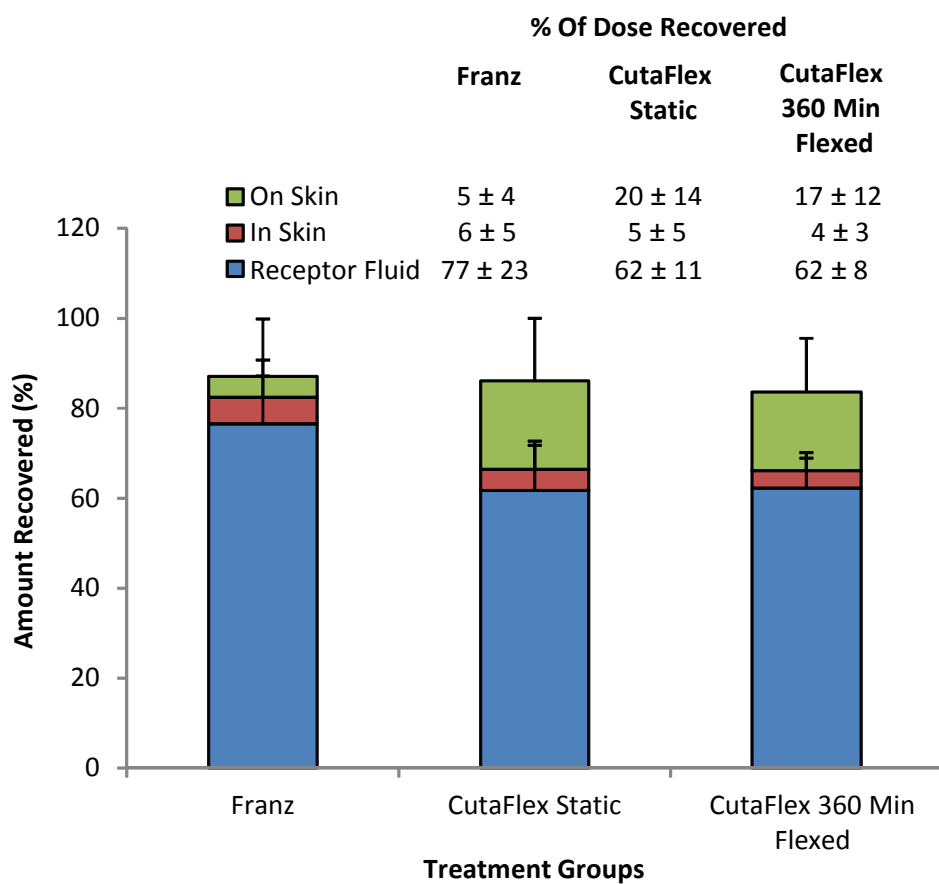


Figure 3.11: Dose Distribution Of ^{14}C -Benzoic Acid From Static (Franz and CutaFlex™ Static) And Flexed (CutaFlex™ 360 Minutes Flexed) Porcine Skin Samples After 51 Hours. Each bar on the graph indicates percentage of the dose applied (40 mg) that was recovered from the skin surface (On Skin), in the skin samples or in the receptor fluid. All bars are mean + standard deviation of n= 6 diffusion cells.

3.3.4.5 ¹⁴C-Caffeine Dermal Absorption Study

Transepidermal Water Loss

There were no significant differences ($p > 0.05$) found between baseline and post-treatment values of transepidermal water loss flux within or between any of the treatment groups (Figure 3.12).

Surface Spreading

There were no significant differences ($p > 0.05$) found in the amount of surface ¹⁴C-caffeine remaining on the skin of any of the treatment groups (Figure 3.13).

Cumulative Penetration

There were no significant differences ($p > 0.05$) found in the cumulative amount of ¹⁴C-caffeine penetrated in the Franz static control as compared to the CutaFlex™ treatment groups (Figure 3.14). The steady-state flux of ¹⁴C-caffeine ranged from 40-49 $\mu\text{g cm}^{-2} \text{h}^{-1}$.

Mass-Balance

There were no significant differences ($p > 0.05$) in the amount of ¹⁴C-caffeine recovered on the skin surface, in the skin samples and in the receptor fluid in any of the treatment groups (Figure 3.15).

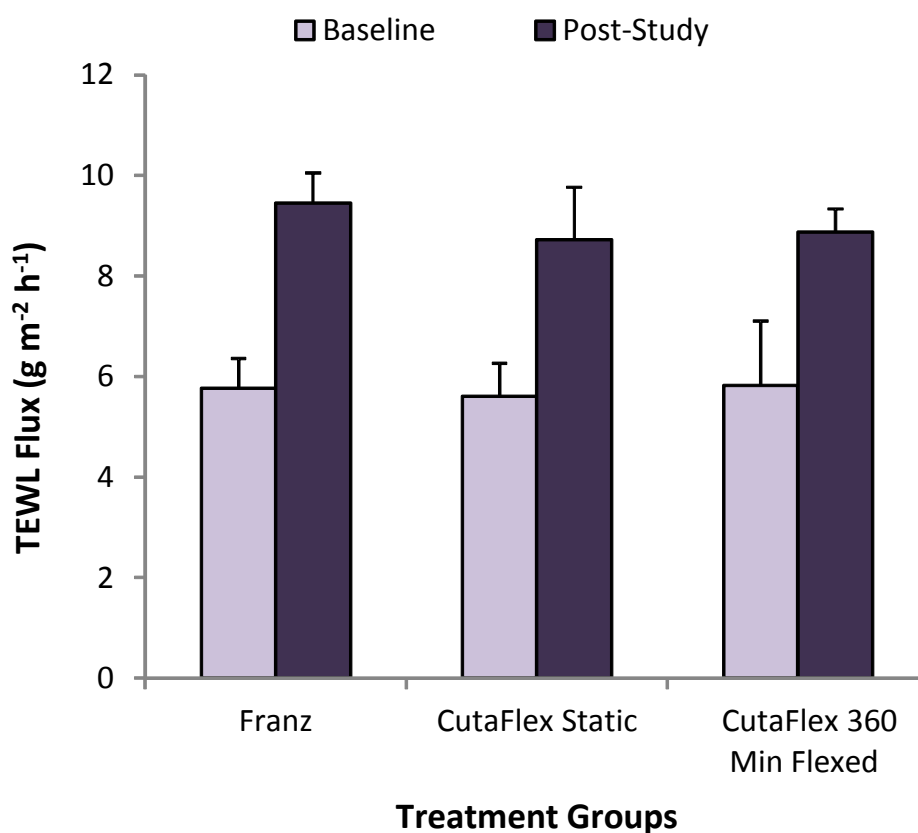


Figure 3.12: Transepidermal Water Loss Flux Before And After ^{14}C -Caffeine Exposure In Static (Franz And CutaFlex™ Static) And Flexed (CutaFlex™ 360 Minutes Flexed) Diffusion Cells. Benzoic acid was applied ($250 \mu\text{l cm}^{-2}$) to the skin surface in a saturated, equilibrated un-filtered solution at a concentration of 84 mg ml^{-1} for 51 hours. All bars are represented as mean + standard deviation of $n= 6$ diffusion cells.

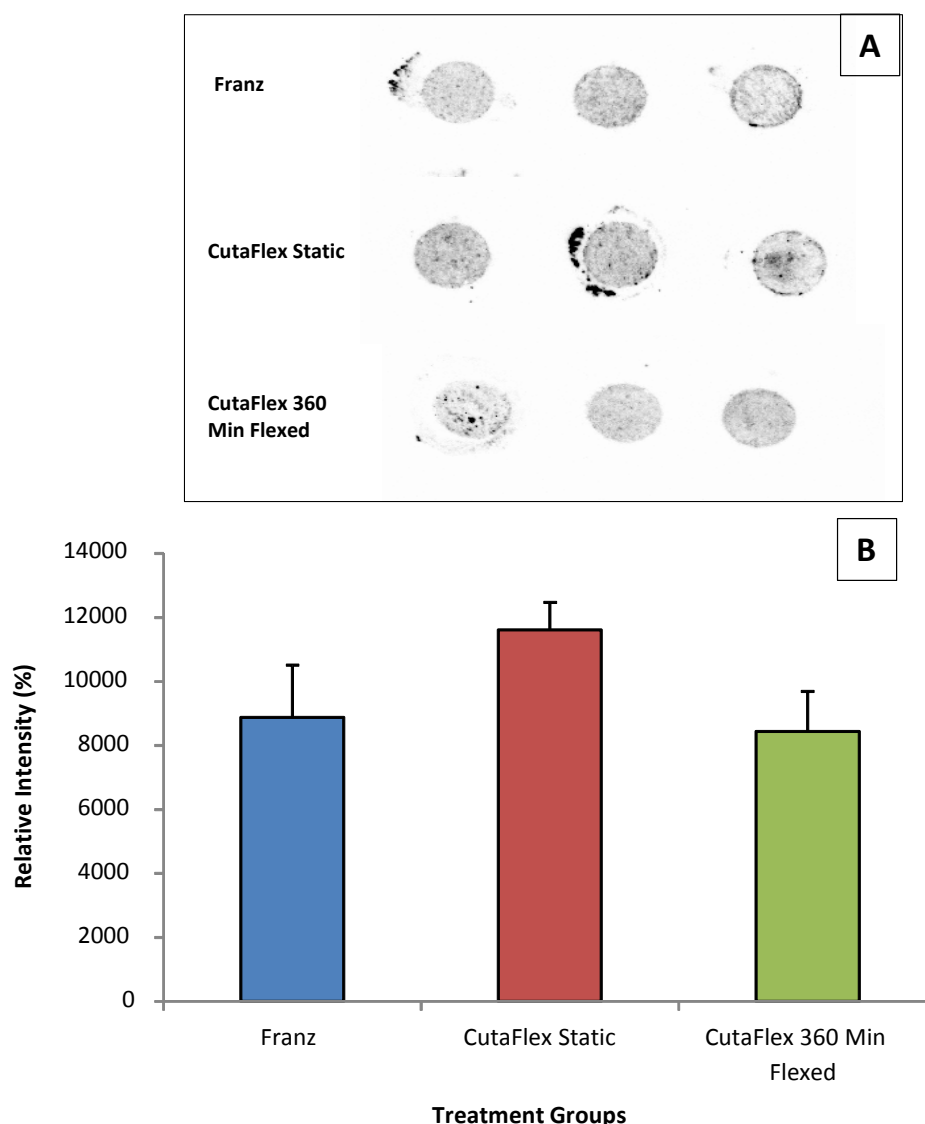


Figure 3.13: Surface Spreading Of ^{14}C -Caffeine Treated Static (Franz And CutaFlex™ Static) And Flexed (CutaFlex™ 360 Min Flexed) Porcine Skin Sections After 51 Hours Of Exposure: Autoradiographs (A) And Intensity Graph (B). Skin was assessed for surface spreading of Carbon-14 using autoradiography images (A). The average intensity of staining was quantified by image analysis to produce a relative intensity score by comparison to un-exposed (control) skin. Caffeine was applied ($250 \mu\text{l cm}^{-2}$) to the skin surface in a saturated, equilibrated un-filtered solution at a concentration of 84 mg ml^{-1} for 51 hours. All points are mean + standard deviation of $n=3$ skin sections.

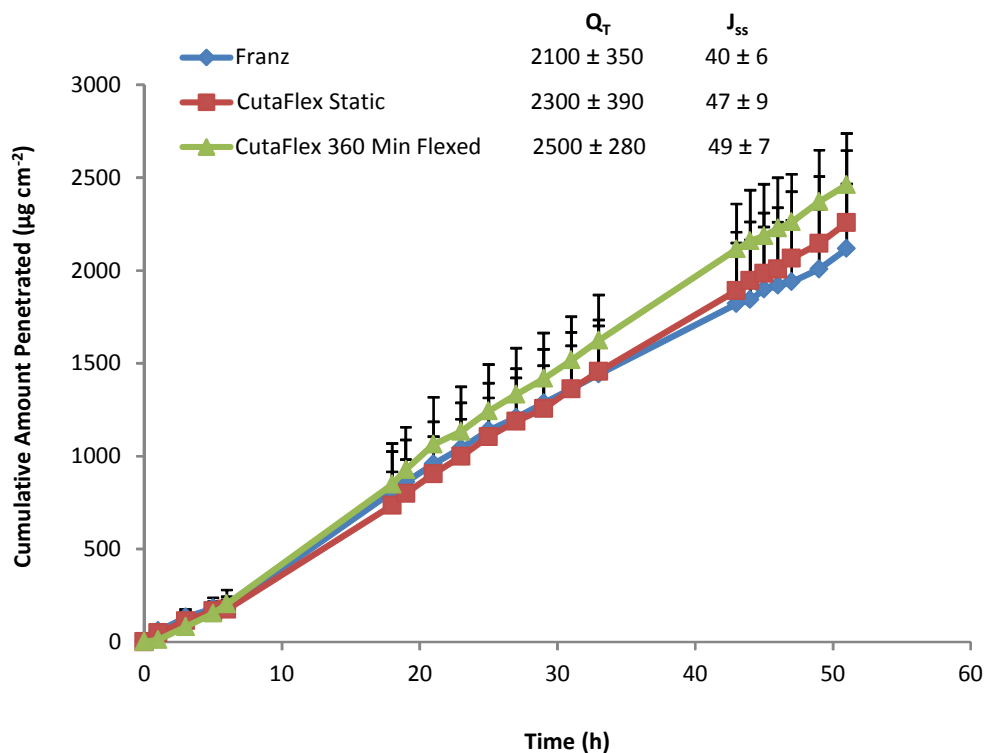


Figure 3.14: Cumulative Amount Of ^{14}C -Caffeine Penetrated Through Static (Franz and CutaFlex[™] Static) And Flexed (CutaFlex[™] 360 Minutes Flexed) Porcine Skin Over 51 Hours. Caffeine acid was applied ($250 \mu\text{l cm}^{-2}$) to the skin surface in a saturated, equilibrated un-filtered solution at a concentration of 84 mg ml^{-1} for 51 hours. Skin mounted in CutaFlex[™] cells was un-flexed (static) or flexed with a maximum amplitude of 6 mm, twice a minute for a duration of 360 minutes. All points are mean + standard deviation of $n=6$ diffusion cells. Values for the cumulative amount penetrated at study end (Q_T) are represented on the graph in units of $\mu\text{g cm}^{-2}$. Steady-state flux (J_{ss}) values are represented on the graph in units of $\mu\text{g cm}^{-2} \text{ h}^{-1}$.

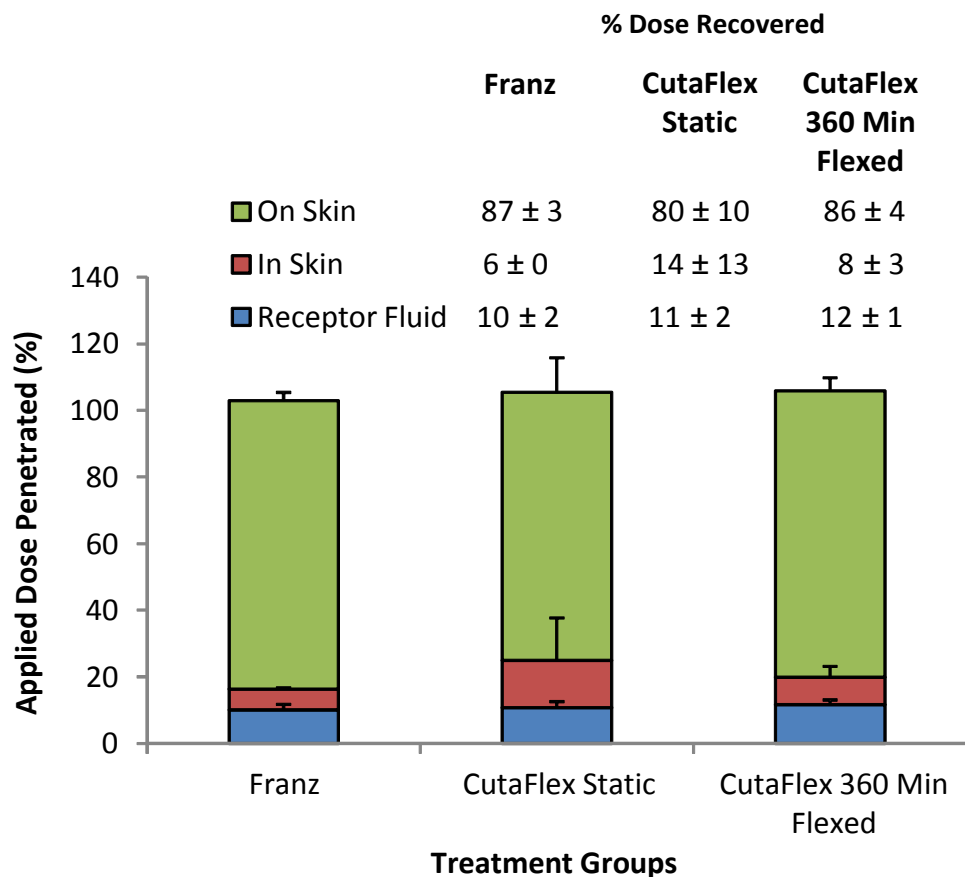


Figure 3.15: Dose Distribution Of ^{14}C -Caffeine Acid From Static (Franz and CutaFlex™ Static) And Flexed (CutaFlex™ 360 Minutes Flexed) Porcine Skin Samples After 51 Hours. Each bar on the graph indicates percentage of the dose (37 mg) applied that was recovered from the skin surface (On Skin), in the skin samples or in the receptor fluid. All bars are mean + standard deviation of n= 6 diffusion cells.

3.3.4.6 ¹⁴C-Testosterone Dermal Absorption Study

Transepidermal Water loss

There were no significant differences ($p > 0.05$) found between baseline and post-treatment values of transepidermal water loss flux within and between any of the treatment groups tested (Figure 3.16).

Surface Spreading

There were no significant differences ($p > 0.05$) between treatment groups of the amount of ¹⁴C-testosterone remaining on the skin surface (Figure 3.17).

Cumulative Amount Penetrated

There were no significant differences ($p > 0.05$) in the cumulative amount of ¹⁴C-testosterone penetrating the skin in Franz static diffusion cells as compared to the CutaFlex™ treatment groups (Figure 3.18). The steady-state flux of ¹⁴C-testosterone ranged from 11-16 $\mu\text{g cm}^{-2} \text{h}^{-1}$.

Mass Balance

There were no significant differences ($p > 0.05$) between the Franz static control as compared to CutaFlex™ static and CutaFlex™ 360 minutes flexed groups in regards to the amount of ¹⁴C-testosterone remaining on the skin surface, in the skin or in the receptor fluid (Figure 3.19).

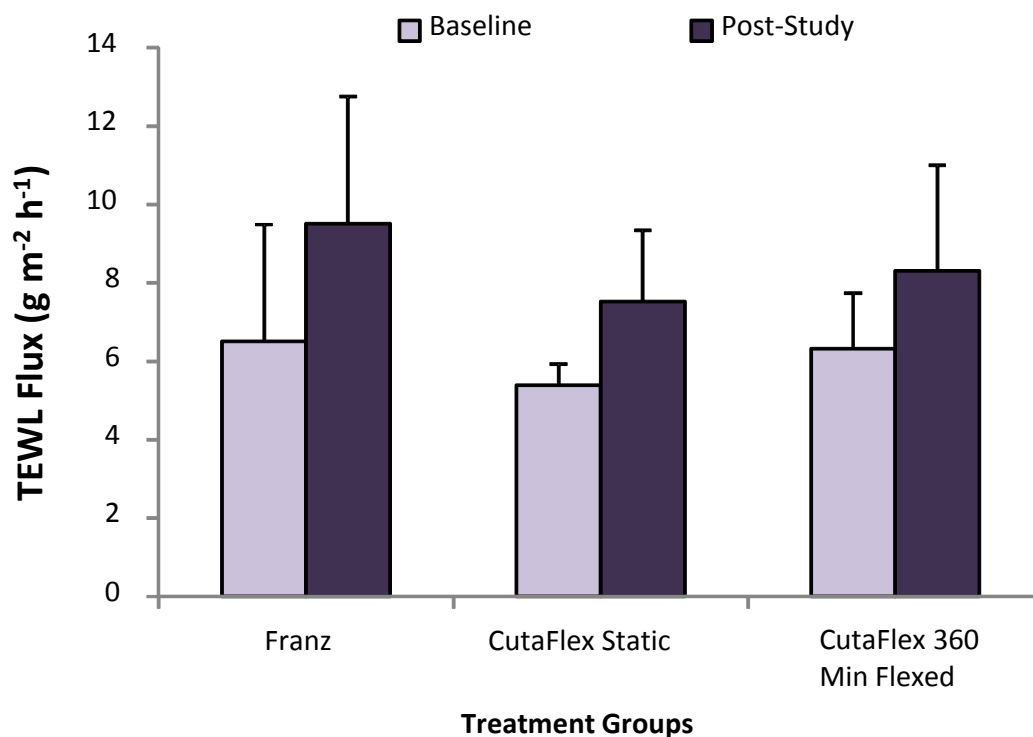


Figure 3.16: Transepidermal Water Loss Flux Before And After ^{14}C -Testosterone Acid Exposure In Static (Franz And CutaFlex™ Static) And Flexed (CutaFlex™ 360 Minutes Flexed) Diffusion Cells. Testosterone was applied ($250 \mu\text{l cm}^{-2}$) to the skin surface in a saturated, equilibrated un-filtered solution at a concentration of 20 mg ml^{-1} for 51 hours. All bars are represented as mean + standard deviation of $n=6$ diffusion cells.

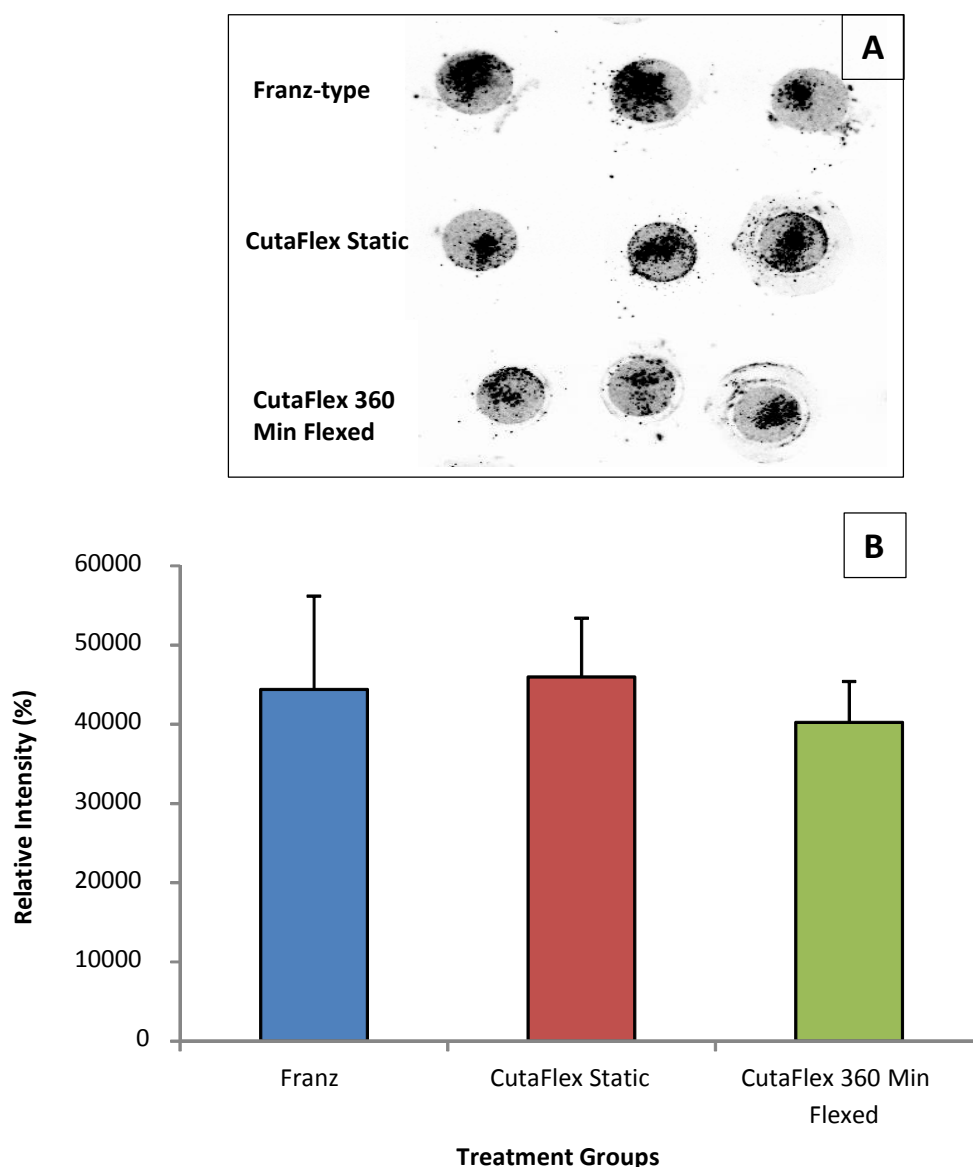


Figure 3.17: Surface Spreading Of ^{14}C -Testosterone Treated Static (Franz And CutaFlex™ Static) And Flexed (CutaFlex™ 360 Min Flexed) Porcine Skin Sections After 51 Hours Of Exposure: Autoradiographs (A) And Intensity Graph (B). Skin was assessed for surface spreading of Carbon-14 using autoradiography images (A). The average intensity of staining was quantified by image analysis to produce a relative intensity score by comparison to un-exposed (control) skin. Testosterone was applied ($250 \mu\text{l cm}^{-2}$) to the skin surface in a saturated, equilibrated un-filtered solution at a concentration of 20 mg ml^{-1} for 51 hours. All points are mean + standard deviation of $n=3$ skin sections.

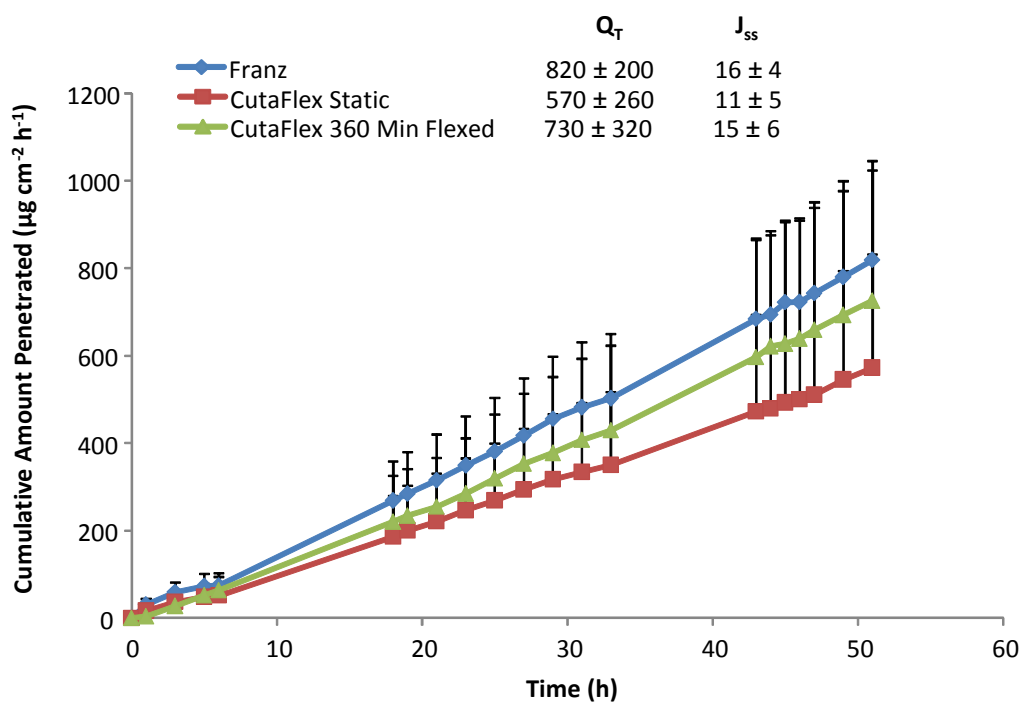


Figure 3.18: Cumulative Amount Of ^{14}C -Testosterone Penetrated Through Static (Franz and CutaFlex™ Static) And Flexed (CutaFlex™ 360 Minutes Flexed) Porcine Skin Over 51 Hours. Testosterone was applied ($250 \mu\text{l cm}^{-2}$) to the skin surface in a saturated, equilibrated un-filtered solution at a concentration of 20 mg ml^{-1} for 51 hours. The cumulative amount ($\mu\text{g cm}^{-2}$) of testosterone penetrated after 51 hours is represented above the graph. All points are mean + standard deviation of $n=6$ diffusion cells. Values for the cumulative amount penetrated at study end (Q_T) are represented on the graph in units of $\mu\text{g cm}^{-2}$. Steady-state flux (J_{SS}) values are represented on the graph in units of $\mu\text{g cm}^{-2} \text{ h}^{-1}$.

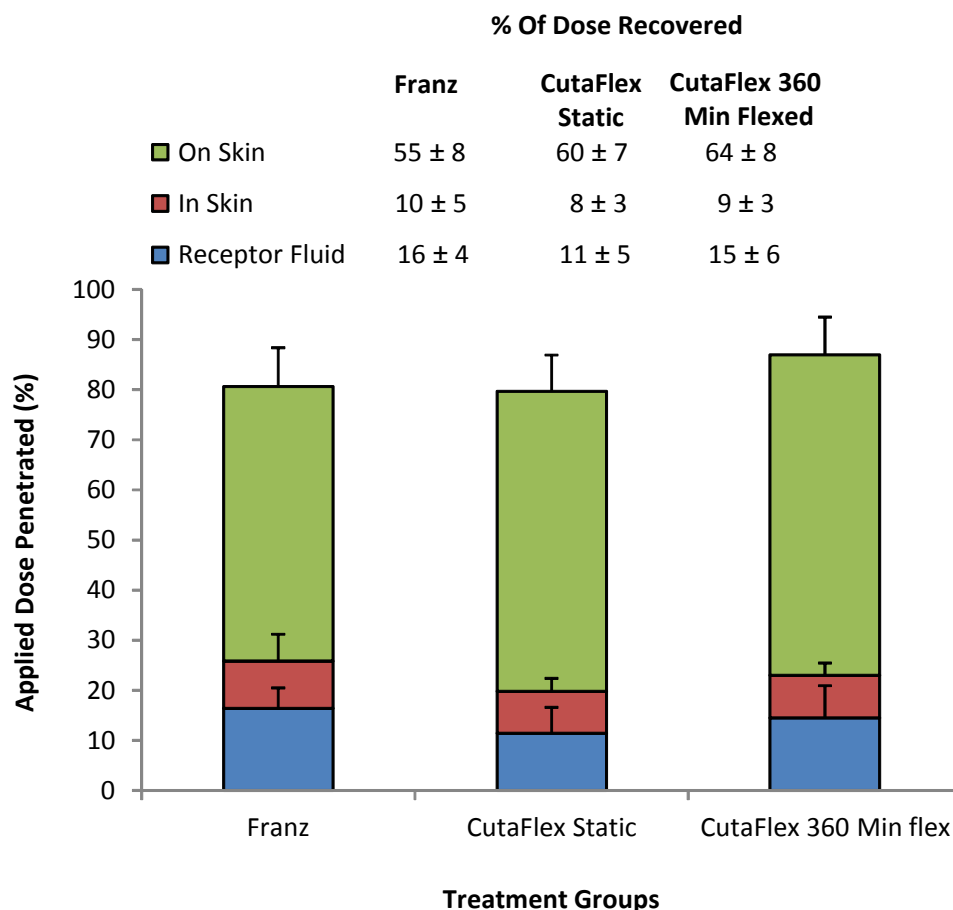


Figure 3.19: Dose Distribution Of ^{14}C -Testosterone From Static (Franz and CutaFlex™ Static) And Flexed (CutaFlex™ 360 Minutes Flexed) Porcine Skin Samples After 51 Hours. Each bar on the graph indicates percentage of the dose applied (8.9 mg) that was recovered from the skin surface (On Skin), in the skin samples or in the receptor fluid. All bars are mean + standard deviation of up to 6 diffusion cells.

3.3.4.7 Dermal Absorption Parameters For All Carbon-14 Chemicals

Dermal absorption parameters of cumulative amount penetrated, steady-state flux, membrane partition coefficient (K_m), permeability coefficient (K_p), diffusion coefficient (D) and lag time (τ) values for benzoic acid, caffeine and testosterone were calculated according to Equations 1.1- 1.5 (pgs. 18- 20) and are listed in Table 3.1. No significant differences in parameters were found between any of the treatment groups for the same chemical. In terms of the rate of dermal absorption (J_{ss}), benzoic acid was the fastest penetrated and testosterone the slowest. However, when presented in terms of $K_p + D$ (which take into account the concentration of penetrant applied to the skin surface), benzoic acid was most able to diffuse through the skin; followed by testosterone and lastly caffeine.

Table 3.1: Dermal Absorption Parameters Measured For Benzoic Acid, Caffeine And Testosterone. Cumulative amount penetrated, steady-state flux, permeability coefficients, diffusion coefficients and lag time were measured for both static skin sections (Franz and CutaFlex™-static) and flexed skin (CutaFlex™ 360 minutes flexed).

	Cumulative Amount Penetrated mg cm ⁻²	Steady State Flux µg cm ⁻² h ⁻¹	Membrane Partition Coefficient (K _m)	Permeability Coefficient (K _p) x 10 ⁻³ cm h ⁻¹	Diffusion Coefficient (D) x 10 ⁻³ cm ² h ⁻¹	Lag Time (τ) minutes
Benzoic Acid			0.065 ± 0.02			
Franz	17.3 ± 5.30	240 ± 136		2.69 ± 1.50	2.07 ± 1.16	20 ± 10
CutaFlex Static	13.7 ± 2.40	200 ± 59		2.17 ± 0.65	1.67 ± 0.50	16 ± 4
CutaFlex Flexed	13.8 ± 1.70	224 ± 56		2.49 ± 0.63	1.91 ± 0.48	14 ± 3
Caffeine			0.060 ± 0.01			
Franz	2.10 ± 0.35	40 ± 6		0.38 ± 0.07	0.23 ± 0.04	107 ± 19
CutaFlex Static	2.30 ± 0.39	47 ± 9		0.47 ± 0.09	0.29 ± 0.06	88 ± 16
CutaFlex Flexed	2.50 ± 0.28	49 ± 7		0.30 ± 0.07	0.30 ± 0.04	84 ± 13
Testosterone			0.069 ± 0.00			
Franz	0.85 ± 0.20	16 ± 4		0.80 ± 0.19	0.58 ± 0.14	46 ± 16
CutaFlex Static	0.57 ± 0.26	11 ± 5		0.57 ± 0.24	0.41 ± 0.18	72 ± 30
CutaFlex Flexed	0.73 ± 0.32	15 ± 6		0.73 ± 0.30	0.53 ± 0.22	55 ± 24

3.4 Discussion

Novel Flexing Diffusion Cell

According to Brain *et al.* (2002), a well-made diffusion cell should encompass the following parameters: be chemically inactive, robust and easy to handle, allow for the use of different sized-membranes, provide thorough mixing of receptor fluid contents, ensure close contact between membrane and receptor phase, maintain a constant temperature, have precisely calibrated volumes and diffusional areas (accurately engineered surface area), maintain membrane integrity, provide easy sampling and replenishment of receptor fluid, provide a good seal between donor and receptor chamber and be available at a reasonable cost.

CutaFlex™ diffusion cell bodies were constructed from polytetrafluoroethylene (PTFE) an inert plastic and the expanding bladder from latex. This novel diffusion cell is based upon the OECD-compliant Franz-type static diffusion cell and as such can accommodate various preparations of skin, several magnetic stir bars and provides close contact between skin and receptor phase. In addition, an insert can be developed to provide support for skin equivalents. CutaFlex™ was also constructed to incorporate a jacketed chamber, which was connected through the diffusion manifold to a heated re-circulating pump, allowing for a consistent skin temperature.

Due to the injection moulding process, each CutaFlex™ cell is identical and therefore will have negligible variations in receptor chamber parameters and diffusional area. Although the CutaFlex™ cell incorporates the use of an additional diaphragm arm, the sampling arm is in the same location as the static Franz cell and provides easy access for sampling receptor fluid as well as replacing media. Due to the manufacturing process (injection moulding) the CutaFlex™ system has been designed

to eliminate high costs. It is expected that CutaFlex™ will cost less than the average glass static Franz cell.

One potential disadvantage of the current CutaFlex™ design is the latex bladder, which may potentially absorb or adsorb penetrants and thus artificially reduce penetrant concentration in the receptor chamber fluid. Indeed, the cumulative amount of penetrant $^3\text{H}_2\text{O}$, benzoic acid and testosterone in CutaFlex™ receptor chambers was consistently less than Franz cells, suggesting that loss of penetrant through bladder adsorption or absorption may have occurred.

Bladder Adherence Studies

Therefore, both tritiated water and carbon-14 chemical bladder adherence studies were performed to determine if chemicals that penetrated through the skin could adhere to the bladder present in the receptor chamber. It was found that the amount of adherence of tritiated water to the latex bladder was consistently approximately 1.16 mg cm^{-2} (0.26 % of the applied dose per cm^{-2}) after 540 minutes. Benzoic acid, caffeine and testosterone were found to adhere to the latex balloon in consistent amounts equating to 0.15 mg cm^{-2} (0.38 % of applied dose per cm^{-2}), 0.64 mg cm^{-2} (1.71 % of applied dose per cm^{-2}) and 0.05 mg cm^{-2} (0.57 % of applied dose per cm^{-2}), respectively after 51 hours. These amounts were not found to explain the small differences in penetration between the Franz and CutaFlex™ cells and so another part of the CutaFlex™ system may be responsible. For example, the PTFE coating of the receptor chamber.

Both tritiated water and TEWL flux rates in this study did not significantly vary from baseline after flexion of skin sections for up to 120 minutes. However, tritiated water and transepidermal water loss measurements did not show a correlation ($r = 0.06$).

Tritiated water measurements after 120-480 minutes of flexion did not differ from the static skin controls. These data demonstrate that under the conditions employed in these studies, skin flexing (2 flexes per minute, 6 mm maximum amplitude) had no measurable effects on baseline TEWL and tritiated water permeability.

Dermal Absorption Of Model Compounds

The OECD 428 guideline states that “thorough characterisation must be performed for a novel diffusion cell” (OECD, 2004). This characterisation consists of “measuring and comparing the absorption of model chemicals to the OECD-compliant models” (OECD, 2004). Model compounds (e.g. benzoic acid, caffeine, testosterone, $^3\text{H}_2\text{O}$ etc.) have been previously used to investigate (i) skin barrier integrity after frozen storage, (ii) comparison of animal and human skin, (iv) quantification of metabolic enzymes in animal and human skin, (v) characterisation of novel diffusion cells and (vi) investigation of skin properties after chemical or physical damage (Franz, 1975, Hawkins and Reifenrath, 1984, Reifenrath *et al.*, 1984, Harrison *et al.*, 1984, Kao *et al.*, 1985, Bronaugh and Stewart, 1985, Hawkins and Reifenrath, 1986, Reifenrath and Kempainen, 1991) (see Sections 1.3.1.3 and 1.4.1.5).

In this study, tritiated water permeation was measured for each treatment group to study the effects of flexing skin from 0-480 minutes. It was imperative to analyse the effect of flexing on skin barrier integrity as damage to the skin barrier layer would impact the percutaneous absorption of both standard chemicals and nanoparticles. *In vitro* flexing of porcine skin from 0-480 minutes did not cause a change in skin barrier integrity when the skin was flexed twice per minute with a maximum displacement height of 6 mm. Tritiated water was applied to the skin surface in a

dose of 250 mg cm^{-2} , allowing for full contact of the skin during exposure for all durations of flexing. This is in agreement to previous *in vitro* studies, in which the surface dose was in contact with flexing skin, however the skin was flexed outside of a diffusion cell system (Tinkle *et al.*, 2003, Rouse *et al.*, 2007). The change in water permeability through the stratum corneum has been documented as a good indicator of changes in permeability of both non-polar and polar chemicals (Bronaugh *et al.*, 1986). Therefore, as no significant differences were found in the amount of tritiated water penetrating immobile sections as compared to skin sections flexed from 30-480 minutes, the flexing conditions (2 flexes per minute, 6 mm maximum displacement) used in this present study did not cause any measurable skin damage in terms of barrier function.

The three carbon-14 model compounds used in this study, namely benzoic acid, caffeine and testosterone differ in physicochemical properties (Table 1.2). These model compounds are studied to provide estimations of dermal absorption for chemicals with similar properties. Benzoic acid has a log P value of 1.83 and the lowest molecular weight of the three compounds studied. Caffeine has a more hydrophilic Log P (e.g. -0.01) and a slightly higher molecular weight (e.g. 194) as compared to benzoic acid. Testosterone has a lipophilic log P (e.g. 3.32) and the highest molecular weight (e.g. 288) compared to benzoic acid and caffeine. A log P value between 1 and 3 is thought to be optimal for dermal absorption (Brain and Chilcott, 2008). Penetration of benzoic acid through the skin was an order of magnitude higher than both caffeine and testosterone. This is not in agreement with the literature, in which researchers using both *in vivo* testing and *in vitro* full- and split-thickness porcine skin observed similarities in the penetration between caffeine and benzoic acid (Reifenrath *et al.*, 1984, Hawkins and Reifenrath, 1986).

Similarities in the general trend of penetration of benzoic acid and caffeine were also seen with in the literature when using human skin (*in vitro*) (Bronaugh and Stewart, 1985). The absolute amounts penetrated for both caffeine and benzoic acid in the present study were greater than those published in the literature; thought to be attributed to the relatively low dose ($4 \mu\text{g cm}^{-2}$), change of vehicle and exposure selected in previous studies in comparison to the saturated, equilibrated solution chosen for the present study (approximately 23 mg cm^{-2}) as well as a change in vehicle.

In contrast to the penetration of benzoic acid and caffeine, testosterone was found to penetrate porcine skin approximately 12-fold and 3-fold less, respectively. This finding is in agreement with the literature, with testosterone found to be the least permeable of all three compounds tested (van de Sandt *et al.*, 2004, Hawkins and Reifenrath, 1984, Hawkins and Reifenrath, 1986). This is to be expected due to the relatively high lipophilicity of testosterone in addition to a high molecular weight, allowing for permeation from vehicle into the stratum corneum but difficulty diffusing through the stratum corneum to the viable epidermis underneath. As seen with caffeine and benzoic acid in the present study, the absolute amounts penetrated from testosterone were higher in this study as compared to the literature, a finding thought to be due to the amount applied in this study (i.e. 5 mg cm^{-2}) as compared to past studies (i.e. $4 \mu\text{g cm}^{-2}$). The dose recovery of ^{14}C -chemical in the skin and in the receptor fluid were not different amongst the treatment groups, which also reiterated the findings that flexion did not cause damage to the skin. However, the amount of ^{14}C -benzoic acid recovered on the skin surface for the Franz treatment group was significantly lower than the CutaFlexTM groups, a fact that could be attributed to experimental design.

In order to determine certain parameters of dermal absorption (e.g. J_{ss} , K_m , K_p , D , and lag time) an infinite dose regime was selected for these studies. Although the infinite dose regime is not thought to reflect an *in vivo* exposure scenario, in order to determine the dermal absorption parameters a concentration that does not appreciably deplete over time is needed. There were no significant differences found between treatment groups in terms of steady-state flux, permeability coefficient (K_p), diffusion coefficient (D) or lag time for each chemical. It is difficult to compare the present parameters to the literature as skin source, skin preparation, compound concentration, vehicle choice and dose regime will impact the findings. However, as previous studies have used different conditions and methods of reporting skin absorption, the only comparison that can be made is that the general pattern of absorption from this study are in broad agreement with the literature. There was no significant difference between CutaFlex™ and Franz cells. Collectively, these data infer that the CutaFlex™ system is comparable to existing OECD compliant diffusion cells for measuring dermal absorption. Moreover, as there were no statistically significant differences in the CutaFlex™ cells flexed for 360 minutes, it can be found that flexing of skin does not cause a decrease in integrity of the skin barrier layer.

The membrane partition coefficient for all three chemicals in this study was found to be similar between benzoic acid and testosterone and lower for caffeine. No comparable measurements of membrane partition coefficients were identified from the available literature. However, it is conceivable that the physicochemical properties for each chemical (i.e. Log P and molecular weight) attributed to differences in membrane partition coefficients, with a more lipophilic molecule showing larger partitioning into the skin than a hydrophilic one (e.g. testosterone compared to caffeine). Aqueous ethanol (50%) has been used as a receptor fluid for

lipophilic chemicals, in order to more realistically model the percutaneous penetration of the *in vivo* scenario (Scott and Ramsey, 1987). Hawkins and Reifenrath (1986) documented that the dermis provided a significant barrier to *in vitro* penetration of compounds with high Log P values, whereas this barrier was not as significant *in vivo*. In this present study, testosterone could have been affected by the hydrophilic dermal tissue present, with much lower amounts of this compound penetrating as compared to the other two more hydrophilic compounds tested.

In these studies it was found that the diffusion coefficient for testosterone was greater than that of caffeine. Testosterone, in comparison to caffeine, is much more lipophilic, a characteristic which seemed to compensate for the larger molecular weight of this compound to caffeine. Caffeine is highly hydrophilic and this no doubt slowed diffusion through the lipophilic stratum corneum. In the present study, lag time was measured for all compounds and found to be greatest for caffeine and benzoic acid as compared to testosterone. Lag time is an important dermal absorption parameter for a compound of interest, however determining *in vitro* lag time has been acknowledged as being difficult (Schaefer and Redelmeier, 1996) . A small change in steady state flux can lead to large changes in the estimation of lag time, and lag time is likely to be dependent upon the apparatus and mixing efficiency (Schaefer and Redelmeier, 1996). Previous studies found in the literature did not use a similar experimental design to the present study (i.e. infinite dose, equilibrated, saturated solution, 51 hours), therefore a comparison could not be drawn between dermal absorption parameters reported between this study and the existing literature.

Skin Damage Studies

Standard methods to measure the viability of skin before the commencement of *in vitro* studies include both transepidermal water loss (TEWL) and tritiated water penetration in static diffusion cells. Both techniques have been recommended by the OECD and ECVAM in assessing skin barrier integrity due to the relatively quick assessment of the quality of skin (OECD, 2004, Howes *et al.*, 1996).

TEWL vs Tritiated Water

Clearly, it would be useful to correlate tritiated water and TEWL methods of barrier integrity measurement in order to increase the ease of determining skin barrier viability. The results of the present *in vitro* studies have shown that baseline values of tritiated water penetration and transepidermal water loss did not correlate ($r = 0.1-0.4$). The correlation between TEWL and tritiated water penetration basal values in excised human skin reported by Chilcott *et al.* (2002) ($r = 0.11$) and Hui *et al.* (2012) from baseline ($r = 0.34$) to 4 hours ($r = 0.37$) are in agreement with those found in this study. This is in contrast to results published by Elmahjoubi *et al.* (2009) which reported a good correlation between TEWL and tritiated water for basal rates ($r = 0.90$). In this study, the *in vitro* spread of baseline values from TEWL data ranged from $7-23 \text{ g m}^{-2} \text{ hr}^{-1}$ in comparison to the applied dose of tritiated water penetrated which ranged from 0.1-4.4% of the applied dose. Thus, the range of tritiated water values were an order of magnitude greater than that of TEWL rates and more variable (e.g. coefficient of variance), which is an indication that tritiated water is a more sensitive measure of barrier function.

Flexion Studies

Using *in vitro* flexion for 360 minutes with model compounds did not show a difference in penetration, steady-state flux, permeability coefficient, diffusion coefficient or lag time. Collectively, these data provide unequivocal evidence that flexing of the skin (2 flexes per minute + 6 mm amplitude) did not cause any measurable effects on skin barrier function. A previous *in vitro* skin flexing device has been documented in the literature. However, that system was not present within a diffusion cell and was used to investigate potential for nanoparticle penetration through the skin (Tinkle *et al.*, 2003, Rouse *et al.*, 2007, Zhang and Monteiro-Riviere, 2008). Previous studies with this device did not report any measurement of skin barrier integrity.

Physical And Chemical Damage Of The Stratum Corneum

When observing tritiated water permeation from chemically damaged skin, it was noted that both static and flexed skin groups showed significant decreases in barrier integrity after SLS treatment. Transepidermal water loss flux results indicated that significant increases in flux had occurred in both static treatment groups as well as the 60 minute flexed skin group, leading to a variation in results. In this study, a poor correlation ($r = 0.6$) was found between tritiated water and transepidermal water loss values after sodium lauryl sulphate damage treatment. This is in agreement with findings published in the literature (Elmahjoubi *et al.*, 2009, Chilcott *et al.*, 2002).

The time after which TEWL measurements can be taken without residual effects from occlusion (i.e. evaporation of excess water) has not yet been conclusively determined. Multiple papers have recommended a 30 minute wait time (Berardesca and Maibach, 1988, Freeman and Maibach, 1988, Goh and Chia, 1988) while others

have taken a more conservative approach and advised either 1 hour (Agner and Serup, 1993) or 3 hours (Baker and Kligman, 1967) waiting time. As TEWL is used as an indication of skin barrier integrity, such a long period of time for a pre-study measurement would not be ideal. This has also been reflected in an OECD recommendation, in that “any pre-study skin evaluation should not take any longer than a few hours and would be performed immediately before application of a test product” (OECD 2004). In the present study, TEWL measurements were taken one hour after occlusion for the model compound. Rates of TEWL were measured directly after flexion and 2 hours after SLS treatment and 3 hours after puncture damage due to the time at which flexing at ceased in the two damage studies. Whilst this complies with OECD guidance, it should be noted that the magnitude of damage measured *in vitro* with TEWL tends to decrease with time (possibly as a result of the water gradient within the skin being re-established) (Chilcott and Farrar, 2000).

In the present study, it was observed that only flexed skin sections (30-120 minutes) mounted in the CutaFlexTM cells presented with significant decreases in barrier integrity through puncturing as measured by tritiated water. When using transepidermal water loss rates, all groups except the Franz static cell, presented with significant decreases in skin integrity after puncture. In this study, there was no correlation ($r = 0.4$) found between tritiated water permeation and transepidermal water loss after physical damage of the skin. These findings agree with what has been documented in the literature (Elmahjoubi *et al.*, 2009, Chilcott *et al.*, 2002). The finding that static skin did not present with a decrease in skin integrity could be credited to swelling (through capillary action) of the skin resulting in the closure of the punctures (Elmahjoubi *et al.*, 2009). Another alternative explanation is that the punctures present in the immobile skin sections could have been re-sealed due to the

elastic properties of the skin (i.e. collagen and elastin). The sealing of the punctures within the flexed skin sections could have been delayed by the flexing motion of the skin. It is conceivable that the difference between tritiated water and TEWL may be partially attributable to small amounts of receptor fluid ejected through the puncture holes during flexing, resulting in liquid on the skin surface. This explanation is supported by the observation that un-flexed skin did not show an increase in tritiated water penetrated, as did half of the static skin groups measured for TEWL rates.

Collectively, these data indicate that skin subject to flexing does not exacerbate the decrease in skin barrier integrity.

In summary, this work demonstrated that:

- The novel flexing diffusion cell provides comparable measurements of dermal absorption to the OECD-compliant Franz-type static cell
- *In vitro* skin flexing from 0-480 minutes does not cause a decrease in skin barrier function
- Skin flexing does not generally exacerbate skin damage caused by SLS/punctures
- Tritiated water permeation is a more sensitive indicator of barrier integrity compared to transepidermal water loss

**Chapter 4: The Effect Of Flexing On Quantum Dot Nanoparticle
Skin Absorption**

4.1. Introduction

Work presented in the preceding chapter confirmed that the novel flexing skin system (CutaFlex™) provides percutaneous penetration measurements for model compounds that are in agreement with a traditional diffusion cell system and other workers (Table 1.3, Table 1.4, Table 1.5 and Table 3.1). The purpose of work reported in this chapter was to use the novel diffusion cell model to investigate the hypothesis that skin flexing could facilitate the dermal absorption of nanoparticles.

In order to achieve this aim, the work was divided into two main stages:

1. Characterisation of 6 quantum dots (QDot 565 and QDot 655; each coated in either PEG-amine, PEG-carboxyl or PEG) in terms of shape, size and distribution in suspension.
2. Develop appropriate methodology for histology, confocal laser microscopy and skin surface fluorescence analysis for the detection and location of QDots 565 and 656 (Figure 4.1) in the presence or absence of flexing. This method development work is not reported further but is mentioned here to demonstrate ‘due diligence’.

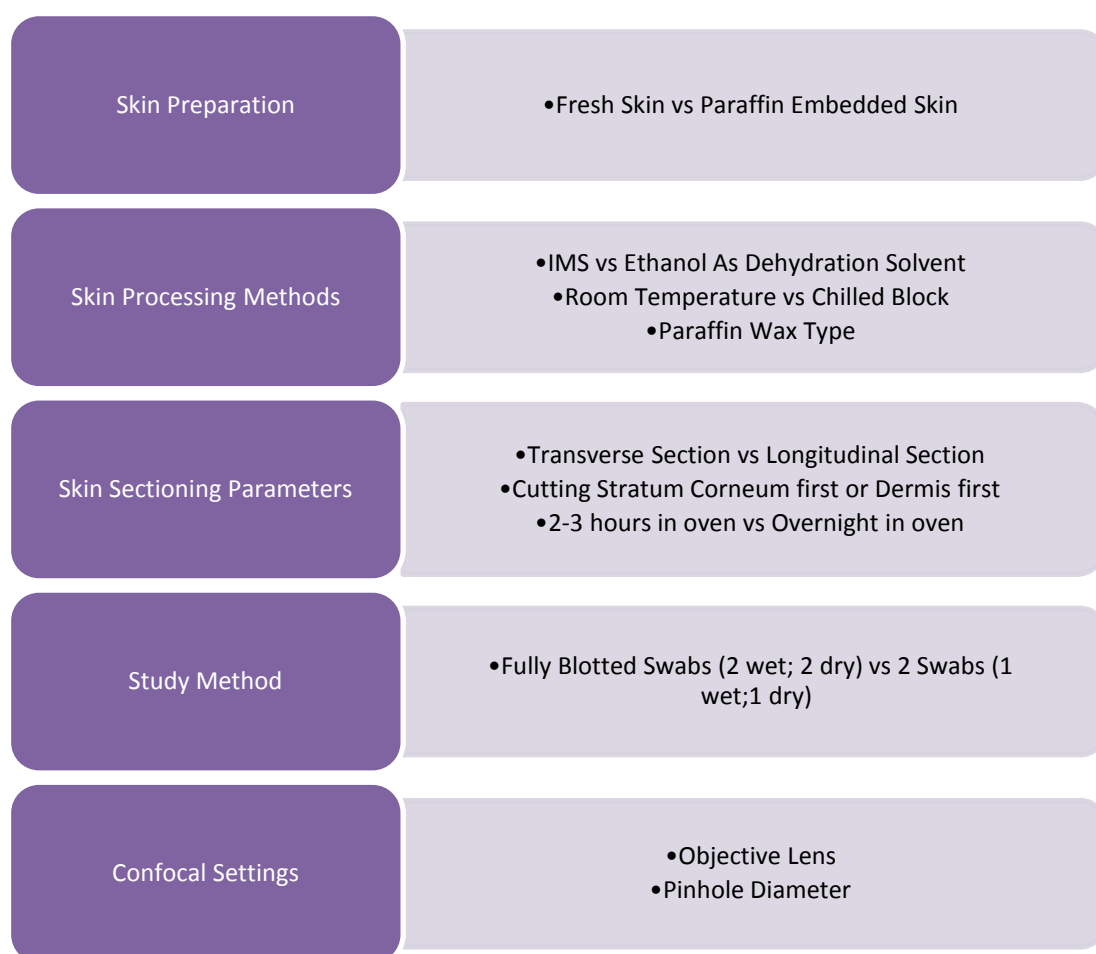


Figure 4.1: Quantum Dot Dermal Absorption Study: Method Development. Parameters that were optimised included skin preparation, skin processing methods, skin sectioning parameters, study method and confocal settings.

4.2. Materials and Methods

Nanoparticle characterisation was performed using transmission electron microscopy (Section 2.1.7.1) and dynamic light scattering (Section 2.1.7.2). Porcine skin and Franz and CutaFlex[™] diffusion cells were prepared as outlined in (Section 2.1.2 and 2.1.3), respectively, according to a nanoparticle skin absorption protocol (Section 2.1.8). Skin samples were subsequently analysed by standard light microscopy (Section 2.1.11.2) and confocal laser microscopy (Section 2.1.12).

Briefly, all quantum dot nanoparticle suspensions were sonicated and characterised prior to dermal absorption studies. Rates of TEWL were measured at baseline and after exposure to quantum dots. Quantum dot nanoparticles 565 and 655 nm with PEG-amine, PEG-carboxyl or PEG attachments as well as the phosphate buffered saline solution (control) were applied to the skin surface at a dose of $169 \mu\text{l cm}^{-2}$ for eight hours. Excess quantum dot suspension was removed from the skin surface using a wet then dry swab and, along with receptor fluid samples, were analysed using a fluorescence spectrophotometer (Section 2.1.9). Skin surface images were then taken under ultra-violet illumination (Section 2.1.10). Skin samples were then processed and wax embedded for H&E staining and imaging on a laser scanning confocal microscope.

This chapter represents a pilot study and is therefore limited in the scope of interpretation due to the relatively small number of skin samples.

4.3. Results

4.3.1. Quantum Dot Nanoparticle Characterisation

Transmission electron microscopy was performed on all QDot nanoparticles for characterisation of both shape and size (Figure 4.2- A). All QDot 565 nm particles were spherical in shape, with diameters ranging from 4 to 6nm (Table 4.1). In contrast, QDot 655 nm nanoparticles were more triangular in shape (Figure 4.2- B) and more consistent along the long (13nm) and short (5 – 6 nm) axis (Table 4.1).

Dynamic light scattering measurements were performed in order to determine hydrodynamic diameters of all quantum dot nanoparticles in phosphate buffered saline solution (Table 4.1). When using the number-based distribution (less affected by large particulates), the hydrodynamic diameter of QDot 565 ranged from 13 nm (PEG-carboxyl) to 23 nm (PEG). The hydrodynamic diameters of QDot 655 were similar in range (Table 4.1).

The polydispersity index of all QDot nanoparticles was found to be approximately 0.5; midway between a small and broad distribution (Table 4.1).

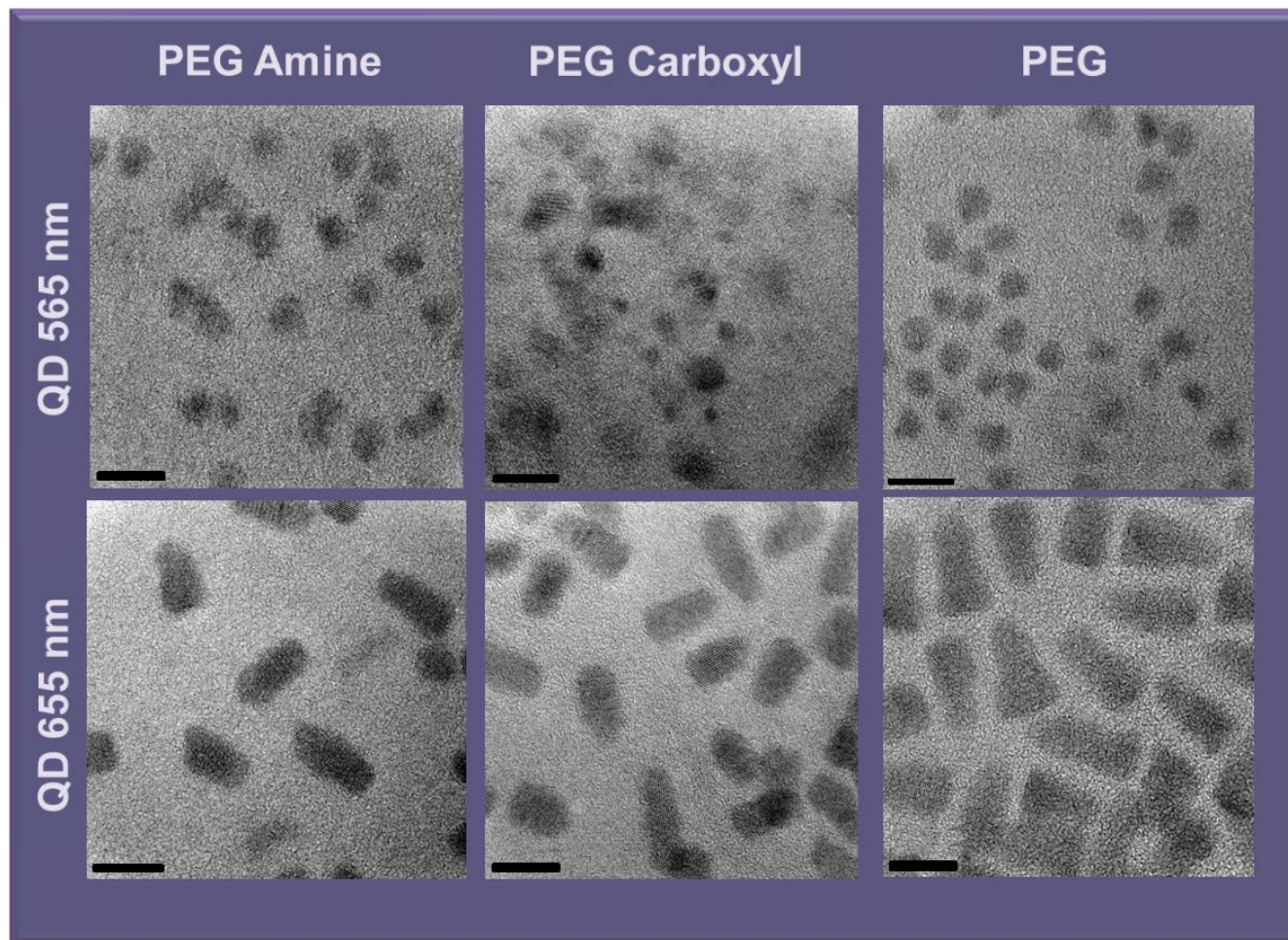


Figure 4.2: Transmission Electron Micrographs Of Quantum Dot 565 nm (Top Row) And 655 nm (Bottom Row) With PEG-Amine (First Column), PEG-Carboxyl (Middle Column) And PEG (Third Column) Attachments. All scale bars (bottom left) are representative of 10 nm. Magnification: 300,000X.

Table 4.1: Size Characterisation Of Quantum Dots 565 And 655 With PEG-Amine, PEG-Carboxyl And PEG Attachments Using Transmission Electron Microscopy And Dynamic Light Scattering. Transmission electron microscopy was used to determine size (d.nm; diameter in nanometers) and QD 655 was expressed as long axis x short axis. Dynamic light scattering individual peak sizes are stated in terms of number-based methods (diameter in nanometers). The polydispersity index is expressed on a 0-1 scale, with 0 representing a fully monodispersed suspension and 1 representing a polydispersed suspension.

Nanoparticle	Transmission Electron Microscopy Images (d. nm)	DLS Peak Size (d.nm)	PDI (Polydispersity Index)
QD 565 PEG-Amine	4	16 ± 1	0.5 ± 0.0
QD 565 PEG-Carboxyl	4.5	13 ± 1	0.6 ± 0.0
QD 565 PEG	6	23 ± 2	0.4 ± 0.0
QD 655 PEG-Amine	13 x 6	13 ± 9	0.4 ± 0.1
QD 655 PEG-Carboxyl	13 x 5	12 ± 2	0.6 ± 0.3
QD 655 PEG	13 x 5	15 ± 3	0.6 ± 0.2

4.3.2. Transepidermal Water Loss Rates

There were no overt changes in the rates of transepidermal water loss (TEWL) following exposure to nanoparticles (Figure 4.3). All TEWL rates were within normal values identified in Chapter 3 (Section 3.3.3) and therefore, the skin barrier integrity was not changed by flexing or nanoparticle exposure.

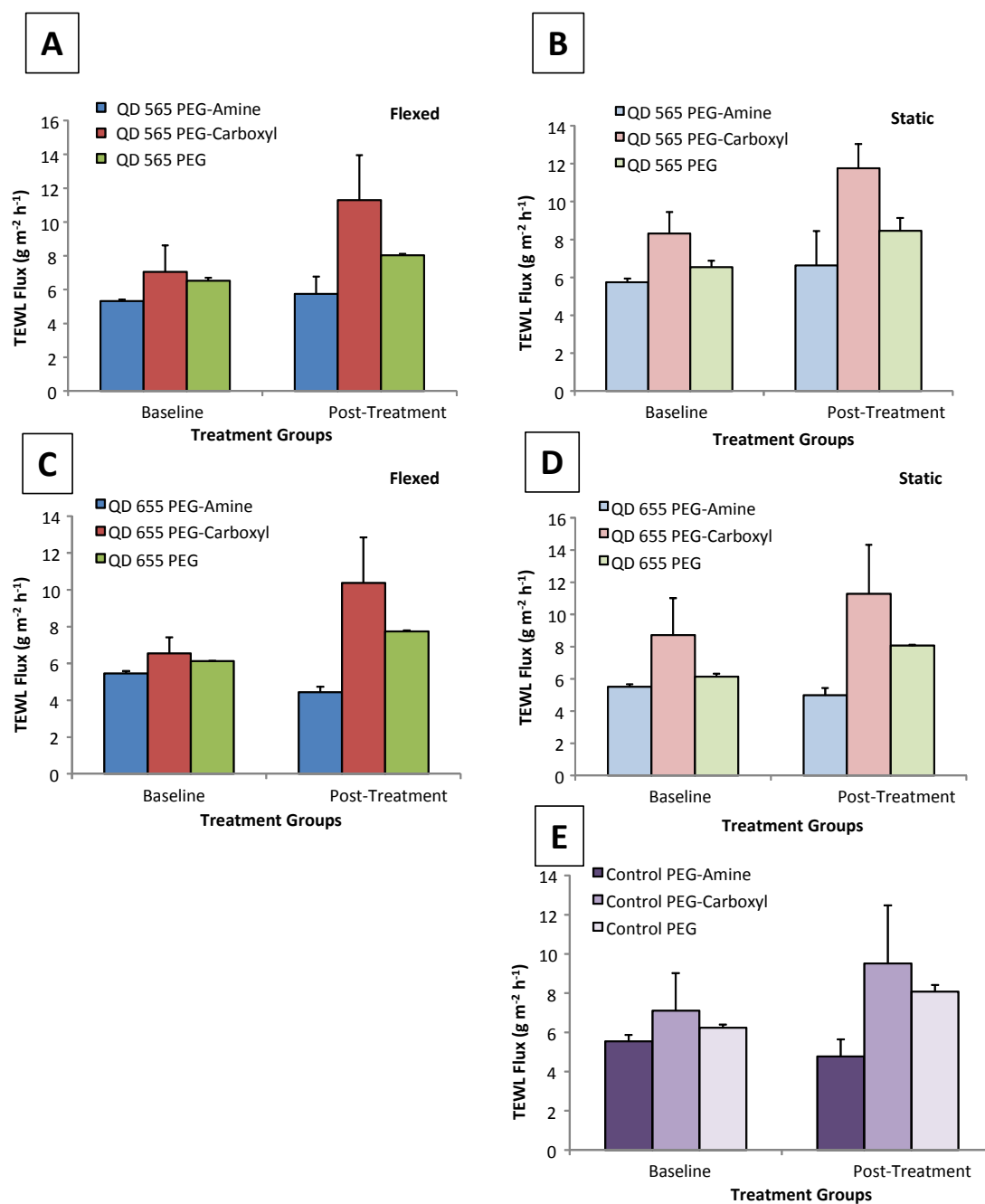


Figure 4.3: *In Vitro* Transepidermal Water Loss Rates Measured From Excised Pig Skin Treated With QDot 565 (A and B), 655(C and D) And PBS (Control-E). Measurements were taken before (baseline) or after exposure (post-treatment) to solutions containing quantum dots 565 (upper) and 655 (middle) or from untreated controls; bottom) in the presence (“Flexed”) or absence (“Static”) of skin flexing. All data are represented as mean + standard deviation of n=3.

4.3.3. Skin Surface Recovery of QDots

The recovery of unabsorbed QDots (from skin surface swabs) was quantified by fluorescence spectroscopy by reference to a range of calibration standards (Section 2.1.9). With the exception of amine coated particles, there was an apparently large recovery of QDot 655 from the skin surface as compared to QDot 565 (Figure 4.4). There was no apparent difference in skin surface recovery between flexed and un-flexed skin (for each QDot). The greatest recovery of fluorescence was observed with PEG-coated particles⁷.

⁷ Due to the limited number of replicates performed ($n = 3$), statistical testing was not performed.

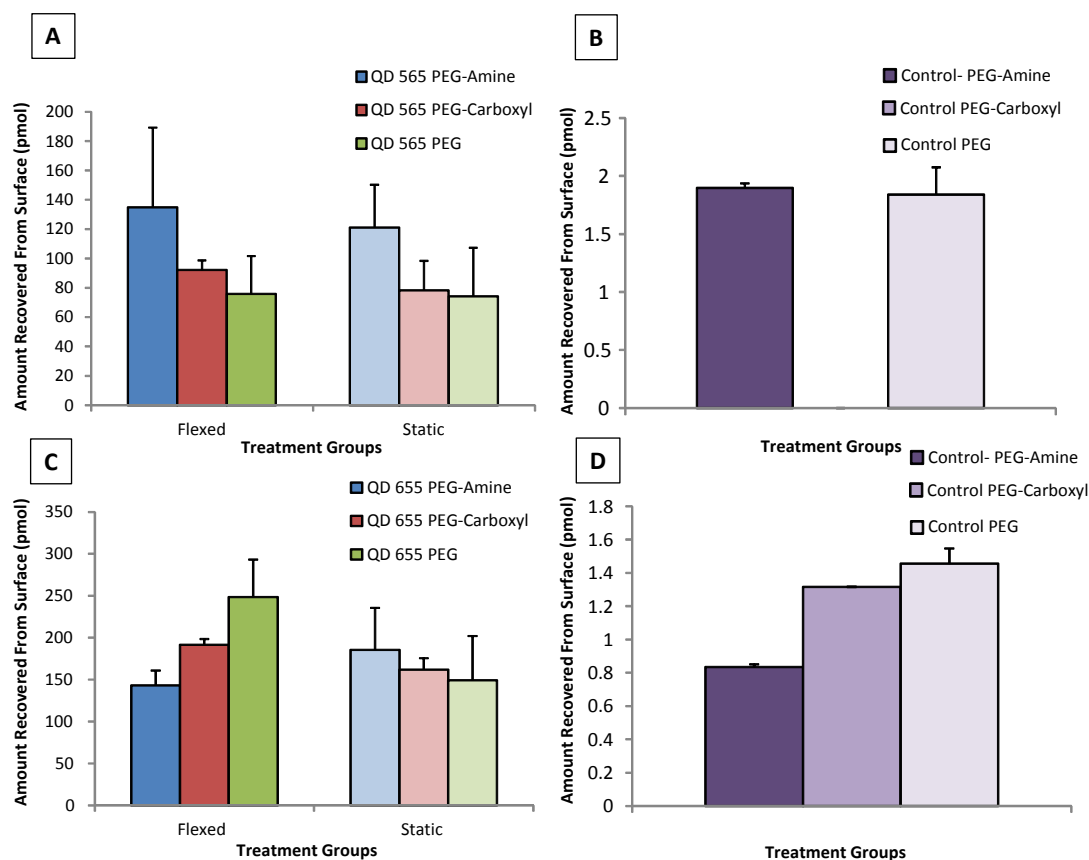


Figure 4.4: Skin Surface Fluorescence Recovery From Quantum Dot 565 (A), Quantum Dot 655 (C) And Control (B and D) Treated Groups. Flexed and static samples are represented in the same graph. Quantum dot 565 and 655 nm were tested with three attachments: PEG-Amine, PEG-Carboxyl and PEG. The control tested was phosphate buffered saline solution. Quantum dot suspension was applied (300 μ l; 300 pmols) to the skin surface for 8 hours. Skin was flexed in CutaFlex™ cells for 6 hours (2 flexes per minute; 6 mm maximum displacement). The same skin donor was used per study (i.e. for QDot and Control groups). All groups (n= 3) are represented as mean \pm standard deviation.

4.3.4. Skin Surface Distribution of QDots

Fluorescence staining of the skin was observed (to varying extents) with all QDot particles (Figure 4.5 and Figure 4.6).

4.3.4.1. Quantum Dot 565 vs 655 nm

All QDot 655 treated skin demonstrated apparently higher fluorescence staining compared to QDot 565 treated skin (Figure 4.5 and Figure 4.6). Thus, QDot 655 nanoparticles seemed to partition into the stratum corneum in greater amounts than QDot 565. However, QD 565 presented with higher fluorescence staining of the hair follicles, as compared to QD 655 treated sections, this effect was most apparent in PEG-Amine and PEG-carboxyl groups. Therefore, charged QD 565 nanoparticles seemed to preferentially partition into hair follicles, in greater amounts than QD 655 treated skin sections.

4.3.4.2. Flexed vs Static Skin Sections

Greater fluorescence was seen in flexed skin treated with carboxylic coated nanoparticles (both QDot 565 and 655) as compared to the static carboxylic treated groups (Figure 4.5 and Figure 4.6). Static skin treated with QDot 565 PEG-Amine and PEG-Carboxyl attachments showed greater staining of the hair follicles than the corresponding flexed skin.

4.3.4.3. PEG-Amine, PEG-Carboxyl And PEG Attachments

The negatively charged QDot attachment (PEG-Carboxyl) showed the greatest fluorescence in staining of the skin surface (both QDot 565 and 655) (Figure 4.5 and Figure 4.6).

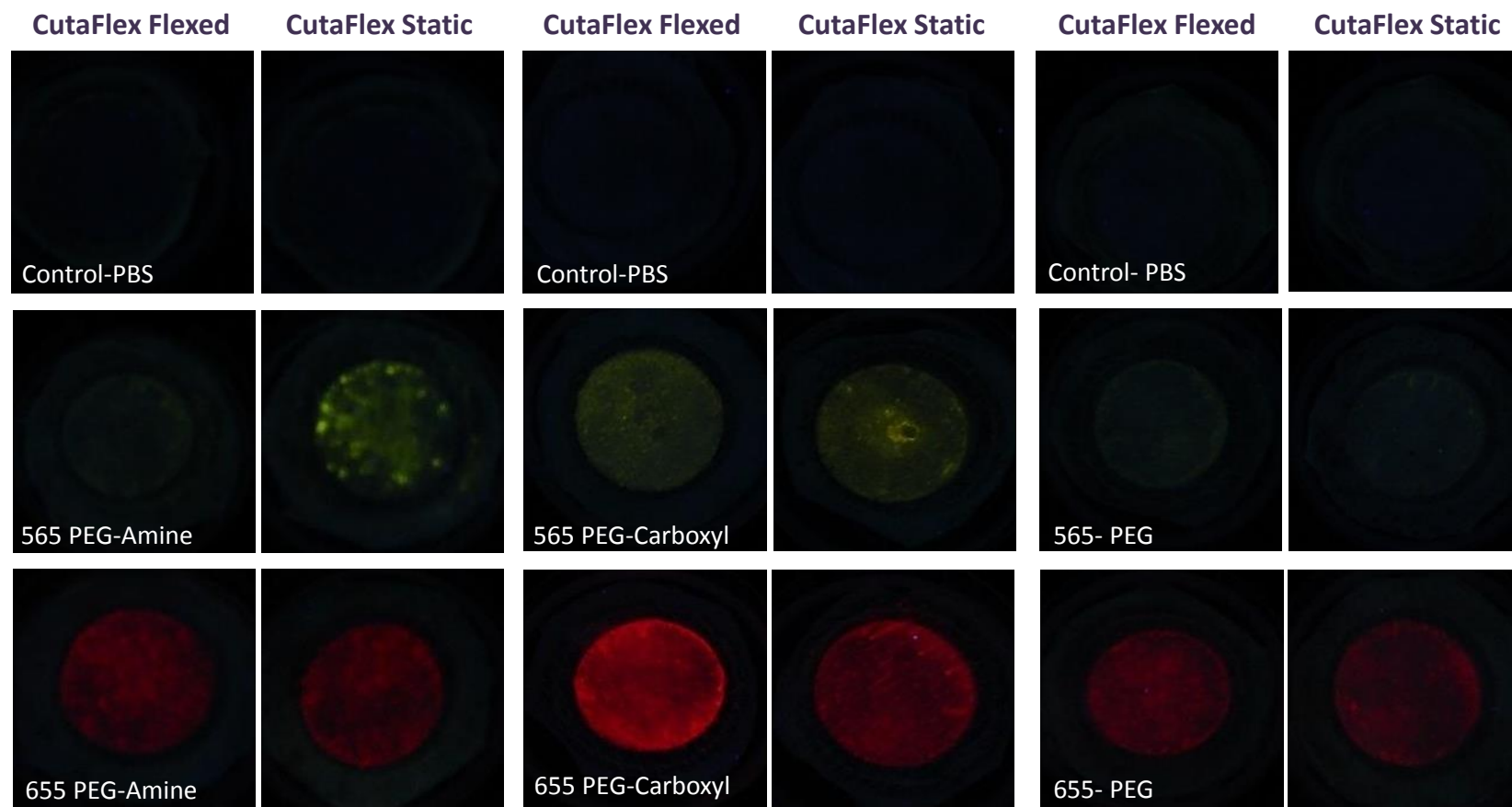


Figure 4.5: Skin Surface Distribution Of Quantum Dot 565 And 655 With PEG-Amine, PEG-Carboxyl And PEG Attachments And Control Skin Sections. Representative sections were selected for each treatment group. Phosphate buffered saline and QDot nanoparticles were applied ($169 \mu\text{l cm}^{-2}$) to flexed or static porcine skin for 8 hours. Fluorescence was then visualised using ultra-violet illumination. Each group consisted of $n=3$ diffusion cells.

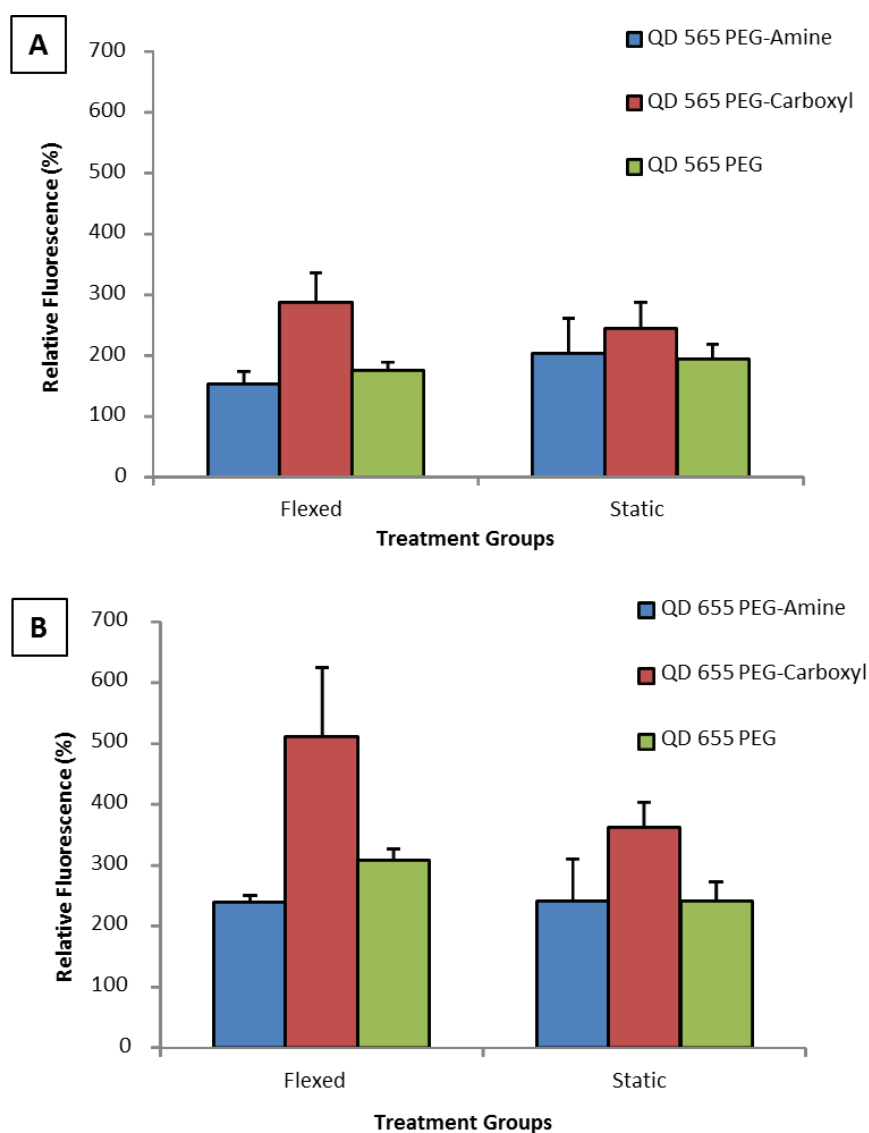


Figure 4.6: Quantum Dot 565 (A) And 655 (B) Skin Surface Relative Fluorescence Using Ultra-Violet Illumination. Fluorescence of quantum dot treated skin is represented in terms of percentage of untreated (phosphate buffered saline) control. Phosphate buffered saline and Quantum dot 565 and 655 nm with PEG-Amine, PEG-Carboxyl or PEG attachments were applied ($169 \mu\text{l cm}^{-2}$) to the skin surface for eight hours. Porcine skin was either flexed (6 hours) or remained static for the duration of the study. All groups ($n=3$) are represented as mean + standard deviation.

4.3.5. Haematoxylin And Eosin Stained Quantum Dot Skin Sections

Haematoxylin and Eosin were used to stain both quantum dot treated skin sections as well as control skin sections in order to visualise skin structure (Figure 4.7, Figure 4.8 and Figure 4.9). Skin sections were visualised with an intact stratum corneum.

Hair follicles were observed in the sections taken for each group. This finding corresponds to the pattern of QDot fluorescence staining (i.e. hair follicles) found with UV-illuminated images of the skin surface.

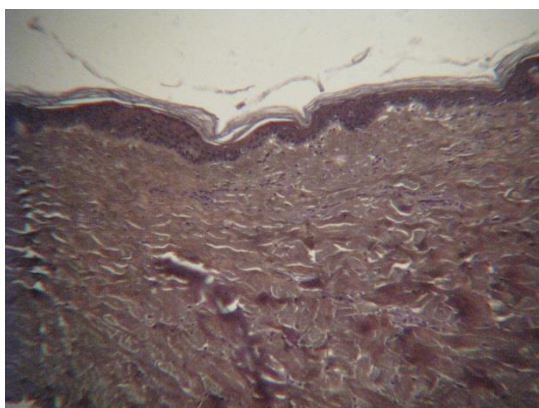
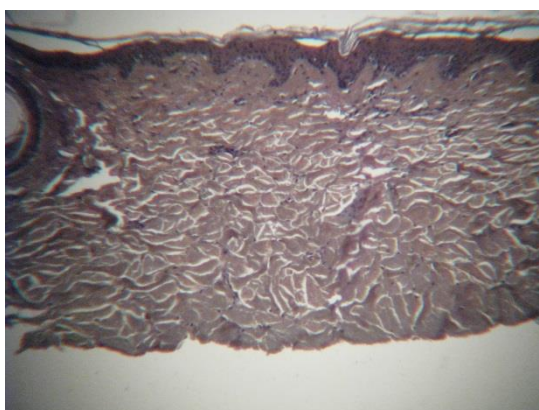
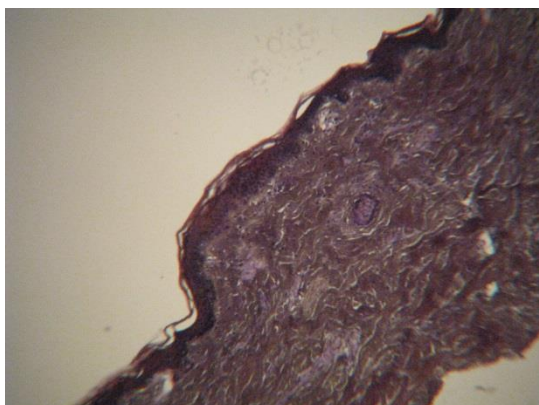
Control- PBS

Figure 4.7: Phosphate Buffered Saline Control Skin Sections From Quantum Dot Treated Porcine Skin Studies Stained With Haematoxylin And Eosin. Representative sections for each group were selected. Porcine Skin Sections Stained With Haematoxylin And Eosin. All skin sections were cut to 5 μm and visualised under a 10 x (0.24 NA) microscope. Groups consisted of n=3 diffusion cells.

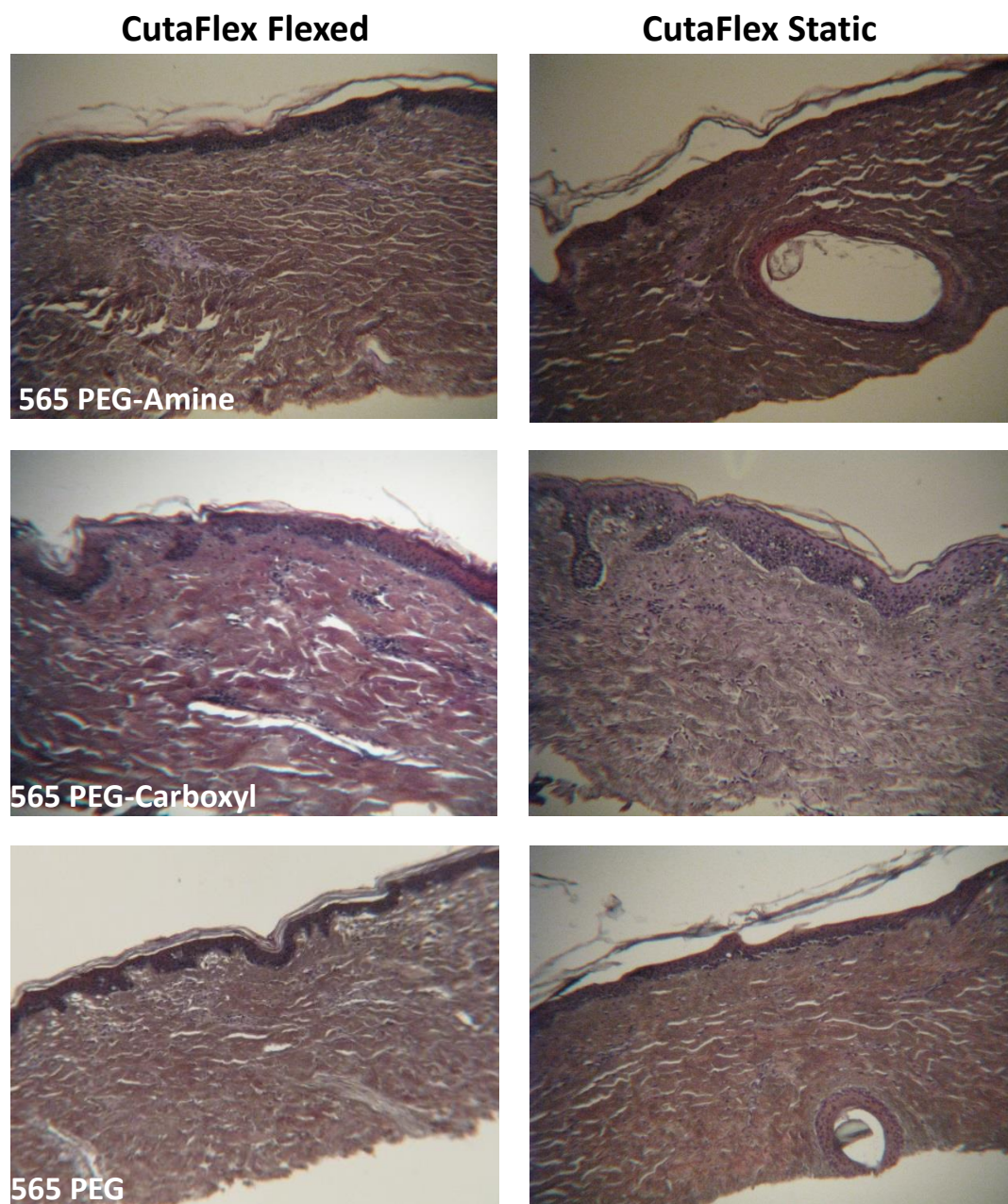


Figure 4.8: Quantum Dot 565 PEG-Amine, PEG-Carboxyl And PEG Treated Flexed And Static Porcine Skin Stained With Haematoxylin And Eosin. Representative sections for each group were selected. All skin sections were cut to 5 μm and visualised under a 10 x (0.24 NA) microscope. Groups consisted of n=3 diffusion cells.

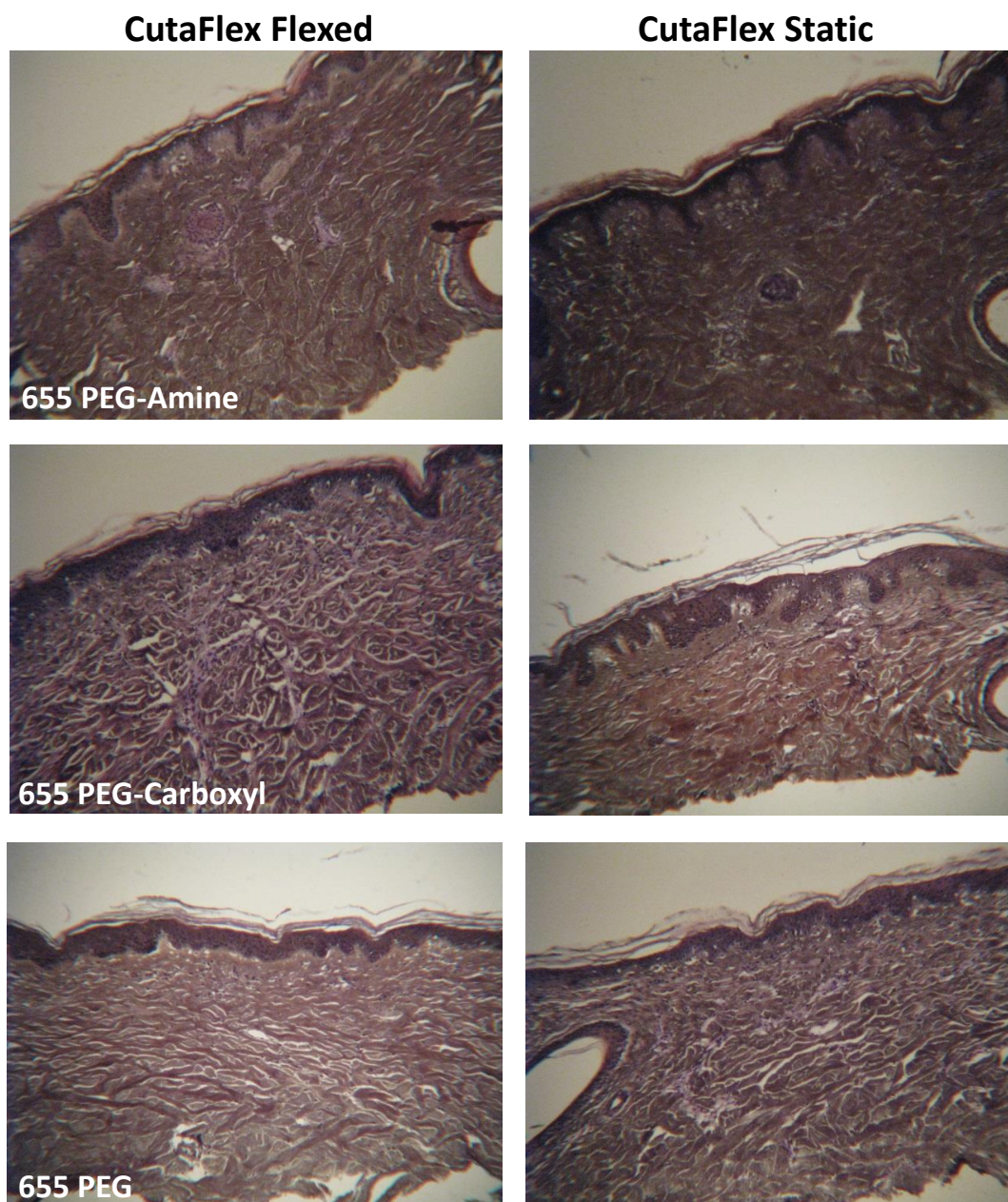


Figure 4.9: Quantum Dot 655 PEG-Amine, PEG-Carboxyl And PEG Treated Flexed And Static Porcine Skin Stained With Haematoxylin And Eosin. Representative sections from each group were selected. All skin sections were cut to 5 μm and visualised under a 10 x (0.24 NA) microscope. Groups consisted of n=3 diffusion cells.

4.3.6. Laser Scanning Confocal Micrographs Of Quantum Dot And PBS Treated Skin Samples

Limited auto-fluorescence of the skin was seen with phosphate buffered saline skin sections (Figure 4.10). Skin structure detail of both PBS and QDot treated sections was visualised with accompanying transmitted light photos of each corresponding skin section (Figure 4.13, Figure 4.14 and Figure 4.15).

All quantum dot nanoparticles were observed in the outermost stratum corneum of both flexed and static skin sections and not deeper (i.e. QDots were not found in the viable epidermis or dermis) (Figure 4.11 and Figure 4.12). Quantum dot 655 nm treated skin sections (all attachments) presented with an apparent increase in fluorescence compared to the corresponding QDot 565 nm nanoparticles (Figure 4.11 and Figure 4.12). There were no visible differences in fluorescence between flexed and static skin sections with either QD 565 nm or QD 655 nm treated sections (Figure 4.11 and Figure 4.12). The PEG-Carboxyl attachment was seen in the outer layers of the stratum corneum moreso than the other two attachments with both QDot 565 and 655 nm nanoparticles (Figure 4.11 and Figure 4.12). The QD 655 PEG attachment was seen to stain the outline of corneocytes in the stratum corneum (Figure 4.12). In general, QDots were found to pool in furrows (Figure 4.11- A and Figure 4.12- A, B and C).

It should be noted that using the confocal microscope laser filter settings were limited and resulted in QDot 565 nm fluorescence demonstrating a red-orange colour, compared to UV-light illumination of the dots where QDot 565 fluorescence was visualised as green.

Control- PBS

Figure 4.10: Phosphate Buffered Saline (Control) Treated Porcine Skin Sections Visualised Using Confocal Microscopy. Representative sections were selected for each group. All skin sections were cut to 5 μm and visualised using a laser scanning confocal microscope with a laser line of 488 nm and an emission wavelength filter of 500-643 nm. Phosphate buffered saline was applied to the skin at 169 $\mu\text{l cm}^{-2}$ for 8 hours. Groups consisted of $n=3$ diffusion cells. Scale bars indicate 100 μm .

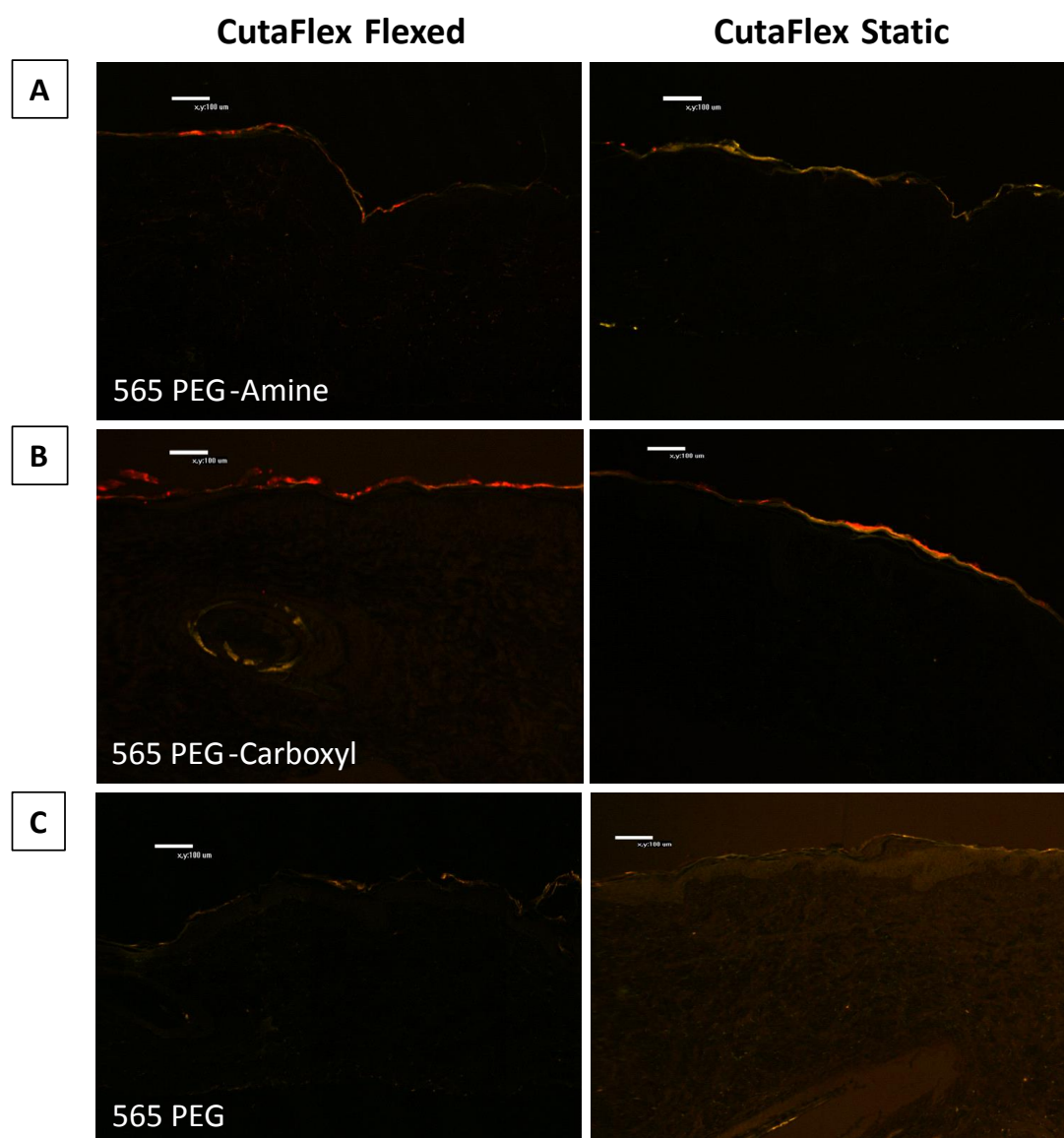


Figure 4.11: Quantum Dot 565 PEG-Amine (A), PEG-Carboxyl (B) And PEG (C) Treated Flexed And Static Porcine Skin Sections Visualised Using Confocal Microscopy. Representative sections for each group were selected. All skin sections were cut to 5 μm and visualised using a laser scanning confocal microscope with a laser line of 488 nm and an emission wavelength filter of 500-643 nm. Quantum dots were applied to the skin at $169 \mu\text{l cm}^{-2}$ for 8 hours. All groups consisted of $n=3$ diffusion cells. Scale bars indicate 100 μm .

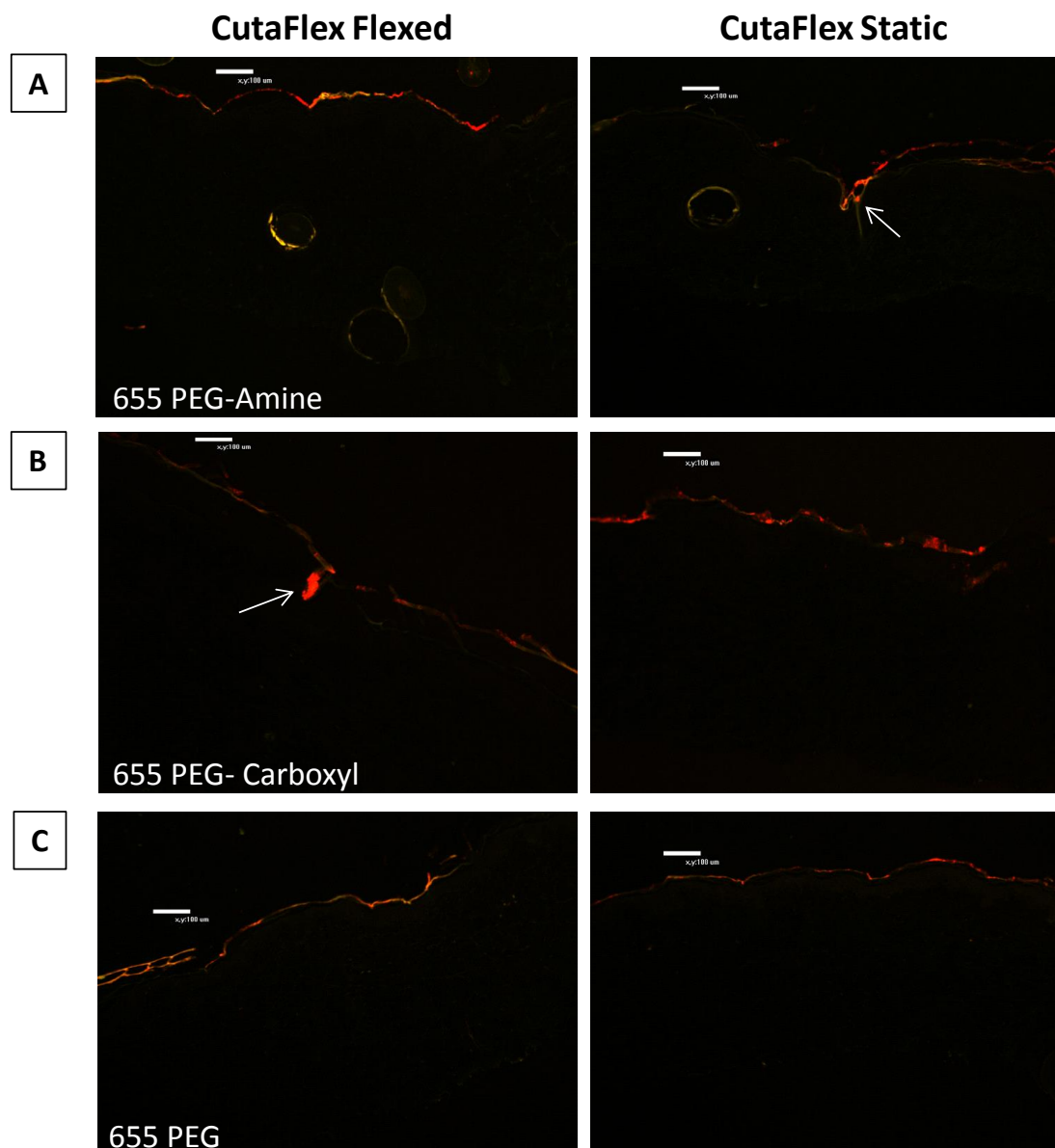


Figure 4.12: Quantum Dot 655 PEG-Amine (A), PEG-Carboxyl (B) And PEG (C) Treated Flexed And Static Porcine Skin Sections Visualised Using Confocal Microscopy. Representative sections for each group were selected. All skin sections were cut to 5 μm and visualised using a laser scanning confocal microscope with a laser line of 488 nm and an emission wavelength filter of 500-643 nm. Quantum dots were applied to the skin at $169 \mu\text{l cm}^{-2}$ for 8 hours. All groups consisted of $n=3$ diffusion cells. Scale bars indicate 100 μm . Arrows indicate accumulation in furrows.

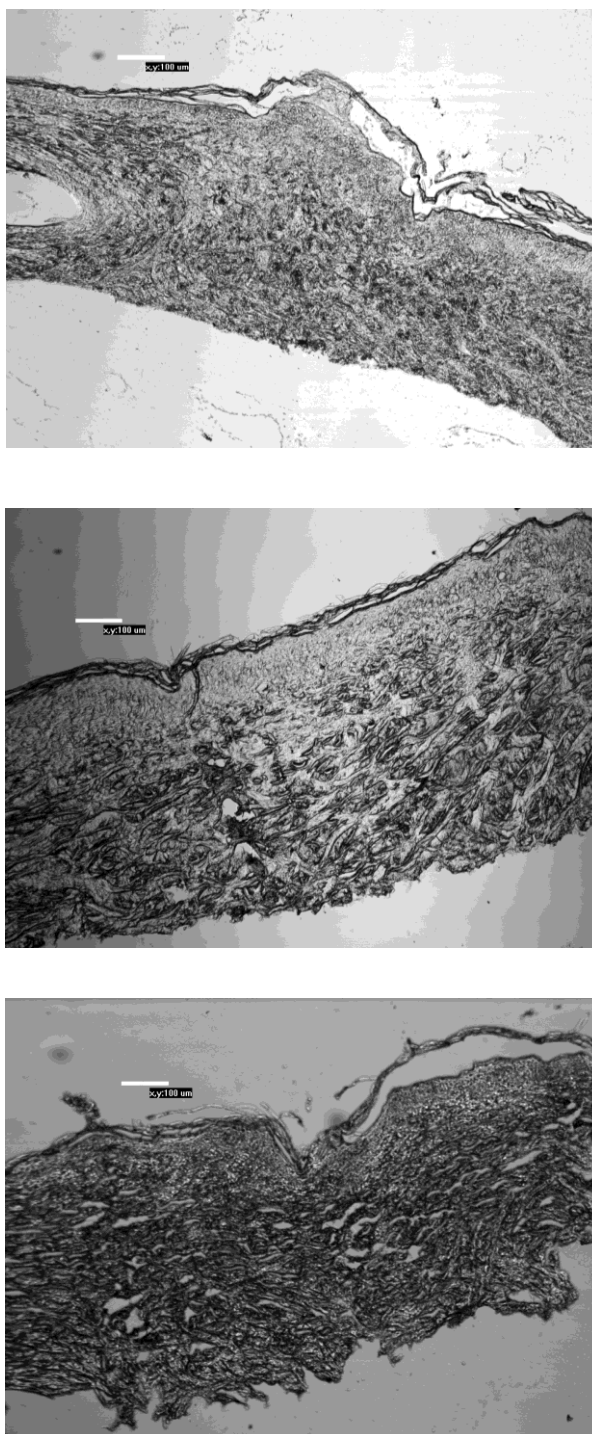
Control- PBS

Figure 4.13: Phosphate Buffered Saline (Control) Treated Porcine Skin– Transmitted Light Images. Representative sections were chosen for each group. All skin sections were cut to 5 μm and visualised for structural details using a laser scanning confocal microscope under the transmitted light channel. Phosphate buffered saline was applied to the skin at $169 \mu\text{l cm}^{-2}$ for 8 hours. All groups consisted of $n=3$ diffusion cells. Scale bars indicate 100 μm .

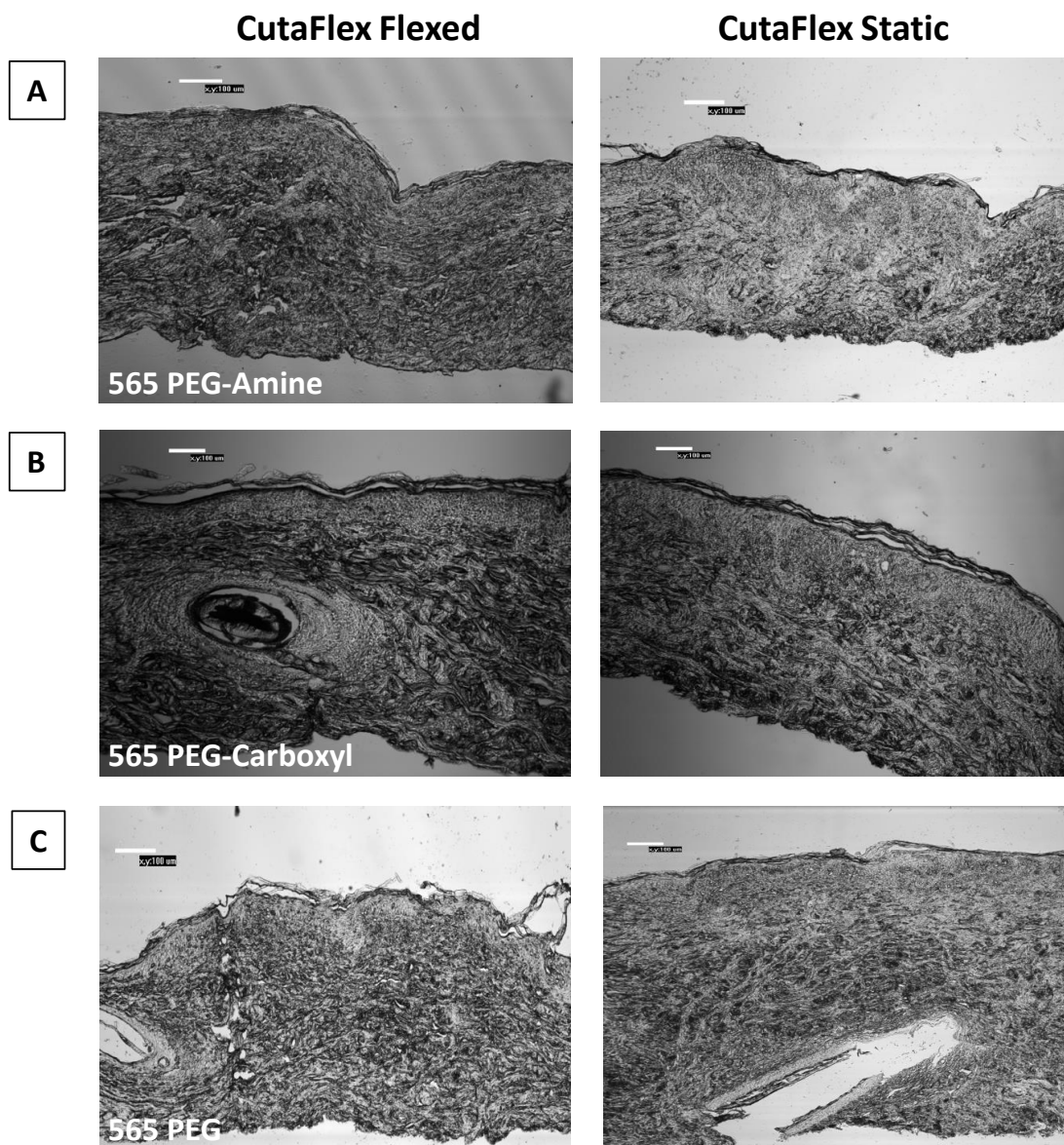


Figure 4.14: Quantum Dot 565 PEG-Amine (A), PEG-Carboxyl (B) And PEG (C) Treated Flexed And Static Porcine Skin Sections- Transmitted Light Images. Representative sections for each group were selected. All skin sections were cut to 5 µm and visualised for structural details using a laser scanning confocal microscope under the transmitted light channel. Quantum dots were applied to the skin at $169 \mu\text{l cm}^{-2}$ for 8 hours. All groups consisted of $n=3$ diffusion cells. Scale bars indicate 100 µm.

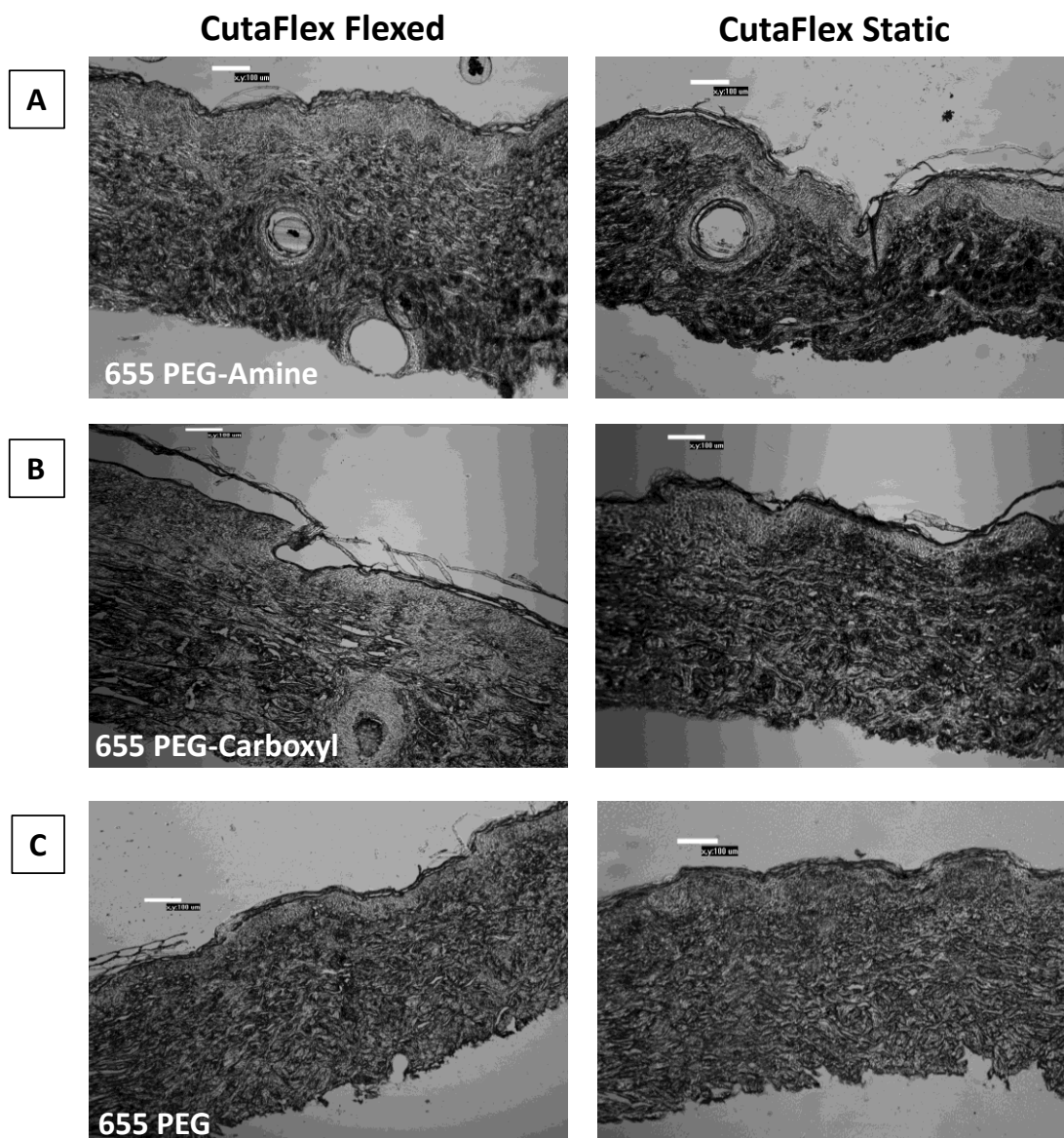


Figure 4.15: Quantum Dot 655 PEG-Amine (A), PEG-Carboxyl (B) And PEG (C) Treated Flexed And Static Porcine Skin Sections- Transmitted Light Images. Representative sections for each group were selected. All skin sections were cut to 5 μm and visualised for structural details using a laser scanning confocal microscope under the transmitted light channel. Quantum dots were applied to the skin at $169 \mu\text{l cm}^{-2}$ for 8 hours. All groups consisted of $n=3$ diffusion cells. Scale bars indicate 100 μm .

4.3.7. Receptor Fluid Fluorescence Recovery Of Quantum Dots

There was no evidence for percutaneous penetration of QDots, as fluorescence measured in samples of receptor chamber fluid collected from QDot exposed skin was identical to that of unexposed (control) receptor fluid (Figure 4.16).

It was observed that the different skin donors used in each QDot study had differences in skin auto-fluorescence, with PEG treated skin presenting with the highest auto-fluorescence (Figure 4.16).

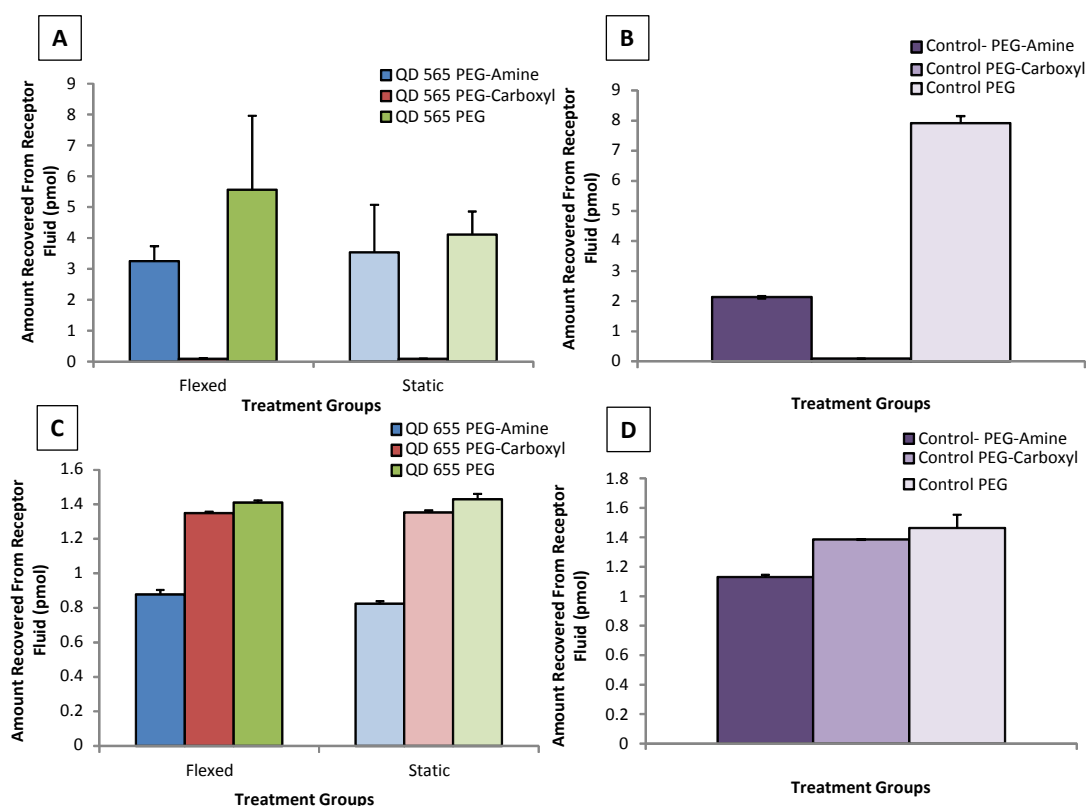


Figure 4.16: Receptor Fluid Fluorescence Recovery From Quantum Dot 565 (A), Quantum Dot 655 (C) And Control (B and D) Treated Skin. Flexed and static samples are represented in the same graph. Quantum dot 565 and 655 nm were tested with three attachments: PEG-Amine, PEG-Carboxyl and PEG. The untreated control was phosphate buffered saline solution. Quantum dot suspension was applied (300 μ l; 300 pmols) to the skin surface for 8 hours. Skin was flexed in CutaFlex™ cells for 6 hours (2 flexes per minute; 6 mm maximum displacement). The same skin donor was used per study (i.e. for QDot and Control groups). All groups (n= 3) are represented as mean \pm standard deviation.

4.4. Discussion

Preliminary findings presented in this Chapter have found that quantum dot nanoparticles applied to flexed or static skin were found in the stratum corneum and no deeper. Quantum dot 565 and 655 nm were characterised and found to be spherical and pyramidal, respectively in shape and within the size limits defined for nanoparticles. Skin surface recovery of QDots demonstrated follicular staining and accumulation in furrows, with the negatively charged particles showing a greater partitioning into the stratum corneum. Quantum dot 655 was shown to have a higher affinity for the stratum corneum than QDot 565. Most importantly, there were no overt differences in QDot partitioning or distribution in the stratum corneum in static skin compared to flexed skin.

Nanoparticle Characterisation

Transmission electron microscopy is a technique favoured for imaging of quantum dot nanoparticles, due to electron properties exhibited by these dots in providing a higher than average contrast and therefore an accompanying increase in detection (Nisman *et al.*, 2004). Transmission electron microscopy can provide both direct measurements of size, shape and partial aggregation state with both qualitative and semi-quantitative techniques, with a spatial resolution of 0.5-3 nm (Soto *et al.*, 2005, Sun *et al.*, 2006, Andrievsky *et al.*, 1999). In the present study, nanoparticle size was measured using both TEM and DLS. Due to the processing methods for TEM (drying on copper grids), this method is not thought to provide a fully accurate representation of the size distribution of particles in suspension (Murdock *et al.*, 2008). It was seen from transmission electron micrographs that quantum dot 655 nm were triangular in shape, in contrast to the spherical quantum dot 565 particles. The

difference in hydrodynamic radius between spherical and oblong particles introduces a variation in mobility and diffusion in both gas and liquid phases (Zuin *et al.*, 2007). Additionally, as the diffusion of a spherical particle through a liquid phase is a key parameter used by DLS to calculate the size (in diameter) of a particle, a difference in sphericity of a particle can create a less accurate measurement. Therefore, both data (i.e. TEM and DLS) need to be interpreted with caution. The hydrophilic coatings of each QDot increased the hydrodynamic diameter by several-fold, due to solvation effects in aqueous solution, a result previously documented in the literature (Ryman-Rasmussen *et al.*, 2006) and demonstrated that the QDots remained nanoscale particles. Nanoparticles which have been suspended in different physiological salt concentrations with differences in vehicle pH values have known to increase to micrometre size due to formation of aggregates with salt molecules (Murdock *et al.*, 2008). The quantum dot nanoparticle shapes and sizes as defined by TEM (and DLS), respectively were very similar in this study as to the values published in the literature (Ryman-Rasmussen *et al.*, 2006).

Alternative characterisation techniques for nanoparticulate size include ultracentrifugation sedimentation, atomic force microscopy and nanoparticle tracking analysis. Hoo *et al.* (2008) found that when comparing characterisation techniques for nanoparticulate suspensions, AFM provided a better tool for distinguishing bimodal distributions whereas DLS could not differentiate between two particles closer than 1:8 of size. Atomic force microscopy also allowed for identification of large bimodal size distributions regardless of particle shape, unlike DLS (Hoo *et al.*, 2008). Dynamic light scattering is known to be both fast and accurate measurement for spherical particle monosized particles in suspension, however relying on the intensity-based sized distribution from DLS may be misleading when analysing

polydisperse mixtures (Hoo *et al.*, 2008). These researchers recommended using number-based distributions in addition to further light scattering techniques or hybrid techniques for particle mixtures with broad particle size distributions.

In this study, all quantum dot suspensions were subject to low frequency sonication (12,700 J) for five minutes before application to the skin surface to ensure optimal dispersion. It has been documented that applying the correct sonication energy and time is important in the optimal dispersion of a nanoparticle suspension (Mandzy *et al.*, 2005). Bihari *et al.* (2008) characterised a number of different nanoparticles (e.g. titanium dioxide, polystyrene latex beads, carbon nanotubes and silver) in terms of size using different sonication parameters and surfactants and recommended sonication before adding surfactants and lastly, suspension in a physiological medium. In the present study, sonication was used before application of the QDots to the skin surface, in order to ensure each suspension was optimally dispersed (i.e. to ensure aggregation of particles was at a minimum).

Skin Integrity

A lengthy discussion on the use of an evaporimeter to measure skin barrier integrity has been covered in Chapter 3 (Section 3.4). A skin integrity measurement should be performed before a dermal absorption study, especially in the case of using previously frozen skin, due to the potential for damage to occur to the barrier layer whilst in storage. In the present study, transepidermal water loss measurements provided an indication (alongside histological and confocal analysis of skin structure) of skin barrier integrity. This was deemed even more important for this study, where some of the skin samples were subject to flexing. Both QDot 565 and 655 nm with carboxyl attachments presented with higher TEWL than other quantum

dot groups, however it was also observed that the control data in this study presented with higher TEWL rates than the corresponding control data in the other studies. The difference in TEWL rates between studies can be attributed to different skin donors, with inter-individual differences noted between skin samples. Importantly, all TEWL values in this study fell below the threshold determined in Chapter 3, and therefore QDot exposed skin was not damaged.

Previous studies investigating quantum dot nanoparticle dermal absorption have not taken skin integrity measurements before or after treatment (Rouse *et al.*, 2007, Ryman-Rasmussen *et al.*, 2006, Zhang and Monteiro-Riviere, 2008, Gratieri *et al.*, 2010). These previous studies have used an *in vitro* flexing device or skin massage, in which case, there was potential for skin barrier damage due to the lack of temperature and fluid control outside of a diffusion cell system, the high rate of flexing (20 flexes per minute) and the additional physical handling/manipulation of the skin. It is therefore hard to interpret the results of these studies as skin viability cannot be confirmed before nanoparticle application. The *in vitro* flexing device, CutaFlex™, tested in this Thesis incorporated *in vitro* flexion within a diffusion cell system, ensuring a constant skin temperature of 32°C, adequate receptor fluid hydration and controlled parameters (2 flexes per minute; 6 mm maximum displacement) of flexing. The present study also incorporated the use of barrier integrity measurements which ensured integrity of skin before nanoparticle application as well as confirmation of structural viability after skin flexion.

Confocal micrographs of each skin section confirmed that quantum dot nanoparticles were not present in any area except for the outermost stratum corneum. The amount of fluorescence in the receptor fluid of each diffusion cell was also quantified, in

order to equate this value with an estimation of the amount of originally applied quantum dot suspension. The values of fluorescence in the receptor fluid chambers of skin sections treated with QDots were identical to data from untreated (control) skin. It is conceivable that inherent auto-fluorescence of the skin samples in each study contributed to the fluorescence seen in the receptor fluid, the extent of which was dependent on the donor.

Experimental Considerations

As previously discussed in Chapter 1 (Section 1.3.1.3), the choice of species of skin is important as animal skin is generally more permeable than human skin (Vecchia and Bunge, 2006, Walker *et al.*, 1986). A large proportion of the *in vitro* quantum dot dermal absorption studies (as outlined in Table 1.7) have chosen to study possible penetration through rat, mouse or porcine skin. It has been demonstrated that porcine skin is closer in structure and permeability to human skin, as compared to rodent skin (Wester and Maibach, 1984). In this study, porcine dorsum skin was selected due to this skin system being both morphologically and functionally closest to human skin as compared to rodent models (Meyer *et al.*, 1978).

In exposing the skin to quantum dot nanoparticles, previous studies have applied QDot nanoparticles to the skin in very small amounts (i.e. 80-320 nmol) (Rouse *et al.*, 2007, Ryman-Rasmussen *et al.*, 2006, Zhang and Monteiro-Riviere, 2008). In addition, the dose applied should be in contact with the skin while flexing conditions are ongoing to simulate physiological movement and contact, which is in agreement with previously conducted studies (Rouse *et al.*, 2007, Zhang and Monteiro-Riviere, 2008, Gratieri *et al.*, 2010). In this Chapter, quantum dot suspensions were in contact with the skin for the duration of the study, including when the skin was flexed. When

studying *in vitro* flexing, it would be optimal for the quantum dot suspension to create a consistent layer on top of the skin surface, which was observed in this study by utilising a dose of $169 \mu\text{l cm}^{-2}$. This layer would then compensate for the transient increase in surface area, allowing for contact of the suspension even when the skin was at maximum displacement height. In this respect (i.e. incorporation of flexion into a diffusion cell and consistency of applied layer) during skin exposure, the CutaFlex™ system is unique.

The pH and lipophilicity of the quantum dot nanoparticle suspension may also affect skin penetration. The stratum corneum has a pH ranging from pH 4 - 6 and is very lipophilic compared to the underlying epidermis which is hydrophilic. As the quantum dot nanoparticle suspensions were prepared for optimum solubility in a water-based vehicle, this would likely discourage partitioning into the stratum corneum. Ryman Rasmussen *et al.* (2006) and Prow *et al.* (2012) demonstrated that quantum dot nanoparticles are able to penetrate intact skin when using suspensions with pH ranging from 8.3-9.0. The use of such a basic pH could have impacted the stratum corneum viability, therefore leading to an increase in penetration. For example, a previous study has demonstrated that increasing the pH of a solution will result in enhanced absorption (Blank and Gould, 1959). The influence of pH on the flux of compounds across the stratum corneum is a complicated issue and relies on the permeability coefficient of the compound, thermodynamic activity of the compound in the solvent and the vehicle stratum corneum partition coefficient (Schaefer and Redelmeier, 1996). As nanoparticles are not thought to follow traditional diffusion through the stratum corneum, the effect of pH on the stratum corneum would likely have resulted in damage (i.e. lipid lamellae disorganisation) in

order for these relatively large particles to pass through into the viable epidermis and dermis.

Quantum Dot Surface Staining

In the present studies, skin surface images of quantum dot fluorescence revealed a greater fluorescence of skin staining with QDot 655 nm (vs QDot 565nm), especially when using the carboxylic attachment. It has been previously documented that *in vitro* flexion of skin samples resulted in an increase in quantum dot fluorescence on the skin surface (Zhang and Monteiro-Riviere, 2008). Massaging of the skin also resulted in altered surface patterns as well as accumulation in furrows and follicles (Gratieri *et al.*, 2010, Wu *et al.*, 2009b). This finding is consistent with results found in the present study, in which skin treated with both charged and neutral QDot 655 particles showed an increase in staining as compared to QDot 565 particles. In addition, skin treated with QD 565 charged particles presented with an increase in follicular staining.

Zhang *et al.*(2008) postulated that the polar groups on quantum dots may bind to hydrated keratin, thereby slowing movement through the stratum corneum. These researchers also found minimal penetration from the QDots with carboxyl attachments, although they were the smallest out of all 6 particles. In this chapter, both UV-Light images of QDot treated skin surfaces and fluorescence spectrophotometer analysis of skin surface swabs in this study postulated that QDot 655 PEG-Carboxyl may have shown a greater affinity for the stratum corneum than the other 5 dots under study. A greater partitioning was thought to have occurred with QDot 655 particles. As previously discussed, the stratum corneum contains both positively and negatively charged groups, however this layer carries a net negative

charge (Brain and Chilcott, 2008). An electronegative charged horizontal field between the stratum granulosum and stratum corneum is thought to repel anions and prevent cations from penetration further into the skin (Montagna, 1962). There is a considerable pH gradient across the stratum corneum. The stratum corneum has been documented to be more permeable to neutral molecules than the salts of weak acids or bases (Swarbrick *et al.*, 1984, Flynn, 1985). In this study, there was a decrease in neutral (PEG) QDot molecules remaining on the skin surface as compared to the charged (PEG-Amine and Carboxyl) QDot particles. In terms of charged molecules, the skin is permselective to cations, based upon iontophoretic evidence in which more current was carried by cations than anions (Burnette and Ongpipattanakul, 1987). Therefore, it was not expected to see an increase of negatively charged quantum on the surface of the skin. Further research into the mechanism of attachment to the stratum corneum will have to be conducted, but could possibly have been due to hydrogen bonding of protein via the ionised carboxyl group.

Previous research has shown quantum dot nanoparticles in skin furrows and in the hair follicle infundibulum and that skin surface swabs did manage to remove QDots in the former but not the latter (Wu *et al.*, 2009b). Pilot studies prior to those described in this Chapter (data not reported here) found that six skin surface swabs removed the majority of quantum dot suspension from the skin surface, presumably from the skin furrows. In the present study, skin surface swabs were seen to remove the majority of neutral QDots (especially in the case of QDot 565), and to a lesser extent the positively charged quantum dots, whilst the negative QDots partitioned into the stratum corneum and thus were not able to be removed to the same extent as the previous QDots.

Skin Flexing

Previous studies have shown that flexing of skin *in vitro* has advanced fullerene-substituted amino acids as well as beryllium and zirconium particles further into the skin, reaching the dermal layers (Tinkle *et al.*, 2003, Rouse *et al.*, 2007). The results of this study have shown that *in vitro* flexion does not influence penetration of quantum dot nanoparticles in the absence of skin damage, as confocal micrographs of both static and flexed skin sections showed these particles contained in the outermost stratum corneum and no further.

Previous studies have shown that flexion does not result in an increase of skin penetration of model penetrants (see Chapter 3). The quantum dot dermal absorption studies were performed under similar conditions as the standard penetrant studies; namely, $169 \mu\text{l cm}^{-2}$ applied dose and 8 hour occluded exposure period. Studies from Chapter 3, representing the percutaneous penetration of compounds with a range of physicochemical properties, also found that *in vitro* skin flexion did not cause a difference in penetration compared to static (unflexed) skin. It was thought that flexion of the skin could cause transient increases of space in the lipid lamellar bilayers, as well as providing additional kinetic energy for particles to move through the lamellar bilayers. However, such transient increases, if present, may also have been expected to affect the permeation and penetration of model compounds in Chapter 3, leading to an increase in penetration from flexing. As this effect was not documented, the ‘transient space theory’ may be discounted. A more credible theory of flexion assisted translocation could lie within the additional kinetic energy imparted to the skin by flexing, which may also impart kinetic energy to particles in the skin, theoretically allowing for deeper skin penetration. In general, quantum dots are known to be too large for diffusion (in comparison to model compounds diffusion

at the molecular level) and too large to fit through individual lipid lamella (capable by individual molecules). In addition, the steric hindrance between adjacent corneocytes would be immense, a situation which can be equated to dropping an elephant between double decker buses which have an elephant-sized (75 nm) gap filled with tennis balls (lipid lamellae). It is theoretically possible in the above theory for the elephant to pass through the tennis balls. However it would require considerable external assistance.

The intercellular pathway has been previously mentioned in the literature as one of the predominant pathways for penetration of quantum dot nanoparticles via skin flexion. This is due to the lateral and horizontal gaps between corneocytes occupied by lipid lamellae, which are thought to be large enough (i.e. 75 nm) for possible penetration of small particles (Elias and Friend, 1975, Rouse *et al.*, 2007). The second most common pathway mentioned in the penetration of nanoparticles is the follicular pathway. It was observed from our previous confocal micrographs (data not shown) that contained hair follicles that quantum dot nanoparticles were present in the follicular infundibulum, a result consistent with the literature (Gratieri *et al.*, 2010). The follicular pathway also has an increased surface area available for absorption. However, the follicular route is likely limited by the presence of sebum (and metabolising enzymes). It is thought the follicular route would not create as much of a shunt to the viable epidermis and dermis as previously suspected, except in the cases of small metal ions (Scheuplein, 1976). If such a shunt existed, this would have been visualised with fluorescence from QDots present in the lower epidermis and dermis of even intact skin, a result not documented in the literature.

The limited superficial ingress of the quantum dot nanoparticles could be attributed to the mechanics of the stratum conjunctum. In contrast, the stratum disjunctum lacks the hemi-desmosomes which bind adjacent corneocytes, thus facilitating desquamation. Moreover, the packing of corneocytes in the most superficial layer is known to be lipid-mediated and therefore has a greater susceptibility to mechanical and chemical induced disruption (Fartasch, 1996). The stratum conjunctum however, is known to be the most tightly packed layer of the stratum corneum, leading to a bottle neck effect in transport of material across the skin (Schatzlein and Cevc, 1998). Additionally, although the stratum corneum is acknowledged as the skin barrier layer, removal of this layer does not eradicate all barrier properties of the skin. Tape stripping of the stratum corneum has been documented to increase water and solute permeability by 10-20 fold, an increase that represented the maximum decrease in barrier function seen in some pathological conditions (Schaefer and Redelmeier, 1996). Conversely, the water permeability was found to be 100 fold less than that observed for a stratified layer of keratinocytes (Schaefer and Redelmeier, 1996). Therefore, maintenance of a barrier could be due to a number of factors such as partial removal of the stratum corneum, homeostatic responses to barrier damage, secretion and coagulation of interstitial fluid and lastly, lipid excretion (from lamellar bodies) located in the stratum spinosum and granulosum (Schaefer and Redelmeier, 1996). Chemicals (or nanoparticles) that have penetrated into both intact and damaged stratum corneum may have also been limited in penetration due to the tight junctions that exist in the stratum granulosum (Bradner, 2009).

In the present study, the robust structure and properties of the stratum corneum (i.e. solubility, steric hindrance, pH) have been shown to impede the penetration of quantum dot nanoparticles when using intact skin. This supports the conclusion of

previous studies using structurally viable skin. Moreover, this limited study has shown that skin flexion does not appear to facilitate translocation of QDots through the stratum corneum. However, it should be emphasised that further work is required to confirm these initial findings based on a limited number of skin samples.

In summary, this work has demonstrated that:

- Quantum dot nanoparticles of different shapes, charges and sizes did not appear to penetrate through intact porcine skin.
- Flexed skin does not show differences in nanoparticle penetration to static skin
- Quantum dot charge influenced the partitioning of dots present into the superficial skin surface.
- Clearly further work is required to substantiate these initial studies.

**Chapter 5: An *In Vitro-In Vivo* Evaluation Of CutaFlex™ For
Assessing Topical Skin Protection Against Methyl Nicotinate**

5.1 Introduction

The purpose of the work reported in this chapter was to investigate the effect of flexing on the *in vitro* performance of a topical skin protectant (RD-1433) during exposure to methyl nicotinate (MN) and to compare the resulting data with an evaluation of the same product under identical conditions when performed *in vivo* using human volunteers.

It should be noted that the human volunteer study was conducted as part of a larger trial to investigate the relative efficacy of RD-1433 and white petroleum jelly B.P. (Vaseline[®]) for preventing or treating incontinence associated dermatitis (IAD): the studies presented here relate to preliminary work designed to identify (i) the optimum thickness of RD-1433 required to impart significant skin protection and (ii) the duration over which an optimum thickness of RD-1433 remains effective. Determination of optimum thickness and duration of efficacy were performed *in vitro* (CutaFlex[™] diffusion cells) with dermatomed pig skin and *in vivo* using human volar forearm skin. The performance of the test products was assessed either by direct measurement of ¹⁴C-MN skin absorption (*in vitro*) or by measuring the rubefacient (erythematous) response to unlabelled MN (*in vivo*).

5.2 Materials and Methods

Skin and diffusion cells were prepared as previously outlined in Sections 2.1.2 and 2.1.3, respectively. A 5 mM solution of ^{14}C -methyl nicotinate (^{14}C -MN) was prepared as described in 2.1.1. Evaporation studies of ^{14}C -methyl nicotinate and tritiated water were performed as outlined in Section 2.1.13.1. Tritiated water and transepidermal water loss barrier integrity measurements were performed as outlined in Section 2.1.4. The barrier cream (RD-1433) was reported to be of clinical research grade and so was in compliance with MHRA requirements as listed in Section 2.1.1. Both RD-1433 and Vaseline were tested *in vitro* for minimum thickness and duration of efficacy according to Section 2.1.13.2 and Section 2.1.13.3, respectively. All *in vitro* studies were quantified using radiometric analysis as described in Section 2.3.1. The details of the clinical trial performed with RD-1433 are outlined in Section 2.2. *In vivo* biophysical measurements were performed as detailed in Section 2.2.1. *In vivo* testing of RD-1433 and Vaseline for optimal thickness and duration of efficacy was performed as outlined in Section 2.2.2 and 2.2.3, respectively. Statistical testing was performed as detailed in Section 2.3.2.

Briefly, both RD-1433 and Vaseline were tested for efficacy against methyl nicotinate. *In vitro* studies involved the use of the novel flexing diffusion cell to test for optimal thickness of both RD-1433 and Vaseline at 0.01, 0.05 and 0.1mm as well as for duration of efficacy for 1, 2, 4 and 6 hours against ^{14}C -methyl nicotinate. *In vivo* biophysical measurements of LDI, TiVi, Visual Erythema and TEWL tested the efficacy of both RD-1433 and Vaseline in human volunteers at the same thicknesses, durations of efficacy and concentration of MN (unlabeled) as *in vitro* studies. *In vitro* techniques were then compared to *in vivo* measurements to give an indication of sensitivity and predictive accuracy.

5.3 Results

5.3.1 *In Vitro* Optimal Thickness Study

5.3.1.1 ¹⁴C-Methyl Nicotinate And ³H-Water Surface Evaporation

The evaporation of ¹⁴C-MN solution was initially linear (approximately 0.11 mgml⁻¹) up to approximately 45 minutes, after which no further evaporation was measurable (Figure 5.1). At 20 minutes (corresponding with the actual duration of exposure *in vitro* and *in vivo*), less than 50% of the applied dose remained. In contrast, the evaporation of water was exponential, with approximately 2% of the applied dose remaining after 20 minutes, after which the amount remaining was negligible (less than 0.02% of the applied dose).

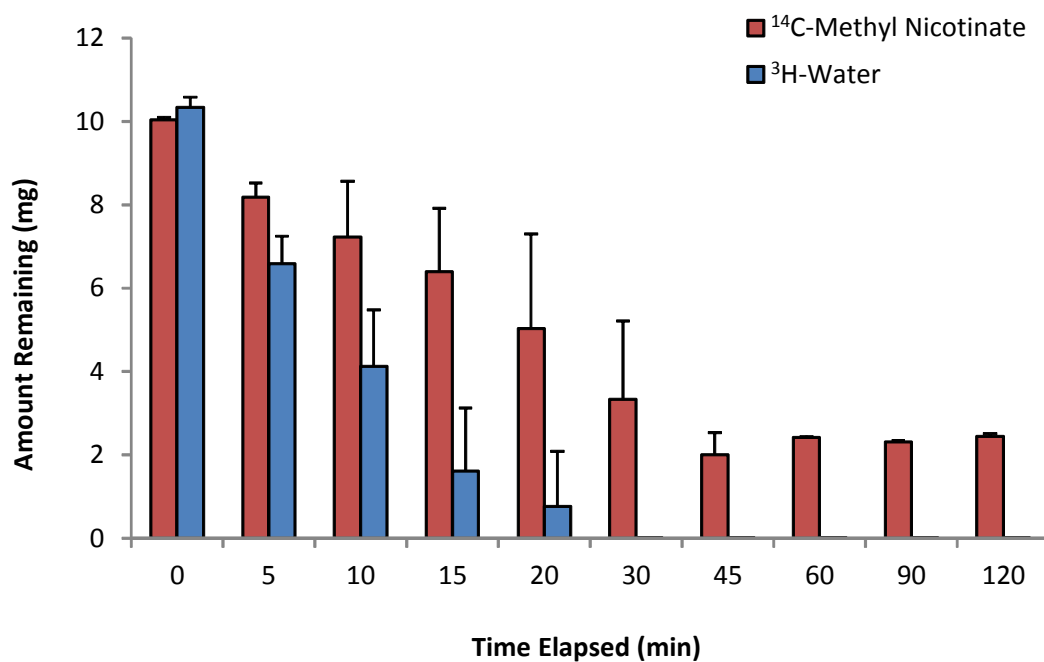


Figure 5.1: Carbon-14 Methyl Nicotinate And Tritiated Water Surface Evaporation. Carbon-14 methyl nicotinate was applied (10 mg; 5mM solution) to aluminium foil for 120 minutes. Tritiated water was applied (10 mg) to aluminium foil for 120 minutes. All data (n =3) are represented as mean + standard deviation.

5.3.1.2 Measured Thickness Applied- RD-1433 and Vaseline®

The actual thickness of RD-1433 applied to the skin samples was consistently lower than the nominal thickness (Figure 5.2). This experimental error was greatest at 0.01 mm (approximately 60% of intended thickness) and approximately 80% for 0.05 and 0.1 mm applications.

In contrast, the dose of Vaseline® applied to the skin surface was closer to the nominal thickness, being approximately 80-90% of the intended dose.

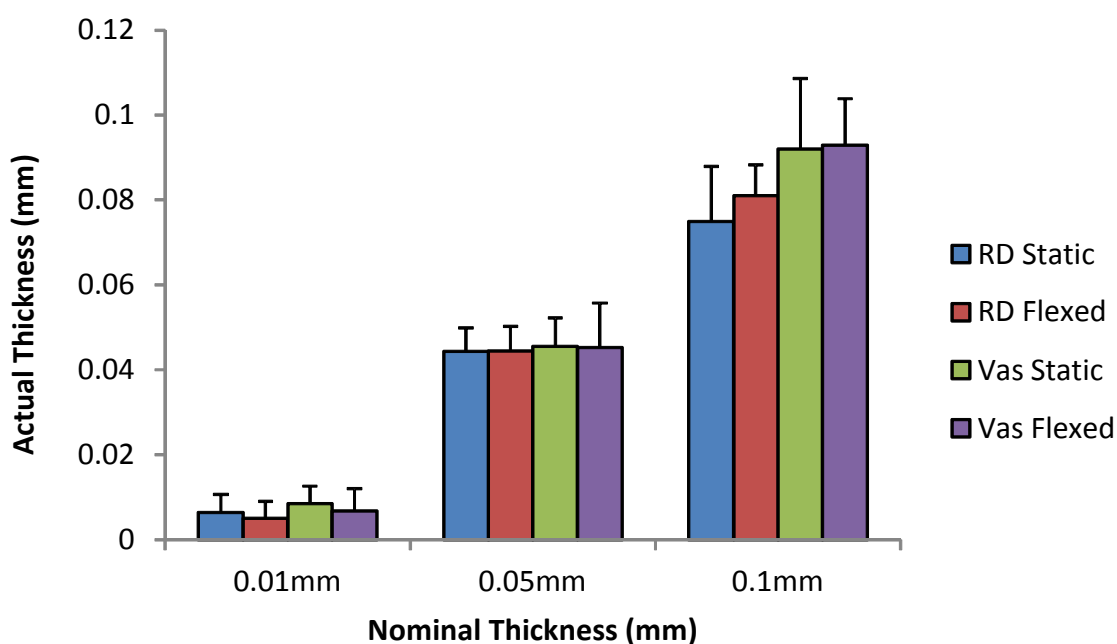


Figure 5.2: *In Vitro* Applied Thickness Of RD-1433 And Vaseline For Optimal Thickness Studies. Glove tips were weighed before and after product application in order to get a total amount applied to the skin surface. Amount was determined after factoring in the density of RD-1433 (2.358 g cm^{-3}) and Vaseline (0.952 g cm^{-3}). All data are represented as mean + standard deviation of 6 diffusion cells.

5.3.1.3 Barrier Viability Measurements

There were no significant differences ($p > 0.05$) found in the transepidermal water loss flux rates or tritiated water penetration between baseline and post-treatment within a group, or between any of the treatment groups (Figure 5.3 and Figure 5.4).

There was no correlation between tritiated water penetrated and transepidermal water loss flux at baseline ($r = 0.08$) and post-treatment ($r = 0.4$) values in RD-1433 treated skin. Similarly there was no correlation for baseline ($r = -0.20$) and post-treatment ($r = 0.19$) values in Vaseline[®] treated skin.

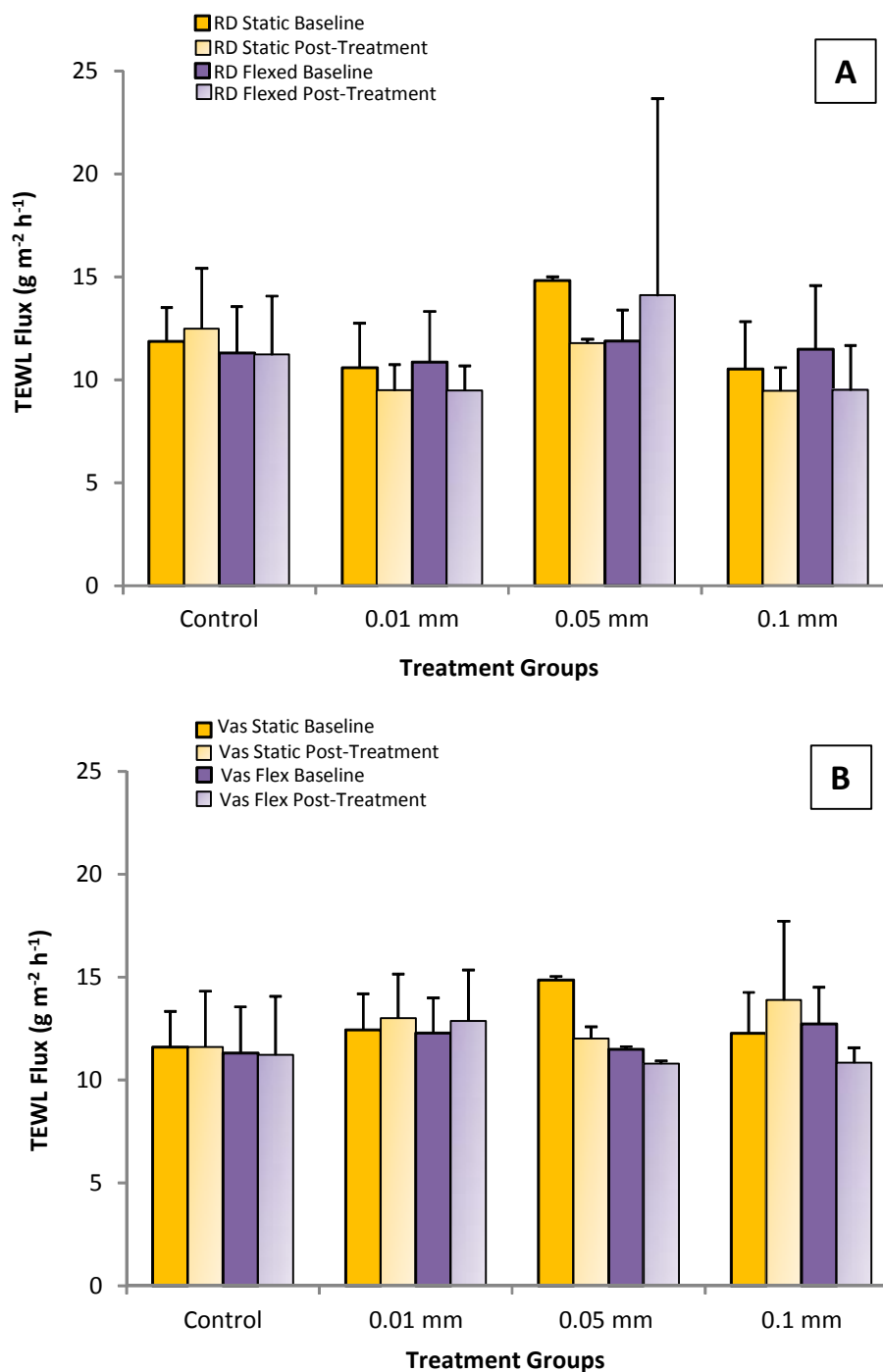


Figure 5.3: *In Vitro* Transepidermal Water Loss Flux Before And After ¹⁴C-Methyl Nicotinate Application In RD-1433 (A) And Vaseline (B) Treated Thickness Groups. Rates of TEWL were measured before test product application and application of 10 μ l (1 μ Ci total) of ¹⁴C-methyl nicotinate (Baseline) and after test product and ¹⁴C-methyl nicotinate removal (Post-Treatment). All data are represented as mean + standard deviation of 6 diffusion cells.

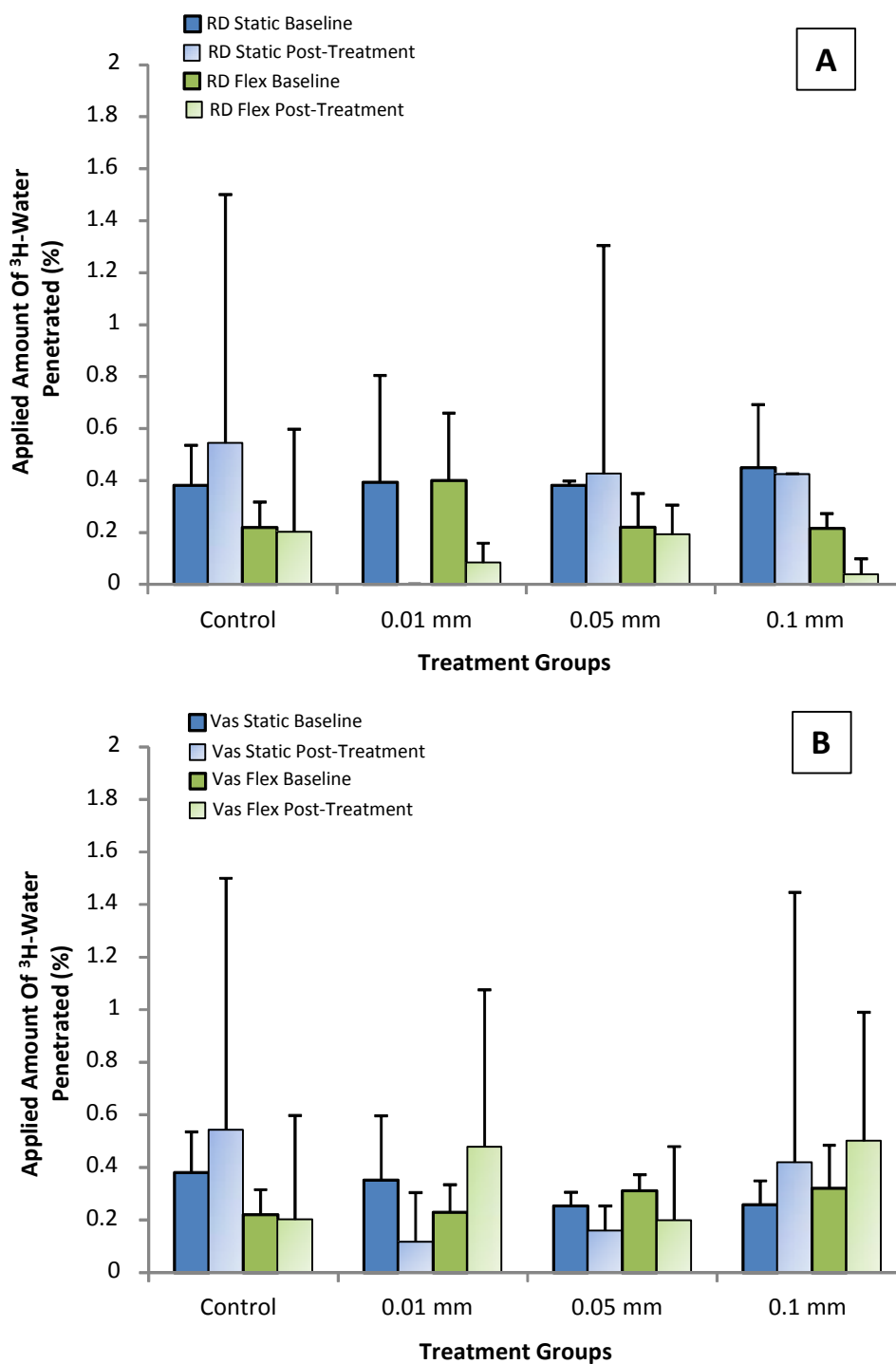


Figure 5.4: *In Vitro* Tritiated Water Penetration Before And After ^{14}C -Methyl Nicotinate Application In RD-1433 (A) And Vaseline (B) Treated Thickness Groups. Tritiated water was applied for 30 minutes before test product application and application of $10\ \mu\text{l}$ ($1\ \mu\text{Ci}$ total) of ^{14}C -methyl nicotinate (Baseline) and after test product and ^{14}C -methyl nicotinate removal (Post-Treatment). All data are represented as mean + standard deviation of 6 diffusion cells.

5.3.1.4 RD-1433 Treated Groups- Optimal Thickness Study

Cumulative Amount Penetrated

The application of RD-1433 at a thickness of 0.05 and 0.1 mm to both static and flexed skin resulted in a significant decrease ($p < 0.05$) in methyl nicotinate penetration. Furthermore, the 0.1 mm application provided 2-fold greater protection than 0.05 mm (Figure 5.5). When applied at 0.01 mm to flexed skin sections, pre-treatment with RD-1433 caused a significant decrease ($p < 0.05$) in ^{14}C -MN penetration compared to the control as well as a 3-fold decrease in penetration compared to corresponding static skin treated with RD-1433 at 0.01 mm. Within flexed skin sections, RD-1433 applied at 0.05 and 0.1 mm provided 3- and 5-fold, protection, respectively, against MN compared to 0.01mm. Within static groups treated with RD-1433 at 0.05 and 0.1 mm, protection of 10- and 16-fold was provided, respectively compared to the 0.01 mm treated sections.

Maximum Flux

Both static and flexed skin treated with RD-1433 at the two higher thicknesses showed significant ($p < 0.05$) 10-fold and 20-fold decreases in maximum flux, respectively compared to the skin treated with 0.01 mm (Figure 5.6). Furthermore, RD-1433 when applied at 0.1 mm significantly reduced the flux of methyl nicotinate by two-fold compared to the groups treated with 0.05 mm. There were no significant differences in the time of onset of maximum flux between all treatment groups.

Thus, RD-1433 provided significant protection against ^{14}C -MN in a dose-dependent manner, decreasing with thicker layers of application, although the thinnest layer tested was inconsistent. Additionally, skin sections (whether immobile or flexed) were significantly more protected against the penetration of methyl nicotinate when using RD-1433 applied at a 0.1 mm thickness.

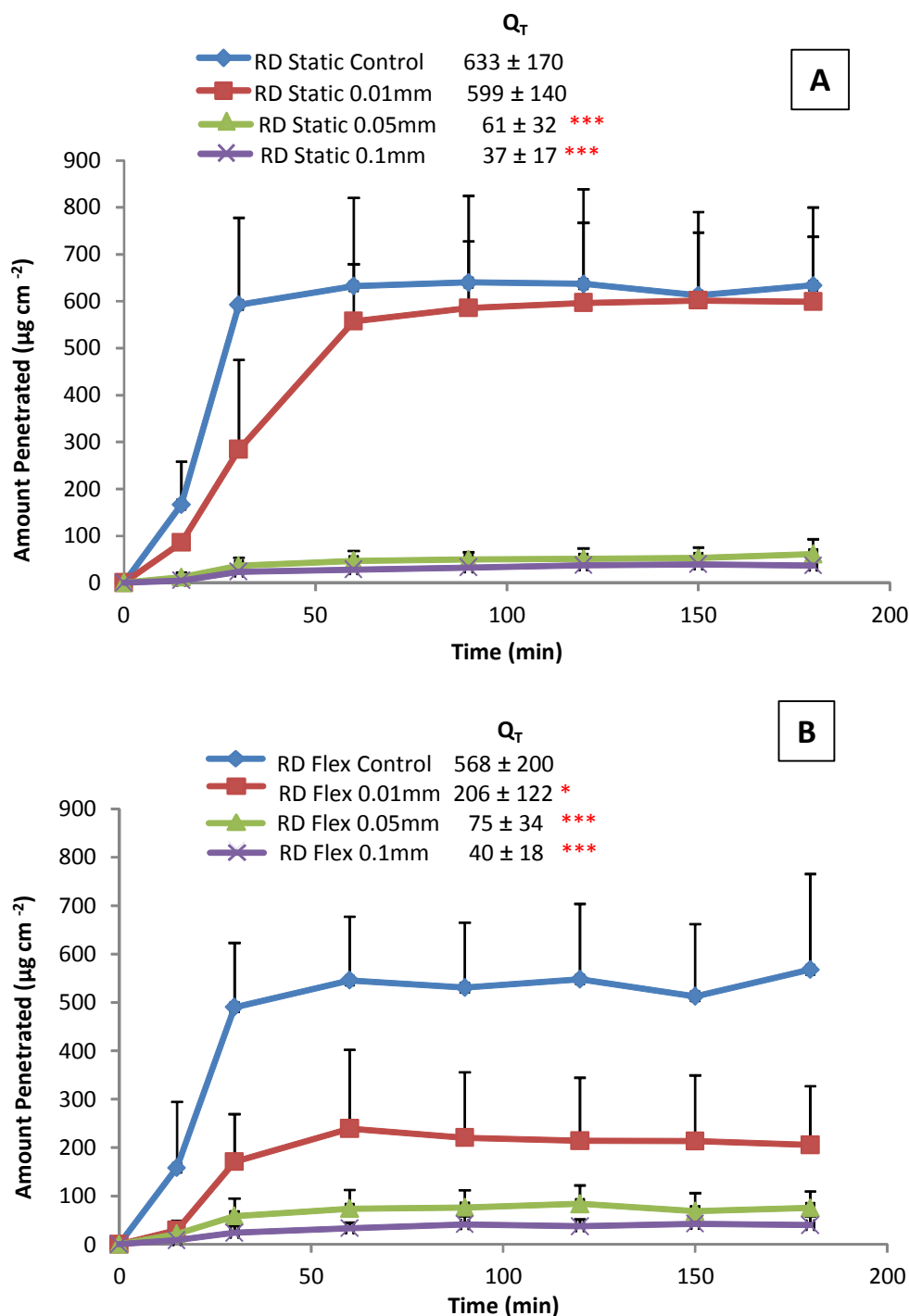


Figure 5.5: Cumulative Amount of ^{14}C -Methyl Nicotinate Penetrated Through Static (A) and Flexed (B) Porcine Skin Treated With RD-1433 Over 180 Minutes. RD-1433 was tested for protective effect against ^{14}C -methyl nicotinate (10 μl , 1 μCi applied) at thicknesses of 0.01, 0.05 and 0.1 mm. Excess nicotinate was removed at 20 minutes and RD-1433 was removed at 120 minutes. Asterisks (* and ***) indicate significant ($p < 0.05$ and 0.001, respectively) reductions in the cumulative amount ($\mu\text{g cm}^{-2}$) of ^{14}C -methyl nicotinate penetrated at 180 minutes compared to the relevant control. Cumulative amount penetrated (Q_T) is represented on the graph as $\mu\text{g cm}^{-2}$. All data are represented as mean + standard deviation of $n=6$ diffusion cells.

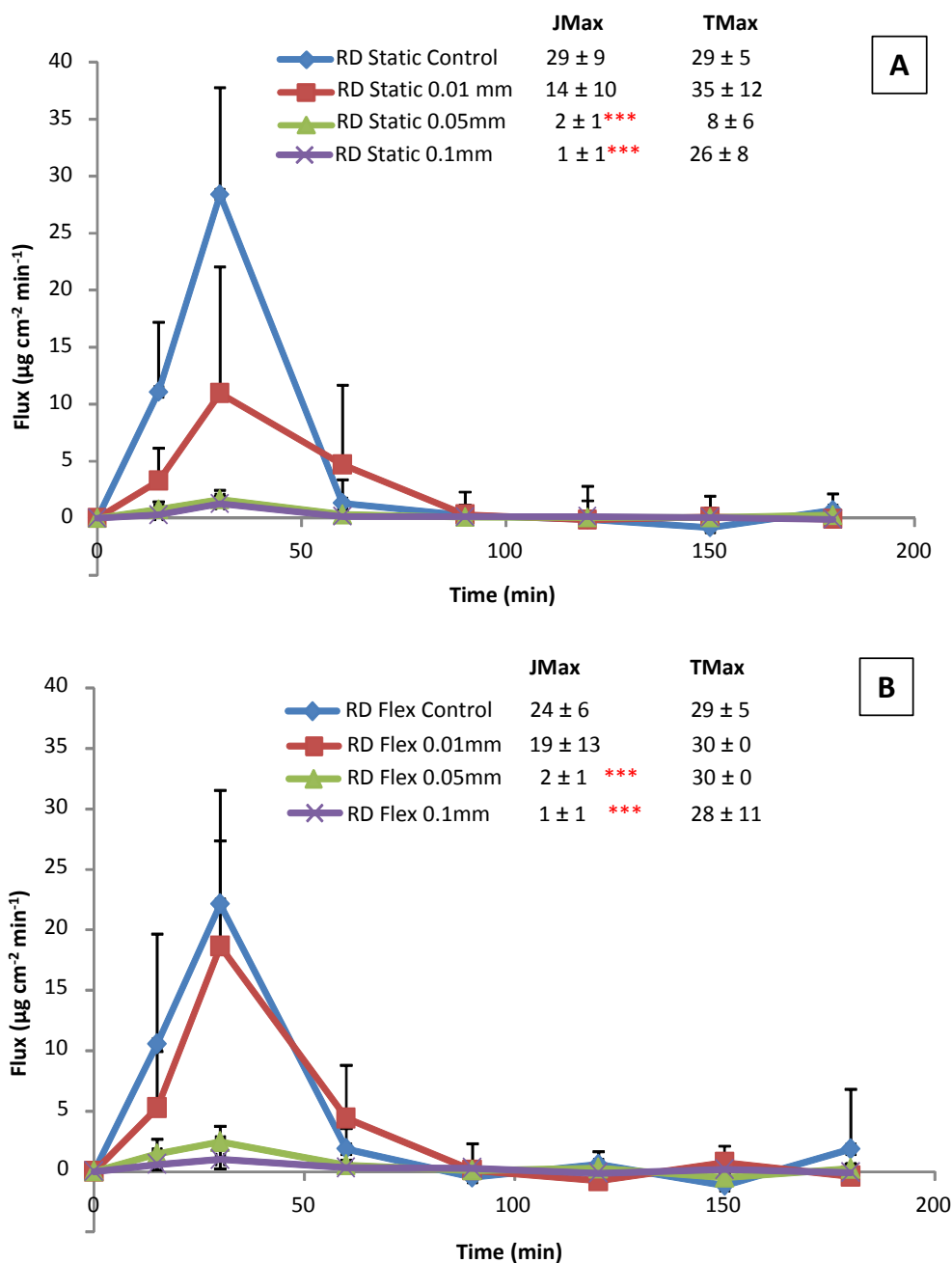


Figure 5.6: *In Vitro* Flux Profile Of ^{14}C -Methyl Nicotinate Penetrated Through Static (A) And Flexed (B) Porcine Skin Treated With RD-1433 Over 180 Minutes. RD-1433 was tested for protective effect against ^{14}C -methyl nicotinate (10 μl ; 1 μCi) at thicknesses of 0.01, 0.05 and 0.1 mm. Excess nicotinate was removed at 20 minutes and RD was removed at 120 minutes. Asterisks (***) indicate significant ($p < 0.001$) reductions in maximum flux (JMax; $\mu\text{g cm}^{-2} \text{min}^{-1}$) compared to the relevant control. Time at which maximum flux occurred (T_{Max}) was also compared. All data are represented as mean + standard deviation of $n=6$ diffusion cells.

5.3.1.5 Vaseline® Treated Groups- Optimal Thickness Study

Cumulative Amount Penetrated

Both immobile and flexed skin treated with Vaseline® at a nominal thickness of 0.05 mm demonstrated significant reductions ($p < 0.05$) in ^{14}C -MN penetration, compared to untreated controls. Moreover, static skin treated with Vaseline® at 0.1 mm also showed a significant reduction in methyl nicotinate penetration compared to the untreated control (Figure 5.7). In comparison to the RD-1433 treated groups, static and flexed skin treated with Vaseline® showed less protection against methyl nicotinate penetration at the highest thickness (0.1 mm) compared to the intermediate (0.05 mm) thickness groups. Moreover, skin sections treated with Vaseline® at 0.05 mm showed 2- 3-fold reductions in methyl nicotinate penetration in flexed and static skin, respectively compared to 0.01 mm Vaseline® treated sections.

When contrasted with Vaseline® treated skin, RD-1433 provided significantly more protection, amounting to 3- and 10-fold, when used at thicknesses of 0.05 and 0.1 mm, respectively in both static and flexed skin.

Maximum Flux

Both static and flexed skin treated with Vaseline® at 0.05 mm showed significant reductions ($p < 0.05$) in flux compared to the untreated control (Figure 5.8). In addition, static skin treated with Vaseline® at 0.1 mm demonstrated significant reduction in flux compared to the untreated control. Application of Vaseline® at 0.05 and 0.1 mm significantly reduced the flux of methyl nicotinate by approximately 2-fold for both static and flexed skin.

In comparison to Vaseline® treated groups, static and flexed skin sections treated with RD-1433 at 0.05 and 0.1 mm thickness provided significant reductions

amounting to approximately 3- to 13-fold, respectively in flux compared to the corresponding Vaseline[®] treated groups at 0.05 and 0.1 mm. In addition, Vaseline[®] treated groups did not show a dose-dependence, with inconsistent results seen between 0.05 and 0.1 mm treated skin.

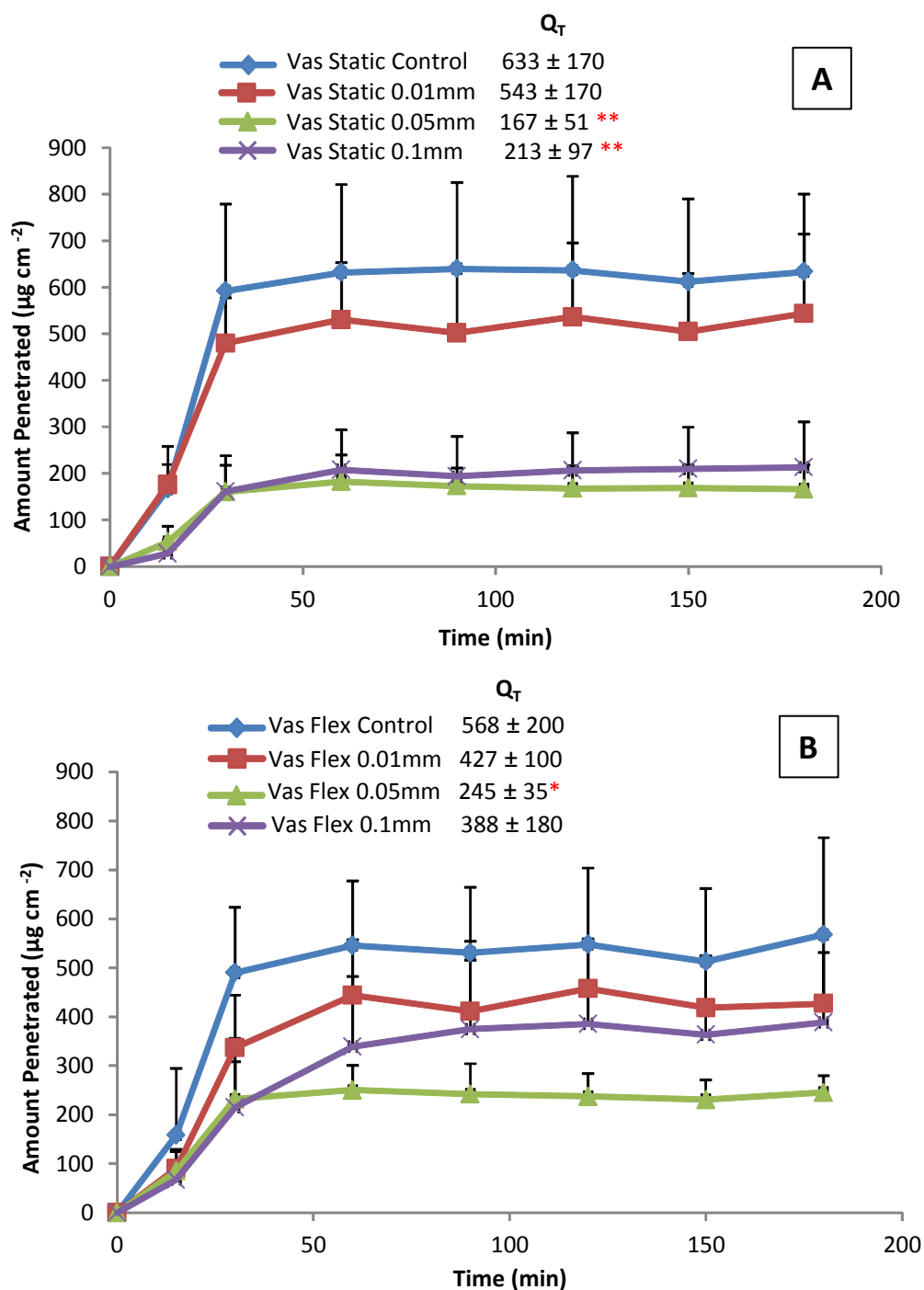


Figure 5.7: Cumulative Amount of ^{14}C - Methyl Nicotinate Penetrated Through Static (A) And Flexed (B) Porcine Skin Treated With Vaseline® Over 180 Minutes. Vaseline® was tested for protective effect against ^{14}C -methyl nicotinate (10 μl ; 1 μCi applied) at thicknesses of 0.01, 0.05 and 0.1 mm. Excess nicotinate was removed at 20 minutes and Vaseline was removed at 120 minutes. Asterisks (* and **) indicate significant ($p < 0.05$ and 0.01 , respectively) reductions in the cumulative amount ($\mu\text{g cm}^{-2}$) of ^{14}C -methyl nicotinate penetrated at 180 minutes compared to the relevant control. Cumulative amount (Q_T) is represented on the graph as $\mu\text{g cm}^{-2}$. All data are represented as mean + standard deviation of $n=6$ diffusion cells.

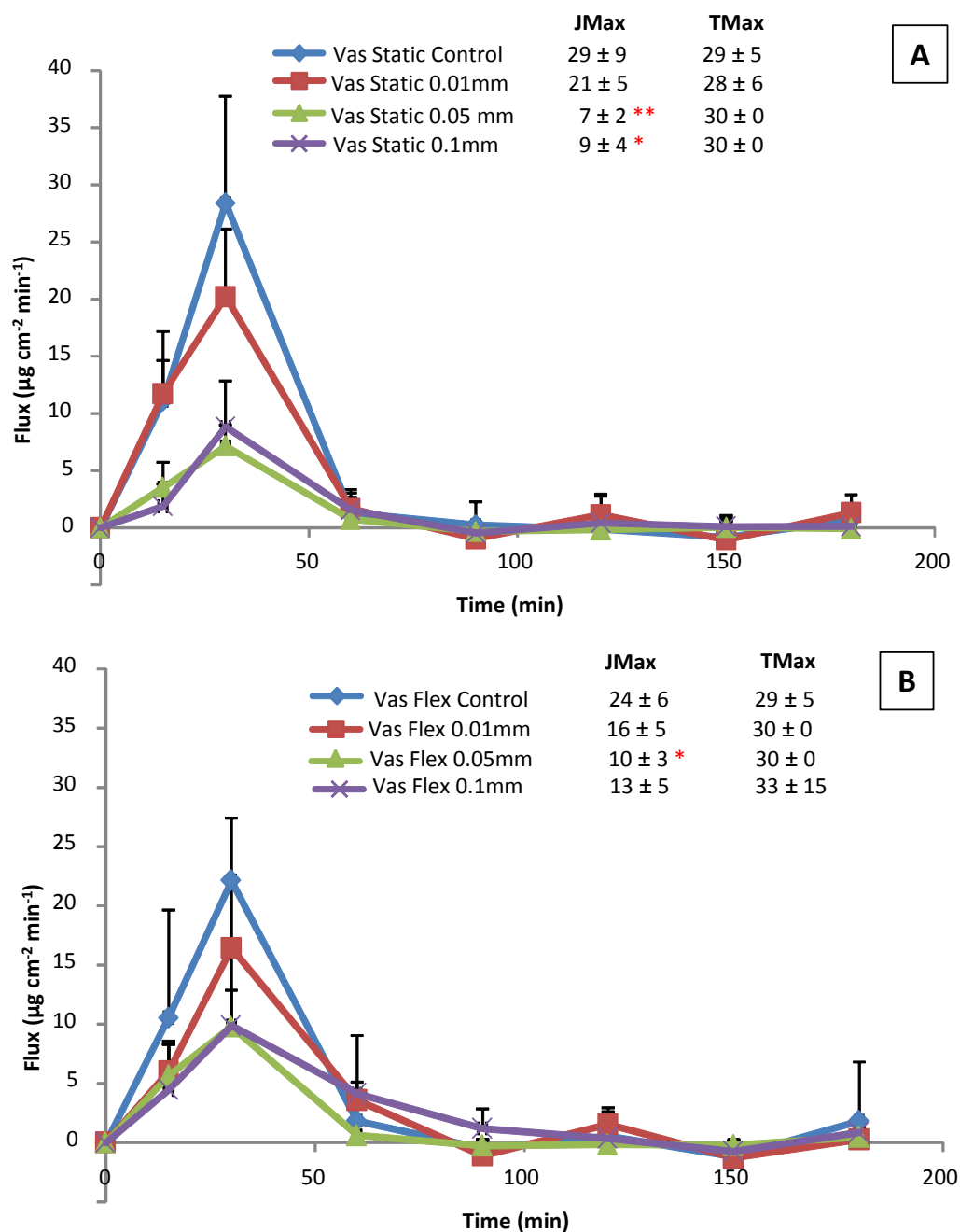


Figure 5.8: *In Vitro* Flux Profile Of ^{14}C -Methyl Nicotinate Penetrated Through Static (A) And Flexed (B) Porcine Skin Treated With Vaseline Over 180 Minutes. Vaseline was tested for protective effect against ^{14}C -methyl nicotinate (10 μl ; 1 μCi) at thicknesses of 0.01, 0.05 and 0.1 mm. Excess nicotinate was removed at 20 minutes and Vaseline was removed at 120 minutes. Asterisks (* and **) indicate significant ($p < 0.05$ and 0.01 , respectively) reductions in maximum penetration rate (JMax; $\mu\text{g cm}^{-2} \text{min}^{-1}$) compared to the relevant control. Time at which maximum flux occurred (T_{Max}) was also studied. All data are represented as mean + standard deviation of $n=6$ diffusion cells.

5.3.1.6 Dose Distribution Of ¹⁴C-Methyl Nicotinate: RD-1433 And Vaseline®

Skin Surface Recovery Of Excess Methyl Nicotinate After 20 Minutes

Both flexed and immobile skin sections treated with RD-1433 and Vaseline® at 0.05 and 0.1 mm showed significant recovery ($p < 0.001$ and 0.01 , respectively) of methyl nicotinate from the skin surface after 20 minutes compared to the untreated control and 0.01 mm treated sections (Figure 5.9). Static and flexed skin treated with 0.01 mm of either RD-1433 or Vaseline® showed significantly decreased ($p < 0.001$) amounts of surface recovery of methyl nicotinate compared to the 0.05 and 0.1 mm treated groups.

Skin Surface Wash Of RD-1433 And Vaseline After 120 Minutes

Both flexed and immobile skin sections treated with RD-1433 at all three thicknesses (0.01, 0.05 and 0.1 mm) showed significant recovery (flexed $p < 0.001$, 0.01 and 0.01; static $p < 0.1$, respectively) of methyl nicotinate after 120 minutes. In contrast, there was no significant recovery ($p > 0.05$) of methyl nicotinate with any of the Vaseline® treated skin.

Skin Recovery Of Methyl Nicotinate

Both static and flexed skin groups treated with RD-1433 at 0.05 mm showed significantly less recovery ($p < 0.05$ and 0.01 , respectively) of methyl nicotinate from skin sections compared to the untreated controls. This result ($p < 0.05$) was also seen with the 0.05 mm flexed Vaseline® treated group.

Control Recovery

The total recovery of methyl nicotinate from control (untreated) groups was approximately 20% of the total applied dose, which was significantly less than the total recovery from RD-1433 and Vaseline® treated groups.

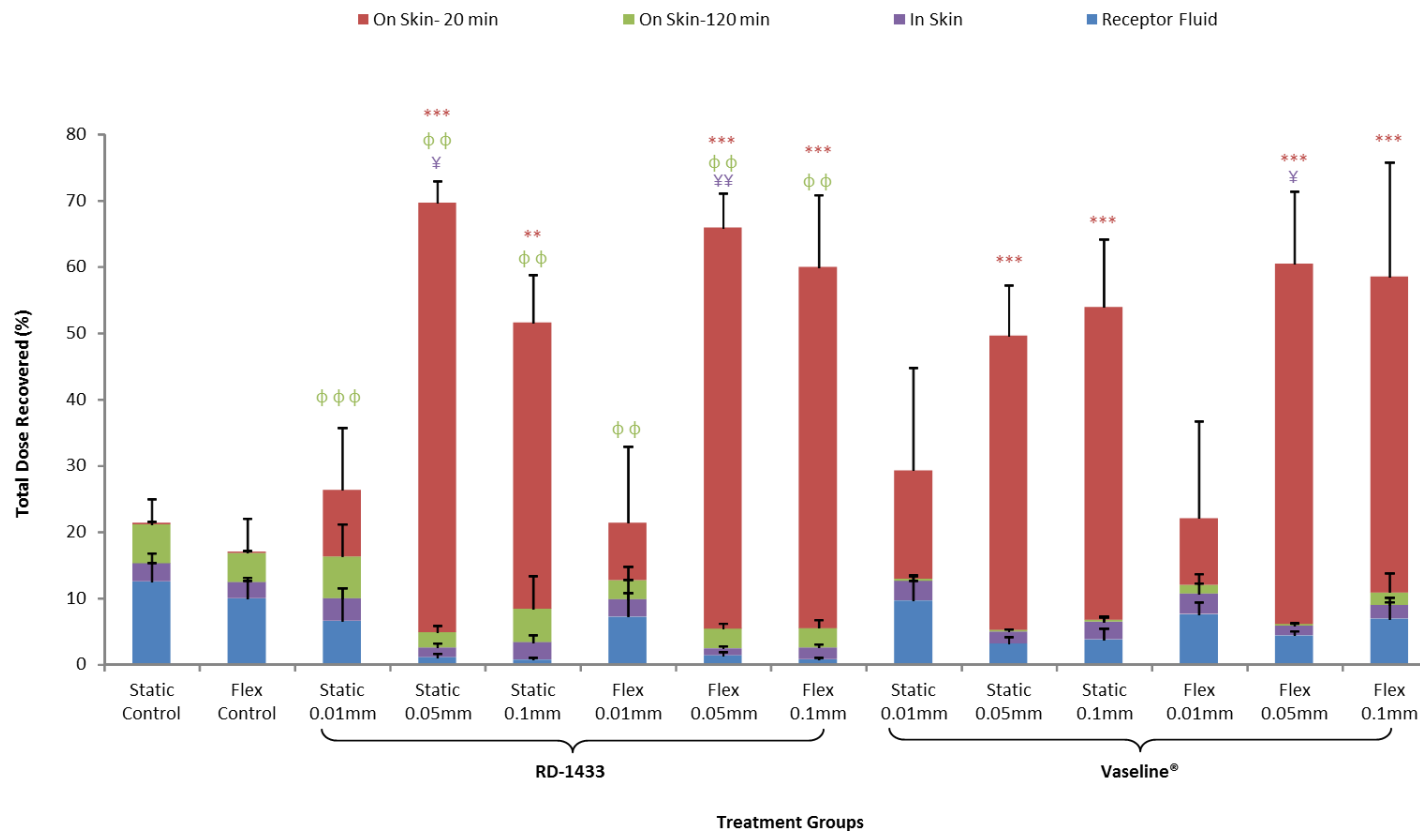


Figure 5.9: Dose Distribution Of ^{14}C -Methyl Nicotinate From Static And Flexed Porcine Skin Samples Treated With RD-1433 And Vaseline® Over 180 Minutes. Test products were treated at thicknesses of 0.01, 0.05 and 0.1 mm. Each bar on the graph indicates percentage of the dose (10.024 mg) applied that was either contained in swabs at 15 minutes (On Skin- 15 min), with RD-1433 and Vaseline after removal at 120 minutes (On Skin- 120 min) in the skin samples or in the receptor fluid. Asterisks (***) indicate significant ($p < 0.001$) increases in the amount of ^{14}C -methyl nicotinate found in the 20 minute swabs compared to the control. Circle and cross symbols (($\phi\phi$ and $\phi\phi\phi$) indicate significant ($p < 0.01$ and 0.001 , respectively) increases in the amount of ^{14}C -methyl nicotinate found in the 120 minutes swabs compared to the control. The Y symbol with 2 parallel lines represents significant decreases ($p < 0.05$ and 0.01 , respectively) in ^{14}C -methyl nicotinate found in the skin compared to the control. All data are represented as mean + standard deviation of 6 diffusion cells.

5.3.2 *In Vivo* Optimal Thickness Study

5.3.2.1 *Thickness Applied*

In contrast to the *in vitro* studies, the actual thickness of both RD-1433 and Vaseline[®] were generally within 80-90% of the intended (nominal) thickness (Figure 5.10).

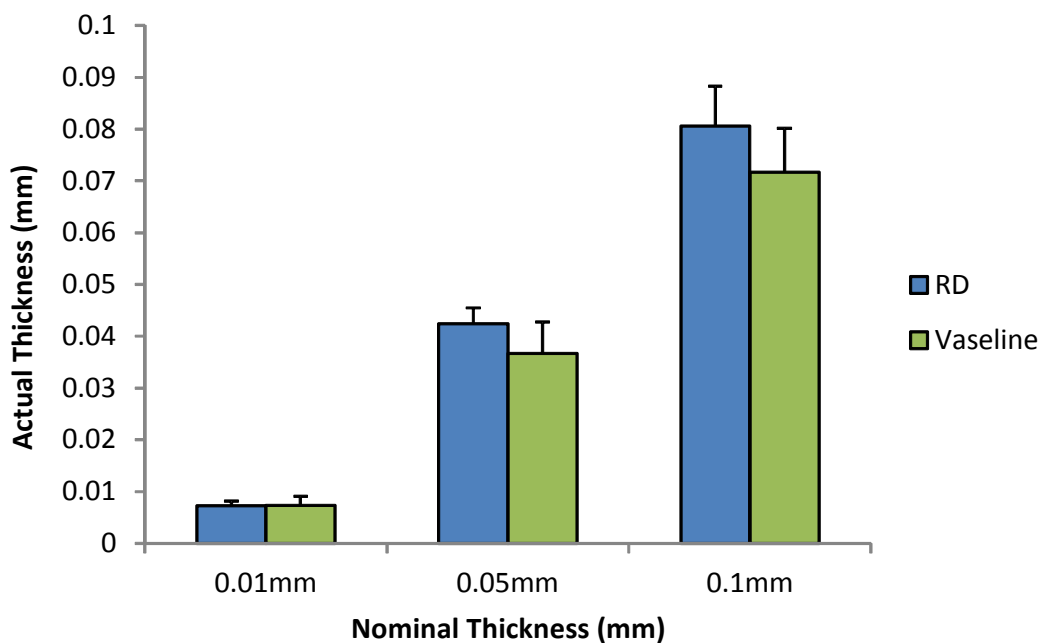


Figure 5.10: *In Vivo* Applied Thickness Of RD-1433 And Vaseline[®] For Optimal Thickness Studies. Glove tips were weighed before and after product application in order to get a total amount applied to the skin surface. This amount was determined after factoring in the density of RD-1433 (2.358 g cm^{-3}) and Vaseline (0.952 g cm^{-3}). All data are represented as mean + standard deviation of 12 volunteers.

5.3.2.2 In Vivo Barrier Integrity Measurement- TEWL

There were no significant differences seen in the transepidermal water loss flux between the baseline and post-treatment values within or between treatment groups (Figure 5.11). Transepidermal water loss flux was consistently lower in all post-treatment measurements.

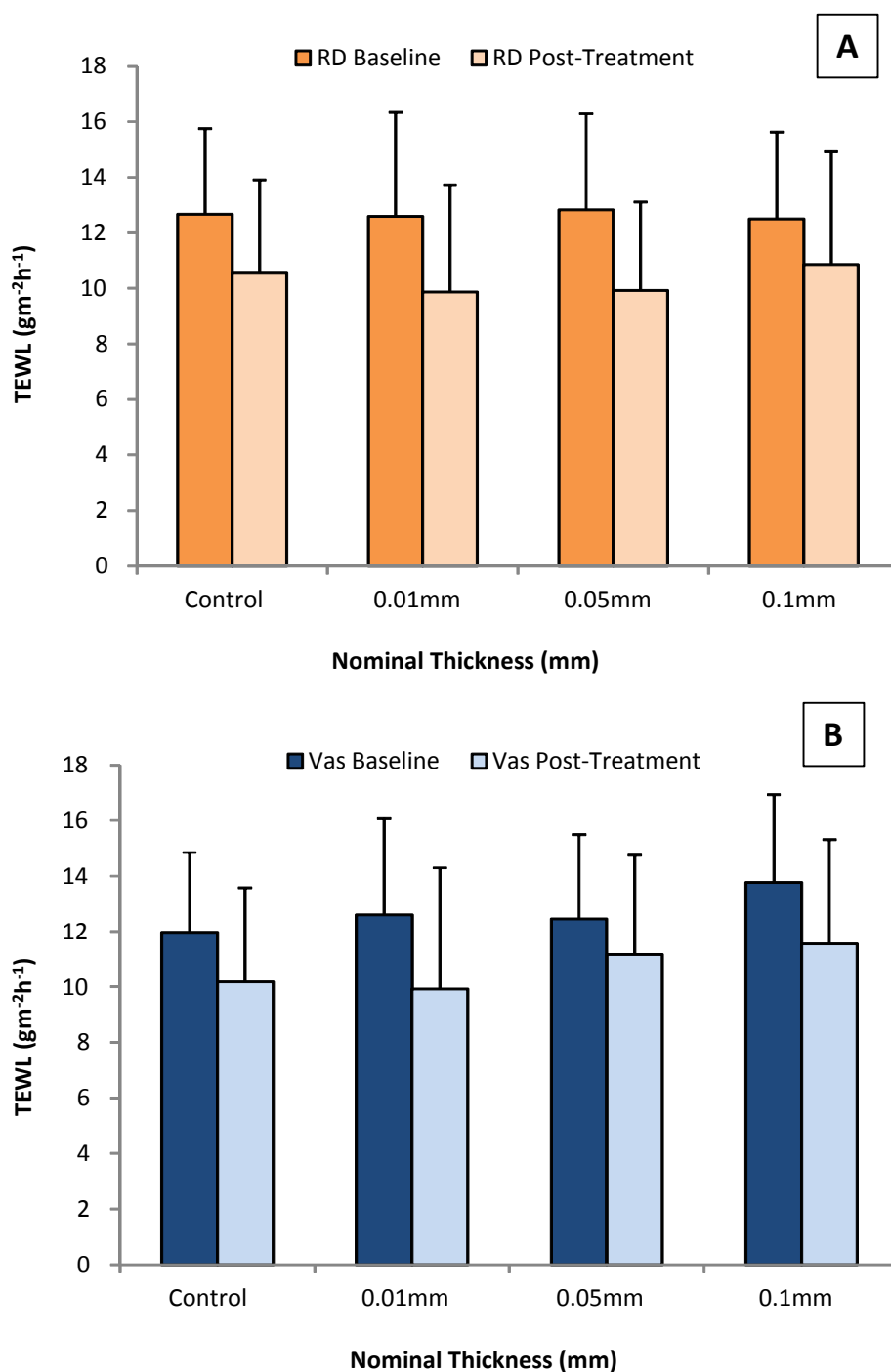


Figure 5.11: *In Vivo* Transepidermal Water Loss Flux Before And After ¹⁴C-Methyl Nicotinate Application In RD-1433 (A) And Vaseline (B) Treated Thickness Groups. TEWL was measured before test product application and application of 10 μ l of methyl nicotinate (A) and after test product and methyl nicotinate removal (B). All data are represented as mean + standard deviation of 12 volunteers.

5.3.2.3 Visual Erythema Scoring

Skin sites treated with RD-1433 at 0.05 and 0.1 mm showed a dose-dependent and significant ($p < 0.05$) decrease in erythema compared to the untreated control (Figure 5.12, A). Vaseline[®] treated sites, when tested at all thicknesses, did not significantly reduce erythema compared to the untreated control (Figure 5.12, B).

Moreover, RD-1433 (when applied at all thicknesses) was found to significantly ($p < 0.05$) reduce erythema compared to the Vaseline[®] treated groups. When applied at 0.01 mm, RD-1433 treated skin showed a 4-fold decrease in erythema compared to the untreated control and a 2-fold decrease compared to erythema with application at 0.05 mm.

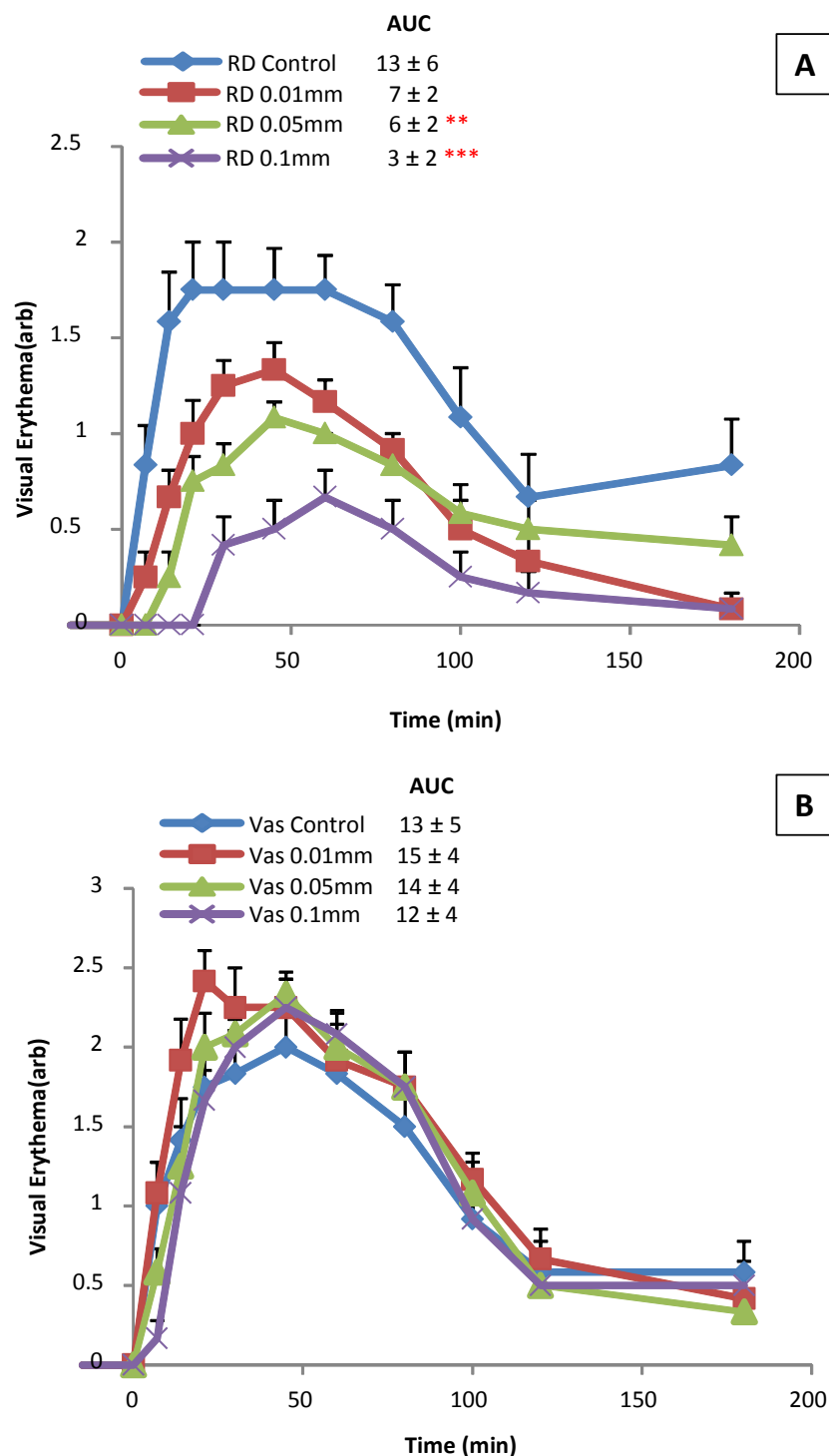


Figure 5.12: Visual Erythema Scoring For Human Volunteers Treated With RD-1433 (A) And Vaseline® (B) Over 180 Minutes. RD-1433 and Vaseline were applied to separate application sites on the volar forearm at thicknesses of 0.01, 0.05 and 0.1 mm before rubefacient application. An untreated control site was present on both arms. Methyl nicotinate was applied (10 μ l; 5 mM) to the forearm at time 0. Excess methyl nicotinate was removed at 20 minutes and products were removed at 120 minutes. All data (n=12) are represented as mean + standard error of the mean. Asterisks (** and ***) represent a significant ($p < 0.05$ and 0.01 , respectively) decrease in visual erythema as compared to the untreated control.

5.3.2.4 Tissue Imaging Viability

Skin sites treated with RD-1433 at both 0.05 and 0.1 mm thicknesses showed significantly ($p < 0.05$) reduced erythema compared to the untreated control. In addition, RD-1433 treated skin showed a dose-dependent decrease in erythema with increasing thicknesses applied. Skin sites treated with Vaseline[®] did not differ significantly in respect to erythema compared to the untreated control (Figure 5.13).

Skin treated with RD-1433 at all thicknesses showed significant reductions ($p < 0.05$) in erythema compared to Vaseline treated sections, equating to an approximate reduction in erythema of 3- to 11-fold with increasing RD-1433 thickness, respectively (Figure 5.13).

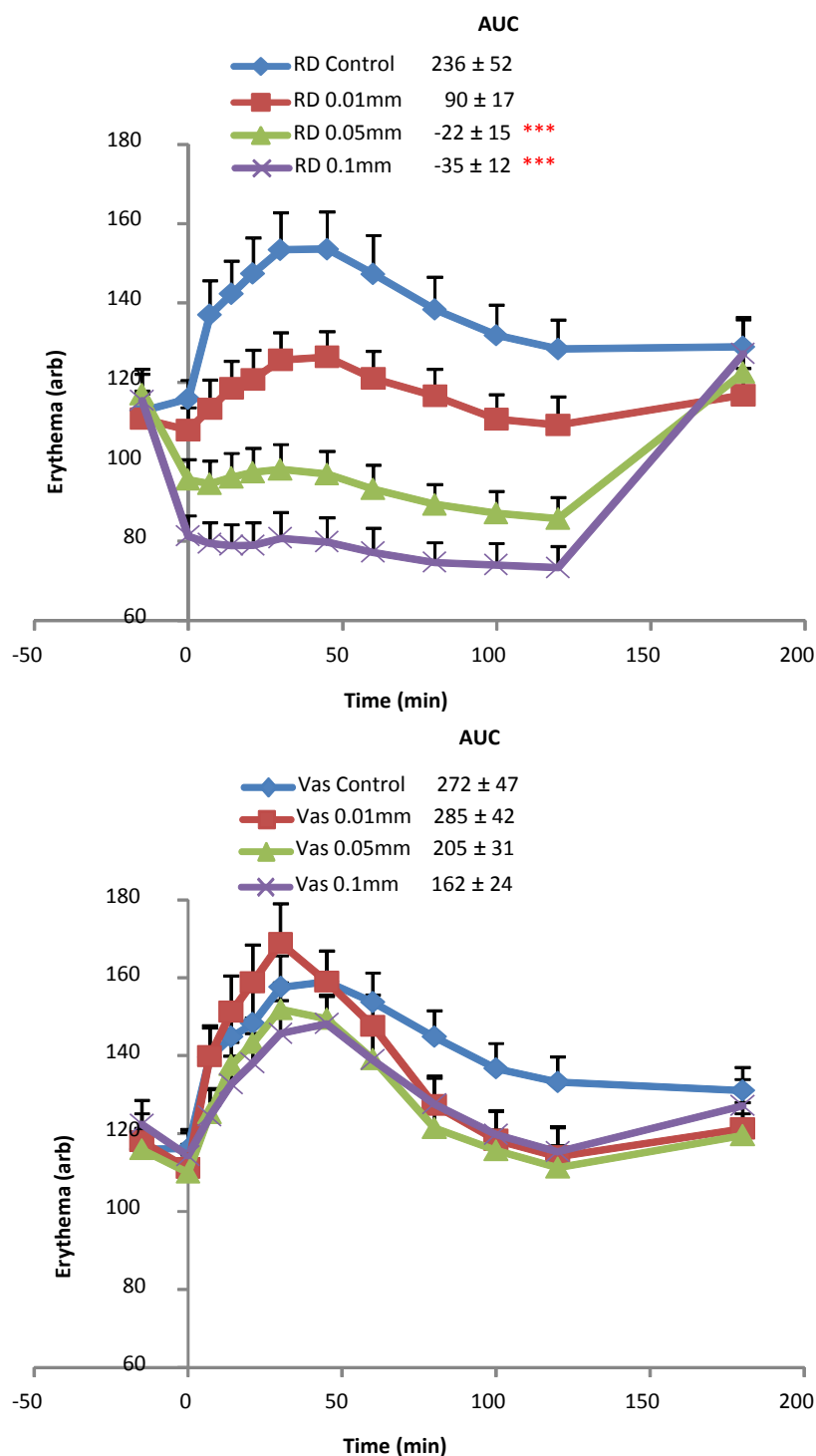


Figure 5.13: Tissue Viability Imaging Of Human Volunteers Treated With RD-1433 (A) And Vaseline® (B) Over 180 Minutes. RD-1433 and Vaseline were applied to separate application sites on the volar forearm at thicknesses of 0.01, 0.05 and 0.1 mm before rubefacient application. An untreated control site was present on both arms. Methyl nicotinate was applied (10 μ l; 5 mM) to the forearm at time 0. Excess methyl nicotinate was removed at 20 minutes and products were removed at 120 minutes. All data (n=12) are represented as mean + standard error of the mean. Asterisks (***) represent a significant ($p < 0.001$) decrease in erythema as compared to the untreated control.

5.3.2.5 Laser Doppler Imaging- Blood Flow

Skin sites treated with RD-1433 at a thickness of 0.05 and 0.1 mm demonstrated significant reductions in blood flow compared to the RD-1433 0.01 mm treated group and the untreated control (Figure 5.14). All skin treated with RD-1433 showed a dose-dependent decrease in blood flow with increasing thickness of product used. Skin sites treated with Vaseline[®] did not show significantly different erythema compared to the untreated control.

All skin sites treated with RD-1433 showed significant decreases ($p < 0.05$) in blood flow compared to corresponding Vaseline[®] treated sites, with decreases approximately 2- fold to 20-fold for increasing RD-1433 treated thicknesses. Skin sites treated with RD-1433 0.1 mm provided more than a 2-fold decrease in blood flow compared to RD-1433 0.05 mm treated sites.

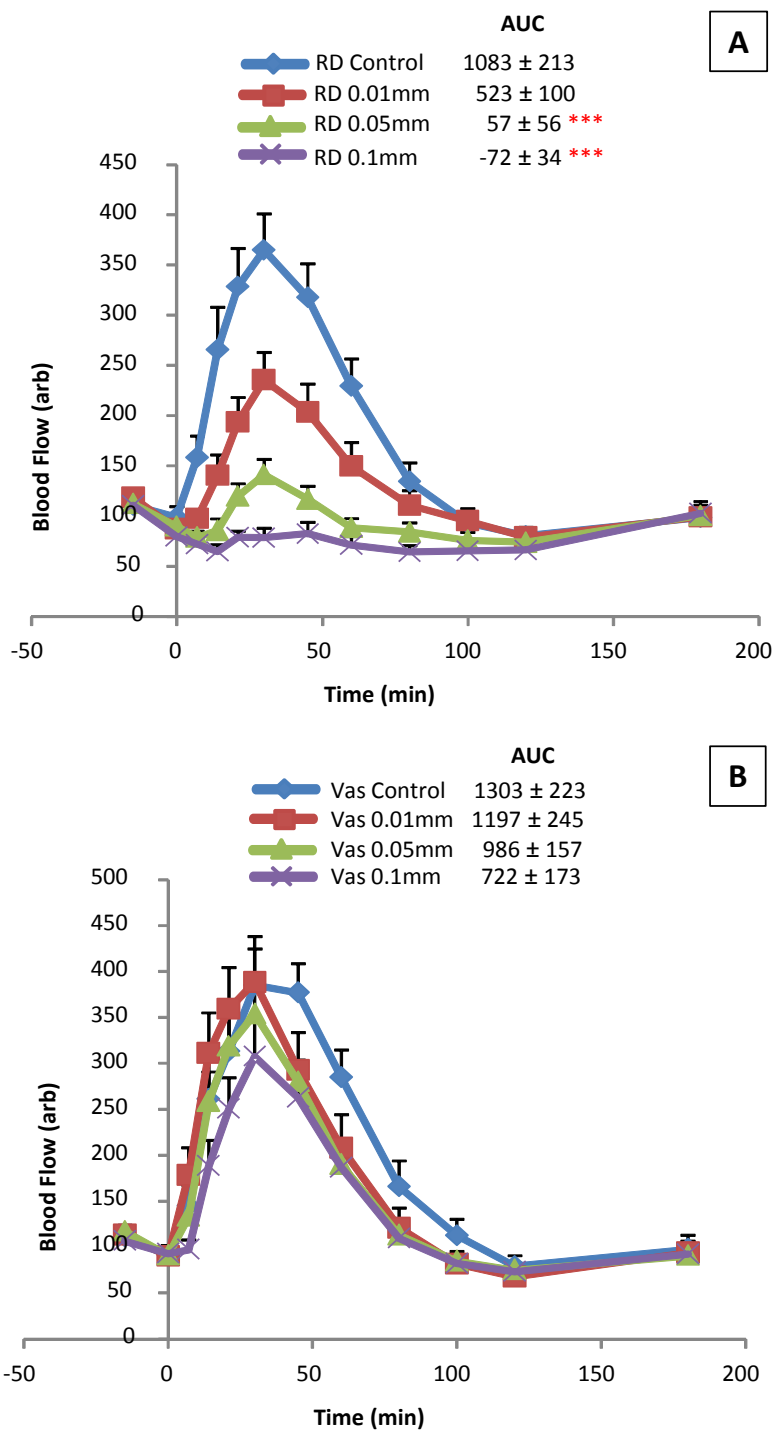


Figure 5.14: Laser Doppler Imaging Of Human Volunteer Blood Flow Of RD-1433 (A) And Vaseline® (B) Over 180 Minutes RD-1433 and Vaseline were applied to separate application sites on the volar forearm at thicknesses of 0.01, 0.05 and 0.1 mm before rubefacient application. An untreated control site was present on both arms. Methyl nicotinate was applied (10 μ l; 5 mM) to the forearm at time 0. Excess methyl nicotinate was removed at 20 minutes and products were removed at 120 minutes. All data (n=12) are represented as mean + standard error of the mean. Asterisks (***) represent a significant ($p < 0.001$) decrease in blood flow as compared to the untreated control.

5.3.2.6 Laser Doppler Imaging- Maximum Blood Flow

Skin sites treated with RD-1433 at a thickness of 0.05 and 0.1 mm presented with significantly ($p < 0.05$) reduced maximum blood flux compared to RD-1433 sites treated at 0.01 mm and the untreated control (Figure 5.15). A dose-dependent decrease was seen in maximum blood flow with increasing RD-1433 thicknesses used. Skin sites treated with Vaseline[®] did not demonstrate maximum blood flow rates distinguishable from the untreated control.

All skin sites treated with RD-1433 showed significant decreases in maximum blood flow compared to sites treated with Vaseline[®]. In addition, RD-1433 skin sites treated with 0.1 mm showed significantly reduced maximum blood flow in comparison to the lesser thicknesses of RD-1433.

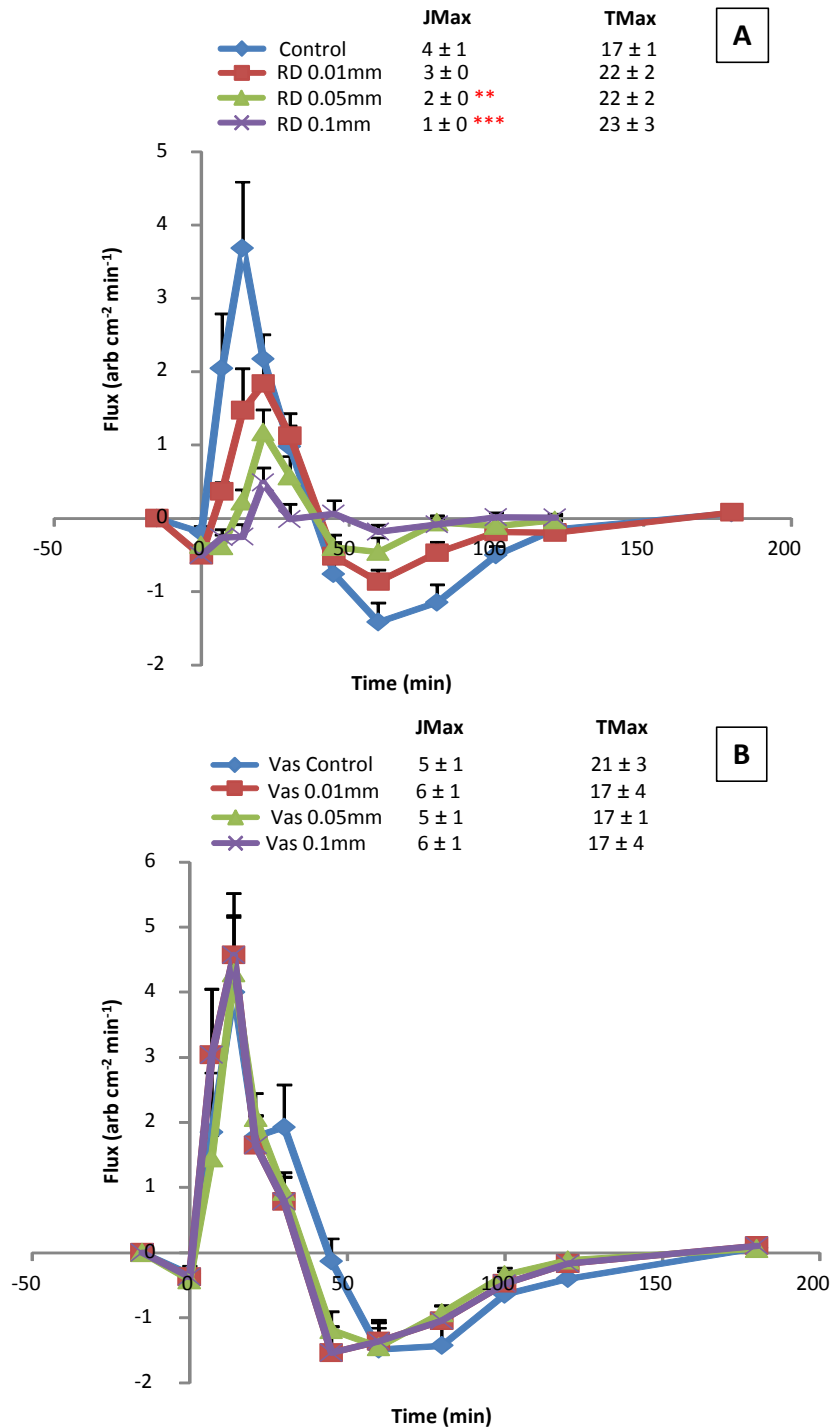


Figure 5.15: Laser Doppler Imaging Of Human Volunteers- Maximum Blood Flow Of RD-1433 (A) And Vaseline® (B) Over 180 Minutes. RD-1433 and Vaseline were applied to separate application sites on the volar forearm at thicknesses of 0.01, 0.05 and 0.1 mm before rubefacient application. An untreated control site was present on both arms. Methyl nicotinate was applied (10 μ l; 5 mM) to the forearm at time 0. Excess methyl nicotinate was removed at 20 minutes and products were removed at 120 minutes. All data (n=12) are represented as mean + standard error of the mean. Asterisks (** and ***) represent a significant ($p < 0.05$ and 0.01, respectively) decrease in visual erythema as compared to the untreated control.

5.3.3 *In Vitro* Duration Of Efficacy Study

5.3.3.1 *Barrier Integrity Measurements*

When evaluating transepidermal water loss flux in both immobile and flexed skin treated with RD-1433 and Vaseline[®], there were no significant differences between baseline and post-treatment values either within or between treatment groups (Figure 5.16). An identical result was seen with tritiated water penetration (Figure 5.17).

There was no correlation between tritiated water penetrated and TEWL flux at both baseline ($r= 0.23$) and post-treatment ($r= 0.35$) in skin treated with RD-1433. There was also no correlation between tritiated water penetrated and TEWL flux at both baseline ($r= 0.20$) and post-treatment ($r= 0.17$) in Vaseline[®] treated groups.

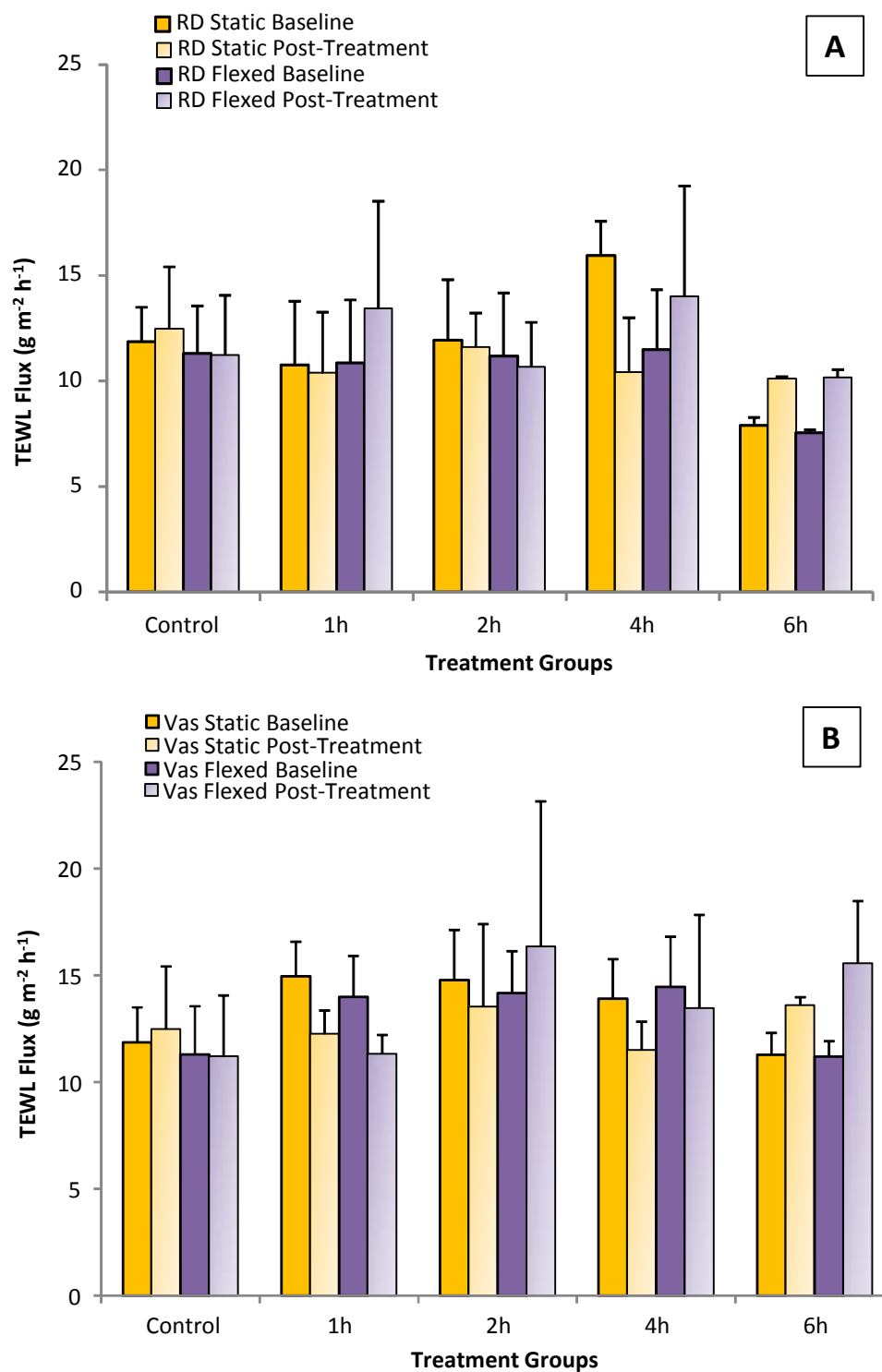


Figure 5.16: Transepidermal Water Loss Flux In Static And Flexed Porcine Skin Exposed To ^{14}C -Methyl Nicotinate And Treated With RD-1433 (A) And Vaseline (B) At Different Durations Of Efficacy. TEWL was measured before test product application and $10\ \mu\text{l}$ ($1\ \mu\text{Ci}$ total) of ^{14}C -methyl nicotinate (Baseline) and after test product and ^{14}C -methyl nicotinate removal (Post-Treatment). All data are represented as mean + standard deviation of 6 diffusion cells.

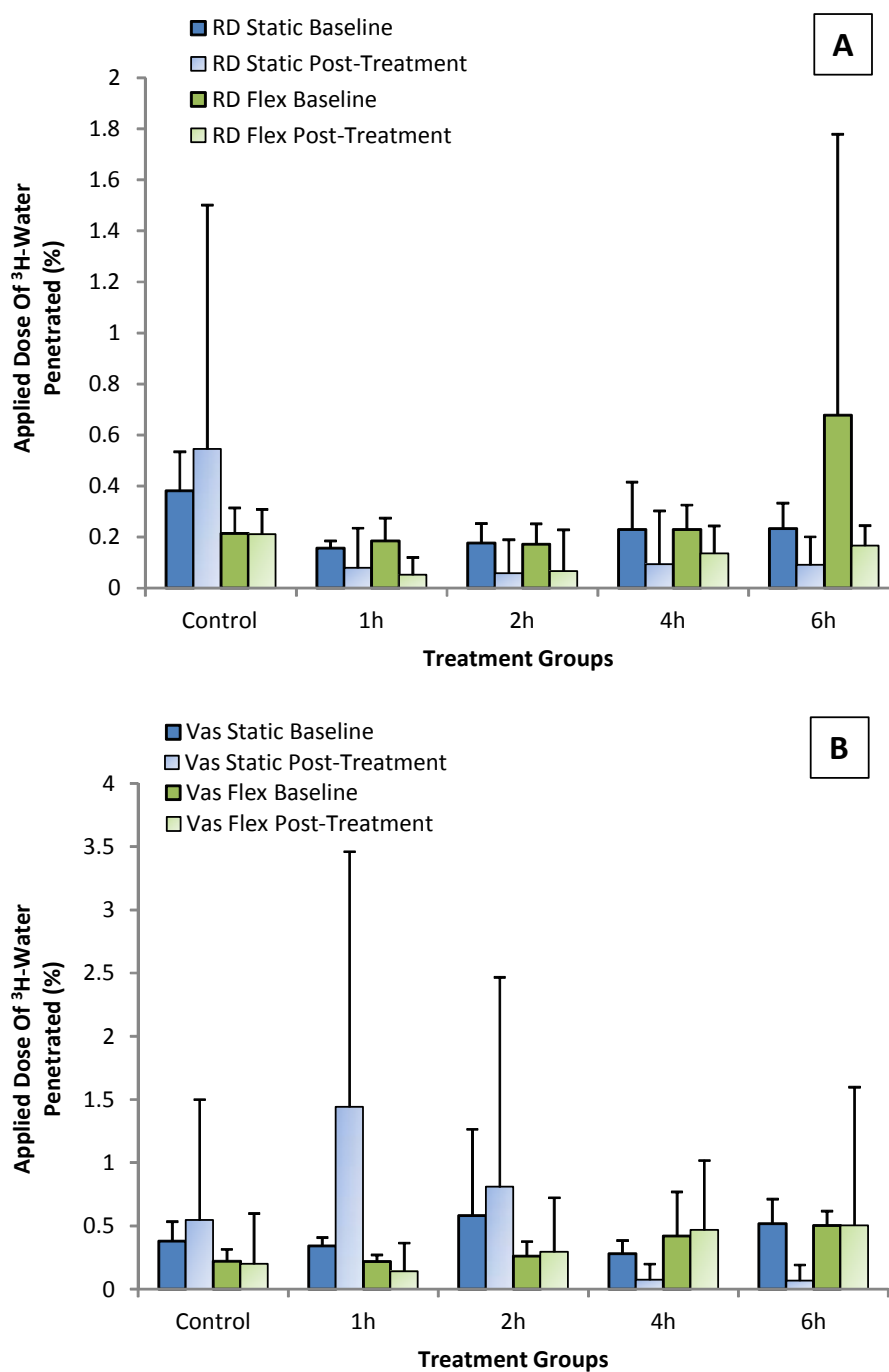


Figure 5.17: Tritiated Water Penetration In Static And Flexed Porcine Skin Treated With RD-1433 (A) And Vaseline (B) Used At Different Durations Of Efficacy. Tritiated water was applied for 30 minutes before test product application and 10 μl (1 μCi total) of ^{14}C -methyl nicotinate (Baseline) and after test product and ^{14}C -methyl nicotinate removal (Post-Treatment). All data are represented as mean + standard deviation of 6 diffusion cells.

5.3.3.2 RD-1433 Treated Groups- Duration Of Efficacy Study

Cumulative Amount Penetrated

Both static and flexed skin treated with RD-1433 from 1-6 hours showed significant decreases ($p < 0.001$) in the cumulative amount of methyl nicotinate penetrated compared to the untreated control (Figure 5.18).

Maximum Flux

Static groups treated with RD-1433 at 1, 2, 4 and 6 hours had significantly ($p < 0.001$) lower maximum flux compared to the static control (Figure 5.19).

Both static and flexed skin treated with RD-1433 for 1-6 hours had significantly lower ($p < 0.001$) maximum flux values compared to the relevant controls. All skin treated with RD-1433 from 1-6 hours showed identical maximum flux rates, which equated to approximately a 29-fold decrease in methyl nicotinate flux compared to the control.

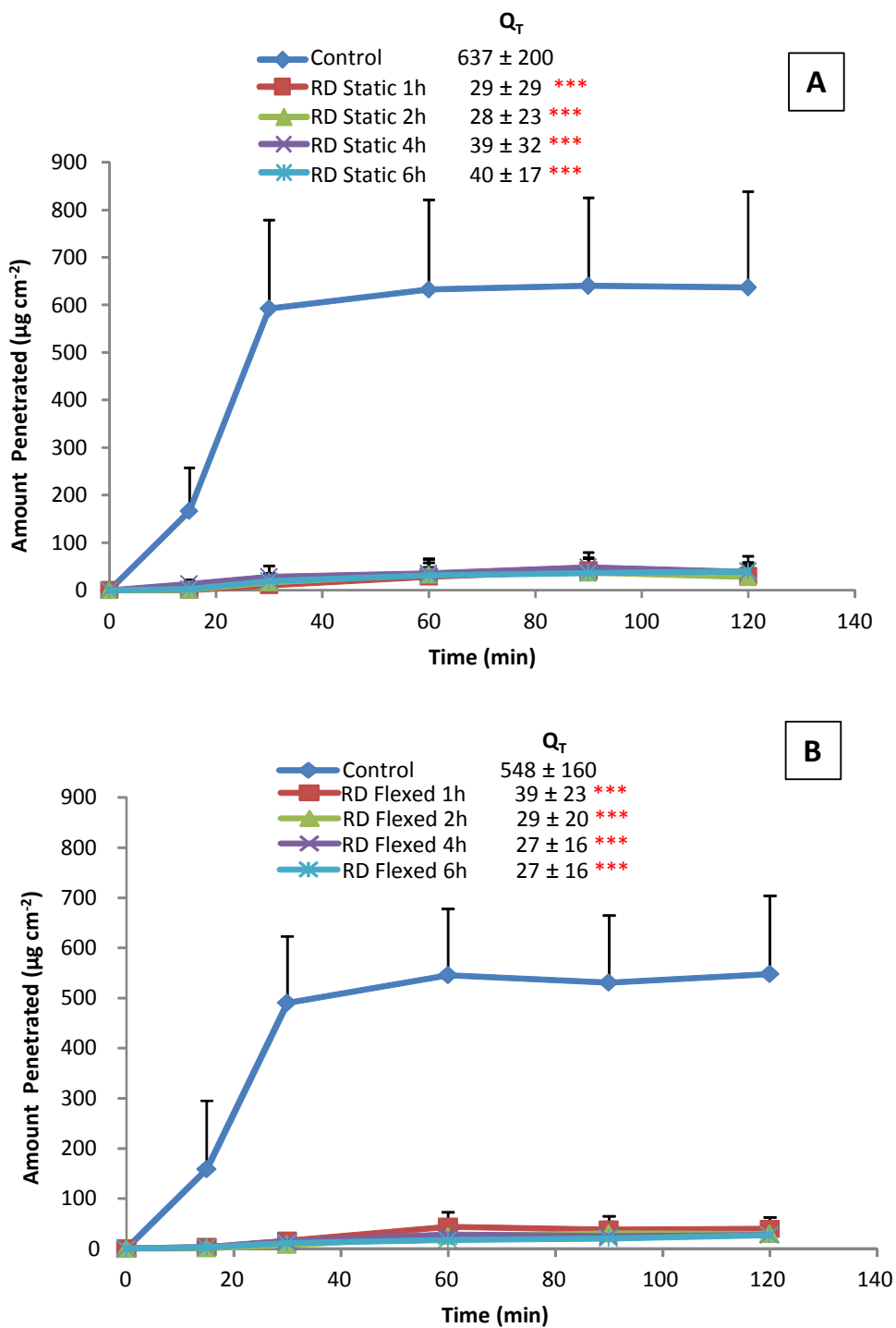


Figure 5.18: Cumulative Amount of ¹⁴C- Methyl Nicotinate Penetrated Through Static (A) And Flexed (B) Porcine Skin Treated With RD-1433 Over 120 Minutes. RD-1433 (0.1 mm thickness) was tested for protective effect against ¹⁴C-methyl nicotinate (10 µl, 1 µCi applied) for durations of 1, 2, 4 and 6 hours. Excess nicotinate was removed at 20 minutes and RD-1433 was removed at 60 minutes. The cumulative amount penetrated at study end (Q_T) is represented on the graph in µg cm⁻² h⁻¹. Asterisks (***) indicate significant (p < 0.001) reductions in the cumulative amount (µg cm⁻²) of ¹⁴C-methyl nicotinate penetrated at 120 minutes compared to the relevant control. All data are represented as mean + standard deviation of n=6 diffusion cells.

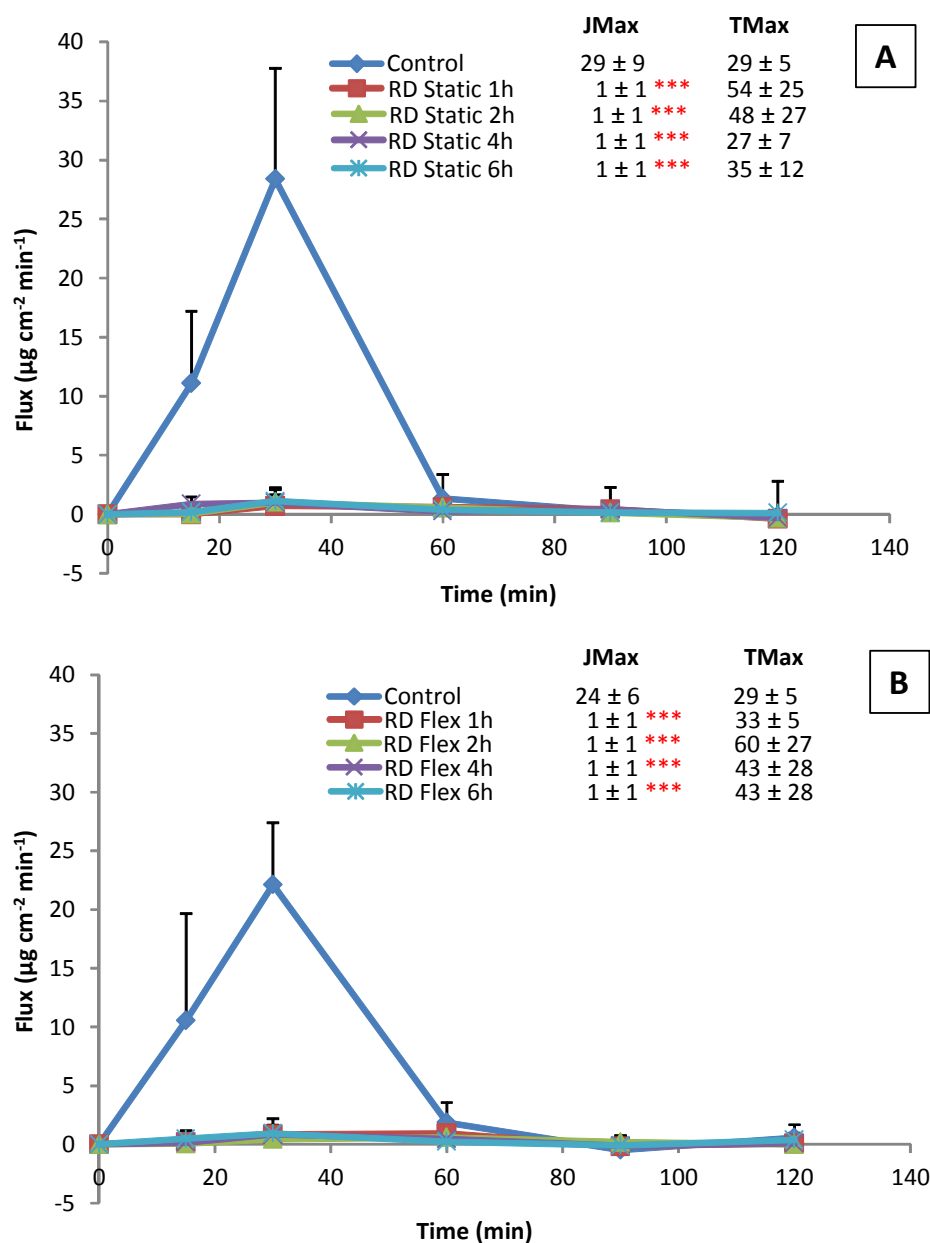


Figure 5.19: Flux Profile Of ^{14}C -Methyl Nicotinate Penetrated Through Static (A) And Flexed (B) Porcine Skin Treated With RD-1433 Over 120 Minutes. RD-1433 (0.1 mm thickness) was tested for protective effect against ^{14}C -methyl nicotinate (10 μl , 1 μCi applied) for durations of 1, 2, 4 and 6 hours. Excess nicotinate was removed at 20 minutes and RD-1433 was removed at 60 minutes. Asterisks (***) indicate significant ($p < 0.001$) reductions in maximum flux (JMax; $\mu\text{g cm}^{-2} \text{min}^{-1}$) compared to the relevant control. All data are represented as mean + standard deviation of $n=6$ diffusion cells.

5.3.3.3 Vaseline[®] Treated Groups- Duration Of Efficacy Study

Cumulative Amount Penetrated

Flexed skin treated with Vaseline[®] for 2 hours showed a significant decrease ($p < 0.05$) in methyl nicotinate penetrated compared to the untreated control (Figure 5.20). In addition, both static and flexed skin treated with Vaseline[®] for 4 hours showed significant decreases ($p < 0.05$) in the penetration of methyl nicotinate compared to the untreated control. Although not significant ($p > 0.05$), Vaseline[®] treated skin from 1-4 hours showed approximately a 5-fold decrease in methyl nicotinate penetrated compared to the untreated control. Skin treated with Vaseline[®] for 6 hours showed higher amounts of methyl nicotinate penetrated compared to the 1-4 hour treated groups.

Both static and flexed skin treated with RD-1433 showed significant decreases ($p < 0.05$) in cumulative penetration of methyl nicotinate compared to the corresponding Vaseline[®] treated groups. The decrease in penetration of methyl nicotinate from 1-6 hours in skin treated with RD-1433 was approximately 10-fold less than that of Vaseline[®] treated skin.

Maximum Flux

Both static and flexed skin treated with Vaseline[®] at 4 hours showed significant decreases ($p < 0.05$) in maximum flux of methyl nicotinate compared to the untreated control (Figure 5.21). Although not significant, skin treated with Vaseline[®] for 1-4 hours showed approximately a 6-fold decrease in maximum flux of methyl nicotinate compared to the untreated control. Skin treated with Vaseline[®] for 6 hours showed higher maximum flux rates compared to the 1-4 hour treated groups.

Skin treated with RD-1433 from 1-6 hours showed significantly lower maximum flux than skin treated with Vaseline[®] from 1-6 hours, equating to approximately 5-fold decreases from the 1-4 hour groups and 10-fold decreases compared to the Vaseline[®] 6 hour treatment group.

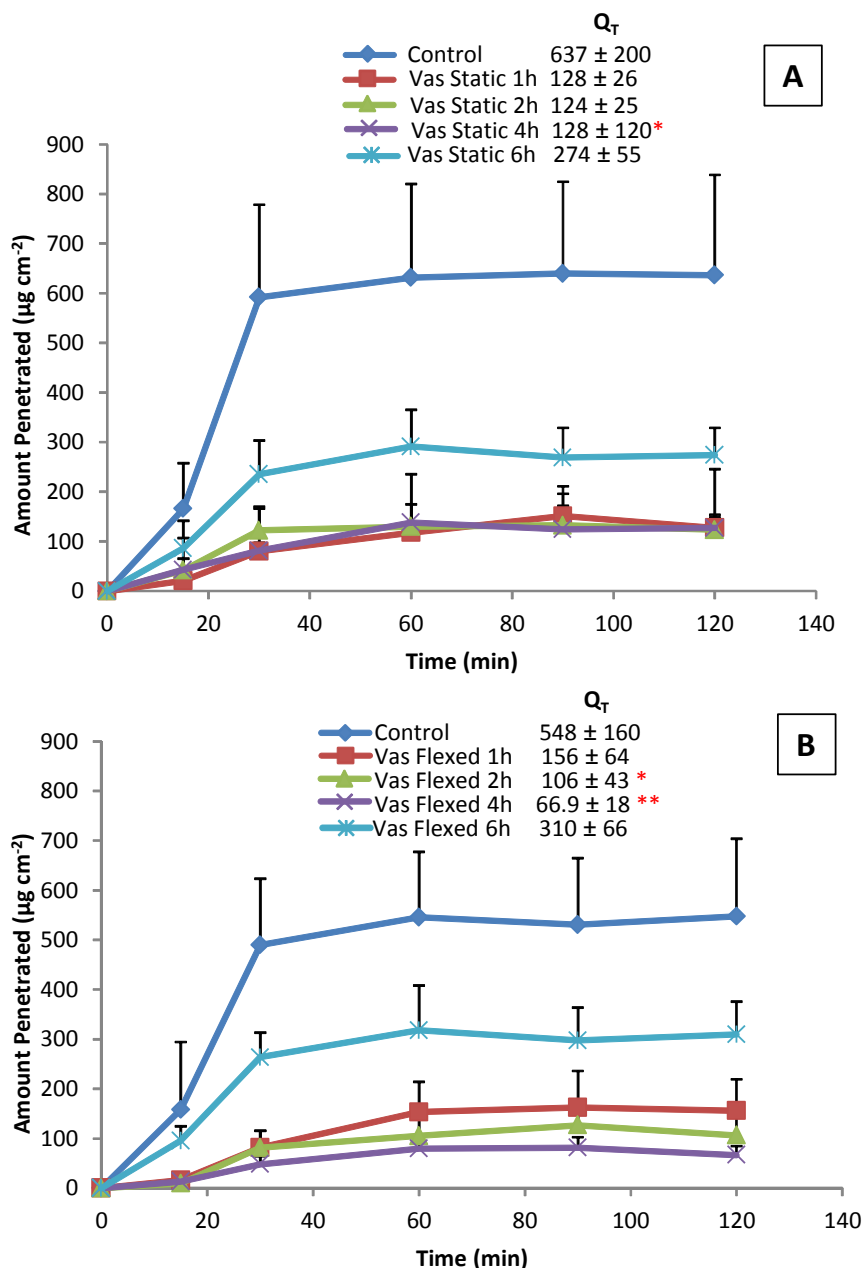


Figure 5.20: Cumulative Amount of ^{14}C - Methyl Nicotinate Penetrated Through Porcine Skin Treated with Vaseline[®] In Static (A) and Flexed (B) Skin Over 120 Minutes. Vaseline[®] (0.1 mm thickness) was tested for protective effect against ^{14}C -methyl nicotinate (10 μl , 1 μCi applied) for durations of 1, 2, 4 and 6 hours. Excess nicotinate was removed at 20 minutes and Vaseline[®] was removed at 60 minutes. The cumulative amount penetrated at study end (Q_T) is represented on the graph in $\mu\text{g cm}^{-2} \text{h}^{-1}$. Asterisks (* and **) indicate significant ($p < 0.05$ and 0.01 , respectively) reductions in the cumulative amount ($\mu\text{g cm}^{-2}$) of ^{14}C -methyl nicotinate penetrated at 120 minutes compared to the relevant control. All data are represented as mean + standard deviation of $n=6$ diffusion cells.

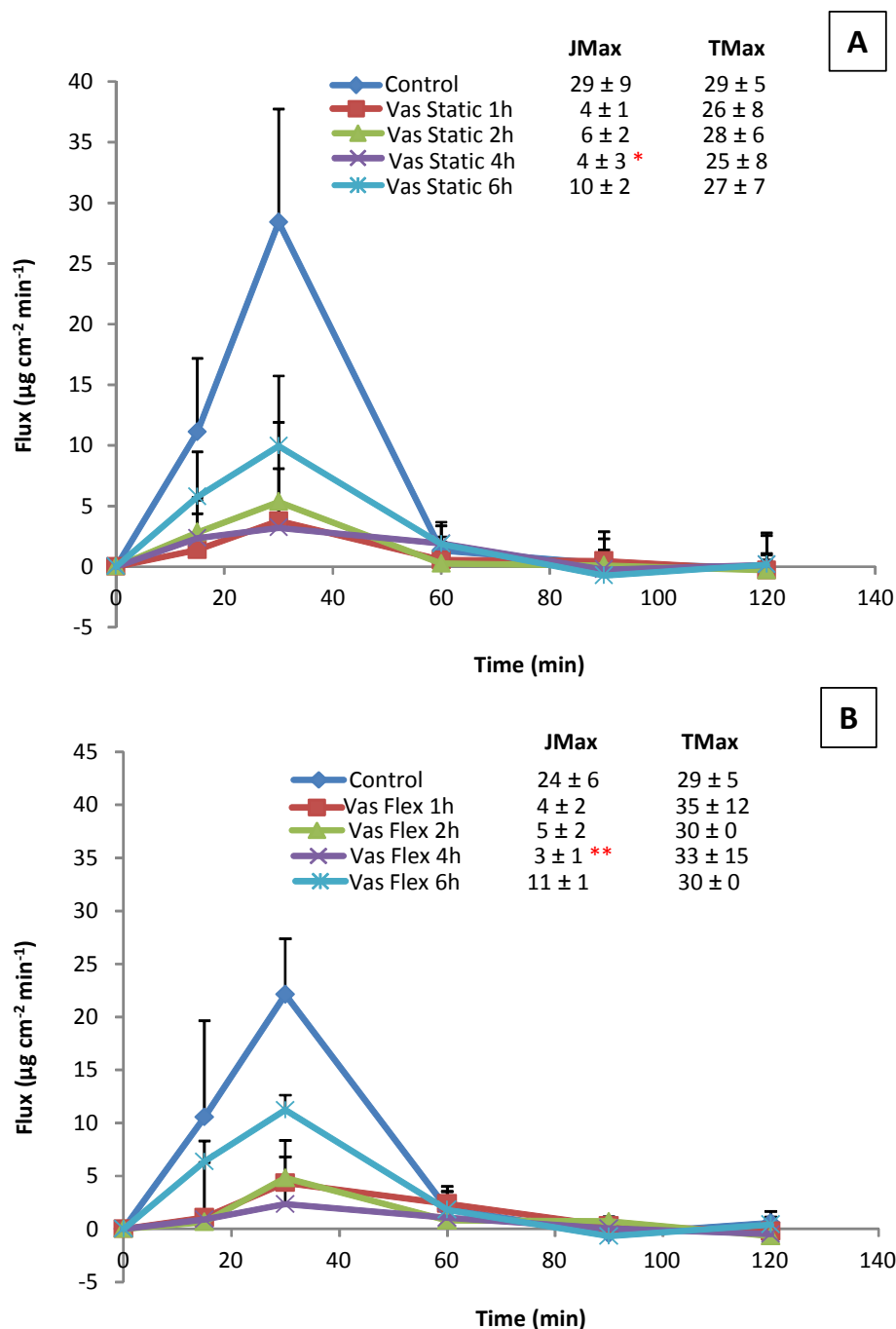


Figure 5.21: Flux Profile Of ^{14}C -Methyl Nicotinate Penetrated Through Static (A) And Flexed (B) Porcine Skin Treated With Vaseline[®] Over 120 Minutes Vaseline[®] (0.1 mm thickness) was tested for protective effect against ^{14}C -methyl nicotinate (10 μl , 1 μCi applied) for durations of 1, 2, 4 and 6 hours. Excess nicotinate was removed at 20 minutes and Vaseline[®] was removed at 60 minutes. Asterisks (* and **) indicate significant ($p < 0.05$ and 0.01 , respectively) reductions in maximum flux (JMax; $\mu\text{g cm}^{-2} \text{h}^{-1}$) compared to the relevant control. All data are represented as mean + standard deviation of $n=6$ diffusion cells.

5.3.3.4 Dose Recovery Of ¹⁴C-Methyl Nicotinate- Duration Of Efficacy Study

Skin Surface Recovery Of Methyl Nicotinate At 20 Minutes

Both static and flexed skin treated with RD-1433 showed significantly ($p < 0.05$) greater recovery of methyl nicotinate at 20 minutes on the skin surface than the untreated control groups (Figure 5.22).

Immobile skin treated with Vaseline[®] for 1, 4 and 6 hours and flexed skin treated with Vaseline[®] for 2, 4 and 6 hours showed significantly ($p < 0.05$) greater recovery of methyl nicotinate at 20 minutes from the skin surface than the untreated controls.

Skin Wash Of RD-1433 And Vaseline At 60 Minutes

All skin treated with RD-1433 showed similar recovery of methyl nicotinate at 60 minutes compared to the untreated control. Similar recovery rates were seen with skin treated with Vaseline[®] for 1, 2 and 4 hours compared to the untreated control, however both 6 hour treated Vaseline[®] groups showed significant decreases in the recovery of methyl nicotinate at 60 minutes compared to the untreated control.

A significant decrease ($p < 0.05$) in the recovery of methyl nicotinate from the skin wash at 60 minutes was seen in both static and flexed skin treated with Vaseline[®] for 6 hours.

Skin Recovery Of Methyl Nicotinate

All static and flexed groups treated with RD-1433 showed similar recovery of methyl nicotinate in the skin compared to the untreated controls. Static and flexed groups treated with Vaseline[®] from 1-4 hours showed similar skin recovery of methyl nicotinate, however groups treated with Vaseline[®] for 6 hours demonstrated

significant ($p < 0.05$) decreases in the amount of methyl nicotinate recovered in the skin compared to the untreated controls.

Control Groups

Both static and flexed untreated skin showed total recoveries of methyl nicotinate totalling approximately 20% of the applied dose, this was significantly ($p < 0.05$) less methyl nicotinate recovered compared to the RD-1433 and Vaseline[®] treated groups.

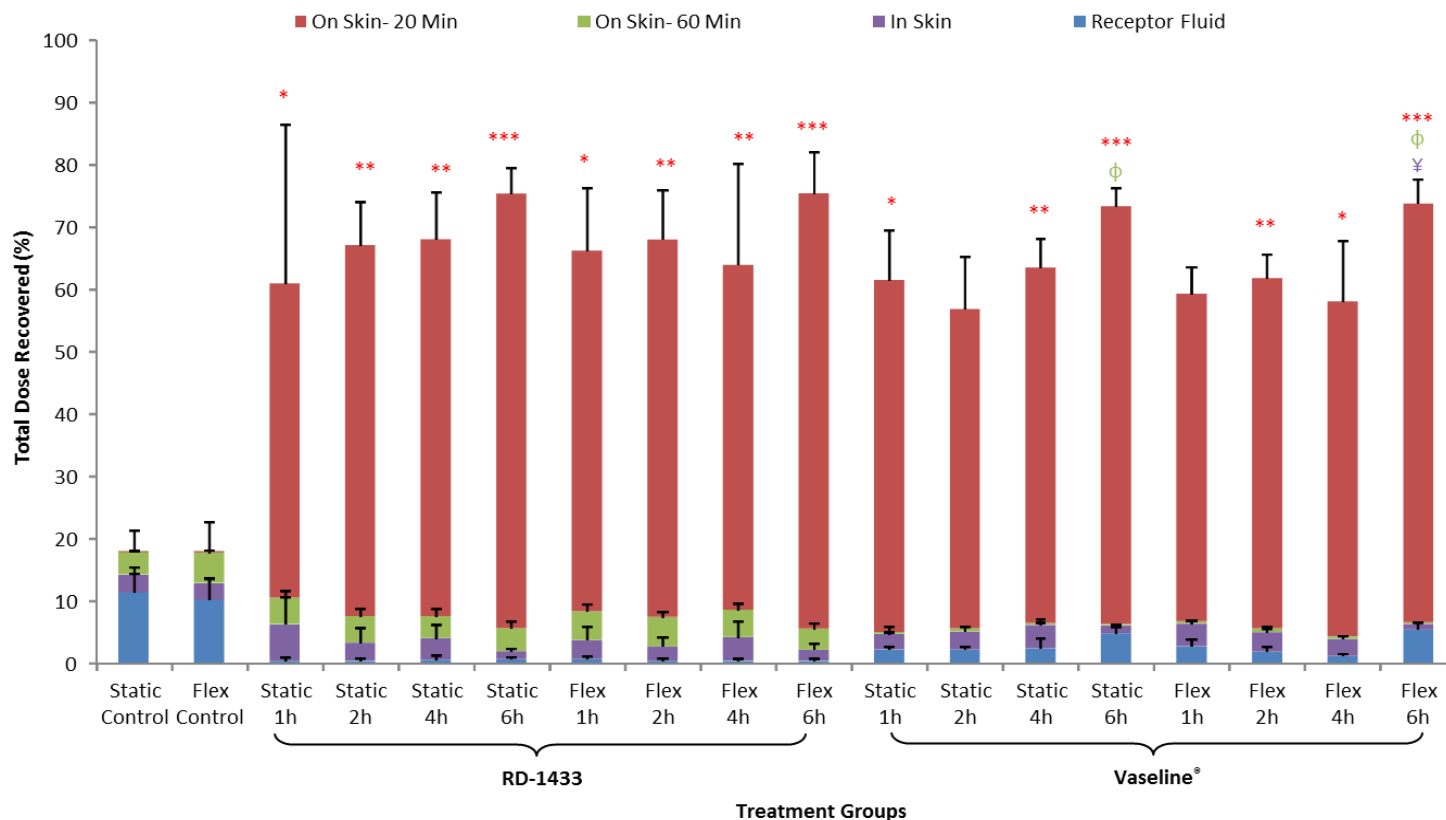


Figure 5.22: Dose Distribution Of ¹⁴C-Methyl Nicotinate From Flexed And Static Porcine Skin Treated With RD-1433 And Vaseline® Over 120 Minutes. Test products were applied to the skin surface at a thickness of 0.1 mm for 1, 2, 4 or 6 hours. Carbon-14 methyl nicotinate was applied at 10 µl (1 µCi total) per diffusion cell at time 0. The percentage of the dose (10.024 mg) applied was found on the skin at 20 minutes (On Skin- 20 Min), with test products at 60 minutes (On Skin- 60 Min), in the skin samples and in the receptor fluid. Asterisks (*, ** and ***) indicate a significant (p < 0.05, 0.01 and 0.001, respectively) increase in the amount of ¹⁴C-methyl nicotinate found in the 20 minute samples compared to the relevant control. The circle with cross symbol indicates a significant (p < 0.05) decrease in the amount of ¹⁴C-MN recovered at 60 minutes compared to the relevant control. The Y symbol with 2 parallel lines represents a significant decrease (p < 0.05) in ¹⁴C-methyl nicotinate found in the skin compared to the control. All data are represented as mean + standard deviation of 6 diffusion cells.

5.3.4 *In Vivo* Duration Of Efficacy Study

5.3.4.1 *Barrier Integrity Measurement- TEWL*

There were no significant differences found in TEWL rate for static and flexed skin sections treated with RD-1433 and Vaseline[®] between baseline and post-treatment values within a treatment group and values between groups (Figure 5.23). All post-treatment values demonstrated lower TEWL rates compared to baseline values.

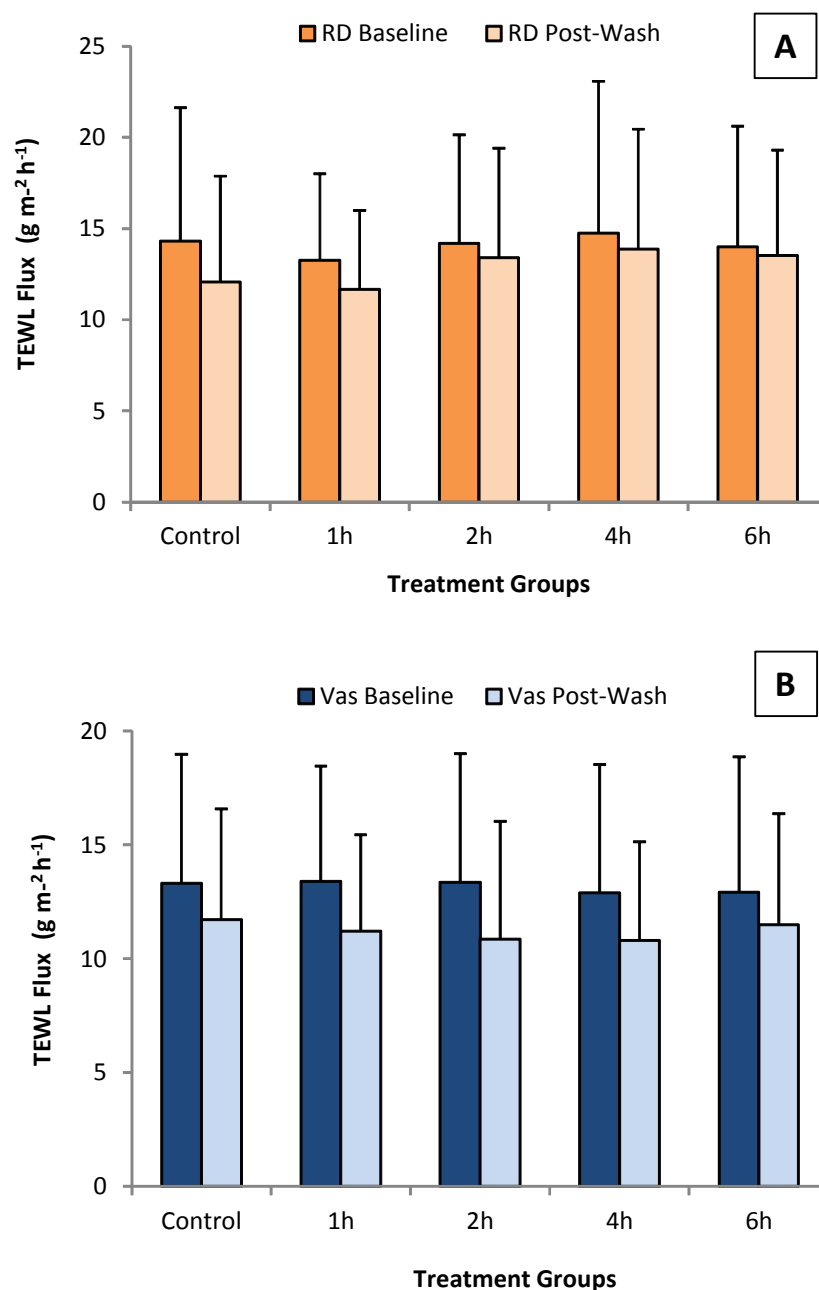


Figure 5.23: *In Vivo* Transepidermal Water Loss Flux Before And After ¹⁴C-Methyl Nicotinate Application In RD-1433 (A) And Vaseline® (B) Duration Of Efficacy Groups. TEWL was measured before test product application and application of 10 μ l of methyl nicotinate (Baseline) and after test product and methyl nicotinate removal (Post-Treatment). All data are represented as mean + standard deviation of 12 volunteers.

5.3.4.2 Visual Erythema

Skin sites treated with RD-1433 for 1, 2 and 4 hours showed significant decreases ($p < 0.001$, 0.01 and 0.001, respectively) in erythema compared to the untreated control (Figure 5.24- A). There were no significant decreases in erythema in the Vaseline[®] treated groups compared to the untreated control (Figure 5.24- B).

Skin sites treated with RD-1433 from 1-6 hours showed significantly ($p < 0.05$) less visual erythema compared to Vaseline[®] treated groups, this equated to an approximate 2- to 3-fold decrease in RD-1433 treated groups.

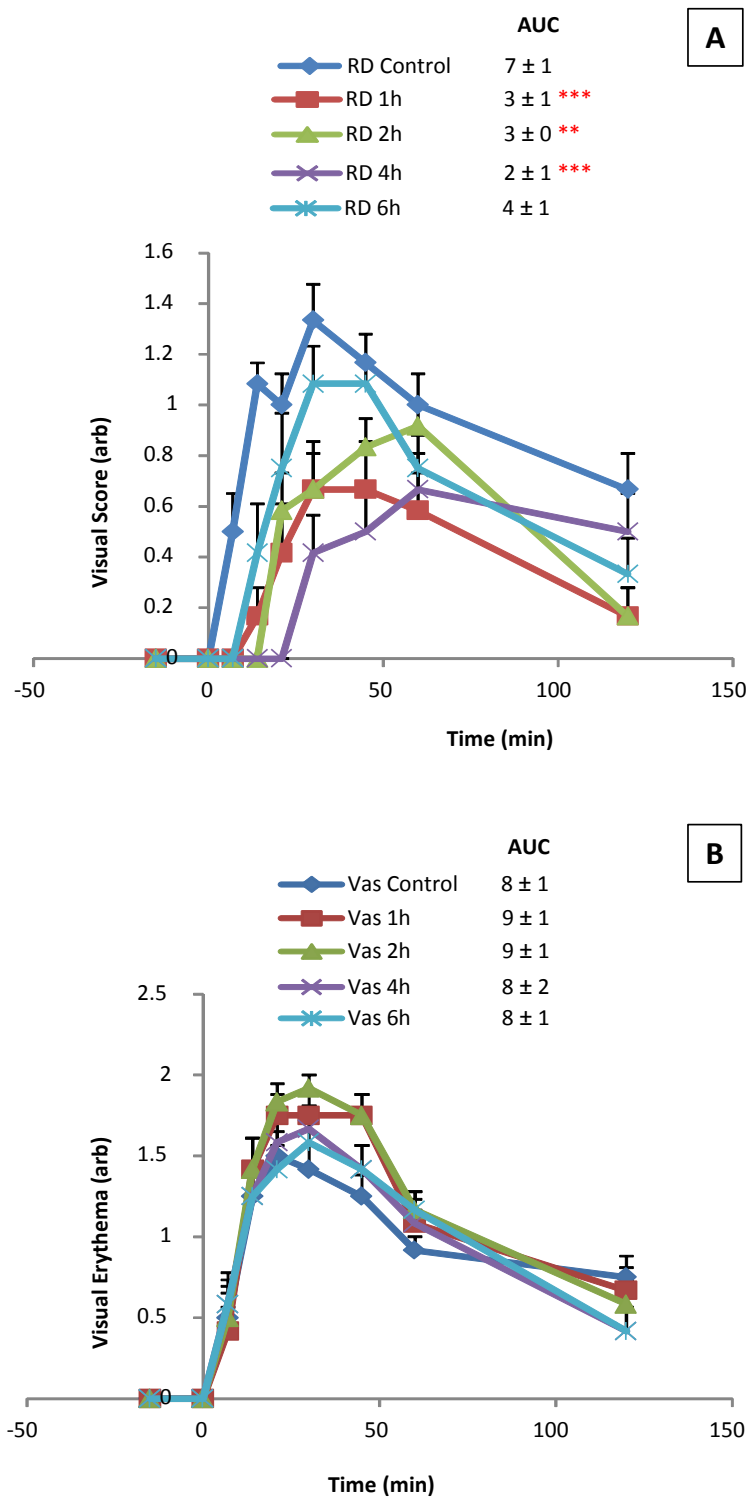


Figure 5.24: Visual Erythema Scoring For Human Volunteers Treated With RD-1433 (A) And Vaseline® (B) For Different Durations. RD-1433 and Vaseline® were applied at 0.1 mm to separate application sites on the volar forearm at 1, 2, 4 and 6 hours before rubefacient application. An untreated control site was present on both arms. Methyl nicotinate was applied (10 μ l; 5 mM) to the forearm at time 0. Excess methyl nicotinate was removed at 20 minutes and products were removed at 60 minutes. All data (n=12) are represented as mean + standard error of the mean. Asterisks (** and ***) represent a significant ($p < 0.05$ and 0.01 , respectively) decrease in visual erythema as compared to the untreated control.

5.3.4.3 Tissue Viability Imaging

Skin sites treated with RD-1433 for 1, 2 and 4 hours showed significant ($p < 0.05$) decreases in erythema compared to the untreated control (Figure 5.25, A). A noticeable decrease in erythema was seen between baseline and application of test product, this is possibly a surface optical effect due to the opacity of the product resulting in a decrease in light penetration through the skin. There were no significant decreases in the Vaseline[®] treated groups compared to the untreated control (Figure 5.25, B).

All skin sites treated with RD-1433 from 1-6 hours showed significant ($p < 0.05$) decreases in erythema compared to the correspondingly treated Vaseline[®] groups. Quantitatively, RD-1433 treated skin showed erythema an order of magnitude lower than from Vaseline treated skin. Although not significant, RD-1433 treated at 1 and 2 hours showed lower erythema responses than RD-1433 treated groups at 4 and 6 hours.

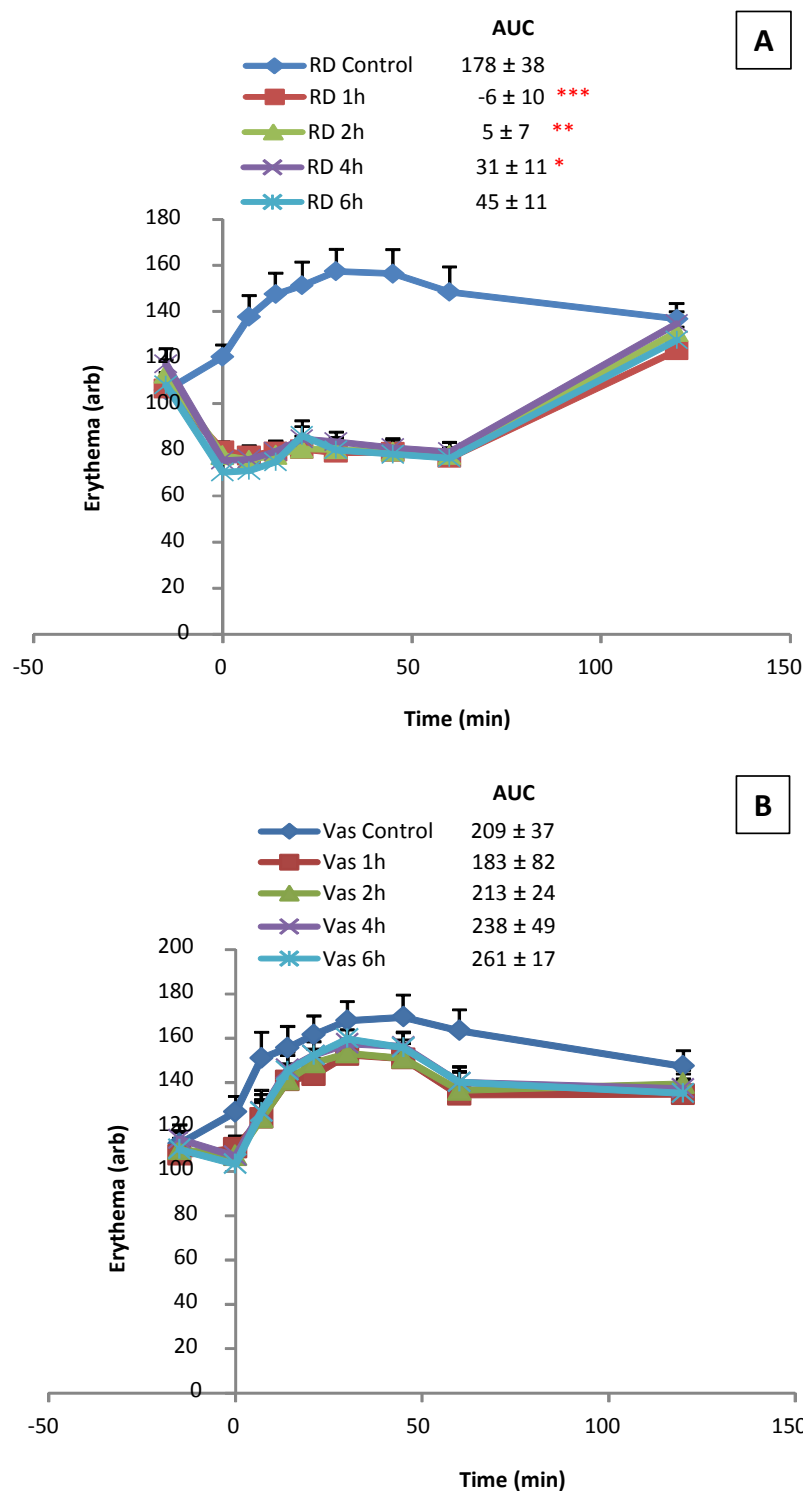


Figure 5.25: Tissue Viability Imaging Of Human Volunteers Treated With RD-1433 (Top) And Vaseline® (Bottom) For Duration Of Efficacy Studies. RD-1433 and Vaseline® were applied at 0.1 mm to separate application sites on the volar forearm at 1, 2, 4 and 6 hours before rubefacient application. An untreated control site was present on both arms. Methyl nicotinate was applied (10 µl; 5 mM) to the forearm at time 0. Excess methyl nicotinate was removed at 20 minutes and products were removed at 60 minutes. All data (n=12) are represented as mean + standard error of the mean. Asterisks (*, ** and ***) represent a significant ($p < 0.05$, 0.01 and 0.001, respectively) decrease in erythema as compared to the untreated control.

5.3.4.4 Laser Doppler Imaging- Blood Flow

Skin sites treated with RD-1433 for 1, 2, 4 and 6 hours showed significant ($p < 0.05$) decreases in blood flow compared to the untreated control (Figure 5.26- A). Skin treated with RD-1433 showed a time-dependent increase in penetration of methyl nicotinate corresponding to an increase in duration. In comparison, no significant differences were found in blood flow between Vaseline[®] treated groups compared to the untreated control (Figure 5.26- B).

All skin sites treated with RD-1433 were shown to have significantly lower ($p < 0.05$) blood flow compared to all corresponding Vaseline[®] treated groups. Quantitatively, RD-1433 treated skin showed blood flow an order of magnitude lower than blood flow from Vaseline[®] treated groups.

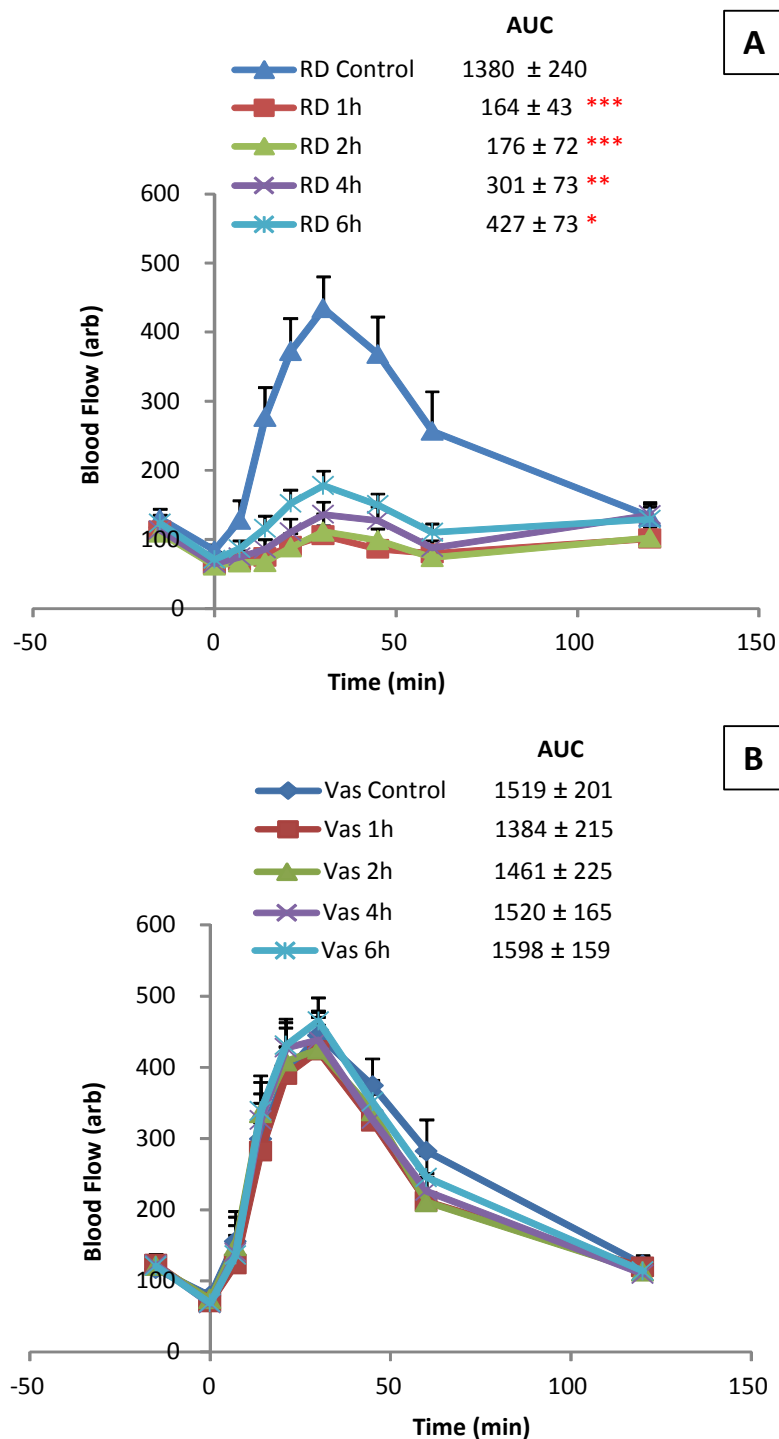


Figure 5.26: Laser Doppler Imaging Of Human Volunteer Blood Flow Of RD-1433 (A) And Vaseline® (B) For Duration Of Efficacy Studies. RD-1433 and Vaseline® were applied at 0.1 mm to separate application sites on the volar forearm at 1, 2, 4 and 6 hours before rubefacient application. An untreated control site was present on both arms. Methyl nicotinate was applied (10 μ l; 5 mM) to the forearm at time 0. Excess methyl nicotinate was removed at 20 minutes and products were removed at 60 minutes. All values (n=12) are represented as mean + standard error of the mean. Asterisks (*, ** and ***) represent a significant ($p < 0.05$, 0.01 and 0.001, respectively) decrease in blood flow as compared to the untreated control.

5.3.4.5 Laser Doppler Imaging- Maximum Blood Flux

Skin sites treated with RD-1433 for 1, 2, 4 and 6 hours showed significant ($p < 0.05$) decreases in maximum blood flow compared to the untreated control (Figure 5.27- A). All skin treated with RD-1433 showed time-dependent increases in methyl nicotinate penetration corresponding to an increase in duration. There were no significant differences ($p > 0.05$) between the Vaseline[®] treated groups compared to the untreated control (Figure 5.27- B).

Skin sites treated with RD-1433 showed significant ($p < 0.05$) decreases in maximum blood flow flux compared to the corresponding Vaseline[®] treated groups. The decreases in maximum blood flow flux ranged from 4- to 7-fold in RD-1433 treated groups compared to the corresponding Vaseline[®] treated groups.

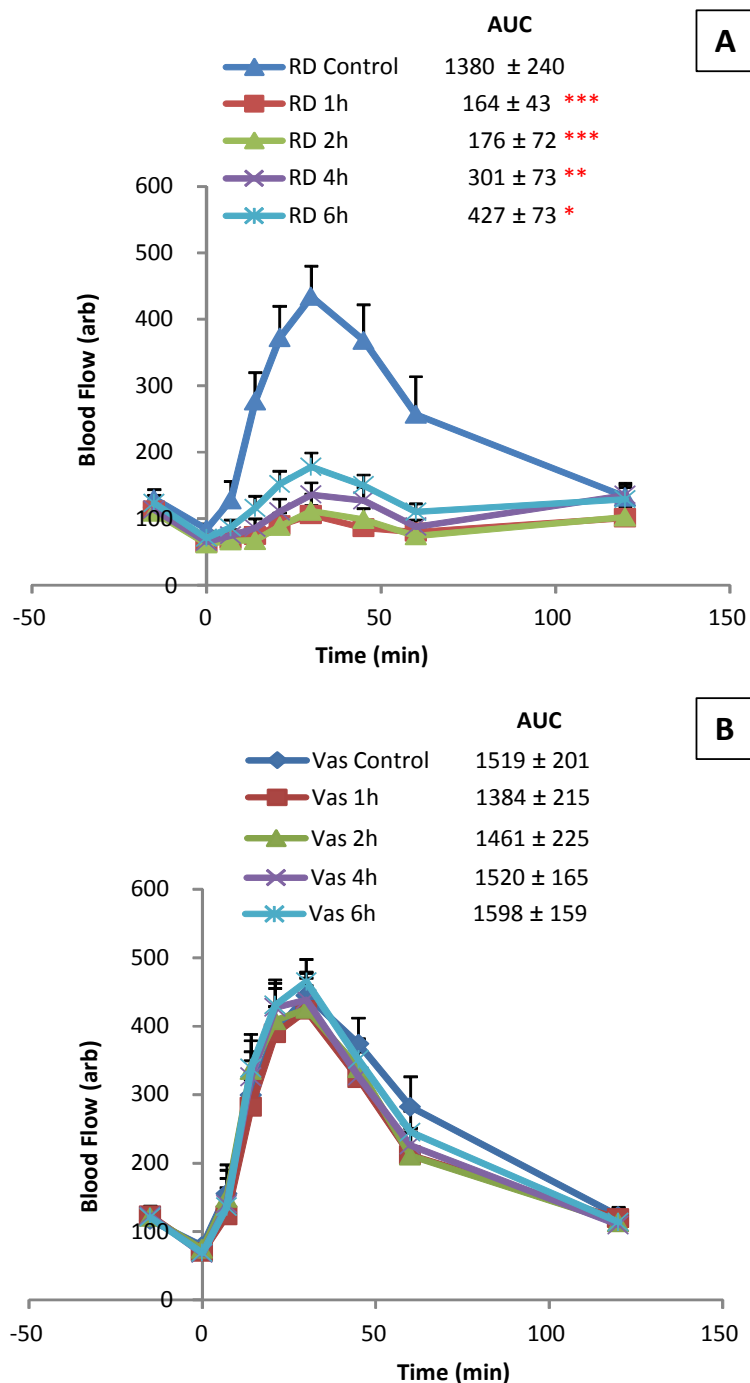


Figure 5.27: Laser Doppler Imaging Of Human Volunteers- Maximum Blood Flow Of RD-1433 (A) And Vaseline® (B) For Duration Of Efficacy Studies. Both RD-1433 and Vaseline® were applied at 0.1 mm to separate application sites on the volar forearm at 1, 2, 4 and 6 hours before rubefacient application. An untreated control site was present on both arms. Methyl nicotinate was applied (10 μ l; 5 mM) to the forearm at time 0. Excess methyl nicotinate was removed at 20 minutes and products were removed at 60 minutes. All data (n=12) are represented as mean + standard error of the mean. Asterisks (*, ** and ***) represent a significant ($p < 0.05$, 0.01 and 0.001, respectively) decrease in maximum blood flow as compared to the untreated control.

5.3.5 Summation Of *In Vitro* And *In Vivo* Results

In general, both *in vitro* and *in vivo* results demonstrated that RD-1433 treated skin provided the most protection against ^{14}C -MN penetration (and resulting flux) as well as erythema and blood flow reductions. When observing optimal thickness, it was shown that *in vitro* radiometric results for skin treated with RD-1433 matched results obtained with all the biophysical measurements (i.e. visual erythema, TiVi and LDI). When investigating the duration of efficacy, it was seen that *in vitro* radiometric measurements for skin treated with RD-1433 from 1 to 4 hours duration matched with all biophysical measurements with the 6 hour duration only observed to match with LDI measurements. Additionally, it was discovered that *in vitro* measurements may have been more sensitive, in detecting small changes in the amounts of ^{14}C -MN in test product treated skin.

Correspondingly, the sensitivity calculated (maximum amount penetrated/twice background) using an *in vitro* radiometric assay was 10 fold, this is in comparison to *in vivo* biophysical measurements (maximum response/twice background) of 1.4 fold and 3.5 fold for tissue viability imaging and laser Doppler imaging, respectively.

A	Parameter	Treatment Thickness (mm)					
		RD1433			Vaseline		
		0.01	0.05	0.1	0.01	0.05	0.1
In vitro	Methyl Nicotinate Cumulative Penetration	Green	Thatched Green	Grey	Grey	Green	Green
	Methyl Nicotinate Maximum Flux	Grey	Thatched Green	Grey	Grey	Grey	Grey
	Transepidermal Water Loss (TEWL)	Grey	Grey	Grey	Grey	Grey	Grey
In vivo	Laser Doppler Imaging	Grey	Thatched Green	Grey	Grey	Grey	Grey
	Visual Scoring (Erythema)	Grey	Thatched Green	Grey	Grey	Grey	Grey
	Tissue Viability Imaging (Erythema)	Grey	Thatched Green	Grey	Grey	Grey	Grey
	Transepidermal Water Loss (TEWL)	Grey	Grey	Grey	Grey	Grey	Grey

B	Parameter	Treatment Duration (h)							
		RD1433				Vaseline			
		1	2	4	6	1	2	4	6
In vitro	Methyl Nicotinate Cumulative Penetration	Green	Green	Green	Green	Grey	Green	Green	Green
	Methyl Nicotinate Maximum Flux	Green	Green	Green	Green	Grey	Green	Green	Green
	Transepidermal Water Loss (TEWL)	Grey	Grey	Grey	Grey	Grey	Grey	Grey	Grey
In vivo	Laser Doppler Imaging	Green	Green	Green	Green	Grey	Grey	Grey	Grey
	Visual Scoring (Erythema)	Green	Green	Green	Green	Grey	Grey	Grey	Grey
	Tissue Viability Imaging (Erythema)	Green	Green	Green	Green	Grey	Grey	Grey	Grey
	Transepidermal Water Loss (TEWL)	Grey	Grey	Grey	Grey	Grey	Grey	Grey	Grey

Figure 5.28: Statistical Summary Of Optimal Thickness Studies (A) And Duration Of Efficacy Studies (B) For *In Vitro* And *In Vivo* Data. Methyl nicotinate was applied at same concentration (5 mM) to both *in vitro* porcine skin (dorsum) and *in vivo* human volunteers (volar forearm). Methyl nicotinate application *in vitro* was quantified using radiometric assays to calculate cumulative penetration and maximum flux. Rates of TEWL were taken at baseline and post-treatment for both *in vitro* and *in vivo* studies. Biophysical measurements were used to quantify an erythematous response (visual erythema, tissue viability imaging) and blood flow (laser Doppler imaging) following application of RD-1433 and Vaseline® and subsequent *in vivo* application of methyl nicotinate. Green areas indicate significant decreases ($p < 0.05$) in methyl nicotinate penetration (*in vitro*) or significant decreases in erythema and blood flow response (*in vivo*) as compared to the untreated controls. Thatched green areas indicate matching statistical results from *in vitro* experimentation to *in vivo* clinical trial data.

5.4 Discussion

Overall, the work presented in this Chapter has demonstrated that a topical skin protectant (RD-1433) can significantly reduce the dermal absorption of methyl nicotinate in a dose-dependent manner. There was a high degree of correlation between the *in vitro* pig skin absorption kinetics of ^{14}C -MN and the corresponding physiological response to MN measured using *in vivo* biophysical techniques with human volunteers. The *in vitro-in vivo* correlation in barrier cream performance was somewhat improved when the skin was flexed *in vitro*, although flexing did not affect the baseline absorption kinetics of MN (in the absence of treatments) as demonstrated in Chapter 3 with model compounds benzoic acid, caffeine and testosterone.

Pig vs Human Skin

Marzulli *et al.* (1969), when using chemical warfare agents of varying physicochemical properties, found that the dorsum of weanling pigs approximated that of the human forearm in regards to permeability characteristics. Although it is acknowledged that human skin is the gold standard for *in vitro* testing of dermal absorption, porcine skin has been shown as a good model for human skin permeability (Walker *et al.*, 1986). In the present studies, porcine skin was used *in vitro* due to ethics surrounding the use of human skin as well as cost, reduced inter-individual variation (i.e. same gene pool, age and gender) and most importantly, the amount of skin available for the multitude of studies needed.

It was ascertained in both the optimal thickness and duration of efficacy studies with both test products, that maximum penetration and time taken to reach maximum, were very similar when using porcine dorsum skin and human volar forearm. Methyl

nicotinate has been documented in producing an erythema intensity that increases to a maximum reaction before fading away until a point as to where it is no longer visually detectable (Fountain *et al.*, 1969, Guy and Maibach, 1982). Both human and porcine skin showed maximum penetration occurring at approximately 30 minutes. Theoretically, the maximum flux of methyl nicotinate *in vitro* should have peaked at a time closer to time zero due to the 2- to 3- fold increase in permeability with porcine skin compared to human skin. Due to the mechanism of methyl nicotinate, blood flow is affected at the level of the papillary plexus (leading to erythema, etc.). *In vitro* porcine skin was dermatomed to 500 μm , a thickness that would include dermal tissue, and this may explain the delay in maximum flux. However, it is thought that the relatively rapid penetration of methyl nicotinate may account for similarities in penetration of MN between pig and human skin. In comparison to model compounds, the penetration of methyl nicotinate was relatively faster. The extremely rapid penetration of MN in both porcine and human skin would reduce the known relative difference between species as compounds penetrating rapidly over a short duration are difficult to measure due to inherent skin variability.

Application Of Test Products

The actual thickness of RD-1433 and Vaseline[®] applied to the skin both *in vitro* and *in vivo* was determined to be very close to the nominal thickness required. However, *in vivo* application of both test products was found to be consistently closer to nominal thickness as compared to *in vitro* application. This result was to be expected as the relative ease in applying the test products *in vivo* (i.e. larger surface area, solid support) contrasted with the relatively difficult application of the test products to a skin section present within a diffusion cell. As the skin sections did not have rigid

inserts for support, a high degree of caution was taken in the spreading of test products, in order to ensure that skin damage did not take place.

Generally, significant decreases in penetration of MN with 0.01 mm treated skin were not seen, and it is possible that this relatively small amount of test product did not provide a consistent layer of protection. This is further evidenced by *in vitro* penetration from the 0.01 mm treated groups demonstrating higher penetration than the 0.05 and 0.1 mm groups and the *in vivo* data indicating that the 0.01 mm groups presented with higher erythema and blood flow than the two higher thicknesses tested. Another potential interference when achieving a consistent layer of barrier cream could be due to skin structure. The skin is not a flat uniform surface, it has been previously estimated that 30% of total skin surface area is due to wrinkles (Kligman *et al.*, 1985b). Wrinkles have also been documented in preventing a uniform covering of the skin surface by a topical product (Brown and Diffey, 1986). As the skin is not uniform, it would be reasonable to infer that any variations in application of products to the skin surface (in identical amounts) could be due to this difference. For example, if applying a barrier cream, it may be difficult to provide a consistent layer due to the furrows of the skin creating more surface area than expected.

In Vitro Flexing

Although there were generally no significant differences between immobile and flexed skin, a difference was observed in that the amount of methyl nicotinate penetrating flexed skin in RD-1433 0.01 mm treated group was less than static skin. This may have been due to the flexing motion resulting in the furrows of the skin cycling between stretched and returning to a static state, in which case barrier cream

from treated areas may have covered an area lacking the product (Figure 5.29). In general, there were no consistent differences in penetration, flux or recovery of ^{14}C -MN on the skin surface in the flexed skin groups compared to the static skin groups. Furthermore, *in vitro* flexing of skin did not show differences in application of test products, with the noticeable exception of the 0.01 mm RD-1433 treated group. In this regard, the 0.01 mm RD-1433 treated group was not shown to be significantly different to the untreated controls when tested *in vivo*, which may have been due to the restriction of movement of the volunteers when MN was applied and biophysical measurements were taken. In general, although *in vitro* flexing did not show a difference to static skin, both measurements correlated well to *in vivo* findings, which would also indicate that CutaFlexTM is a good measure of dermal absorption and consistent to an OECD-compliant model.

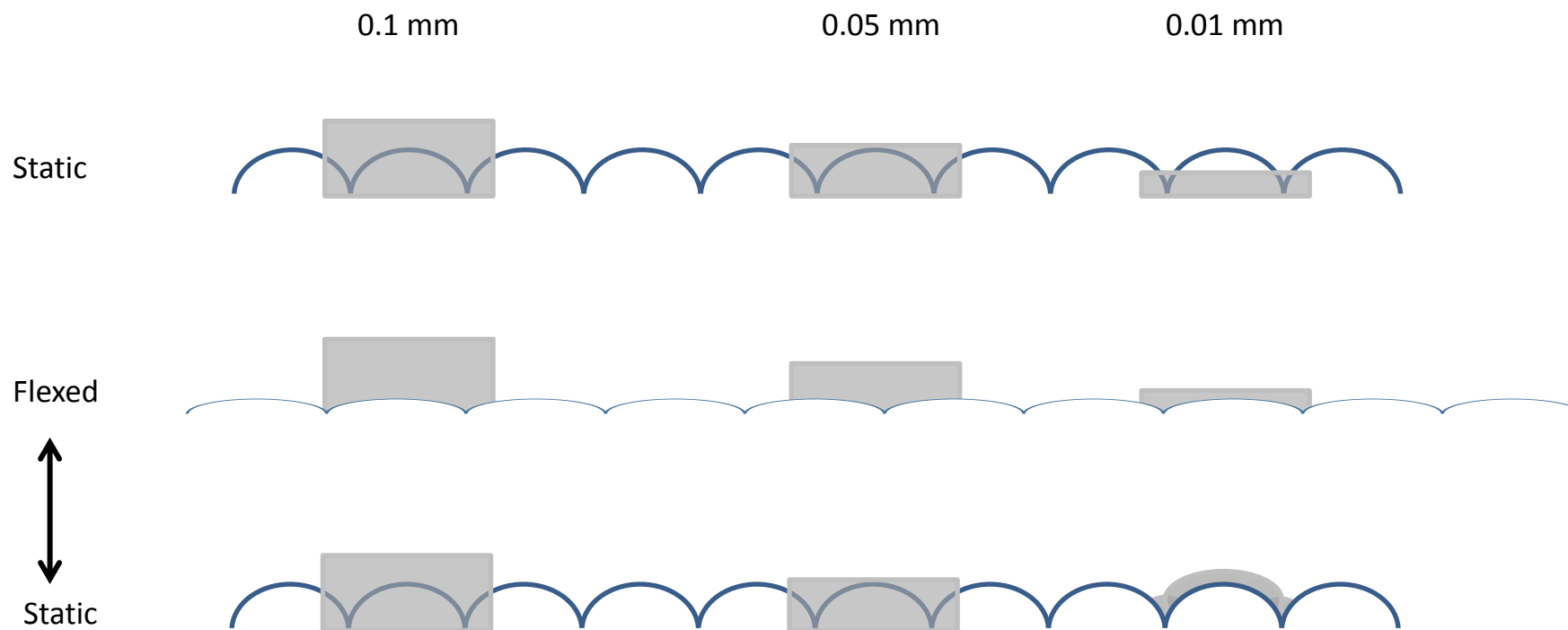


Figure 5.29: Schematic Of RD-1433 Spreading On The Skin Surface After Skin Flexing. Test product RD-1433 was applied to static and flexed skin at nominal thicknesses of 0.01, 0.05 and 0.1 mm. When applying RD-1433 *in vitro* at 0.05 and 0.1 mm, the skin surface was consistently covered (both furrows and surface), which was not the case when applying a nominal thickness of 0.01 mm to the skin surface. However, when skin treated with RD-1433 at a thickness of 0.01 mm is subsequently flexed, areas which were untreated come into contact with areas with barrier cream, allowing for spreading of the barrier cream more consistently and increased protection against ^{14}C -MN compared to static skin (Viegas, 2014).

Relative Endpoints

It has been thoroughly documented that the use of *in vitro* systems is not without several disadvantages, most notably the absence of systemic uptake and distribution, limited metabolic response, lack of systemic metabolism and finally an absence of an inflammatory-mediated response (Pendlington, 2008). Arguably, the absence of an inflammatory response limits the extent of comparison between *in vitro* measurements of methyl nicotinate to *in vivo* studies. To compound this, previously frozen porcine skin was also used, resulting in a possible decrease in enzymatic activities. As the mechanism of action of methyl nicotinate involves both action of the compounds on the papillary plexus and radial spreading through the capillaries, neither of the two effects would be present *in vitro* when using previously frozen skin. The active metabolism of prostaglandin molecules in skin cells (which lead to erythema) are not seen *in vitro*. However, *in vitro* kinetics should correlate to some degree with a physiological response *in vivo* if using skin models and experimental conditions that are comparable. For example, methyl nicotinate penetration should be similar *in vitro* and *in vivo* if *in vitro* skin viability was maintained and if concentration and exposure time were identical.

The benefit of using methyl nicotinate is the direct and rapid action in producing a response, in comparison to an inflammatory response caused by resulting histamine. Therefore, as a histamine-mediated immune response would be a longer process to initiate, it is thought that methyl nicotinate may still be relevant to study *in vitro* as skin can be dermatomed or epidermal sheets created to mimic the level of the capillaries (i.e. level of response).

If using a viable porcine skin preparation, it has been noted that the phenotype of enzyme expression in the skin of the domestic pig is similar to human patterns (Meyer and Neurand, 1976). However, *in vitro* correlation between human and porcine skin with ethyl nicotinate saw a difference in dermal penetration due to a difference in esterase activities (Ngawhirunpat *et al.*, 2004). Esterases are ubiquitously expressed in mammalian tissues and activities are known to be preserved after skin freezing processes (Wilkinson, 2008). As the present study used previously frozen porcine skin, esterase activity was not monitored or quantified prior to evaluation of barrier creams. It is possible that residual esterase activity in porcine skin may have contributed to the *in vitro* response to MN being similar to the *in vivo* response.

Sensitivity Of In Vitro Detection Versus In Vivo Detection

With the present *in vitro* studies, percutaneous penetration of ^{14}C -methyl nicotinate was directly quantified with collection in the receptor chamber allowing for detection down to as small as 0.5% (0.05 mg) of the applied dose. Guy *et al.* (1983) found that the response of methyl nicotinate was hampered by lower drug concentrations, which delayed the onset and magnitude of the response as well as shortening the duration of which changes in the microvasculature were seen. In the present study, the lowest amounts of methyl nicotinate penetrated were in the 0.1 mm RD-1433 treatment groups, in which both erythema and blood flow were still detected above baseline. Therefore, the concentration and exposure duration of MN chosen for the present studies provided a detectable response (even when providing significant protection against MN penetration) using both biophysical and radiometric measurements.

In terms of sensitivity within biophysical measurements, *in vivo* measurements of visual erythema and tissue viability imaging found that RD-1433 was only efficacious from 1-4 hours, whereas laser Doppler imaging found that RD-1433 was efficacious up to 6 hours a result that is in agreement with the quantitative amounts recovered *in vitro*. *In vivo* measurements of Vaseline[®] treated groups found Vaseline[®] to be ineffective at all time periods tested a result largely consistent with *in vitro* conclusions. Laser Doppler imaging is an important measure of skin health due to direct links between blood flow to thermoregulation and immune defence in addition to providing sensitive and rapid detection of vasodilators (i.e. methyl nicotinate (Taylor, 2008, Wester and Maibach, 1984). Laser Doppler imaging measures the response of a chemical in the skin through the Doppler effect whereas tissue viability imaging detects a depolarisation of reflected visible light. The main difference between LDI and TiVi is that the former detects superficial differences in blood flow, while the latter identifies deeper (reticular) changes in blood flow. In terms of methyl nicotinate detection and quantification (i.e. papillary plexus) LDI may provide a superior *in vivo* method of detection compared to TiVi. When sensitivity between techniques was semi-quantified, it was found that *in vitro* radiometric analysis provided a 10-fold increase whereas biophysical measurements of TiVi produced a 1.4-fold increase and LDI provided a 3.5-fold increase between minimum and maximum values (i.e. baseline and maximum response from MN). This would then seem to indicate that LDI may provide a better sensitivity and a closer one to that found with *in vitro* methodology. The increased sensitivity of *in vitro* testing also supplements other such advantages of lower inter-individual variability, lower costs and high-throughput data methods for this type of testing.

In terms of experimentation, both *in vitro* and *in vivo* procedures have advantages and disadvantages relating to detection of methyl nicotinate response and both work as complimentary techniques in order to detect erythema and blood flow changes as well as quantify amounts penetrating through the skin.

TEWL Measurements

Rates of transepidermal water loss flux were not found to differ between treatment groups or between the untreated controls both *in vitro* and *in vivo*. No correlation was found between TEWL rates and tritiated water penetrated, a result also documented in Chapter 3. An advantage that exists when using *in vitro* TEWL measurements is that the skin sections are not prone to effects such as diurnal variation, which are clearly seen with the *in vivo* TEWL rate decrease from baseline to post-treatment (Chilcott and Farrar, 2000).

In Vitro and In Vivo Measurements Of Optimal Thickness And Duration Of Efficacy

In the optimal thickness study, skin sections treated with RD-1433 at 0.05 and 0.1 mm showed significantly lower penetration of methyl nicotinate and accompanying maximum flux (*in vitro*) compared to the untreated control as well as RD 0.01 mm treated groups and all Vaseline[®] treated groups. Comparable decreases in erythema and blood flow (dose-dependent) were found with RD-1433 0.05 and 0.1 mm treated groups when using *in vivo* biophysical measurements. Between the two highest thicknesses used, 0.1 mm consistently provided better protection, at a minimum 2-fold greater than the 0.05 mm treated groups.

Although Vaseline[®] treated skin was statistically different from the untreated control, the values of methyl nicotinate penetrated and accompanying flux were much higher than RD-1433 treated skin and Vaseline[®] was not thought to provide consistent

results. Most importantly, these results agree with *in vivo* biophysical measurement findings that Vaseline[®] treated skin sites were not found to be different than the untreated control for both erythema and blood flow.

In the present study, it was also noted that all RD-1433 groups contained a greater amount of ¹⁴C-methyl nicotinate in the 60 (and 120) minute swabs than the corresponding Vaseline treated groups. This is thought to be attributed to the chemical constituents making up the RD-1433 formulation. RD-1433 is an overall amphiphobic formulation which provides a broad-spectrum of liquid repellence from chemicals, whereas Vaseline[®] is a hydrophobic formulation consisting of a mixture of hydrocarbon molecules 20-25 carbons in length. Results from the present studies have shown a small amount of methyl nicotinate (~ 5%) was still present on the skin surface after 60-120 minutes, with removal only taking place after washing of the skin. As already highlighted with the evaporation study with tritiated water (i.e. 0 mg left after 30 minutes), the methyl nicotinate remaining would have been spread on the skin surface as a fine powder. It is conceivable that the formulation of RD-1433 and associated low surface energy acted as a liquid repellent, and as such kept MN on the skin surface and available for removal. In addition, Vaseline[®] and associated lipophilic chains intercalating in the stratum corneum, could have assisted the translocation of methyl nicotinate from the formulation into the skin.

When contrasting both *in vitro* and *in vivo* results, it can be seen in the statistical table provided in Section 5.3.5 that *in vitro* and *in vivo* measurements are in broad agreement. However, *in vitro* results were found to identify additional significant decreases in MN penetration than *in vivo* findings, this was thought to be due to the sensitivity of the *in vitro* technique. Additionally, as quantitative amounts of MN

penetration cannot be taken from *in vivo* biophysical measurements (only response is measured), it is difficult to draw a comparison to the amount of MN penetrated *in vitro*.

In the duration of efficacy studies, both static and flexed skin treated with RD-1433 showed significant decreases in methyl nicotinate penetration from 1-6 hours after treatment. This result was similarly seen *in vivo* with laser Doppler blood flow. Furthermore, Vaseline[®] presented with inconsistent decreases in methyl nicotinate penetration from 1-4 hours, in addition to static and flexed skin showed a marked increase in methyl nicotinate penetration (and resulting flux) in the 6 hour treated group. *In vivo* measurements demonstrated consistently that Vaseline[®] treated groups did not show decreases in either erythema or blood flow that were significantly different to the control. The range of protective property exhibited by RD-1433 groups at one hour through to six hours, compared to Vaseline[®] groups, corresponded to a 4- to 11-fold protection.

A significant decrease in the amount of ¹⁴C-MN found in the skin was also found in the 6 hour flexed Vaseline[®] group. This result corresponds to a significantly higher penetration (and rate) of methyl nicotinate in the 6 hour group. It is thought that interaction of the petrolatum chains with the stratum corneum lipids may be responsible for this effect as this would create a disruption in the lipid bilayer of the stratum corneum. Previous results in the literature have documented the effect of Vaseline[®] in advancing barrier repair *in vivo* through the same mechanism (intercalating hydrocarbon chains with stratum corneum lipids) (Ghadially *et al.*, 1992). However, biophysical measurements indicate that RD-1433 also showed increases in both erythema and blood flow at 6 hours (although not significant)

compared to groups treated from 1-4 hours. As both products showed a similar trend of increased methyl nicotinate penetration/response, it is reasonable to presume that a contact duration of 6 hours may have resulted in possible hyperhydration of the stratum. However, this may not have been the case with skin treated with RD-1433 as the perfluorinated formulation is generally permeable to water vapour. Hyperhydration of the stratum corneum has documented in producing damage to the skin barrier layer (Wester and Maibach, 1995, Warner *et al.*, 1999). As both erythema and blood flow are biophysical indicators of a response by MN, it is thought that the *in vivo* results (although not quantitative) are more useful, as *in vitro* results showed that Vaseline[®] treated groups (difference between *in vitro* and *in vivo*) provided very inconsistent results against the penetration of methyl nicotinate.

Therefore, after a thorough assessment of three different test product thicknesses, it was determined through both radiometric and biophysical confirmation of significant decreases in methyl nicotinate penetration, erythema response and blood flow, that a thickness of 0.1 mm for RD-1433 would provide the best protection of the skin. Additionally, after testing of both test products for duration of efficacy from 1-6 hours it can be seen that RD-1433 provides significantly better protection through lower penetration (and flux) of methyl nicotinate, erythema response and blood flow from 1-6 hours compared to Vaseline.

Experimental Considerations

The dose recovery data (Figure 5.9 and Figure 5.22) demonstrated considerable loss of ¹⁴C-methyl nicotinate from all diffusion cells, with up to 80% unaccounted for in the (untreated) controls. This could not have been accounted for by the volatility of MN, which is reported to be extremely low (approximately 0.4 hPa at 25°C; Merck

Millipore, 2014). Therefore, the rate of vapour loss of $^3\text{H}_2\text{O}$ and ^{14}C -MN from an inert surface (foil) within the diffusion cells was measured. Surprisingly, MN initially evaporated quickly, with approximately 80% of the applied dose evaporating at 45 minutes (Figure 5.1). However, there was no further measurable loss after this time. This unusual behaviour can be explained by the concurrent loss of tritiated water, which evaporated completely by 45 minutes (Figure 5.1). When there was no further water available, the methyl nicotinate stopped evaporating. Thus, it appears highly likely that the relatively low recovery of ^{14}C -MN *in vitro* was due to co-evaporation with the (aqueous) vehicle, resulting in considerable (80%) loss of radioactivity in dose recoveries.

Due to exposure to the environment, the amount of methyl nicotinate available for dermal absorption after 20 minutes on untreated skin was less than half of what was originally applied to the skin surface. It has been previously discussed that a major factor affecting dermal absorption is volatility, with more volatile chemicals presenting with less of a dermal absorption hazard (Chilcott, 2012). This is attributed to the amount of chemical potentially available to penetrate through the epidermis being less than that of a non-volatile substance.

In Summary

- RD-1433 provided significantly better protection against ^{14}C -MN than Vaseline, especially at a thickness of 0.1 mm.
- RD-1433 was proven to provide a protective effect against ^{14}C -MN up to 6 hours. Vaseline treated skin could not provide an adequate level of protection.
- *In vitro* static and flexed skin treated with RD-1433 correlated well to *in vivo* techniques.

- Skin flexed in the CutaFlex™ system provided a good correlation to human skin treated with methyl nicotinate.

Chapter 6: General Discussion

6.1. General Discussion

The main aim of this Thesis was to develop and characterise a novel skin diffusion cell that would facilitate controlled flexing of the skin during dermal absorption studies. To date, all *in vitro* diffusion cell studies have been performed using un-flexed (static) skin. This is clearly not representative of the real-life situation, in which skin may be subject to various flexional forces, especially at jointed anatomical locations (e.g. elbow, knee, wrist, fingers). Therefore, the successful introduction of skin movement within a diffusion cell would represent a substantial refinement of existing *in vitro* dermal absorption models.

A further need to establish a flexing system exists due to the recent rise in products incorporating nanomaterials and the subsequent potential risk arising from dermal exposure to nanoparticles (Royal Society Of Chemistry, 2012, European Commission, 2006). Whilst it is accepted that nanoparticles exceed the established molecular weight limit for percutaneous penetration (by several orders of magnitude) and inherent molecular dimensions should physically impede permeation through the stratum corneum, it is conceivable that skin flexion may provide the necessary external force to assist translocation between adjacent corneocytes. Standard (non-flexing) diffusion cells cannot be used to test such a hypothesis, therefore further highlighting the need for modifying current *in vitro* dermal absorption models.

A series of pilot studies (not reported in this Thesis) assessed a number of flexing cell prototypes before establishing the current “CutaFlex™” design. At that stage of development, it became crucial to address a number of issues, specifically;

1. Does flexing of skin within the CutaFlex™ system cause damage to skin barrier function?

2. Are dermal absorption measurements of model (well-studied) compounds attained within the CutaFlex™ system in agreement with historical values?
3. Does the CutaFlex™ system exacerbate existing damage to skin barrier function?

In addressing these issues, the CutaFlex™ system could then be deemed appropriate to investigate the hypothesis that skin flexion may assist in the translocation of nanoparticles through the stratum corneum. In support of this aim, additional studies were performed which contributed to the current debate on the relationship between skin permeability (measured directly with tritiated water) and transepidermal water loss (TEWL). Furthermore, the effects of skin flexing on the performance of topical skin protectants such as barrier creams was investigated.

Initial work reported in Chapter 3 addressed the fundamental issues of the CutaFlex™ system in relating the effects of skin flexing on (i) normal barrier function, (ii) the percutaneous penetration of model compounds and (iii) exacerbation of existing skin damage. It was demonstrated that skin flexing (2 flexes per minute; 6 mm maximum amplitude for up to 8 hours) did not cause any measurable disruption in normal skin barrier function, as evidenced by no significant change in the skin absorption kinetics of $^3\text{H}_2\text{O}$ (Figure 3.6), benzoic acid (Figure 3.10), caffeine (Figure 3.14) and testosterone (Figure 3.18) to those acquired with an OECD-compliant Franz-type static cell. Generally, dermal absorption patterns in this Thesis agreed with historic model compound data (Hawkins and Reifenrath, 1986, van de Sandt *et al.*, 2004). In addition, flexing of skin did not generally exacerbate prior chemical and physical damage (Figure 3.2 and Figure 3.3).

Interestingly, no correlation was shown to exist between tritiated water penetration and TEWL flux (Figure 3.4 and Figure 3.5), with the former method providing a more sensitive indicator of barrier integrity. A number of studies have been published purporting to support the use of TEWL as a surrogate measure of skin barrier integrity (Nangia *et al.*, 1998, Fluhr *et al.*, 2006). In contrast, only two studies have indicated that TEWL does not necessarily correlate with permeability of the skin to water (Chilcott *et al.*, 2002, Hui *et al.*, 2012). The results of this present study tend to support the argument that TEWL is not a good indicator of skin barrier function. It is tempting to conclude that this may be due, at least in part, to the relative insensitivity of evaporimeters compared to tritiated water measurements (Section 3.4).

Overall, the data presented in Chapter 3 indicated that the CutaFlex™ system (when used within current parameters) provides an equivalent measure of *in vitro* dermal absorption to the standard well-characterised Franz cell and does not impair skin barrier function.

The CutaFlex™ system was then applied to investigate the hypothesis that skin flexing may facilitate translocation of nanoparticles through the skin. In Chapter 4, it was found that quantum dot nanoparticles (of a variety of shapes, sizes and charges) were not able to penetrate intact porcine skin in the presence or absence of flexing (Figure 4.11 and Figure 4.12). In general, flexed skin did not show differences in nanoparticle partitioning or penetration compared to static skin (Figure 4.4, Figure 4.5, Figure 4.6, Figure 4.11 and Figure 4.12). However, quantum dot charge was indicated as a factor influencing the extent to which QDots partitioning into the superficial layers of the stratum corneum, with negatively charged particles being

superficially absorbed to a greater extent than neutral or positively charged particles. It needs to be emphasised that the work reported in Chapter 4 represents a pilot study due to the limited number of skin samples (n=3) used in each treatment group. Therefore, further work involving a larger population of skin samples is needed to substantiate these initial findings, ideally with an additional treatment group to assess the effects of vehicle pH to confirm the findings of Prow *et al.* (2012) that skin barrier disruption (caused by alkaline conditions) may facilitate the dermal absorption of nanoparticles.

Data presented in Chapter 5, whilst relevant to finding new preventative treatments against incontinence-associated dermatitis (IAD), was studied to examine the possibility that skin flexing could potentially affect the topical distribution (and hence performance) of barrier creams. These studies used measurements of the dermal absorption of radiolabelled methyl nicotinate to quantify the protective effects of RD-1433 (and a comparator product, Vaseline®). A particular feature of this study was that it was subject to replication in a human volunteer study. This presented an opportunity to directly compare the predictive capability of the *in vitro* CutaFlex™ system (containing pig skin) with indirect measurements of methyl nicotinate penetration through human skin *in vivo* (by quantification of the erythematous response). From a clinical perspective, the novel barrier cream RD-1433 was found to provide consistently better protection against ¹⁴C-MN penetration than the comparator product. For example, RD-1433 provided a 3- to 10-fold increase in protection against ¹⁴C-MN compared to Vaseline® when used at 0.05 and 0.1 mm thickness and was effective for up to 6 hours in comparison to Vaseline® treated skin (Figure 5.5 vs. Figure 5.7 and Figure 5.18 vs Figure 5.20), a conclusion which was reproduced in the *in vivo* study (Figure 5.14 and Figure 5.26). Interestingly, skin

flexing appeared to influence the performance of RD1433 when applied at the smallest (0.01 mm) thickness (Figure 5.5). This effect was tentatively ascribed to the cream undergoing a redistribution on the skin surface (thus providing a protective coating to skin which was not dosed during the application – see Figure 5.29). Most importantly, the rate, duration and extent of MN penetration measured *in vitro* was in excellent agreement with the *in vivo* biophysical measurements, particularly blood flow (laser Doppler imaging). These data strongly suggest that the *in vitro* CutaFlex™ system is predictive of the human skin absorption of MN *in vivo*. Moreover, the CutaFlex™ system was deemed to be more sensitive in terms of ability to quantify dermal absorption of MN (as opposed to biophysical measurements of the physiological effects of MN *in vivo*).

6.2. Summary

Overall, the work reported in this Thesis has successfully demonstrated the practical feasibility of designing, manufacturing and characterising a skin flexing diffusion cell system which produces measurements of dermal absorption that are generally in good agreement with historical values of skin permeability to a range of model compounds. Flexing of excised skin samples had no measurable effect on the dermal absorption of model compounds, quantum dot nanoparticles or efficacy of barrier cream protection, although some evidence of an effect was observed in the protective performance of a barrier cream applied at a low dose (0.01 mm thickness).

6.3. Future Studies

Although data reported in this Thesis has addressed many relevant issues, there are also a number of interesting questions subsequently raised regarding additional

flexion scenarios. In particular, it is recommended that the following work be performed:

- Assessment of dermal absorption of human skin within the CutaFlex™ system
- Further skin damage studies (e.g. SLS, punctures, tape stripping) involving assessment of the percutaneous absorption of benzoic acid, caffeine and testosterone through a damaged skin barrier layer. In addition, an evaluation of QDot penetration through skin compromised through chemical or physical means (e.g. pH damage).
- An evaluation of an extended range of nanomaterials (e.g. metal ions, solid lipid nanoparticles, gold, silver) in the CutaFlex™ system applied to both flexed and static skin in the presence and absence of controlled skin damage.
- The use of several different concentration ranges of methyl nicotinate to determine minimum and maximum limits of detection in terms of an *in vivo* dose-response curve (to quantify the difference in sensitivity between *in vitro* and *in vivo* measurements).
- Further study to quantify the extent to which esterase activity affects methyl nicotinate penetration in both fresh and previously frozen porcine skin compared to human skin.

References

- Aalto-Korte, K. & Turpeinen, M. 1993. Transepidermal water loss and absorption of hydrocortisone in widespread dermatitis. *Br J Dermatol*, 128, 635-663.
- Adams, J. & Watts, F. 1993. Regulation and development and differentiation by the extracellular matrix. *Development*, 117, 1183-1198.
- Agner, T. & Serup, J. 1993. Time course of occlusive effects on skin evaluated by measurement of transepidermal water loss (TEWL): Including patch tests with sodium lauryl sulphate and water. *Contact Dermatitis*, 28, 6-9.
- Albery, W.J. & Hadgraft, J. 1979a. Percutaneous absorption: *In vivo* experiments. *J Pharm Pharmacol*, 31, 140-147.
- Albery, W.J. & Hadgraft, J. 1979b. Percutaneous absorption: Interfacial transfer kinetics. *J Pharm Pharmacol*, 31, 65-68.
- Albery, W.J. & Hadgraft, J. 1979c. Percutaneous absorption: Theoretical description. *J Pharm Pharmacol*, 31, 65-68.
- Allenby, A.C., Fletcher, J., Schock, C. & Tees, T.F.S. 1969. The effect of heat, pH and organic solvents on the electrical impedance and permeability of excised human skin. *Br J Dermatol*, 8, 31-39.
- Alvarez-Román, R., Naik, A., Kalia, Y.N., Guy, R.H. & Fessi, H. 2004. Skin penetration and distribution of polymeric nanoparticles. *J Control Release*, 99, 53-62.
- Aly, R., Shirley, C., Cunico, B. & Maibach, H.I. 1978. Effect of prolonged occlusion on the microbial flora, pH, carbon dioxide and transepidermal water loss on human skin. *J Invest Dermatol*, 71, 378-381.
- Anderson, B.D. 1993. Prodrugs and their topical uses. *In: Shah, V. P. & Maibach, H. I. (eds.) Topical drug bioavailability: Bioequivalence and penetration*. New York: Plenum Press.
- Andrievsky, G.V., Klochkov, V.K., Karyakina, E.L. & Mchedlov-Petrosyan, N.P. 1999. Studies of aqueous colloidal solutions of fullerene C₆₀ by electron microscopy. *Chem Phys Lett*, 300, 392-396.
- Baker, B.S., Fountain, R.B., Hadgraft, J.W. & Sarkany, I. 1969. A comparison of some physical properties of four vehicles used in dermatological preparations. *Br J Dermatol*, 81, 60-64.
- Baker, H. & Kligman, A.M. 1967. Measurement of transepidermal water loss by electrical hygrometry. *Arch Dermatol*, 96, 441-452.
- Balls, M., Botham, P.A., Bruner, L.H. & Spielmann, H. 1995. The EC/HO international validation study on alternatives to the draize. *Toxicol In Vitro*, 9, 871-929.
- Baroli, B., Ennas, M.G., Loffredo, F., Isola, M., Pinna, R. & Lopez-Quintela, M.R. 2007. Penetration of metallic nanoparticles in human full-thickness skin. *J Invest Dermatol*, 127, 1701-17012.
- Barry, B.W. & Williams, A.C. 1995. Permeation enhancement through skin. *In: Swarbrick, J. & Boylan, J. C. (eds.) Encyclopedia of pharmaceutical technology, Volume 11*. New York: Marcel Dekker.
- Bartek, M.J., LaBudde, J.A. & Maibach, H.I. 1972. Skin permeability *in vivo*: Comparison in rat, rabbit, pig and man. *J Invest Dermatol*, 58, 114-123.
- Benfledt, E. & Serup, J. 1999. Effect of barrier perturbation on cutaneous penetration of salicylic acid in hairless rats: *In vivo* pharmacokinetics using microdialysis and non-invasive quantification of barrier function. *Arch Dermatol Res*, 291, 517-526.

- Benowitz, N.L., Jacob, P.I., Olsson, P. & Johansson, C.J. 1992. Intravenous nicotinate retards transdermal absorption of nicotine: Evidence of blood flow-limited percutaneous absorption. *Clin Pharmacol Ther*, 52, 223-230.
- Berardesca, E. & Maibach, H.I. 1988. Racial differences in sodium lauryl sulphate induced cutaneous irritation: Black and white. *Contact Dermatitis*, 18, 65-70.
- Bergstresser, P.R. & Chapman, S.L. 1980. Maturation of normal human epidermis without an ordered structure. *Br J Dermatol*, 102, 641-648.
- Bettley, F.R. & Grice, K.A. 1967. The influence of ambient humidity on transepidermal water loss. *Br J Dermatol*, 78, 575-581.
- Bhatia, K.S. & Singh, K. 1998. Mechanism of transport enhancement of LHRH through porcine epidermis by terpenes and iontophoresis: Permeability and lipid extraction studies. *Pharm Res*, 15, 1857-1862.
- Bihari, P., Vippola, M., Schultes, S., Praetner, M., Khandoga, A.G., Reichel, C.A., Coester, C., Tuomi, T., Rehberg, M. & Krombach, F. 2008. Optimized dispersion of nanoparticles for biological *in vitro* and *in vivo* studies. *Particle Fibre Toxicol*, 5, 1-14.
- Blank, I.H. 1952. Factors which influence the water content of the stratum corneum. *J Invest Dermatol*, 18, 433-440.
- Blank, I.H. 1953. Further observations on factors which influence the water content of the stratum corneum. *J Invest Dermatol*, 21, 259-269.
- Blank, I.H. & Gould, E. 1959. Penetration of anionic surfactants (surface active agents) into skin. I. Penetration of sodium laurate and sodium dodecyl sulfate into excised human skin *J Invest Dermatol*, 33, 327-336.
- Blank, I.H. & Scheuplein, R.J. 1969. Transport into and within the skin. *Br J Dermatol*, 81, 4-10.
- Blume, U., Ferracin, J., Vershoore, M., Czernielewski, J.M. & Schaefer, H. 1991. Physiology of the vellus hair follicle: Hair growth and sebum excretion. *Br J Dermatol*, 124, 21-28.
- Blundell, G., Henderson, W.J. & Price, E.W. 1989. Soil particles in the tissues of the foot in endemic elephantiasis of the lower legs. *Ann Trop Med Parasit*, 83, 381-385.
- Borchert, K., Bliss, D.Z., Savik, K. & Radosevich, D.M. 2010. The incontinence associated dermatitis and its severity instrument: development and validation. *J Wound Ostomy Continence Nurs*, 37, 527-535.
- Borm, P.J.A., Robbins, D., Haubold, S., Kuhlbusch, T., Fissan, H., Donaldson, K., Schins, R.P.F., Stone, V., Kreyling, W., Lademann, J., Krutmann, J., Warheit, D. & Oberdörster, G. 2006. The potential risks of nanomaterials: A review conducted out for ECETOC. *Particle Fibre Toxicol*, 3, 1-35.
- Bos, J.D. & Meinardi, M.M.H.M. 2000. The 500 Dalton rule for the skin penetration of chemical compounds and drugs. *Exp Dermatol*, 9, 165-169.
- Bradner, J.M. 2009. Tight junctions and tight junction proteins in mammalian epidermis. *Eur J Pharm Biopharm*, 72, 289-294.
- Brain, K.R. & Chilcott, R.P. 2008. Physicochemical factors affecting skin absorption. In: Chilcott, R. P. & Price, S. (eds.) *Principles and practice of skin toxicology*. Chichester: John Wiley & Sons.
- Briggaman, R.A. & Wheeler, C.E. 1975. The epidermal-dermal junction. *J Invest Dermatol*, 65, 71-84.
- Bronaugh, R., Stewart, R.F. & Congdon, E.R. 1982. Methods for *in vitro* percutaneous absorption studies II. Animal models for human skin. *Toxicol Appl Pharmacol*, 62, 481-488.

- Bronaugh, R.L. 1995a. Methods for *in vitro* percutaneous absorption. *Toxicol Methods*, 5, 265-273.
- Bronaugh, R.L. 1995b. Methods for *in vitro* skin metabolism studies. *Toxicol Methods*, 5, 275-281.
- Bronaugh, R.L. 1996. Methods for *in vitro* skin metabolism studies *In: Marzulli, F. M. & Maibach, H. I. (eds.) Dermatotoxicology Fifth Edition*. Washington: Taylor & Francis.
- Bronaugh, R.L., Congdon, E.R. & Scheuplein, R.J. 1981. The effect of cosmetic vehicles on the penetration of N-Nitrosodiethanolamine through excised human skin. *J Invest Dermatol*, 76, 94-96.
- Bronaugh, R.L. & Stewart, R.F. 1985. Methods for *in vitro* percutaneous absorption studies V: Permeation through damaged skin. *J Pharm Sci*, 74, 1062-1066.
- Bronaugh, R.L., Stewart, R.F. & Simon, M. 1986. Methods for *in vitro* percutaneous absorption studies VII: Use of excised human skin. *J Pharm Sci*, 75, 1094-1097.
- Brown, M.B., Traynor, M.J., Martin, G.P. & Akomeah, F.K. 2008. Transdermal drug delivery systems: Skin perturbation devices. *Methods Mol Biol*, 437, 119-139.
- Brown, S. & Diffey, B.L. 1986. The effect of applied thickness on sunscreen protection: *In vivo* and *in vitro* studies. *Photochem Photobiol*, 44, 509-513.
- Bucks, D.A.W. & Maibach, H.I. 1999. Occlusion does not uniformly enhance penetration *in vivo*. *In: Bronaugh, R. L. & Maibach, H. I. (eds.) Percutaneous absorption: Drugs, cosmetics, mechanisms, methodology. Third Edition*. New York: Marcel Dekker.
- Burnette, R.R. & Ongpipattanakul, B. 1987. Characterization of the permselectivity properties of excised human skin during iontophoresis. *J Pharm Sci*, 76, 765-773.
- Calabrese, E.J. 1984. Gastrointestinal and dermal absorption: Interspecies differences. *Drug Metab Rev*, 15, 1013-1032.
- Calvo, P., Thomas, C., Alonso, M.J., Vilajato, J.L. & Robinson, J.R. 1994. Study of the mechanism of interaction of poly(epsilon-caprolactone) nanocapsules with the cornea by confocal laser-scanning microscope. *Int J Pharm*, 103, 283-291.
- Chan, F.L. & Inoue, S. 1994. Lamina lucida of basement membrane: An artefact. *Microsc Res Tech*, 28, 48-59.
- Chan, W.C.W., Maxwell, D.J., Gao, X., Bailey, R.E., Han, M. & Nie, S. 2002. Luminescent quantum dots for multiplexed biological detection and imaging. *Curr Opin Biotechnol*, 13, 40-46.
- Chan, W.C.W. & Nile, S. 1998. Quantum dot bioconjugates for ultrasensitive non-isotopic detection. *Science*, 281, 2016-2018.
- Chilcott, R.P. 2008. Cutaneous anatomy and function. *In: Chilcott, R. P. & Price, S. (eds.) Principles and practice of skin toxicology*. Chichester: John Wiley & Sons Ltd.
- Chilcott, R.P. 2012. Chemical warfare agents. *In: Wilhelm, K.-P., Zhai, H. & Maibach, H. I. (eds.) Dermatotoxicology Eighth Edition*. London: Informa Healthcare.
- Chilcott, R.P., Dalton, C.H., Emmanuel, A.J., Allen, C.E. & Bradley, S.T. 2002. Transepidermal water loss does not correlate with skin barrier function *in vitro*. *J Invest Dermatol*, 118, 871-875.
- Chilcott, R.P. & Farrar, R. 2000. Biophysical measurements of human forearm skin *in vivo*: Effects of site, gender, chirality and time. *Skin Res Technol*, 6, 64-69.

- Cho, S.J., Maysinger, D., Jain, M., Roder, B., Hackbarth, S. & Winnik, F.M. 2007. Long-term exposure to CdTe quantum dots causes functional impairments in live cells. *Langmuir*, 23, 1974-1980.
- Choi, H.S., Liu, W., Misra, P., Tanaka, E., Zimmer, J.P., Ipe, B.I., Bawendi, M.G. & Frangioni, J.V. 2007. Renal clearance of nanoparticles. *Nat Biotechnol.*, 25, 1165-1170.
- Christophers, E. & Kligman, A.M. 1965. Percutaneous absorption in aged skin. *In: Montagna, W. (ed.) Advances in biology of skin*. Oxford: Pergamon.
- Christophers, E., Wolff, H.H. & Laurence, E.B. 1974. The formation of epidermal cell columns. *J Invest Dermatol*, 62, 555-559.
- Clowes, H.M., Scott, R.C. & Heylings, J.R. 1994. Skin absorption- Flow-through or static diffusion cells. *Toxicol In Vitro*, 8, 827-830.
- Corachan, M., Tura, J.M., Campo, E., Soley, M. & Traveria, A. 1988. Podoconiosis in aequatorial Guinea. Report of two cases from different geological environments. *Trop Geogr Med* 40, 359-364.
- Cornell, P.M. & Barry, B.W. 1995. Effects of penetration enhancer treatment on the statistical distribution of human skin permeabilities. *Int J Pharm*, 117, 101-112.
- Crank, J. 1975. *The diffusion equations*, Oxford, Clarendon Press.
- Cronin, E. & Stoughton, R.B. 1962. Percutaneous absorption of nicotinic acid and ethyl nicotinate in human skin. *Nature*, 195, 1103-1104.
- Crutcher, W. & Maibach, H.I. 1969. The effect of perfusion rate on *in vitro* percutaneous penetration. *J Invest Dermatol*, 53, 264-269.
- Dailey, L.A., Kleemann, E., Wittmar, M., Gessler, T., Schmehl, T., Roberts, C., Seeger, W. & Kissel, T. 2003. Surfactant-free biodegradable nanoparticles for aerosol therapy based on the branched polyesters, DEAPA-PVAL-gPLGA. *Pharm Res*, 20, 2011-2020.
- DeLong, C.W., Thompson, R.C. & Kornberg, H.A. 1954. Percutaneous absorption of tritium oxide. *Am J Roent Rad Ther Nucl Med*, 71, 1038-1045.
- Denk, W., Strickler, J.H. & Webb, W.W. 1990. Two-photon laser scanning fluorescence microscopy. *Science*, 248, 73-76.
- Downing, D.T., Stewart, M.E., Wertz, P.W. & Strauss, J.S. 1993. Lipids of the epidermis and sebaceous glands. *In: Fitzpatrick, T. B., Eisen, A. Z., Wolff, K., Freedberg, I. M. & Austen, K. F. (eds.) Dermatology in general medicine*. New York: McGraw-Hill.
- Draize, J.H., Woodard, G. & Calvery, H.O. 1944. Methods for the study of irritation and toxicity of substances applied topically to the skin and mucous membrane. *J Pharmacol Exp Ther*, 82, 377-390.
- Dupuis, D., Rougier, A., Rouget, R., Lotte, C. & Kalopissis, G. 1984. *In vivo* relationship between horny layer reservoir effect and percutaneous absorption in human and rat. *J Invest Dermatol*, 82, 353-356.
- Eastman, J. 2005. Colloidal stability. *In: Cosgrove, T. (ed.) Colloid science: Principles, methods and applications*. Oxford: Blackwell Publishing.
- Eckert, R.L. 1989. Structure, function and differentiation of the keratinocyte. *Physiol Rev*, 69, 1316-1345.
- Effendy, I. & Maibach, H.I. 1996. Detergent and skin irritation. *Clin Dermatol*, 14, 15-21.
- Egelrud, T., Lundström, A. & Sondell, B. 1996. Stratum corneum cell cohesion and desquamation in maintenance of the skin barrier. *In: Marzulli, F. M. &*

- Maibach, H. I. (eds.) *Dermatotoxicology. Fifth Edition*. Washington, D.C.: Taylor & Francis.
- Elias, P.M. 1983. Epidermal lipids, barrier function and desquamation. *J Invest Dermatol*, 80, S44-49.
- Elias, P.M. & Friend, D.S. 1975. The permeability barrier in the mammalian epidermis. *J Cell Biol*, 65, 180-191.
- Elias, P.M. & Menon, G.K. 1991. Structural and lipid biochemical correlates of the epidermal permeability barrier. *Adv Lipid Res*, 24, 1-26.
- Elmahjoubi, E., Frum, Y., Eccleston, G.M., Wilkinson, S.C. & Meidan, V.M. 2009. Transepidermal water loss for probing full-thickness skin barrier function: Correlation with tritiated water flux, sensitivity to punctures and diverse surfactant exposures. *Toxicol In Vitro*, 23, 1429-1435.
- Enkema, L., Holloway, G.A., Piraino, D.W., Harry, D., Zick, G.L. & Kenny, M.A. 1981. Laser Doppler velocimetry vs heater power as indicators of skin perfusion during transcutaneous O₂ monitoring. *Clin Chem*, 27, 391-396.
- European Commission 1993. Council Directive 93/42/EEC of 14 June 1993 concerning medical devices (OJ L 169).
- European Commission 2006. SCENIHR modified opinion (after public consultation) on the appropriateness of existing methodologies to assess the potential risks associated with engineered and adventitious products of nanotechnologies.
- Everett, D.H. 1994. *Basic principles of colloid science*, London, The Royal Society Of Chemistry.
- Fartasch, M. 1995. Human barrier formation and reaction to irritation. In: Burg, G. (ed.) *Current problems in dermatology: Irritant dermatitis- New clinical and experimental aspects*. Basel: Karger Verlag.
- Fartasch, M. 1996. The nature of the epidermal barrier: Structural aspects. *Adv Drug Deliv Rev*, 18, 273-282.
- Fartasch, M. 1997. Ultrastructure of the epidermal barrier after irritation. *Microsc Res Tech*, 37, 193-199.
- Fasano, W.J., Manning, L.A. & Green, J.W. 2002. Rapid integrity assessment of rat and human epidermal membranes for *in vitro* dermal regulatory testing: Correlation of electrical resistance with tritiated water permeability. *Toxicol In Vitro*, 16, 731-740.
- Feldmann, R.J. & Maibach, H.I. 1965. Penetration of ¹⁴C-hydrocortisone through normal skin: The effect of stripping and occlusion. *Arch Dermatol*, 91, 661-666.
- Feldmann, R.J. & Maibach, H.I. 1967. Regional variation in percutaneous penetration of ¹⁴C-cortisol in man *J Invest Dermatol*, 48, 181-183.
- Ferrara, D.E., Weiss, D., Carnell, P.H., Vito, R.P., Vega, D., Gao, X., Nie, S. & Taylor, W.R. 2006. Quantitative 3D fluorescence technique for the analysis of en-face preparations of arterial walls using quantum dot nanocrystals and two-photon excitation laser scanning microscopy. *Am J Physiol Regul Integr Comp Physiol*, 290, R114-123.
- Fluhr, J.W., Feingold, K.R. & Elias, P.M. 2006. Transepidermal water loss reflects permeability status: Validation in human and rodent *in vivo* and *ex vivo* models. *Exp Dermatol*, 15, 483-492.
- Flynn, G.L. 1985. Mechanism of percutaneous absorption from physiological evidence. In: Bronaugh, R. L. & Maibach, H. I. (eds.) *Percutaneous absorption*. New York: Marcel Dekker.

- Flynn, G.L. 1990. Physicochemical determinants of skin absorption. *In: Gerrity, T. R. & Henry, C. J. (eds.) Principles of route-to-route extrapolation for risk assessment.* Amsterdam: Elsevier Science Publishing.
- Forbes, P.D. 1969. Vascular supply of the skin and hair in swine. *In: Montagna, W. & Dobson, R. L. (eds.) Hair growth, Advances in biology of skin.* Oxford: Pergamon.
- Fountain, R.B., Baker, B.S., Hadgraft, J.W. & Sarkany, I. 1969. The rate of absorption and duration of action of four different solutions of methyl nicotinate. *Br J Dermatol*, 81, 202-206.
- Fourier, J.B.J. 1878. *The analytical theory of heat by Joseph Fourier; translated with notes by Alexander Freeman*, Cambridge, University Press.
- Franz, T.J. 1975. Percutaneous absorption on the relevance of *in vitro* data. *J Invest Dermatol*, 64, 190-195.
- Franz, T.J. 1978. The finite dose technique as a valid *in vitro* model for the study of percutaneous absorption in man. *Curr Probl Dermatol*, 7, 58-68.
- Freeman, S. & Maibach, H.I. 1988 Study of irritant contact dermatitis produced by repeat patch testing with sodium lauryl sulphate and assessed by visual methods, transepidermal water loss and laser Doppler velocimetry. *J Am Acad Dermatol*, 19, 277-283.
- Froebe, C.L., Simion, F.A., Rhein, L.D., Cagan, R.H. & Kligman, A. 1990. Stratum corneum lipid removal by surfactants: Relation to *in vivo* irritation. *Dermatologica*, 181, 277-283.
- Frosch, P.J. & Kligman, A.M. 1979. The Durhing chamber. *Contact Dermatitis*, 5, 73-81.
- Frosch, P.J., Schulze-Dirks, A., Hoffmann, M. & Axthelm, I. 1993. Efficacy of skin barrier creams (II). Ineffectiveness of a popular 'skin protector' against various irritants in the repetitive irritation test in the guinea pig. *Contact Dermatitis*, 29, 74-77.
- Fuchs, E. 1993. Epidermal differentiation and keratin gene expression. *J Cell Sci*, 17 (suppl), 197-208.
- Fulton, G.P., Farber, E.M. & Moreci, A.P. 1959. The mechanism of action of rubefaciants. *J Invest Dermatol*, 33, 317-325.
- Galey, W.R., Lonsdale, H.K. & Nacht, S. 1976. The *in vitro* permeability of skin and buccal mucosa to selected drugs and tritiated water. *J Invest Dermatol*, 67, 713-717.
- Gamer, A., Leibold, E. & van Ravenzway, B. 2006. The *in vitro* absorption of microfine ZnO and TiO₂ through porcine skin. *Toxicol In Vitro* 20, 301-307.
- Gerion, D., Pinaud, F., Williams, S.C., Parak, W.J., Zanchet, D., Weiss, S. & Alivisatos, A.P. 2001. Synthesis and properties of biocompatible water-soluble silica-coated CdSe/ZnS semi-conductor quantum dots. *J Phys Chem B*, 105, 8861-8871.
- Ghadially, R., Halkier-Sorensen, L. & Elias, P.M. 1992. Effects of petrolatum on stratum corneum structure and function. *J Am Acad Dermatol*, 26, 387-396.
- Gilchrest, B.A. 1984. Age-associated changes in normal skin. *In: Gilchrest, B. A. (ed.) Skin and the ageing process.* Boca Raton: CRC Press.
- Gilpin, S.J., Hui, X. & Maibach, H.I. 2009. Volatility of fragrance chemicals: Patch testing implications. *Dermatitis*, 20, 200-207.
- Goh, C.L. & Chia, S.E. 1988. Skin irritancy to sodium lauryl sulphate as measured by skin vapour loss by sex and race. *Clin Exp Dermatol*, 13, 16-19.

- Gopee, N.V., Roberts, D.W., Webb, P., Cozart, C.R., Siitonen, P.H., Latendresse, J.R., Warbitton, A.R., Yu, W.W., Colvin, V.L., Walker, N.J. & Howard, P.C. 2009. Quantitative determination of skin penetration of PEG-coated CdSe quantum dots in dermabrased but not intact SKH-1 hairless mouse skin. *Toxicol Sci*, 111, 37-48.
- Gopee, N.V., Roberts, D.W., Webb, P., Cozart, C.R., Siitonen, P.H., Warbitton, A.R., Yu, W.W., Colvin, V.L., Walker, N.J. & Howard, P.C. 2007. Migration of intradermally injected quantum dots to sentinel organs in mice. *Toxicol Sci*, 98, 249-257.
- Gorelik, J., Shevchuk, A., Ramalho, M., Elliott, M., Lei, C., Higgins, C.F., Lab, M.J., Klenerman, D., Krauzewicz, N. & Korchev, Y. 2002. Scanning surface confocal microscopy for simultaneous topographical and fluorescence imaging: Application to single virus-like particle entry into a cell. *Proc Nat Acad Sci USA*, 99, 16018-16023.
- Gratieri, T., Schaefer, U.F., Jing, L., Gao, M., Kostka, K.-H., Lopez, R.F.V. & Schneider, M. 2010. Penetration of quantum dot particles through human skin. *J Biomed Nanotechnol*, 6, 586-595.
- Gray, M. 2010. Optimal management of incontinence-associated dermatitis in the elderly. *Am J Clin Dermatol*, 11, 201-210.
- Gray, M., Black, J.M., Baharestani, M.M., Bliss, D.Z., Colwell, J.C., Goldberg, M., Kennedy-Evans, K.L., Logan, S. & Ratliff, C.R. 2011. Moisture-associated skin damage: overview and pathophysiology. *J Wound Ostomy Continence Nurs*, 38, 233-241.
- Gray, M., Bliss, D.Z., Doughty, D.B., Ermer-Seltun, J., Kennedy-Evans, K.L. & Palmer, M.H. 2007. Incontinence-associated dermatitis: a consensus. *J Wound Ostomy Continence Nurs*, 34, 45-54.
- Grayson, S., Johnson-Winegar, A.G., Wintraub, B.U., Isserhof, R.R., Epstein, E.H. & Elias, P.M. 1985. Lamellar body-enriched fractions from neonatal mice: Preparative techniques and partial characterization. *J Invest Dermatol*, 85, 285-289.
- Guy, R.H. & Maibach, H.I. 1982. Rapid radial transport of methyl nicotinate in the dermis. *Arch Dermatol Res*, 273, 91-95.
- Guy, R.H., Wester, R.C., Tur, E. & Maibach, H.I. 1983. Non-invasive assessments of the percutaneous absorption of methyl nicotinate in humans. *J Pharm Sci*, 72, 1077-1079.
- Hadgraft, J. 2001. Skin, the final frontier. *Int J Pharm*, 224, 1-18.
- Hadgraft, J., Hadgraft, J.W. & Sarkany, I. 1972. The effect of glycerol on the percutaneous absorption of methyl nicotinate. *Br J Dermatol*, 87, 30-36.
- Hadgraft, J., Hadgraft, J.W. & Sarkany, I. 1973. The effect of thermodynamic activity on percutaneous absorption. *J Pharm Pharmacol*, 25, 122-123.
- Halbhuber, K.J. & Konig, K. 2003. Modern laser scanning microscopy in biology, biotechnology and medicine. *Ann Anat*, 185, 1-20.
- Harding, C.R. & Scott, I.R. 1983. Histidine-rich proteins (filaggrins): Structural and functional heterogeneity during epidermal differentiation. *J Mol Bio*, 170, 651-673.
- Harrison, S.M., Barry, B.W. & Dugard, P.H. 1984. Effects of freezing on human-skin permeability. *J Pharm Pharmacol*, 36, 261-262.
- Hawkins, G.S. & Reifenrath, W.G. 1984. Development of an *in vitro* model for determining the fate of chemicals applied to skin. *Fund Appl Toxicol*, 4, s133-144.

- Hawkins, G.S. & Reifenrath, W.G. 1986. Influence of skin source, penetration, cell fluid and partition coefficient on *in vitro* skin penetration. *J Pharm Sci*, 75, 378-381.
- Higuchi, T. 1960. Physical chemical analysis of percutaneous absorption process from creams and ointments. *J Soc Cosmet Chem*, 11, 85-97.
- Higuchi, W.I. & Yu, C.-D. 1987. Prodrugs in transdermal delivery. In: Kydonieus, A. F. & Berber, B. (eds.) *Transdermal delivery of drugs*. Boca Raton: CRC Press.
- Hilliges, M., Wang, M. & Johansson, O. 1995. Ultrastructural evidence for nerve fibers within all vital layers of the human epidermis. *J Invest Dermatol*, 104, 134-137.
- Ho, Y.P. & Leong, K.W. 2010. Quantum dot-based theranostics. *Nanoscale*, 2, 60-68.
- Holbrook, K.A. & Odland, G.F. 1974. Regional differences in the thickness (cell layers) of the human stratum corneum: An ultrastructural analysis. *J Invest Dermatol*, 62, 415-422.
- Holloway, G.A. 1980. Cutaneous blood flow responses to injection trauma measured by laser Doppler velocimetry. *J Invest Dermatol*, 74, 1-4.
- Holloway, G.A. & Watkins, D.W. 1977. Laser doppler measurement of cutaneous blood flow. *J Invest Dermatol*, 69, 306-309.
- Hoo, C.M., Starostin, N., West, P. & Mecartney, M.L. 2008. A comparison of atomic force microscopy (AFM) and dynamic light scattering (DLS) methods to characterize nanoparticle size distributions. *J Nanopart Res*, 10, 89-96.
- Hori, M., Satoh, S. & Maibach, H.I. 1990. Classification of percutaneous penetration enhancers: A conceptual diagram. *J Pharm Pharmacol*, 42, 71-72.
- Hoshino, A., Fujioka, K., Oku, T., Suga, M., Sasaki, Y.F., Ohta, T., Yasuhara, M., Suzuki, K. & Yamamoto, K. 2004. Physicochemical properties and cellular toxicity of nanocrystal quantum dots depend on their surface modification. *Nanolett*, 4, 2163-2169.
- Hou, S.Y.E., Mitra, A.K., White, S.H., Menon, G.K., Ghadially, R. & Elias, P.M. 1991. Membrane structures in normal and essential fatty acid-deficient stratum corneum: Characterization by ruthenium tetroxide staining and X-ray diffraction. *J Invest Dermatol*, 96, 215-223.
- Howes, D., Guy, R.H., Hadgraft, J., Heylings, J.R., Hoeck, U., Kemper, F., Maibach, H.I., Marty, J.-P., Merk, H.F., Parra, J., Rekkas, D., Rondelli, I., Schaefer, H., Tauber, U. & Verbiess, N. 1996. Methods for assessing percutaneous absorption. The report and recommendations of ECVAM workshop 13. *ATLA*, 24, 81-106.
- Hui, X., Elkeeb, R., Chan, H. & Maibach, H.I. 2012. Ability to estimate relative percutaneous penetration via a surrogate marker- Transepidermal water loss? *Skin Res Technol*, 18, 108-113.
- Hull, M.T. & Warfel, K.A. 1983. Age-related changes in the cutaneous basal lamina: Scanning electron microscopic study. *J Invest Dermatol*, 81, 378-380.
- Idson, B. 1973. Water and the skin. *J Soc Cosmet Chem*, 24, 197-212.
- Imokawa, G., Akasaki, S., Minematsu, Y. & Kawai, M. 1989. Importance of intercellular lipids in water-retention properties of the stratum corneum: Induction and recovery study of surfactant dry skin. *Arch Dermatol Res*, 281, 45-51.

- Jakasa, I., Mohammadi, N., Krüse, J. & Kezic, S. 2004. Percutaneous absorption of neat and aqueous solutions of 2-butoxyethanol in volunteers. *Int Arch Occup Environ Health*, 77, 79-84.
- Jimbow, K., Quevedo, W.C., Fitzpatrick Jr, T.B. & Szabo, G. 1993. Biology of melanocytes. In: Fitzpatrick, T. B., Eisen, A. Z., Wolff, H. H., Freedberg, I. M. & Austen, K. F. (eds.) *Dermatology in general medicine*. New York: McGraw-Hill.
- Kao, J. & Carver, M.P. 1990. Cutaneous metabolism of xenobiotics. *Drug Metab Rev*, 22, 363-410.
- Kao, J., Hall, J., Shugert, L.R. & Holland, J.M. 1984. An *in vitro* approach to studying cutaneous metabolism and disposition of topically applied xenobiotics. *Toxicol Appl Pharmacol*, 75, 289-298.
- Kao, J., Patterson, F.K. & Hall, J. 1985. Skin penetration and metabolism of topically applied chemicals in six mammalian species, including man: An *in vitro* study with benzo[a]pyrene and testosterone. *Toxicol Appl Pharmacol*, 81, 502-516.
- Kasting, G.B. & Bowman, L.A. 1990. DC electrical properties of frozen, excised human skin. *Pharm Res*, 7, 134-143.
- Katz, M. & Poulson, B.J. 1971. Absorption of drugs through the skin. In: Brobie, B. B. & Gillette, J. (eds.) *Handook of experimental pharmacology*. Berlin: Springer.
- Kemp, S.J., Thorley, A.J., Gorelik, J., Seckl, M.J., O'Hare, M.J., Arcaro, A., Korchev, Y., Goldstraw, P. & Tetley, T.D. 2008. Immortalization of human alveolar epithelial cells to investigate nanoparticle uptake. *Am J Respirat Cell Molec Biol*, 39, 591-597.
- Kertész, Z.S., Szikszai, Z., Gontier, E., Moretto, P., Surleve-Bazeille, J.E., Kiss, B., Juhasz, I., Hunyadi, J. & Kiss, A.Z. 2005. Nuclear microprobe study of TiO₂-penetration in the epidermis of human skin xenografts. *Nuc Instr Meth B*, 231, 280-285.
- Khan, G.M., Frum, Y., Sarheed, O., Eccleston, G.M. & Meidan, V.M. 2005. Assessment of drug permeability distributions in two different model skins. *Int J Pharm*, 303, 81-87.
- Kim, D.-K. & Holbrook, K.A. 1995. The appearance, density and distribution of Merkel cells in human embryonic and fetal skin: Their relation to sweat gland and hair follicle development. *J Invest Dermatol*, 104, 411-416.
- Kim, S., Lim, Y.S., Soltesz, E.G., De Grand, A.M., Lee, J., Nakayama, A., Parker, J.A., Mihaljevic, T., Laurence, R.G., Dor, D.M., Cohn, L.H., Bawendi, M.G. & Frangioni, J.V. 2004. Near-infrared fluorescent type II quantum dots for sentinel lymph node mapping. *Nat Biotechnol*, 22, 93-97.
- Kligman, A.M. 1963. The uses of sebum. *Br J Dermatol*, 75, 307-319.
- Kligman, A.M. & Balin, A.K. 1989. Aging of human skin. In: Balin, A. K. & Kligman, A. M. (eds.) *Aging and skin*. New York: Raven Press.
- Kligman, A.M., Grove, G.L. & Balin, A.K. 1985a. Aging of human skin. In: Finch, C. E. & Schneider, E. L. (eds.) *Handbook of the biology of aging*. New York: Van Nostrand Reinhold.
- Kligman, A.M., Zheng, P. & Lavker, R.M. 1985b. The anatomy and pathogenesis of wrinkles. *Br J Dermatol*, 113, 37-42.
- Kulvietis, V., Zurauskas, E. & Rotomskis, R. 2013. Distribution of polyethylene glycol coated quantum dots in mice skin. *Exp Dermatol*, 22, 141-159.

- Labouta, H.I., El-Khordagui, L.K., Kraus, T. & Schneider, M. 2011. Mechanism and determinants of nanoparticle penetration through human skin. *Nanoscale*, 3, 4989-4999.
- Lademann, J., Weigmann, H.-J., Rickmeyer, C., Barthelmes, H., Schaefer, H., Mueller, G. & Wolfram, S. 1999. Penetration of titanium dioxide microparticles in a sunscreen formulation into the horny layer and the follicular orifice. *Skin Pharmacol Appl Skin Physiol*, 12, 247-256.
- Lademann, L. 1986. Epidermal permeability barrier: Transformation of lamellar-granule disks into intercellular sheets by a membrane-fusion process: A freeze-fracture study. *J Invest Dermatol*, 98, 202-209.
- Lademann, L. 1988. The epidermal permeability barrier. *Anat Embryol*, 178, 1-13.
- Lamaud, E., Lambrey, B., Schalla, W. & Schaefer, H. 1984. Correlation between transepidermal water loss and penetration of drugs. *J Invest Dermatol*, 82, 556.
- Lampe, M.A., Burlingame, A.L., Whitney, J., Williams, M.L., Brown, B.E., Roitman, E. & Elias, P.M. 1983. Human stratum corneum lipids: Characterisation and regional differences. *J Lipid Res*, 24, 120-130.
- Langemo, D., Hanson, D., Hunter, S., Thompson, P. & Oh, I.E. 2011. Incontinence and incontinence-associated dermatitis. *Adv Skin Wound Care*, 24, 126-140.
- Larese, F.F., D'Agostin, F., Crosera, M., Adami, G., Renzi, R., Bovenzi, M. & Maina, G. 2009. Human skin penetration of silver nanoparticles through intact and damaged skin. *Toxicol*, 33-37.
- Larson, D.R., Zipfel, W.R., Williams, R.M., Clark, S.W., Bruchez, M.P., Wise, F.W. & Webb, W.W. 2003. Water-soluble quantum dots for multiphoton fluorescence imaging *in vivo*. *Science*, 300.
- Lauer, A.C., Ramachandran, C., Lieb, L.M., Niemiec, S. & Weiner, N.D. 1996. Targeted delivery to the pilosebaceous unit via liposomes. *Adv Drug Deliv Rev*, 18, 311-324.
- Lavker, R.M. 1979. Structural alterations in exposed and unexposed aged skin. *J Invest Dermatol*, 73, 59-66.
- Lavker, R.M., Zheng, P. & Dong, G. 1986. Morphology of aged skin. *Dermatol Clin*, 4.
- Lavker, R.M., Zheng, P. & Dong, G. 1987. Aged skin: A study by light, transmission electron and scanning electron microscopy. *J Invest Dermatol*, 88, 44s-51s.
- Lee, W.-R., Shen, S.-C., Al-Suwayeh, S.A., Yang, H.-H., Li, Y.-C. & Fang, J.-Y. 2013. Skin permeation of small-molecule drugs, macromolecules and nanoparticles mediated by a fractional carbon dioxide laser: The role of the hair follicles. *Pharm Res*, 30, 792-802.
- Leveque, J.L., Corcuff, P., de Rigal, J. & Agache, P. 1984. *In vivo* studies of the evolution of physical properties of the human skin with age. *Int J Dermatol*, 23, 322-329.
- Lévêque, J.L., De Rigal, J., Saint-Léger, D. & Billy, D. 1993. How does sodium lauryl sulfate alter the skin barrier function in man? A multiparametric approach. *Skin Pharmacol*, 6, 111-115.
- Lévêque, J.L., Poelman, M.C., de Rigal, J. & Kligman, A.M. 1988. Are corneocytes elastic. *Dermatologica*, 176, 65-59.
- Lippold, B.C. & Schneemann, H. 1984. The influence of vehicles on the local bioavailability of betamethasone-17 benzoate from solution- and suspension-type ointments. *Int J Pharm*, 22, 31-43.

- Liu, D.K., Wannemacher, R.W., Snider, T.H. & Hayes, T.L. 1999. Efficacy of the topical skin protectant in advanced development. *J Appl Toxicol*, 19, S40-45.
- Lopez, R.F.V., Seto, J.E., Blankschtein, D. & Langer, R. 2011. Enhancing the transdermal delivery of rigid nanoparticles using the simultaneous application of ultrasound and sodium lauryl sulfate. *Biomaterials*, 32, 933-941.
- Lotte, C., Rougier, A., Wilson, D. & Maibach, H.I. 1987. *In vivo* relationship between transepidermal water loss and percutaneous penetration of some organic compounds in man: Effect of anatomic site. *Arch Dermatol Res*, 279, 351-356.
- Lyklema, J. 2000. *Fundamentals of interface and colloid science: Liquid-fluid interfaces*, London, Academic Press.
- Lynch, I., Cedervall, T., Lundqvist, M., Cabaleiro-Lago, C., Linse, S. & Dawson, K. 2007. The nanoparticle-protein complex as a biological entity: A complex fluids and surface science challenge for the 21st century. *Adv Colloid Interfac*, 134-135, 167-174.
- Maibach, H.I., Feldman, R.J., Mitby, T.J. & Serat, W.F. 1971. Regional variation in percutaneous penetration in man: Pesticides. *Arch Environ Health*, 23, 208-211.
- Malten, K.E. & den Arend, J. 1978. Topical toxicity of various concentrations of DMSO recorded with impedance measurements and water vapor loss measurements. *Contact Dermatitis*, 4, 80-92.
- Malten, K.E., den Arend, J. & Wiggers, R.E. 1979. Delayed irritation: Hexanediol diacrylate and butanediol diacrylate. *Contact Dermatitis*, 5, 178-184.
- Malten, K.E. & Thiele, F.A.J. 1973. Evaluation of skin damage. II. Water loss and carbon dioxide release measurements related to skin resistance measurements. *Br J Dermatol*, 89, 565-569.
- Manabe, M. & O'Guin, W.M. 1992. Keratohyalin, trichohyalin and keratohyalin-trichohyalin hybrid granules: An overview. *J Dermatol*, 19, 749-755.
- Mandzy, N., Grulke, E. & Druffel, T. 2005. Breakage of TiO₂ agglomerates in electrostatically stabilized aqueous dispersions. *Powder Technol*, 160, 121-126.
- Marks, R. 2004. The stratum corneum barrier: The final frontier. *J Nutr*, 134, S2017-2021.
- Marks, R. & Barton, S.P. 1983. The significance of size and shape of corneocytes. *In: Marks, R. & Plewig, G. (eds.) Stratum corneum*. Berlin: Springer.
- Martin, E., Neeilssen-Subnel, M.T.A., de Haan, F.H.N. & Bodde, H.E. 1996. A critical comparison of methods to quantify stratum corneum removed by tape stripping. *Skin Pharmacol*, 9, 69-77.
- Marzulli, F.M. 1962. Barriers to skin penetration. *J Invest Dermatol*, 39, 387-390.
- Marzulli, F.N., Brown, D.W.C. & Maibach, H.I. 1969. Techniques for studying skin penetration. *Toxicol Appl Pharmacol*, 14, 76-83.
- Mattoussi, H.M., Mauro, M., Goldman, E.R., Anderson, G.P., Sundar, V.C., Mikulec, F.V. & Bawendi, M.G. 2000. Self-assembly of CdSe-ZnS quantum dot bioconjugates using an engineered recombinant protein. *J Am Chem Soc*, 122, 12142-12150.
- Mavon, A., Miquel, C., Lejeune, O., Payre, B. & Moretto, P. 2007. *In vitro* percutaneous absorption and *in vivo* stratum corneum distribution of an organic and a mineral sunscreen. *Skin Pharmacol Physiol*, 20, 10-20.

- McMullen, E. & Gawkröeder, D.J. 2006. Physical friction is under-recognised as an irritant that can cause or contribute to contact dermatitis. *Br J Dermatol*, 154, 154-156.
- Menon, G.K., Feingold, K.R. & Elias, P.M. 1992a. The lamellar secretory response to barrier disruption. *J Invest Dermatol*, 95, 279-289.
- Menon, G.K., Williams, M.L., Ghadially, R. & Elias, P.M. 1992b. Lamellar bodies as delivery systems of hydrolytic enzymes: Implications for normal and abnormal desquamation. *Br J Dermatol*, 126, 337-345.
- Menzel, F., Reinert, T., Vogt, J. & Butz, T. 2004. Investigations of percutaneous uptake of ultrafine TiO₂ particles at the high energy ion nanoprobe LIPSION. *Nuc Instr Meth B*, 219-220, 82-86.
- Merck Millipore. 2014. *Methyl Nicotinate* [Online]. Available: http://www.merckmillipore.com/GB/en/product/Methyl-nicotinate,MDA_CHEM-818713 [Accessed June 25, 2014].
- Meyer, W. & Neurand, K. 1976. The distribution of enzymes in the skin of the domestic pig. *Lab Anim*, 10, 237-247.
- Meyer, W., Schwarz, R. & Neurand, K. 1978. The skin of domestic mammals as a model for human skin, with special reference to the domestic pig. *Curr Probl Dermatol*, 7, 39-52.
- Michaels, A.S., Chandrasekaran, S.K. & Shaw, S.E. 1975. Drug permeation through human skin: Theory and *in vitro* experimental measurement. *AIChE Journal*, 21, 985-996.
- Mils, V., Vincent, C., Croute, F. & Serre, G. 1992. The expression of desmosomal and corenodesmosomal antigens shows specific variations during terminal differentiation of epidermis and hair follicle epithelia. *J Histochem Cytochem*, 40, 1329-1337.
- Milstone, L.M. 2004. Epidermal desquamation. *J Invest Dermatol*, 36, 131-140.
- Mitragotri, S., Edwards, D., Blankschtein, D. & Langer, R. 1995. A mechanistic study of ultrasonically enhanced transdermal drug delivery. *J Pharm Sci*, 84, 697-706.
- Monash, S. & Blank, H. 1958. Location and reformation of the epithelial barrier to water vapor. *Arch Dermatol*, 78, 710-714.
- Montagna, W. 1961. *The structure and function of the skin*, New York, Academic.
- Montagna, W. 1962. *The epidermis*, New York, Academic Press.
- Montagna, W. & Yun, J.S. 1964. The skin of the domestic pig. *J Invest Dermatol*, 43, 11-21.
- Monteiro-Riviere, N.A. 1991. Comparative anatomy, physiology and biochemistry of mammalian skin. In: Hobson, D. W. (ed.) *Dermal and ocular toxicology: Fundamentals and methods*. Boca Raton: CRC Press.
- Monteiro-Riviere, N.A. 1996. Anatomical factors affecting barrier function. In: Marzulli, F. N. & Maibach, H. I. (eds.) *Dermatotoxicology Fifth Edition*. Fifth ed. Washington: Taylor & Francis.
- Monteiro-Riviere, N.A. 2006. Structure and function of skin. In: Riviere, J. E. (ed.) *Dermal absorption models in toxicology and pharmacology*. Boca Raton: Taylor & Francis.
- Monteiro-Riviere, N.A. & Riviere, J.E. 1996. The pig as a model for cutaneous pharmacology and toxicology research. In: Tumbleson, M. E. & Shook, L. B. (eds.) *Advances in swine in biomedical research*. New York: Plenum Press.

- Moon, S.H., Wester, R.C. & Maibach, H.I. 1990. Diseased skin models on the hairless guinea pig: In vivo percutaneous absorption. *Dermatologica*, 180, 8-12.
- Mordon, S., Sumian, C.C. & Devoisselle, J.M. 2003. Site-specific methylene blue delivery to pilosebaceous structures using highly porous nylon microspheres: An experimental evaluation. *Lasers Surg Med*, 33, 119-125.
- Morris-Jones, R., Robertson, R.J., Ross, J.S., White, I.R., McFadden, J.P. & Rycroft, R.J.G. 2002. Dermatitis caused by physical irritants. *Br J Dermatol*, 147, 270-275.
- Mortensen, L.J., Jatana, S., Gelein, R., DeBenedetto, A., Bentley, K.L.D., Beck, L.A., Elder, A. & DeLouise, L.A. 2013. Quantification of quantum dot murine skin penetration with UVR barrier impairment. *Nanotox*, 7, 1386-1398.
- Moser, K., Kriwet, K., Naik, A., Kalia, Y.N. & Guy, R.H. 2001. Passive skin penetration enhancement and its quantification *in vitro*. *Eur J Pharm Biopharm*, 52, 103-112.
- Moss, G.P., Sun, Y., Davey, N., Adams, R.G., Wilkinson, S.C. & Gullick, D.R. 2014. The application of gaussian processes in the prediction of permeability across a polydimethyl siloxane membrane. *In: Brain, K. R. & Chilcott, R. P. (eds.) Advances in dermatological sciences*. Cambridge: RSC Publishing.
- Murdock, R.C., Braydich-Stolle, L., Schrand, A.M., Schlager, J.J. & Hussain, S.M. 2008. Characterization of nanomaterial dispersion in solution prior to *in vitro* exposure using dynamic light scattering technique. *Toxicol Sci*, 101, 239-253.
- Nangia, A., Patil, S., Berner, B., Boman, A. & Maibach, H.I. 1998. *In vitro* measurement of transepidermal water loss: A rapid alternative to tritiated water permeation for assessing skin barrier functions. *Int J Pharm*, 170, 33-40.
- Nazzaro-Porto, M., Passi, S., Boniforti, L. & Belsito, F. 1979. Effects of aging on fatty acids in skin surface lipids. *J Invest Dermatol*, 73, 112-117.
- Netzlaff, F., Schaefer, I.F., Lehr, C.M., Meiers, P., Stahl, J., Kietzmann, M. & Niedorf, F. 2006. Comparison of bovine udder skin with human and porcine skin in percutaneous permeation experiments. *Atla-Altern Lab Animal*, 34, 499-513.
- Newman, D., Preston, A. & Salazar, S. 2007. Moisture control, urinary and faecal incontinence and perineal skin management. *In: Krasner, D., Rodeheaver, G. & Sibbald, R. (eds.) Chronic wound care: A clinical source book for healthcare professionals. Fourth edition*. Malvern: HMP Communications.
- Ng, K.M., Chu, I., Bronaugh, R.L., Franklin, C.A. & Somers, D.A. 1992. Percutaneous absorption and metabolism of pyrene, benzo[a]pyrene and di(2-ethylhexyl) phthalate: Comparison of *in vitro* and *in vivo* results in the hairless guinea pig. *Toxicol Appl Pharmacol*, 115, 216-223.
- Ngawhirunpat, T., Opanasopit, P. & Prakongpan, S. 2004. Comparison of skin transport and metabolism of ethyl nicotinate in various species. *Eur J Pharm Biopharm*, 58, 645-651.
- Nicolaides, N., Fu, H.C. & Rice, G.R. 1968. The skin surface lipids of man compared with those of eighteen species of animals. *J Invest Dermatol*, 51, 83-89.
- Nisman, R., Dellaire, G., Ren, Y., Li, R. & Bazett-Jones, D.P. 2004. Application of quantum dots as probes for correlative fluorescence, conventional and

- energy-filtered transmission electron microscopy. *J Histochem Cytochem*, 52, 13-18.
- Oberdörster, G., Oberdörster, E. & Oberdörster, J. 2005. Nanotoxicology: An emerging discipline evolving from studies of ultrafine particles. *Environ Health Perspect*, 113, 823-839.
- Odland, G.F. & Holbrook, K.A. 1987. The lamellar granules of epidermis. *Curr Probl Dermatol*, 9, 29.
- OECD 2004. Guideline for testing of chemicals. Skin absorption *in vitro* method 428. Paris.
- Ohl, L., Mohaupt, M., Czeloth, N., Hintzen, G., Kiafard, Z., Zwirner, J., Blankenstein, T., Henning, G. & Förster, R. 2004. CCR7 governs skin dendritic cell migration under inflammatory and steady-state conditions. *Immunity*, 21, 279-288.
- Paddock, S.W. 1999. An introduction to confocal imaging. *In: Paddock, S. W. (ed.) Confocal Microscopy: Methods and protocols*. New Jersey: Humana Perss Inc.
- Paliwal, S., Menon, G.K. & Mitragotri, S. 2006. Low-frequency sonophoresis: Ultrastructural basis for stratum corneum permeability assessed using quantum dots. *J Invest Dermatol*, 126, 1095-1101.
- Patil, S.M., Patrick, E. & Maibach, H.I. 1996. Animal, human and *in vitro* test methods for predicting skin irritation. *In: Marzulli, F. M. & Maibach, H. I. (eds.) Dermatotoxicology Fifth Edition*. Washington: Francis & Taylor.
- Paulsson, M. 1992. Basement membrane proteins: Structure, assembly and cellular interactions. *Crit Rev Biochem Mol Bio*, 27, 93-127.
- Pendlington, R.U. 2008. *In vitro* percutaneous absorption measurements. *In: Chilcott, R. P. & Price, S. (eds.) Principles and practice of skin toxicology*. Chichester: John Wiley & Sons.
- Pendlington, R.U., Whittle, E., Robinson, J.A. & Howes, D. 2001. Fate of ethanol topically applied to skin. *Food Chem Toxicol*, 39, 169-174.
- Pflücker, F., Wendel, V., Hohenberg, H., Gartner, E., Witt, T., Pfeiffer, S., Wepf, R. & Gers-Berlag, H. 2001. The human stratum corneum layer: An effective barrier against dermal uptake of different forms of topically applied micronised titanium dioxide. *Skin Pharmacol Appl Skin Physiol*, 14, S157-S163.
- Pinnagoda, J., Tupker, R.A., Agner, T. & Serup, J. 1990. Guidelines for transepidermal water loss (TEWL) measurement. *Contact Dermatitis*, 22, 164-178.
- Potts, R.O. & Francoeur, M.L. 1991. The influence of stratum corneum morphology on water permeability. *J Invest Dermatol*, 96, 495-499.
- Powers, K.W., Brown, S.C., Krishna, V.B., Wasdo, S.C., Moudgil, B.M. & Roberts, S.M. 2006. Research strategies for safety evaluation of nanomaterials: Part VI: Characterization of nanoscale particles for toxicological evaluation. *Toxicol Sci*, 90, 296-303.
- Prow, T.W., Monteiro-Riviere, N.A., Inman, A.O., Grice, J.E., Chen, X., Zhao, X., Sanchez, W.H., Gierden, A., Kendall, M.A.F., Zvyagin, A.V., Erdmann, D., Riviere, J.E. & Roberts, M.S. 2012. Quantum dot penetration into viable human skin. *Nanotox*, 6, 173-185.
- Pugh, W.J. & Chilcott, R.P. 2008. Principles of diffusion and thermodynamics. *In: Chilcott, R. P. & Price, S. (eds.) Principles and practice of skin toxicology*. Chichester: John Wiley & Sons.

- Qiao, G.L., Williams, P.L. & Riviere, J.E. 1994. Percutaneous absorption, biotransformation, and systemic disposition of parathion *in vivo* in swine. I. Comprehensive pharmacokinetic model. *Drug Metab Dispos*, 22, 459-471.
- Rapaport, M. 1973. The aging skin. *J Am Geriatr Soc*, 21, 206-207.
- Reichert, U., Michels, S. & Schmidt, R. 1993. The cornified envelope: A key structure of terminally differentiated keratinocytes. In: Darmon, M. & Blumenberg, M. (eds.) *The keratinocytes*. San Diego: Academic Press.
- Reifenrath, W.G., Chellquist, E.M., Shipwash, E.A., Jederberg, W.W. & Krueger, G.G. 1984. Percutaneous penetration in the hairless dog, weanling pig and grafted athymic nude mouse: Evaluation of models for predicting skin penetration in man. *Br J Dermatol*, 111, 123-135.
- Reifenrath, W.G. & Kemppainen, B.W. 1991. Skin storage conditions. In: Bronaugh, R. & Maibach, H. I. (eds.) *In vitro percutaneous absorption: Principles, fundamentals and applications*. Boca Raton: CRC.
- Reifenrath, W.G. & Spencer, T.S. 1985. Evaporation and penetration from skin. In: Bronaugh, R. & Maibach, H. I. (eds.) *Percutaneous absorption: Mechanisms, methodology and drug delivery*. New York: Marcel Dekker.
- Roberts, M.S. 2004. Skin structure and function. Proceedings of the preconference course "Fundamentals of percutaneous penetration". *Perspectives in Percutaneous Penetration*. La Grande Motte, France.
- Roberts, M.S. & Walker, M. 1993. Water: The most natural penetration enhancer. In: Walters, K. A. & Hadgraft, J. (eds.) *Pharmaceutical skin penetration enhancement*. New York: Marcel Dekker.
- Rolland, A., Wagner, N., Chatelus, A., Shroot, B. & Schaefer, H. 1993. Site-specific drug delivery to pilosebaceous units using polymeric microspheres. *Pharm Res*, 10, 1738-1744.
- Rosell, J., Colominas, J., Riu, P., Pallas-Areny, R. & Webster, J.G. 1998. Skin impedance from 1 Hz to 1 MHz. *IEEE Trans Biomed Eng*, 35, 649-651.
- Rougier, A., Dupuis, D., Lotte, C., Rouget, R., Wester, R.C. & Maibach, H.I. 1986. Regional variation of percutaneous penetration in man: Measurement by the stripping method. *Arch Dermatol Res*, 278, 465-469.
- Rougier, A., Lotte, C., Corcuff, P. & Maibach, H.I. 1988. Relationship between skin permeability and corneocyte size according to anatomic site, age and sex in man. *J Soc Cosmet Chem*, 39, 15-26.
- Rouse, J.G., Yang, J., Ryman-Rasmussen, J.P., Barron, A.R. & Monteiro-Riviere, N.A. 2007. Effects of mechanical flexion on the penetration of fullerene amino acid-derivatized peptide nanoparticles through skin. *Nano Lett*, 7, 155-160.
- Royal Society & Royal Academy of Engineering 2004. Nanoscience and nanotechnologies: Opportunities and uncertainties. London.
- Royal Society Of Chemistry 2012. Royal society of chemistry view on nanoscience and nanotechnology.
- Ryman-Rasmussen, J.P., Riviere, J.E. & Monteiro-Riviere, N.A. 2006. Penetration of intact skin by quantum dots with diverse physicochemical properties. *Toxicol Sci*, 9, 159-165.
- Sadauskas, E., Wallin, H., Stoltenberg, M., Vogel, U., Doering, P., Larsen, A. & Danscher, G. 2007. Kupffer cells are central in the removal of nanoparticles from the organism. *Part Fibre Toxicol*, 4, 1-7.

- Sage, B.H., Huke, R.H., McFarland, A.C. & Kowalczyk, K. 1993. The importance of skin pH in iontophoresis of peptides. *In: Brain, K., James, V. & Walters, K. A. (eds.) Prediction percutaneous penetration.* Cardiff: STS Publishing.
- Saint-Léger, D. 1994. Physiology of the pilosebaceous follicle. *Rev Prat*, 43, 2315-2319.
- Sampol, E., Jacquet, A., Viggiano, M., Bernini, V., Manelli, J.C., Lacarelle, B. & Durand, A. 2000. Plasma, urine and skin pharmacokinetics of cefepime in burns patients. *J Antimicrob Chemother*, 6, 315-317.
- Sato, K., Imai, Y. & Irimura, R.T. 1998. Contribution of dermal macrophage trafficking in the sensitization phase of contact hypersensitivity. *J Immunol*, 161, 6835-6844.
- Sato, K., Sugibayashi, K. & Morimoto, Y. 1991. Species differences in percutaneous absorption of nicorandil. *J Pharm Sci*, 80, 104-107.
- Schaefer, H. & Redelmeier, T.E. 1996. *Skin Barrier: Principles of percutaneous penetration*, Basel, Karger.
- Schatzlein, A. & Cevc, G. 1998. Non-uniform cellular packing of the stratum corneum and permeability barrier function of intact skin: A high-resolution confocal laser scanning microscopy study using highly deformable vesicles (Transfersomes). *Br J Dermatol*, 138, 583.
- Scheuplein, R.J. 1965. Mechanism of percutaneous absorption I. Routes of penetration and influence of solubility. *J Invest Dermatol*, 45, 334-346.
- Scheuplein, R.J. 1966. Analysis of permeability data for the case of parallel pathways. *Biophys J*, 6, 1-17.
- Scheuplein, R.J. 1976. Percutaneous absorption after twenty-five years: Or "old wine in new wineskins". *J Invest Dermatol*, 67, 31-38.
- Scheuplein, R.J. & Blank, I.H. 1971. Permeability of the skin. *Phys Rev*, 51, 701-747.
- Scheuplein, R.J. & Bronaugh, R.L. 1983. Percutaneous absorption. *In: Goldsmith, L. A. (ed.) Biochemistry and physiology of the skin: Volume 2.* New York: Oxford University Press.
- Scheuplein, R.J. & Morgan, L.J. 1967. "Bound-water" in keratin membranes measured by a microbalance technique. *Nature*, 214, 456-458.
- Scheuplein, R.J. & Ross, L. 1970. Effects of surfactants and solvents on the permeability of epidermis. *J Soc Cosmet Chem*, 21, 853-873.
- Schliemann, S., Petri, M. & Elsner, P. 2013. Preventing irritant contact dermatitis with protective creams: Influence of the application dose. *Contact Dermatitis*, 70, 19-26.
- Schluter-Wigger, W. & Elsner, P. 1996. Efficacy of 4 commercially available protective creams in the repetitive irritation test (RIT). *Contact Dermatitis*, 34, 278-283.
- Schulz, J., Hohenberg, F., Pflücker, F., Gartner, B., Will, T., Pfeiffer, S., Wepf, R., Wendel, V., Gers-Berlag, H. & Wittern, K.P. 2002. Distribution of sunscreens on skin *Adv Drug Deliv Rev*, 54, S157-S163.
- Schwarz, M.A., Owaribe, J., Kartenbeck, J. & Franke, W.W. 1990. Desmosomes and hemidesmosomes; Constitutive molecular components. *Annu Rev Cell Biol*, 6, 461-491.
- Scott, R.C. & Ramsey, J.D. 1987. Comparison of the *in vivo* and *in vitro* percutaneous absorption of a lipophilic molecule (cypermethrin, a pyrethroid insecticide). *J Invest Dermatol*, 89, 142-146.

- Senzui, M., Tamura, T., Miura, K., Ikarashi, Y., Watanabe, Y. & Fujii, M. 2010. Study on penetration of titanium dioxide (TiO₂) nanoparticles into intact and damaged skin *in vitro*. *J Toxicol Sci*, 35, 107-113.
- Seto, J.E., Polat, B.E., Lopez, R.F.V., Blankschtein, D. & Langer, R. 2010. Effects of ultrasound and sodium lauryl sulphate on the transdermal delivery of hydrophilic permeants: Comparative *in vitro* studies with full-thickness and split-thickness pig and human skin. *J Control Release*, 145, 26-32.
- Simon, G.A. & Maibach, H.I. 2000. The pig as an experimental animal model of percutaneous permeation in man: Qualitative and quantitative observations-an overview. *Skin Pharmacol Appl Skin Physiol*, 13, 229-234.
- Smith, H.W., Clowes, G.H.A. & Marshall, E.K. 1919. On dichloroethylsulfide (mustard gas) IV. The mechanism of absorption by the skin. *J Pharmacol Exp Ther*, 13, 1-30.
- Soto, K.F., Carrasco, A., Powell, T.G., Garza, K.M. & Murr, L.E. 2005. Comparative *in vitro* cytotoxicity assessment of some manufactured nanoparticulate materials characterized by transmission electron microscopy. *J Nanopart Res*, 7, 145-169.
- Steinert, P.M. 1993. Structure, function and dynamics of keratin intermediate filaments. *J Invest Dermatol*, 100, 729-733.
- Stern, M.D. 1975. *In vivo* evaluation of microcirculation by coherent light scattering. *Nature*, 254, 56-58.
- Stern, M.D., Lappe, D.L., Bowen, P.D., Chimosky, J.E., Holloway, G.A., Keiser, H.R. & Bowman, R.L. 1977. Continuous measurement of tissue blood flow by laser Doppler spectroscopy. *Am J Physiol*, 232, H441-448.
- Steven, A.C., Bisher, M.E., Roop, D.R. & Steinert, P.M. 1990. Biosynthetic pathways of filaggrin and loricrin- Two major proteins expressed by terminally differentiated epidermal keratinocytes. *J Struct Biol*, 104, 150-162.
- Stingl, G., Hauser, C. & Wolff, K. 1993. The epidermis: An immunological environment. In: Fitzpatrick, T. B., Eisen, A. Z., Wolff, K., Freedberg, I. M. & Austen, K. F. (eds.) *Dermatology in general medicine*. New York: McGraw-Hill.
- Stoughton, R.B., Clendenning, W.E. & Kruse, D. 1960. Percutaneous absorption of nicotinic acid and derivatives. *J Invest Dermatol*, 35, 337-341.
- Sumian, C.C., Pitre, F.B., Gauthier, B.E., Bouclier, M. & Mordon, S.R. 1999. A new method to improve penetration depth of dyes into the follicular duct: Potential application for laser hair removal. *J Am Acad Dermatol*, 41, 172-175.
- Sun, Y.-P., Li, X.-Q., Cao, J., Zhang, W.-X. & Wang, H.P. 2006. Characterization of zero-valent iron nanoparticles. *Adv Colloid Interf Sci*, 120, 47-56.
- Svesson, C.K. 2009. Biotransformation of drugs in human skin. *Drug Metab Dispos*, 37, 247-253.
- Swarbrick, J., Lee, G., Brom, J. & Gensmantel, N.P. 1984. Drug permeation through human skin. II. Permeability of ionizable compounds. *J Pharm Sci*, 73, 1352-1355.
- Szikszai, Z., Kertesz, Z.S., Bodnar, E., Major, I., Borbiro, I., Kiss, A.Z. & Hunyadi, J. 2010. Nuclear microprobe investigation of the penetration of ultrafine zinc oxide into intact and tape-stripped human skin. *Nuc Instr Meth B*, 268, 2160-2163.
- Takahashi, M., Tezuka, T. & Katunuma, N. 1992. Phosphorelated cystain alpha is a natural substrate of epidermal transglutaminase for formation of skin cornified cell envelope. *FEBS Lett*, 308, 79-82.

- Tan, M.H., Commens, C.A., Burnett, L. & Snitch, P.J. 1996. A pilot study on the percutaneous absorption of microfine titanium dioxide from sunscreens. *Australas J Dermatol*, 37, 185-187.
- Taylor, H. 2008. Instruments for measuring skin toxicity. In: Chilcott, R. P. & Price, S. (eds.) *Principles and practice of skin toxicology*. Chichester: John Wiley & Sons, Ltd.
- Teumer, J., Zezulak, K. & Green, H. 1994. Measurements of specific mRNA content of keratinocytes of different sizes in relation to growth and differentiation. In: Leigh, I. M., Lane, E. B. & Watt, F. M. (eds.) *The keratinocyte handbook*. Cambridge: Cambridge University Press.
- Tezuka, T. & Takahashi, M. 1987. The cysteine-rich envelope protein from human epidermal stratum corneum cells. *J Invest Dermatol*, 88, 47-51.
- Tinkle, S.S., Antonini, J.M., Rich, B.A. & Roberts, J.R. 2003. Skin as a route of exposure and sensitization in chronic beryllium disease. *Environ Health Perspect*, 111, 1202-1208.
- Toll, R., Jacobi, U., Richter, H., Schaefer, H. & Blume-Peytavi, U. 2004. Penetration profile of microspheres in follicular targeting of terminal hair follicles. *J Invest Dermatol*, 123, 168-176.
- Tsai, J.C., Shen, L.C., Sheu, H.M. & Lu, C.C. 2003. Tape stripping and sodium dodecyl sulfate treatment increase the molecular cutoff of polyethylene glycol penetration across murine skin. *Arch Dermatol Res*, 295, 169-174.
- Tsuji, J.S., Maynard, A.D., Howard, P.C., James, J.T., Lam, C., Warheit, D.B. & Santamaria, A.B. 2006. Research strategies for safety evaluation of nanomaterials, Part IV: Risk assessment of nanoparticles. *Toxicol Sci*, 89, 42-50.
- Tur, E., Maibach, H.I. & Guy, R.H. 1983. Percutaneous penetration of methyl nicotinate at three anatomic sites: Evidence for an appendageal contribution to transport? *Skin Pharmacol*, 4, 230-234.
- UK NanoSafety Partnership Group 2012. Working safely with nanomaterials in research & development.
- van de Sandt, J.J.M., van Burgsteden, J.A., Cage, S., Carmichael, P.L., Dick, I., Kenyon, S., Korinth, G., Larese, F., Limasset, J.C., Maas, W.J.M., Montomoli, L., Nelson, J.B., Payan, J.-P., Robinson, E., Sartorelli, P., Schaller, K.H., Wilkinson, S.C. & Williams, F.M. 2004. *In vitro* predictions of skin absorption of caffeine, testosterone and benzoic acid: A multi-centre comparison study. *Regul Toxicol Pharm*, 39, 271-281.
- van der Merwe, D., Tawde, S., Pickrell, J.A. & Erickson, L.E. 2009. Nanocrystalline titanium dioxide and magnesium oxide *in vitro* dermal absorption in human skin. *Cutan Ocul Toxicol*, 28, 78-82.
- van der Molen, R.G. & Riviere, J.E. 2005. Effects of vehicles and sodium lauryl sulphate on xenobiotic permeability and stratum corneum partitioning in porcine skin. *Toxicology*, 289, 514-518.
- Vecchia, B.E. & Bunge, A. 2006. Animal models: A comparison of permeability coefficients for excised skin from humans and animals. In: Riviere, J. E. (ed.) *Dermal absorption models in toxicology and pharmacology*. Boca Raton: CRC Press.
- Viegas, V.A. 2014. *Characterisation of a novel flexing diffusion cell (CutaFlex™) for assessing dermal exposure to nanoparticles*. Doctor of Philosophy, University of Hertfordshire.

- Voegeli, D. 2012. Moisture-associated skin damage: aetiology, prevention and treatment. *Br J Nurs*, 21, 517-521.
- von Zglinicki, T., Lindberg, M., Roomans, G.M. & Forslind, B. 1993. Water and ion distribution profiles in human skin *Acta Derm Venereol (Stockh)*, 73, 340-343.
- Walczyk, D., Bombelli, F.B., Monopoli, M.P., Lynch, I. & Dawson, K. 2010. What the cell "sees" in bionanoscience. *Journal of the American Chemical Society*, 132, 5761-5768.
- Walker, M., Dugard, P.H. & Scott, R.C. 1986. A comparison of the *in vitro* permeability properties of human and some laboratory animal skin. *Int J Cos Sci*, 8, 189-194.
- Warner, R.R., Boissy, Y., Lilly, N.A., Spears, M.J., McKillop, K., Marshall, J.L. & Stone, K.J. 1999. Water disrupts stratum corneum lipid lamellae: Damage is similar to surfactants. *J Invest Dermatol*, 113, 960-966.
- Warner, R.R., Myers, M.C. & Taylor, D.A. 1988. Electron probe analysis of human skin: Determination of the water concentration profile. *J Invest Dermatol*, 90, 218-224.
- Warner, R.R., Stone, K.J. & Boissy, Y.L. 2003. Hydration disrupts the human stratum corneum ultrastructure. *J Invest Dermatol*, 120, 275-284.
- Watkins, D.W. & Holloway, G.A. 1978. An instrument to measure cutaneous blood flow using the Doppler shift of laser light. *IEEE Trans Biomed Eng*, BME-25, 28-33.
- Weinstein, G.D. 1966. Comparison of turnover time and of keratinous protein fractions in swine and human epidermis. In: Bustad, L. K. & McClellan, R. O. (eds.) *Swine in biomedical research*. Seattle: Frayn.
- Werth, J.H., Linsenbuhler, M., S.M., D., Farkas, Z., Hinrichsen, H., Wirth, K.-E. & Wolf, D.E. 2003. Agglomeration of charged nanopowders in suspension. *Powder Technol*, 133, 106-112.
- Wertz, P.W., Madison, K.C. & Downing, D.T. 1989. Covalently bound lipids of the stratum corneum. *J Invest Dermatol*, 92, 109-111.
- Wester, R.C. & Maibach, H.I. 1984. Advances in percutaneous absorption. In: Drill, V. & Lazar, P. (eds.) *Cutaneous Toxicity*. New York: Raven Press.
- Wester, R.C. & Maibach, H.I. 1993. Animal models for percutaneous absorption. In: Shaw, V. P. & Maibach, H. I. (eds.) *Topical drug bioavailability, bioequivalence and penetration*. New York: Plenum Press.
- Wester, R.C. & Maibach, H.I. 1995. Penetration enhancement by skin hydration. In: Smith, E. W. & Maibach, H. I. (eds.) *Percutaneous penetration enhancers*. Boca Raton: CRC Press.
- Whitesides, G.M., Mathias, J.P. & Seto, C.T. 1991. Molecular self-assembly and nanochemistry: A chemical strategy for the synthesis of nanostructures. *Science*, 254, 1312-1319.
- Wigger-Alberti, W., Rougier, A., Richard, A. & Elsner, P. 1998. Efficacy of protective creams in a modified repeated irritation test. Methodological aspects. *Acta Derm Venereol*, 78, 270-273.
- Wilkinson, S.C. 2008. Biochemistry of the skin. In: Chilcott, R. P. & Price, S. (eds.) *Principles and practice of skin toxicology*. Chichester: John Wiley & Sons.
- Williams, A.C., Cornell, P.M. & Barry, B.W. 1992. On the non-Gaussian distribution of human skin permeabilities. *Int J Pharm*, 86, 69-77.
- Williams, R.M., Zipfel, W.R. & Webb, W.W. 2001. Multiphoton microscopy in biological research. *Curr Opin Chem Biol*, 5, 603-608.

- Wu, J., Liu, W., Xue, C., Zhou, S., Lan, F., Bi, L., Xu, H., Yang, X. & Zeng, F. 2009a. Toxicity and penetration of TiO₂ nanoparticles in hairless mice and porcine skin after subchronic dermal exposure. *Toxicol Lett*, 191, 1-8.
- Wu, X., Price, G.J. & Guy, R.H. 2009b. Disposition of nanoparticles and an associated lipophilic permeant following topical application to the skin. *Mol Pharmacol*, 6, 1441-1448.
- Yancey, K.N. 1995. Adhesion molecules. II. Interactions of keratinocytes with epidermal basement membrane. *J Invest Dermatol*, 104, 1008-1014.
- Young, B. & Heath, J.W. 2000. Organ systems- Skin. In: Young, B. & Heath, J. W. (eds.) *Wheater's functional histology*. London: Churchill Livingstone, Harcourt Publishers Ltd.
- Zhai, H. & Maibach, H.I. 2002. Occlusion versus skin barrier function. *Skin Res Technol*, 8, 1-6.
- Zhang, L.W. & Monteiro-Riviere, N.A. 2008. Assessment of quantum dot penetration into intact, tape-stripped, abraded and flexed rat skin. *Skin Pharmacol Physiol*, 21, 166-180.
- Zuin, S., Pojana, G. & Marcomini, A. 2007. Effect-oriented physicochemical characterization of nanomaterials. In: Monteiro-Riviere, N. A. & Tran, C. L. (eds.) *Nanotoxicology: Characterisation, dosing and health effects*. New York: Informa Healthcare USA Inc.